MRI-guided electrophysiology for the assessment and ablation of ventricular tachycardia substrate

Mukherjee, Rahul

Awarding institution:
King's College London

Take down policy

If you believe that this document breaches copyright please contact librarypure@kcl.ac.uk providing details, and we will remove access to the work immediately and investigate your claim.

MRI-guided electrophysiology for the assessment and ablation of ventricular tachycardia substrate

Dr Rahul Kumar Mukherjee

MBBS BSc(Hons) MRCP

A dissertation submitted for the degree of

Doctor of Philosophy

School of Biomedical Engineering and Imaging Sciences

King's College London

University of London

For Anjali and Selina

Abstract:

Real-time magnetic resonance imaging (MRI)-guided electrophysiology (MR-EP) offers a number of potential advantages over conventional electroanatomic mapping (EAM) systems, including improved assessment of arrhythmia structural substrate using late gadolinium enhancement (LGE) scar imaging, navigation of catheters using dedicated tracking techniques and monitoring of ablation lesion formation with soft tissue visualisation. Registration errors due to changes in the volume, orientation, rhythm, cardiac or respiratory motion between the time of pre-procedural imaging and EAM, as is typical with image integration approaches, are also minimised during real-time MR-EP. Although the majority of real-time MR-EP studies published to date have focused on the atria, where significant challenges remain for accurate substrate evaluation, the full potential of substrate and lesion assessment afforded by such systems is likely to be realised in the context of ventricular tachycardia (VT) ablation.

This thesis explores the use of a real-time MR-EP system for the assessment of structural and electrical substrate in the ventricle. Furthermore, the accuracy of the system is evaluated in the delivery of radiofrequency (RF) ablation lesions and online monitoring of lesions using dedicated imaging techniques. Chapters 1 and 2 review the literature on the electrophysiology of ventricular tachycardia and magnetic resonance imaging. Chapter 3 describes in detail the methods common to the data chapters including the animal model, imaging approaches and MR-EP workflow. In Chapter 4, a method of contrast delivery using a slow infusion of gadolinium (contrast steady-state) is used to enable LGE scar imaging over a prolonged period, thereby enhancing the spatial resolution of 3D sequences and improve the characterisation of structural substrate. A porcine ischaemia-reperfusion model is used to

compare post-contrast 3D sequences under consistent contrast conditions whilst the technique is also applied in a feasibility cohort of ischaemic cardiomyopathy patients.

In Chapter 5, the contrast steady-state technique is then used to acquire high resolution 3D scar imaging in the porcine model with the real-time MR-EP system. The relationship between structural and electrical substrate with the system is assessed. In Chapter 6, the accuracy of the MR-EP system to deliver ablation lesions in target regions is evaluated and lesion sizes measured using temperature mapping (MR-thermometry and dosimetry) and a non-contrast sequence (gradient-echo with a long inversion time) are compared to gross pathological examination. Chapter 7 summarises the results and describes further studies to advance the field.

Statement of originality

This thesis is submitted as a 'thesis incorporating publication' in accordance with the King's College London guidelines. All publications were published with an open access CC-BY licence and permission has been granted by the publishers to reproduce published manuscripts. I declare that the work described in this thesis has been primarily carried out by me. I declare that this thesis has not been submitted elsewhere for a higher degree.

Material from the following publications, which I have authored, have been adapted and reproduced within this thesis:

1. Mukherjee RK, O'Neill L, O'Neill MD. Prophylactic catheter ablation for ventricular tachycardia: Are we there yet? Arrhythmia and Electrophysiology Review 2017; 6(3):125-8. PMID: 29018520 - Chapter 1

2. Mukherjee RK, Chubb H, Roujol S, Razavi R, O'Neill MD. Advances in real-time MRI-guided electrophysiology. Current Cardiovascular Imaging Reports 2019; 12: 6. PMID: 31501689 - Chapters 2 and 3

3. Mukherjee RK, Whitaker J, Williams SE, Razavi R, O'Neill MD. Magnetic resonance imaging guidance for the optimization of ventricular tachycardia ablation. Europace 2018; 20; 1721-32. PMID: 29584897 - Chapter 2

4. Mukherjee RK, Costa CM, Neji R, Harrison JL, Sim I, Williams SE, Whitaker J, Chubb H, O'Neill L, Schneider R, Lloyd T, Pohl T, Roujol S, Niederer SA, Razavi R, O'Neill MD. Evaluation of a real-time magnetic resonance imaging-guided electrophysiology system for structural and electrophysiological ventricular tachycardia substrate assessment. Europace 2019; June 20; Epub ahead of print. PMID: 31219547 - Chapter 5

5. Mukherjee RK, Roujol S, Chubb H, Harrison J, Williams S, Whitaker J, O'Neill L, Silberbauer J, Neji R, Schneider R, Pohl T, Lloyd T, O'Neill M, Razavi R. Epicardial electroanatomical mapping, radiofrequency ablation and lesion imaging in the porcine left ventricle under real time magnetic resonance imaging guidance – an in-vivo feasibility study. Europace 2018: 20(FI2): f254-f262. PMID: 29294008 - Chapter 6

Table of contents

Table of Figures

Table of Tables

SECTION ONE:

BACKGROUND

1 Ventricular tachycardia

1.1 Introduction

Ventricular tachycardia (VT) is an abnormal heart rhythm originating from the left or right ventricle and includes a spectrum of clinical disease that may occur in the presence or absence of structural heart disease ranging from benign, idiopathic premature ventricular complexes (PVC) to monomorphic or polymorphic VT (Tanawuttiwat et al. 2016). In the presence of structural heart disease, VT is a life-threatening cardiac arrhythmia and a major cause of sudden cardiac death, the incidence of which is estimated to range from 50-100 per 100,000 in the general population (Rajat et al. 2012). Although the use of implantable cardioverter-defibrillators (ICDs) can reduce the risk of sudden cardiac death due to ventricular arrhythmias, recurrent ICD shocks can lead to psychological morbidity, reduce quality of life and have no impact on the underlying arrhythmogenic substrate (Poole et al. 2008; Wissner et al. 2012).

Anti-arrhythmic medications such as amiodarone can be used to suppress VT and reduce both appropriate and inappropriate ICD therapies (Santangeli et al. 2016) but have variable efficacy and are associated with significant adverse effects (Sapp et al. 2016). Catheter ablation using radiofrequency energy has emerged as a useful adjunct to ICD implantation and anti-arrhythmic medications in the management of VT. However, VT ablation remains limited by modest long-term success rates (Della Bella et al. 2013). Treatment failure can be due to the inability to deliver radiofrequency energy in a transmural fashion, difficulties in accessing regions of arrhythmogenic tissue and lack of robust procedural end-points. There are also significant procedural risks including vascular complications, cardiac tamponade, stroke and death.

The aim of this thesis is to develop and evaluate a real-time magnetic resonance imaging (MRI)-guided electrophysiology (MR-EP) solution for VT ablation which has the potential to improve the safety and efficacy of catheter ablation. This chapter provides an overview of the current classification of ventricular tachycardia, pathophysiology, electroanatomic mapping techniques and ablation strategies.

1.1.1   Idiopathic ventricular tachycardia

Around 10% of ventricular arrhythmias occur in the absence of structural heart disease defined by imaging and coronary angiography and are termed 'idiopathic' (Pathak et al. 2019). The mechanisms underlying idiopathic VT include abnormal automaticity, triggered activity and re-entry. Increased automaticity or spontaneous depolarisation of a focal region of tissue can result in extrasystoles which can precipitate tachycardia. Triggered activity can occur when oscillations in the transmembrane potential during or after repolarisation of the cardiac action potential is sufficient to breach the threshold potential and generate a spontaneous action potential. If repolarisation of the original cardiac action potential is interrupted resulting in a second spontaneous potential, this is referred to as an early afterdepolarisation (EAD) whilst a spontaneous potential occurring after the end of full repolarisation is referred to as a delayed afterdepolarisation (DAD). These 'triggered events' can also lead to extrasystoles and precipitate VT. The majority of idiopathic VT, particularly those related to the outflow tracts, are due to triggered activity secondary to DADs (Dukkipati et al. 2017). Re-entry requires the presence of alternate pathways of conduction where unidirectional block in one pathway may lead to circus movement or 're-entry' between the conventional and alternate pathways, culminating in tachycardia.

Idiopathic VT can be classified according to the anatomic site of origin. The most common location is in the right ventricular outflow tract (RVOT) which accounts for 80% of

idiopathic VTs. Other cardiac structures in close proximity including the left ventricular outflow tract (LVOT), aortic cusp and pulmonary artery can also give rise to outflow tract tachycardias. Similar to atrial fibrillation, where sleeves of myocardial tissue extending into the pulmonary veins can trigger ectopic beats, myocardial sleeves extending into the great vessels (aorta and pulmonary artery) may account for outflow tract VT.

The conduction system accounts for 10-15% of idiopathic VT with involvement of the left anterior or posterior fascicle. Fascicular VT is usually due to re-entry with a zone of slow conduction in the interventricular septum. These tachycardias are highly sensitive to the administration of calcium-channel blockers such as verapamil which can rapidly terminate the arrhythmia. VT may also originate from intra-cavitary structures such as the papillary muscles accounting for 5-12% of all idiopathic VT (Dukkipati et al. 2017). The posteromedial LV papillary muscle is the most common location followed by the anterolateral papillary muscle and rarely the right ventricular papillary muscles. The mitral and tricuspid annuli can also be a sources of idiopathic VT.

In general, catheter ablation can be offered with or without a trial of medical therapy in patients with symptomatic idiopathic VT and is associated with a relatively low risk of complications. For outflow tract VT, catheter ablation is highly efficacious with significant reductions in PVC burden and recurrence-free survival of >80% at 1-year in selected cases (Ling et al. 2014; Bogun et al. 2007). Fascicular VT ablation has comparable procedural efficacy with an initial success rate of 87% after the index procedure and 93.5% after multiple procedures (Creta et al. 2019). Catheter ablation of papillary muscle VT can be more challenging due to their complex structures, deep location of sites of origin, poor catheter stability and contact force during ablation (Doppalapudi et al. 2008).

1.1.2   Ventricular tachycardia in structural heart disease

Ventricular tachycardia associated with structural heart disease (SHD) is a major cause of
sudden death and ICDs can be used for primary and secondary prevention in selected patients
to reduce this risk. Catheter ablation may be considered as an adjunctive therapy in patients
with recurrent VT who cannot tolerate anti-arrhythmic medications or where they prove
ineffective (Deyell et al. 2018). The most common anatomic substrate for VT associated with
SHD is scar-related re-entrant VT post myocardial infarction (Josephson ME et al. 1978).

Following a myocardial infarction, there may be three different types of tissue present: dense
scar which is electrically unexcitable, normal myocardium and borderzone tissue. Infarct
heterogeneity can occur due to variability in myocardial perfusion, restoration of blood flow
after an infarct following primary percutaneous coronary intervention and subsequent
remodelling during the healing phase of the infarct (Schmidt et al. 2007). The infarct
borderzone region may contain a mixture of non-excitable scar tissue and surviving
'channels' of myocardial tissue. These regions provide the substrate for VT as a combination
of slow conduction and fixed anatomical block from dense scar produce non-uniform
anisotropy and promote re-entry (Ashikaga et al. 2007) - *Figure 1-1*. In ischaemic scar, the
substrate for VT is mainly detected in the endocardium but epicardial substrate may
sometimes also be present (Hayashi et al. 2018).
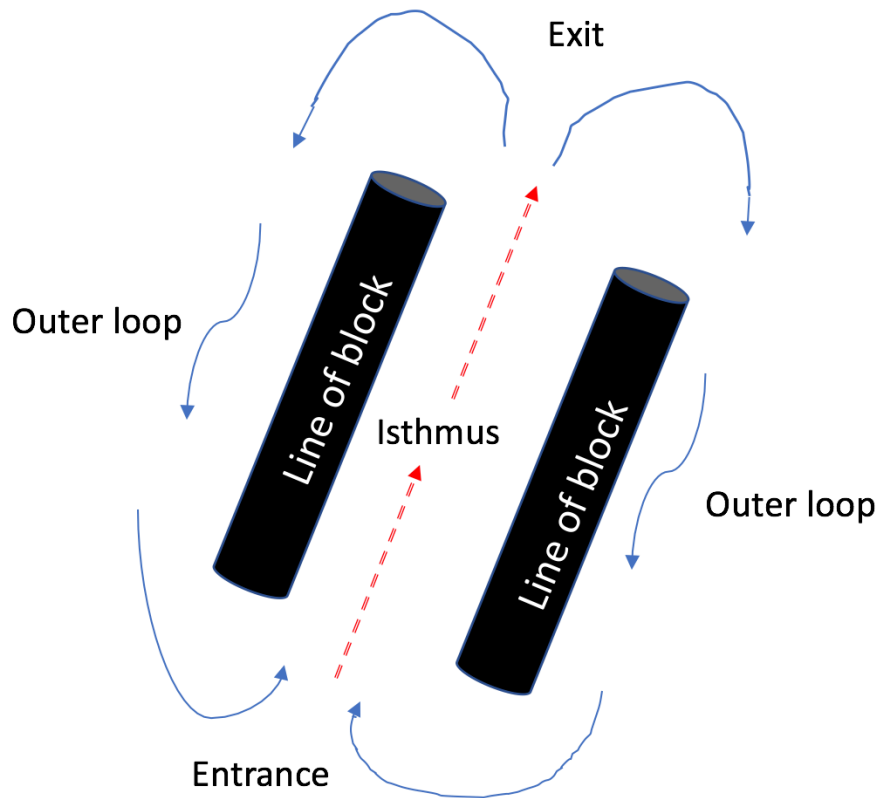
Figure 1-1: Figure-of-eight re-entry circuit.

Classical figure-of-eight re-entrant ventricular tachycardia circuit with an entrance, common isthmus and exit. The isthmus is bounded by two lateral lines of block which may be fixed or functional. Animal studies have demonstrated that conduction velocities are slowest at the inward curvature to the isthmus entrance, slightly faster at the outward curvature and almost normal in the central isthmus. The arrows denote the direction of electrical activation wavefronts.

Not all patients with ischaemic scar develop VT - patients with larger regions of low voltage and electrogram fractionation (a sign of asynchronous activation in the region of the recording electrode) appear to have a greater risk of developing monomorphic VT (Haqqani et al. 2009). Furthermore, in patients post infarct with spontaneous VT, channels of surviving myocytes supporting VT are longer and have a reduced conduction velocity compared to channels that do not support VT (Nayyer et al. 2018; Nayyer et al. 2014). Non-ischaemic cardiomyopathies can also result in VT and can be more challenging to manage as substrate may be located in the endocardium, epicardium or in intramural myocardium (Nakahara et al. 2010). In non-ischaemic dilated cardiomyopathy (DCM), the presence of myocardial replacement fibrosis can provide the substrate for re-entrant VT. The presence of mid wall

fibrosis on late gadolinium enhancement magnetic resonance imaging (LGE-MRI) is an independent risk factor for sudden cardiac death in this cohort (Gulati et al. 2013; Halliday et al. 2017). Other mechanisms for VT in DCM include enhanced automaticity, triggered activity and bundle-branch re-entry (Dukkipati et al. 2017). Frequently epicardial ablation may be required in addition to endocardial ablation in DCM, especially in the presence of inferolateral scars (Piers et al. 2013).

Arrhythmogenic right ventricular cardiomyopathy (ARVC) is characterised by fibro-fatty replacement of RV myocardium occurring classically in the RV free wall, outflow tract and RV apex forming the so-called 'triangle of dysplasia.' Scar-related re-entry is the main mechanism of VT in these patients and can present early during the natural history of the disease (Sen-Chowdhry et al. 2006). In patients with hypertrophic cardiomyopathy (HCM), sudden cardiac death may be caused by ventricular fibrillation or polymorphic VT. Monomorphic VT is rare but can be caused by the presence of myocardial scar. Due to the increased wall thickness in HCM, combined endo-epicardial approaches to catheter ablation may also be required to fully eliminate VT substrate (Dukkipati et al. 2011).

Sarcoidosis is a systemic inflammatory disorder characterised by non-caseating granulomas and can affect the heart in around 25% of cases (Dukkipati et al. 2017). Ventricular tachycardia can occur due to re-entry, triggered activity or abnormal automaticity but the inflammatory substrate is often best managed early using immunosuppression with corticosteroids and/or anti-arrhythmic medications. In selected cases resistant to medical management, catheter ablation may be considered but is associated with poor efficacy (Papageorgiou et al. 2018).

In this thesis, substrate assessment with MRI and evaluation of the MR-EP system for electroanatomic mapping and ablation will be assessed in models of ischaemic cardiomyopathy and the remainder of the thesis will focus on VT in this context.

1.2   Electroanatomical mapping

1.2.1   Background and technical aspects

Intra-cardiac electrophysiological mapping can be used to infer local tissue structural characteristics, which may reveal pro-arrhythmic substrate and also provide a direct assessment of arrhythmia mechanism. Catheters introduced percutaneously record local electrograms (EGM), their characteristics including timing, amplitude and location and are used for substrate assessment and arrhythmia diagnosis. The EGM represents local electrical activity and is the difference between signals recorded from two electrodes. A unipolar EGM is the signal detected between one electrode at the recording site and an indifferent electrode at a point of zero reference. The unipolar signal incorporates both near and far-field signal components as the signal is a representation of myocardial electrical activity spanning the distance between electrodes. A bipolar EGM is the signal detected between a pair of closely spaced recording electrodes (comprising the recording bipole) and is created through subtraction of two unipolar EGMs. As a result, bipolar EGMs are less influenced by larger amplitude far-field signals from surrounding myocardium and are useful to evaluate the local characteristics of abnormal tissue.

As unipolar signals are comprised of both local and remote influences, they are more susceptible to far-field influences but are of greatest use in locating sites of earliest activation or exit points of re-entrant circuits as information on the direction of impulse propagation can be derived (de Groot et al. 2003). Bipolar signals, although less susceptible to far-field

effects, are influenced by multiple factors including the catheter orientation relative to the surface tissue (angle of incidence), recording electrode size, inter-electrode spacing, direction of activation wavefront, filtering techniques and tissue contact (Tschabrunn et al. 2016).

These extrinsic factors can introduce artefacts during EGM recordings in several ways. Poor catheter contact can lead to low-amplitude EGMs leading to potentially misleading annotation of regions of normal myocardium as scar. Catheter stability is also important during EGM recordings - catheter motion can artificially lead to recording of fractionated EGMs (low amplitude EGMs with high frequency deflections). The presence of electromagnetic interference (e.g. as is present inside a MRI scanner) can also introduce high frequency noise and obscure the timing and morphology of the local EGM. Signal filtering is used in the electrophysiology laboratory to enhance segments of the frequency spectrum whilst rejecting undesirable aspects of the spectrum. A combination of high-pass and low-pass filters with or without an optional notch filter can be used to reject electrical interferences from DC voltages, baseline drift and suppress line-related noise to optimise the quality of signal acquisition. The application of filtering can attenuate peak-to-peak signal amplitude depending on the filter settings and needs careful interpretation. Given the additional sources of electromagnetic interference present during MR-EP procedures, filtering techniques have required re-interpretation and adaptation to preserve EGM fidelity and reduce artifacts induced by MR sequences during mapping inside the MRI environment (Elbes et al. 2017).

Residual electrical activity within regions of scar may manifest as abnormal EGMs due to the transverse uncoupling of myocytes due to fibrosis. Abnormal EGMs can be categorised as fractionated, isolated and late (Bogun et al. 2005). A normal ventricular EGM may contain

sharp biphasic or triphasic deflections with an amplitude ≥ 3mV and duration <70ms. In contrast, a fractionated potential exhibits multiple deflections (≥ 3 deflections) from the isoelectric line or continuous electrical activity without an isoelectric line and typically an amplitude ≤0.5mV with duration ≥133ms (Rostock et al. 2006). These may reflect non-uniform activation of a mass of surviving myocardial bundles within a region of scar. An isolated or disassociated potential is defined as a potential distinct and separated from the local ventricular EGM by an isoelectric interval or very low amplitude noise and of a duration >20ms at a gain of 40-80mm/mV (Hsia et al. 2009). These may represent electrical activation from surviving myocardial bundles insulated by dense scar and poorly coupled to remaining myocardium. EGMs containing isolated potentials may have double or multiple potentials. A higher incidence of these late potentials have been recorded near a VT isthmus compared to the entrance or exit sites (Hsia et al. 2009) - *Figure 1-2.*
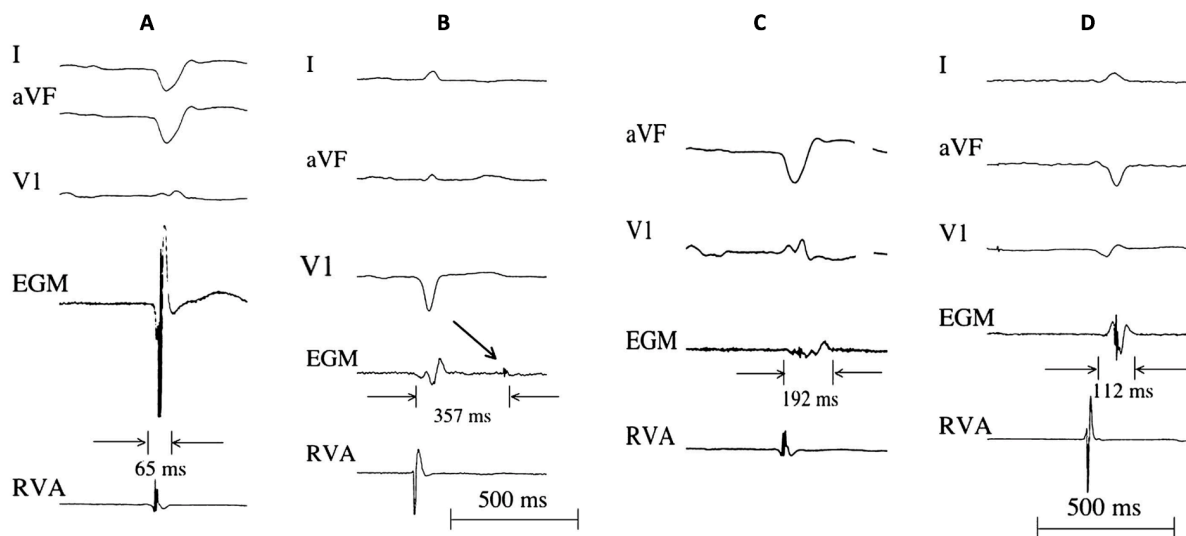
Figure 1-1: Normal and abnormal electrograms.

Example tracings of normal and abnormal electrograms. Recordings from surface leads (I, aVF, V1), intra-cardiac recordings from the left ventricle and right ventricular apex are shown. Normal EGM (A) with an amplitude of 7.8mV and duration 65ms. Isolated potential (B) is clearly visible and separated from the ventricular EGM by 210ms. A fractionated electrogram (C) with an amplitude of 0.37mV and duration of 192ms is seen. An abnormal local electrogram is present (D) with an amplitude of 0.7mV and duration 112ms. Adapted with permission from Bogun et al 2005).

More recently, (Jais et al. 2012) have sought to define abnormal EGMs in a more precise manner incorporating data on the amplitude and timing of potentials in relation to the QRS,

local or far-field signals. Local abnormal ventricular activities (LAVA) were defined as sharp, high-frequency ventricular potentials, distinct from the far-field ventricular EGM occurring during or after the far-field ventricular EGM in sinus rhythm or before the far-field ventricular EGM during VT. Elimination of LAVAs during VT ablation was associated with improved VT-free survival in a cohort of patients with structural heart disease (Jais et al. 2012).

1.2.2 *Electroanatomic mapping systems*

Local electrophysiological data acquired from recording catheters such as activation time, unipolar or bipolar voltage and the presence of abnormal electrograms can be displayed on 3D shells of cardiac chambers using contemporary electroanatomic mapping (EAM) systems. These provide a static representation of time-dependent electrical activation and can be used to assess underlying substrate and guide catheter ablation. All EAM systems provide three basic functions (Knackstedt et al. 2008):

1. Non-fluoroscopic localisation and display of catheter position in real-time

2. Reconstruction of 3D surface anatomy of cardiac chambers from serial acquisition of catheter localisation data

3. Annotation of reconstructed surface geometry with local electrophysiological data and location of ablation lesions

The major systems which are widely used in current electrophysiology practice include CARTO® (Biosense Webster), PRECISION™ (Abbott) and RHYTHMIA™ (Boston Scientific). Catheter location in conventional EAM systems is triangulated using magnetic-based sensing and/or impedance-based tracking. The CARTO system uses magnetic-sensor based tracking incorporating a magneto-sensor in the tip of the catheter which measures

magnetic field strength around it. Magnetic generators are located beneath the patient on the operating table and allows the triangulation of catheter tip position and orientation based on magnetic field strength at the catheter tip. Additional patches are applied on the patient's back to record inadvertent patient movement and correct navigational error (Gepstein et al. 1997; Kautzner et al. 2003; Maury et al. 2018).

Localisation of catheters with the PRECISION system is based on measurements of electrical impedance. Skin patches are applied to the patient's chest through which a high frequency, low amplitude current is delivered to create a voltage gradient along the x,y and z-axes. A catheter then measures impedance changes to compute its location in 3D space in relation to the reference. In order to compensate for respiratory changes, the position of each intra-cardiac electrode is determined during a period of recording and correlated to changes in intra-thoracic impedance as detected by the skin patches. By monitoring surface impedance changes, the system can then adjust electrode position accordingly. The RHYTHMIA system uses a combination of magnetic-sensor based and impedance-based tracking for catheter localisation. The accuracy of these tracking techniques has been estimated at 0.5mm for magnetic-sensor based tracking and 0.6mm for impedance-based tracking (Maury et al. 2018).

Using the localisation data provided by catheters, sequential movements made by manipulating the catheter around the cardiac chamber of interest can be used to generate 3D surface geometry. Electrical information can be collected, if required, at each contact site during the collection of points for geometry. Pre-procedural imaging data from cardiac computed tomography (CT) or MRI can also be merged through image integration with the 3D reconstructions of chamber geometry to refine the accuracy of anatomical maps as well as

reducing errors from geometry acquisition. Imaging-derived data on arrhythmogenic substrate (e.g. wall thinning on CT or LGE on MRI) may be integrated into the navigation system during VT ablation procedures to inform additional mapping in regions of interest as well as to guide epicardial access in those patients with relevant substrate (Yamashita et al. 2016).

The 3D reconstructed shell is annotated with local electrophysiological data during an EAM procedure - *Figure 1-3*. Local activation time of the wavefront of depolarisation can be depicted using colour-coded maps with each colour representing a fixed time frame in the depolarisation cycle. An animation can also be created with all conventional EAM systems to represent wavefront propagation thereby permitting an appreciation of the dynamic pattern of activation. The amplitude of unipolar or bipolar EGMs can also be represented as colour-coded voltage maps which allow discrimination between dense scar, borderzone regions and normal myocardium. Conventionally, a bipolar voltage threshold of ≤0.5mV is used to represent dense scar, 0.5-1.5mV is used to represent borderzone tissue and regions with a bipolar voltage >1.5mV is classified as normal myocardium. These thresholds were originally defined using point-by-point, non-contact, force-sensing mapping catheters and validated in models of ischaemic cardiomyopathy (Reddy et al. 2003). Recent data suggests that normal bipolar voltage thresholds are likely to be catheter and patient-specific and strict voltage cut-offs may not be truly reflective of scar biology, especially in regions of scar heterogeneity (Mukherjee et al. 2018).

Depending on the EAM system used, additional maps can be generated to display EGM fractionation and pace-maps can be used to evaluate the degree of overlap between a paced beat from a given site and a spontaneous beat of tachycardia (Hsia et al. 2003). Acquisition of

points can also be performed automatically using multi-polar catheters and preset electrogram acceptance criteria, thereby precluding the need to manually check and annotate each point. Threshold settings for cycle length tolerance, signal-to-noise threshold and force permit the collection of high-quality data reproducibly and with accuracy, which in turn can reduce procedure times.
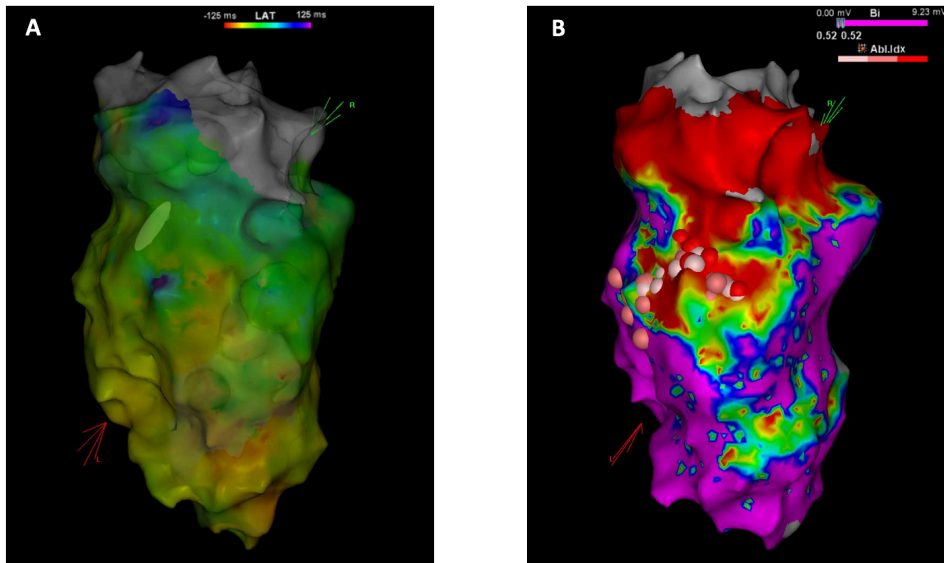
Figure 1-2: Three dimensional electroanatomical maps

Example of three dimensional electroanatomical maps (inferior view) acquired using the CARTO system (Biosense Webster). Local activation time (LAT) (A) and voltage maps (B) acquired in sinus rhythm showing the left ventricle in a patient with a large inferior infarct. Scar is denoted in green/red/blue and healthy tissue in purple on the voltage map (B). NB: Upper threshold for scar shown on the voltage map is 0.52mV whilst standard presentation for low voltage is 0.5 - 1.5mV.

1.2.3   Activation mapping

In order to localise exit sites and determine possible ablation targets, it is desirable to perform EAM either during spontaneous or induced VT. If spontaneous VT is not readily seen, programmed electrical stimulation can be performed at the start of a mapping procedure in order to initiate VT. Induction is typically performed through pacing from the RV apex with a current strength at twice the capture threshold and a pulse width of 2ms. Premature extra-stimuli with progressively shorter coupling intervals can then be delivered down to the ventricular effective refractory period (VERP). If stimulation from the RV apex fails to induce VT, the procedure can be repeated from a different pacing site (e.g. RVOT or the left

ventricle) or a non-selective beta agonist (e.g. isoprenaline) administered (Tschabrunn et al. 2016). If the VT is sustained and haemodynamically tolerated, activation mapping can then be performed using a mapping catheter and a fixed timing reference, typically a dominant QRS deflection on the surface ECG or a diagnostic catheter positioned elsewhere within the heart, often in the right ventricle (in the case of left ventricular VT). The site of earliest activation, prior to the QRS onset during VT may represent an exit site from the zone of myocardium harbouring the diastolic pathway. If using a single electrode catheter, a pre-systolic potential may be seen near an exit site and as the catheter is moved further into the associated scar (away from the exit site), this potential may be seen in the mid-diastolic phase of the tachycardia. Using a multi-electrode catheter, continuous electrical activity consistent with a re-entrant circuit may be demonstrated using the different recording electrodes during activation mapping of VT - *Figure 1-4.*

Activation mapping of a macro-re-entrant VT is considered complete when the following criteria are fulfilled (Anter et al. 2016):

- ≥90% of the tachycardia cycle length is mapped

- A common channel 'isthmus' is identified

- Sufficient mapping density in regions of slow conduction is acquired to limit interpolation between points to ≤ 3mm
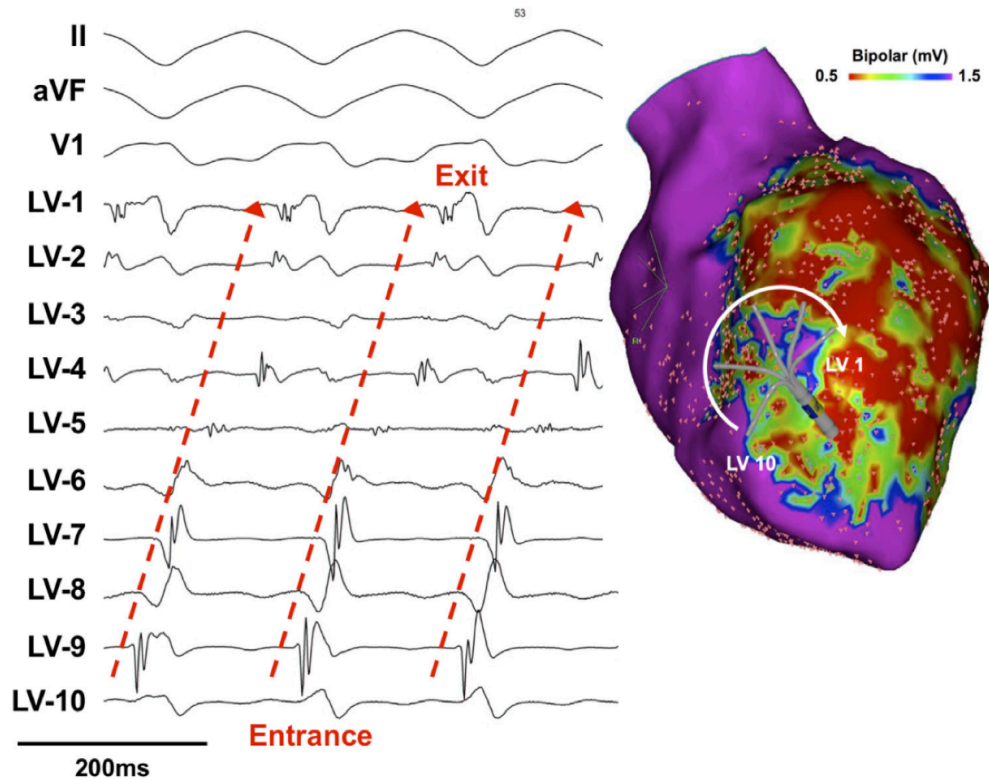
Figure 1-3: Activation map of ventricular tachycardia.

Endocardial recordings made during activation mapping of ventricular tachycardia using a multi-electrode catheter. Continuous electrical activity is recorded throughout the tachycardia cycle length including in diastole representing the re-entrant circuit. The bipolar voltage map with the mapping catheter positioned in the anteroseptum is shown on the right. Reproduced with permission from Tschabrunn et al. 2016.

1.2.4   Entrainment mapping

Following activation mapping, overdrive pacing can be performed at selected sites identified from the activation map in order to 'entrain' the tachycardia. Entrainment mapping can be performed during tachycardia in order to determine the mechanism of the arrhythmia and establish the relationship of an individual pacing site to the re-entry circuit and thereby identify the critical and non-critical parts of a circuit. Entrainment refers to continuous resetting of a re-entrant tachycardia through delivery of a series of consecutive beats in a pacing train where each pacing beat 'resets' the tachycardia - either through advancing or delaying the subsequent tachycardia beat. A re-entrant VT circuit will contain an 'excitable gap' whereby a wave of depolarisation will leave a region of tissue refractory to a further

28

stimulus for a given period of time prior to recovery. This is due to the refractory period of each point in the circuit being shorter than the time interval taken for the wavefront of depolarisation to propagate around the circuit once (Stevenson et al. 1997). A critically timed pacing stimulus can therefore be programmed to enter and affect the tachycardia circuit.

Following the application of a stimulus to a given site during VT, if the site has recovered and the stimulus is applied prior to the arrival of the next wavefront of depolarisation, the stimulus will capture the myocardium. This will lead to activation wavefronts that will travel in a direction which is orthodromic to the tachycardia wavefront and in an opposite direction (antidromic) to the tachycardia wavefront. The antidromic wavefront will collide with the head of the returning orthodromic wavefront from the tachycardia. However, the orthodromic wavefront generated from the pacing stimulus will traverse the circuit and reset the tachycardia. Following termination of pacing, the last paced beat will traverse the circuit at the pacing cycle length; depending on how far from a re-entrant circuit the pacing site lies, the returning orthodromic wavefront following the last paced beat will reach the pacing site in less than 30ms if within the circuit and in more than 30ms if outside the circuit.

If the following features are present on pacing during tachycardia, it suggests that entrainment has occurred and proves re-entry as the mechanism of the tachycardia:

- Constant fusion of complexes during pacing at a constant cycle length (the morphology of the paced complex is intermediate between that of a fully paced complex and a VT complex)

- Progressive fusion during pacing at different pacing rates (i.e. during pacing at faster rates, there is a progressive increase in the extent of myocardium activated from the pacing site ultimately leading to a fully paced complex)

- Conduction block to an orthodromic site that terminates the tachycardia circuit which is followed by activation of that site by the paced wavefront from the opposite direction (Kumar et al. 2017)

In order to determine the relationship of the pacing site relative to the VT circuit, the following electrophysiological parameters can be examined during or after entrainment:

- Post-pacing interval (PPI) following entrainment
- QRS configuration during entrainment
- Stimulus-to-QRS interval (S-QRS) during entrainment

The PPI after entrainment represents a measure of the proximity of the pacing site to the re-entry circuit. A pacing site close to or within the re-entry circuit will give a PPI which is close to the tachycardia cycle length (TCL). If the pacing site is distant from the VT circuit and entrains the tachycardia (i.e. a bystander site), the PPI will be longer than the TCL by at least 30ms. Therefore, the difference between the PPI and TCL can be used to determine the likelihood an individual site is close to or within the circuit. In patients with post-infarct VT, ablation sites with a PPI-TCL during entrainment which was <30ms, had a higher likelihood of terminating VT (Stevenson et al. 1993).

The QRS configuration during entrainment is the result of the myocardial activation sequence from the pacing site. If the pacing site during entrainment is distant from the VT circuit, the QRS morphology will be altered and will be a product of the activation wavefront propagating from the pacing site and the activating wavefront coming out of the VT exit site (fused QRS). If the pacing site is within the re-entry circuit, pacing during VT will not change the surface QRS morphology, therefore there will be no fusion at the surface ECG level - this is referred to entrainment with concealed fusion. The 'fusion' may be detectable by local EGMs within the scar as a small mass of tissue is depolarised by the antidromic wavefront of the VT before collision with the orthodromic wavefront of the pacing stimulus (Kumar et al. 2017).

The S-QRS interval is a representation of conduction time from the site of pacing to the VT circuit during entrainment with concealed fusion. If the pacing site is within the circuit, the time from the local EGM to surface QRS is also an indication of this conduction time, therefore the S-QRS interval during concealed fusion can be used to approximate the EGM-QRS time during tachycardia. When pacing from a bystander site, the S-QRS time will not approximate the EGM-QRS interval (Stevenson et al. 1997). A S-QRS interval during entrainment with concealed fusion which is <70% of the TCL in a given pacing site has a higher likelihood of tachycardia termination during ablation and is likely to represent an isthmus site (Stevenson et al. 1997).

Based on the above criteria, the different features of mapping sites from re-entrant circuits can be classified as isthmus sites, exit, inner and outer loop sites, adjacent and remote bystander sites. These are summarised in the flowchart below (Stevenson et al. 1997) - *Figure 1-5*:
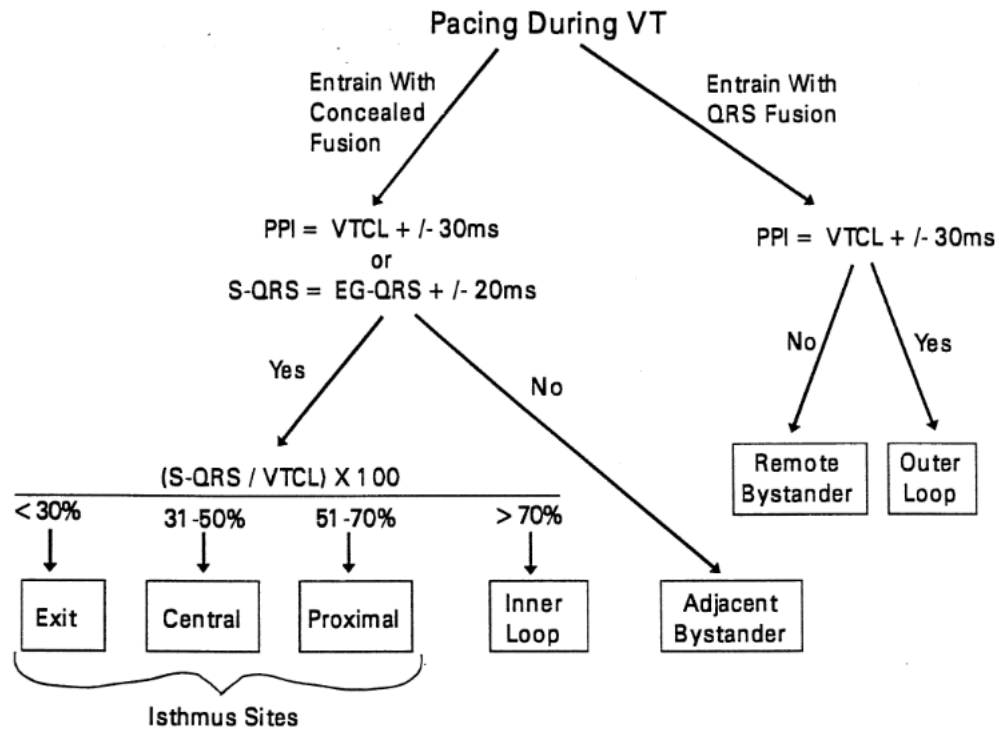
Figure 1-4: Entrainment mapping

During entrainment with concealed fusion, a PPI-TCL ≤ 30ms, S-QRS to EGM-QRS ≤ 20ms or S-QRS <70% of TCL is likely to represent an isthmus site. Sites where these criteria are not met may be classified as inner loop sites, outer loop, adjacent bystander and remote bystander sites as shown above. Reproduced with permission from Stevenson et al. 1997.

In order to perform either activation or entrainment mapping, VT has to be hemodynamically tolerated or the use of mechanical circulatory support devices established in unstable VT. Currently, the majority of VTs induced in the electrophysiology laboratory are not hemodynamically tolerated and alternative substrate-based strategies have developed to identify critical sites for VT.

1.2.5 Pace-mapping

Pace-mapping is a surrogate of the activation map in sinus rhythm to locate the origin of VT. During pace-mapping, the QRS morphology during pacing at a given site is examined and compared to the QRS morphology obtained from a 12-lead ECG recorded during the clinical VT. The QRS morphology within each lead can be assessed and if the morphology in all 12

leads during the clinical VT matches that of the pacing site, this is considered an 'excellent'

site for ablation. If the QRS morphology from the paced site only matches 10-11 out of 12

leads, this is considered a 'good' site. The degree of matching between the paced QRS and

12-lead ECG of the clinical VT can be assessed both qualitatively or through the use of

automated algorithms incorporated into clinical EAM systems which express the degree of

matching as a percentage value through a correlation calculation.

An additional parameter that can be obtained during pace-mapping *in sinus rhythm* is

measurement of the S-QRS interval. This technique has been proposed as a means to locate

the exit site of a VT circuit. A S-QRS delay of ≥ 40ms may indicate a region of slow

conduction away from the pacing site whilst a S-QRS delay ≥ 80ms represents marked delay.

VT ablation sites are more likely to be found in regions of marked S-QRS latency although

the sensitivity is moderate (Brunckhorst et al. 2003).

If the pacing site is located close to the exit site of an isthmus, there will be an 'excellent'

matched QRS morphology and a short S-QRS interval. If the pacing site is moved within the

isthmus, the matched QRS morphology should remain 'excellent' but the S-QRS interval

should become longer. There may then be a sudden transition point within the core of the

isthmus when the matched QRS morphology becomes poor when pacing closer to the

entrance site. This is due to the activation wavefront spreading more rapidly to the entrance

zone when pacing closer to the entrance, followed by ventricular depolarisation. When

pacing closer to the exit zone, the activation wavefront will spread more rapidly to the exit

and depolarise the ventricle from a different site, leading to a significantly different QRS

morphology (de Chillou et al. 2014).

Following identification of an exit/entrance zone, pace-mapping can be performed around adjacent sites in order to identify the lateral boundaries of the isthmus and an isochronal colour-coded pace-map of correlation between QRS morphologies and/or S-QRS intervals generated. Catheter ablation can then be guided by the location of the VT isthmus, aiming to transect this region (de Chillou et al. 2017). There are a number of factors that can reduce the precision of pace-mapping such as large inter-electrode distances within the mapping catheter which may lead to a larger region of myocardial depolarisation and therefore reduce the spatial resolution of the technique. High-output pacing may also increase the likelihood of far-field capture. A high pacing rate could lead to small alterations in QRS morphology and pacing at a rate close to that of the clinical VT cycle length is recommended (de Chillou et al. 2017).

1.2.6   Substrate mapping during sinus rhythm

Activation and entrainment mapping require that VT is both inducible and haemodynamically tolerated as a pre-requisite. Given that the majority of clinical VTs induced result in haemodynamic compromise, substrate-based strategies in sinus rhythm to identify VT ablation targets may serve as an alternative approach. Abnormal electrical substrate evaluated during sinus rhythm comprising low amplitude peak-to-peak voltage and abnormal EGM characteristics (e.g. split, isolated late potentials, fractionated potentials and LAVA) have been used to identify the critical target sites of re-entrant VT.

Both bipolar and unipolar peak-to-peak voltage may be attenuated by abnormal myocardium. Using a combination of animal studies in a model of ischaemic cardiomyopathy (Callans et al. 1999), limited human histopathological evaluation (Deneke et al. 2005) and statistical definitions of normal voltages derived from values >95th centile of amplitude distributions from patients without scar (Marchlinski et al. 2000), a bipolar voltage cut-off of <1.5mV has

been universally implemented to define abnormal myocardium. A cut-off <0.5mV has been used to define dense scar and values 0.5-1.5mV to define borderzone tissue or regions with intermediate degrees of fibrosis. These values were largely validated for transmural scar whilst patchy scar may be missed using these cut-offs. Adjusting the bipolar voltage cut-offs to higher values (e.g. 2.0mV or 2.5mV) may identify a more confluent area of scar which incorporates all abnormal signals (Santangeli et al. 2016). Similarly, when voltage mapping identifies a large area of scar, adjustment of the lower bipolar voltage cut-off to <0.5mV (e.g. 0.1mV or 0.2mV) will help identify dense fibrosis and may facilitate delineation of conduction channels within the scar (Hsia et al. 2006).

Bipolar voltage mapping has a limited field of view, however which can lead to difficulty in the identification of intramural or epicardial substrate. Unipolar voltage mapping, with a larger field of view, has been used to identify epicardial substrate which is more prevalent in patients with non-ischaemic cardiomyopathy. Using statistical distributions of normal signal amplitude from a cohort of healthy patients, a unipolar voltage of >8.27mV has been used to define normal myocardium within the LV endocardium (Hutchinson et al. 2011) and 5.5mV in the thinner free wall of the RV (Polin et al. 2011).

Abnormal EGMs recorded from mapping sites may also represent the substrate for VT. These signals may result from poor cell-to-cell coupling of surviving tissue within regions of fibrosis and represent anisotropic 'zig-zag' conduction (Santangeli et al. 2016). As discussion in Section 1.2.1, abnormal EGMs may be classified as fractionated, split, late, or as LAVA. Different investigators have adopted substrate-based ablation strategies aimed at eliminating all abnormal EGMs (e.g. late potential abolition, LAVA elimination or scar homogenisation)

(Arenal et al. 2013; Vergara et al. 2012; Silberbauer et al. 2014; Jais et al. 2012; Di Biase et al. 2012) with variable success rates.

There are a number of factors that may affect these strategies including sampling bias in regions of abnormal substrate, use of different mapping catheters with variations in recording electrode size and inter-electrode spacing and the direction of activation wavefront during recording of EGMs. These factors may affect the detection, location and characterisation of abnormal signals and impact on the chosen ablation strategy (Santangeli et al. 2016). Recently, in an elegant study, (Anter et al. 2018) used high-resolution mapping in a porcine infarct model to generate activation maps, assess EGM shape, amplitude and conduction velocity. All electrophysiological parameters used to assess substrate in sinus rhythm had a poor specificity and positive predictive value (PPV) in the identification of the VT isthmus. For example, a bipolar voltage <1.5mV had a sensitivity of 72%, specificity of 56% and PPV of only 24% in identifying a VT isthmus location. Of the different EGM abnormalities, the presence of LAVA had the best sensitivity (82%) but all types of abnormal EGMs had poor specificity (38%-64%) and PPV (28% - 48%) (Anter et al. 2018). Interestingly, regions of local conduction velocity slowing - termed steep activation gradients, had the best specificity (80%) and PPV (60%) for isthmus identification. These data highlight the limitation of substrate-based strategies to target VT ablation sites and emphasise the importance of functional assessment to identify the vulnerable zones for re-entrant VT (Anter et al. 2018).

1.2.7 Limitations

There are several limitations of EAM as a means to assess VT substrate. Bipolar voltage is affected by several factors which are independent of the histological characteristics of the underlying tissue as discussed in Section 1.2.1. The assumption that low voltage means

histological scar is therefore not necessarily accurate. Given that catheters with smaller electrodes with reduced inter-electrode spacing may be able to distinguish surviving myocardial bundles with greater sensitivity (Tschabrunn et al. 2016), catheter-specific thresholds may be needed to better define abnormal substrate. EGM configuration and timing is also affected by activation wavefront - late potentials may be visible during RV pacing but not during sinus rhythm and vice versa (Josephson and Anter, 2015). The regions of myocardium designated as harbouring LAVAs may be larger when the wavefront of propagation is perpendicular versus parallel to the line of block along the boundary of an isthmus (Martin et al. 2019).

Activation mapping, whilst being the gold standard for accurate characterisation of the VT circuit, is only possible in a small proportion of VTs due to haemodynamic instability. The use of haemodynamic support devices may facilitate activation mapping in otherwise unstable VT but their use can result in significant complications with unclear clinical benefits (Luni et al. 2019). Problems with entrainment mapping include an inability to capture myocardium with consequent increases in the pacing output delivered. This can lead to a larger volume of tissue capture and result in misleading calculation of isthmus location and dimensions. There are also inherent limitations to pace-mapping - pacing in sinus rhythm from a point source may not mimic the pattern of impulse propagation of scar-related re-entrant VT. The presence of functional block may only be apparent during tachycardia and may be absent during pace-mapping. S-QRS measurements during pace-mapping may therefore not be directly comparable to S-QRS measurements during entrainment (Tung et al. 2012).

The optimal mapping density within regions of scar in the ventricle remains unclear - a lower mapping resolution may underestimate the dimensions of VT target sites due to the interpolation of activation times in under-sampled areas (Anter et al. 2016). EAM is a time-consuming procedure with mean procedural time of 3.5 ± 1.2 hours with a substrate modification protocol (Fernandez-Armenta et al. 2016); the addition of substrate mapping with different activation wavefronts or strategies to unmask slow conduction with extrastimulus pacing protocols (Acosta et al. 2018) can therefore be challenging to deliver in patients with a poor physiological reserve. Given the variety of mapping strategies, the process has significant operator-dependence with implications on the reproducibility of each technique.

1.3   Catheter ablation for ventricular tachycardia in structural heart disease

1.3.1   General considerations

Ablation strategies typically use a combination of activation and entrainment mapping, if possible, pace-mapping and assessment of substrate to delineate target sites. If VT induction is performed, at least two sites are selected with two different cycle lengths and up to three extra-stimuli at progressively shorter coupling intervals to attempt to stimulate VT (Emami et al. 2019). The morphology, cycle length and stability of all induced VTs are recorded. Activation and entrainment mapping can then be performed if the tachycardia is stable. If programmed stimulation is not performed and a substrate-based strategy is selected, local EGMs are recorded with the peak-to-peak voltage and EGM morphology assessed. Additionally, pace-mapping can be performed if a 12-lead ECG of the clinical VT is available and measurement of S-QRS intervals can be made.

1.3.2   Ablation strategies

Activation mapping can be used to identify the earliest site of electrical activation during tachycardia. This data is useful to localise VT exit sites along the border of scar and potentially record EGMs during diastole which could represent critical components of the circuit and are targeted for catheter ablation (Santengeli et al. 2016). Diastolic activation may also be present in bystander sites which are not part of the circuit. Entrainment mapping uses overdrive pacing to locate target sites with a PPI-TCL ≤ 30ms, S-QRS - EGM-QRS ≤ 20ms or S-QRS which is <70% of the VT cycle length as discussed in Section 1.2.4. These sites are more likely to signify the location of an isthmus and successfully terminate VT. Pace-mapping is a surrogate of the activation map - sites with an 'excellent' match of the paced QRS morphology to the clinical VT may be targeted for ablation. An abrupt change in QRS morphology within the mid-isthmus can also be used to unmask target sites for catheter ablation as discussed in Section 1.2.5.

Substrate-based ablation strategies can be classified into those that target the entire abnormal substrate and those that target discrete regions within scar that have been shown to be relevant to the inducible tachycardia through physiologic manoeuvres. Strategies that target the entire abnormal substrate include late potential or LAVA elimination and scar homogenisation whilst strategies that target limited regions of substrate include scar dechanneling, linear ablation and core isolation (Santengeli et al. 2016).

Late potentials have been targeted for ablation by several investigators (Arenal et al. 2003; Nogami et al. 2008; Vergara et al. 2012) but the definition of these potentials have varied significantly between studies. Sampling bias is a major limitation of this technique whilst late potential elimination is not always possible even with extensive ablation. Far-field potentials

from remote sites may contribute to persistence of a signal despite adequate ablation in a given site (Santangeli et al. 2016).

LAVAs first decribed by (Jais et al. 2012) are a more precise definition of abnormal EGMs that may be related to VT circuits, however they suffer from similar limitations to that of late potential ablation including sampling bias. The optimal pacing strategy to systematically record LAVAs also remains unclear (Santangeli et al. 2016). Scar homogenisation represents an extensive ablation strategy whereby all abnormal EGMs within scar defined using conventional bipolar voltage criteria are targeted for ablation - *Figure 1-6*. This approach has been shown to be superior to limited ablation of clinical VT in ischaemic cardiomyopathy within the randomised multi-centre VISTA study (Di Biase et al. 2015). Additionally, in patients with non-ischaemic cardiomyopathy, a scar homogenisation approach improved freedom from VT compared to limited substrate-based ablation, although the success rate was lower than that of patients with ischaemic cardiomyopathy (Gokoglan et al. 2016).

The scar homogenisation approach may be difficult to achieve in patients with large substrates without sufficient physiological reserve for extensive ablation. The strategy also invariably targets bystander regions that do not participate in the VT circuit.
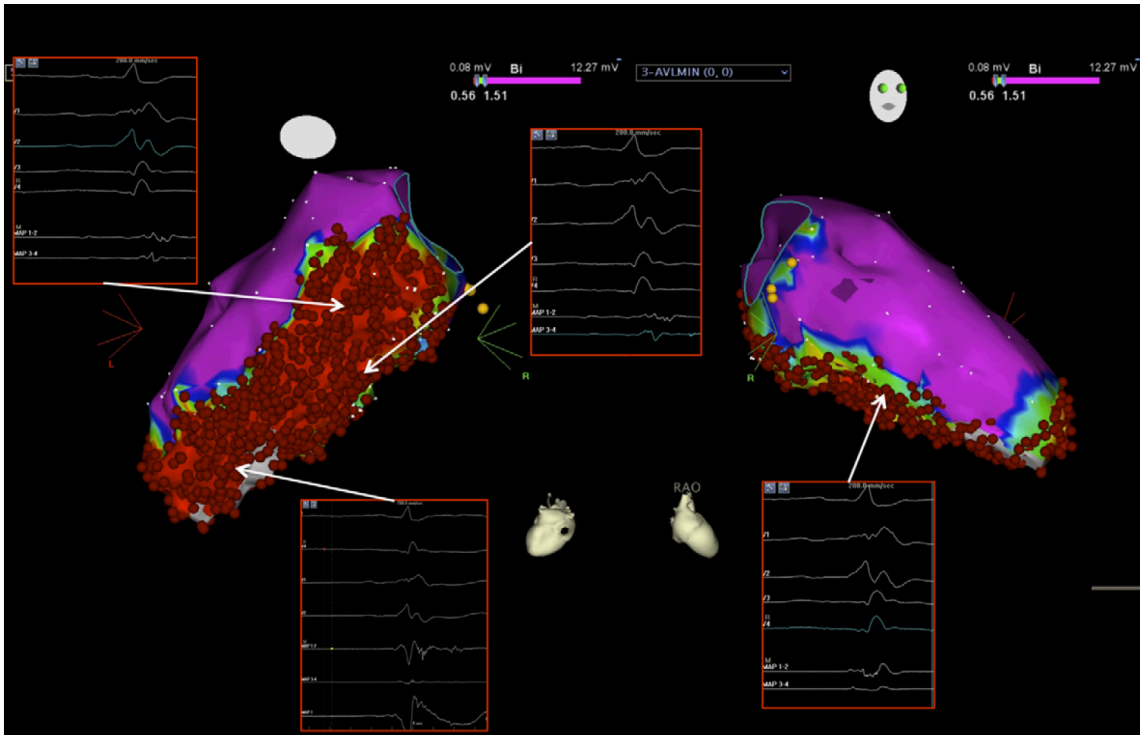
Figure 1-5: Scar homogenisation

Bipolar endocardial voltage map in a patient who has received extensive ablation (scar homogenisation). Red regions indicate scar whilst purple represents healthy myocardium. Red dots represent regions where ablation has been applied. Representative EGMs from sites targeted for ablation are shown. Reproduced with permission from Di Biase et al. 2012.

Limited substrate-based strategies such as linear ablation aim to create contiguous lesions from the scar borderzone to an anatomic structure. The strategy is reliant on the use of pace-mapping to identify VT exit sites within the abnormal substrate. Linear ablation was first described by (Marchlinski et al. 2000) who reported encouraging success rates (75% at median 8 months follow-up) in a small cohort of patients with structural heart disease and was subsequently used in the SMASH-VT trial (Reddy et al. 2007). However, it can be challenging to achieve conduction block across a linear lesion due to the need to deliver transmural lesions. The strategy also requires the presence of fixed anatomic barriers near the relevant substrate (Santangeli et al. 2016).

Scar dechanneling is another substrate-based strategy that aims to identify channels of slow conduction using high-output, unipolar pacing within low voltage regions. Alternatively, a

high-density voltage map can be acquired and regions of abnormal EGMs marked within the substrate to locate channels which may contain surviving myocardial bundles. Scar dechanneling involves ablating inter-connected channels within the substrate and has been shown to have a shorter duration of radiofrequency application and improved event-free survival in those patients where complete conducting channel elimination was possible (Berruezo et al. 2015).

The 'core isolation' approach involves identification of a discrete region of interest within scar using conventional methods (e.g. voltage mapping, pace-mapping, abnormal EGM localisation, entrainment mapping). The critical region identified is then ablated with lesions surrounding the region of interest or extending to anatomical barriers. The demonstration of electrical unexcitability of the core region of interest serves as the procedural end-point. Core isolation has been associated with good VT-free survival whilst also limiting the ablation target size (Tzou et al. 2015). The end-point of electrical isolation of the target region also serves as a reproducible end-point beyond VT inducibility.

1.3.3   Procedural end-points

Traditionally, following the end of a VT ablation procedure, programmed stimulation is applied to evaluate if VT remains inducible. The probabilistic nature of programmed stimulation makes it difficult to apply in a reproducible fashion. The presence of oedema around an ablation lesion site may inhibit induction of VT immediately after an ablation procedure whereas days or weeks after a procedure, after oedema has resolved, VT may once again become inducible. In patients with structural heart disease, anti-arrhythmics such as amiodarone are frequently used prior to VT ablation - their use may suppress inducibility both up-front and at the end of an ablation procedure.

Despite its limitations, non-inducibility has been widely implemented as a procedural end-point during VT ablation. Some investigators have used non-inducibility of the clinical VT as a minimum end-point whilst others have used non-inducibility of all VTs as a more comprehensive end-point. In a large observational cohort, non-inducibility of all VTs was associated with improved cardiac mortality, compared to inducibility of non-documented VT and non-inducibility of clinical VT at the end of a procedure (Della Bella et al. 2013). A meta-analysis of non-inducibility as an end-point in post-infarct VT ablation however found no significant association between rates of non-inducibility and recurrence at follow-up (Santengeli et al. 2014).

Non-invasive programmed stimulation (NIPS) whereby programmed stimulation is performed via the ICD a few days after VT ablation has also been used to identify patients at increased risk of recurrence (Frankel et al. 2012). Although not technically a procedural end-point, NIPS-positive patients might benefit from early repeat ablation and the use of this end-point warrants further investigation (Santangeli et al. 2014).

For substrate-based ablation, additional end-points have been investigated depending on the ablation strategy used. The efficacy of linear ablation lesions has been assessed using the end-point of electrical unexcitability (failure of capture) during high-output pacing along the ablation line and demonstration of a change in QRS morphology during pacing from each side of the ablation line (Santangeli et al. 2014). Alternative surrogate parameters that can be used to support demonstration of effective lesion delivery include assessment of catheter-tissue contact using intra-cardiac echocardiography (ICE), monitoring of impedance and elimination of high-frequency potentials that may represent near-field activation (Santangeli et al. 2014). There is, however, no established electrophysiological end-point that best

demonstrates completeness of linear lesions in the ventricle as the optimal pacing output required to demonstrate failure to capture within a region of pre-existing scar remains unknown. In addition, it is challenging to distinguish between block and severe conduction delay across a lesion line.

Substrate-based strategies that aim to eliminate all abnormal EGMs have used a combination of demonstration of elimination of all abnormal EGMs during scar re-mapping and failure to capture with high-output pacing. Although the end-point of abnormal EGM elimination (e.g. LAVA elimination) has been shown to result in improvement in VT-recurrence and mortality in those patients in whom it could be achieved (Jais et al. 2012), this was only possible in 70% of patients. The presence of late potentials may persist in regions of ablation and the demonstration of local capture with exit block during high-output pacing may be useful to determine if sufficient ablation has been performed (Santangeli et al. 2014). Complete elimination of abnormal EGMs may require time-consuming and extensive ablation whilst also inadvertently targeting bystander sites where late potentials may be recorded but do not participate in a VT circuit. Whether scar re-mapping from different pacing sites is required to demonstrate comprehensive elimination of abnormal EGMs also remains unclear and this strategy would prolong procedure times still further.

Imaging techniques such as ICE or MRI represent alternative modalities to judge procedural end-points. ICE has been used to monitor lesion formation in real-time through demonstration of increased echogenicity within ablated tissue whilst lesion size on imaging appeared to correlate with size at pathology in a pre-clinical study (Ren et al. 2001). In this thesis, a method of evaluating ablation lesion formation in real-time using MRI temperature

mapping (MR-thermometry and dosimetry) is evaluated as a possible novel end-point for VT ablation.

1.3.4 Clinical outcomes

A number of clinical trials have examined the impact of catheter ablation on outcomes in patients with VT. In general, non-ischaemic cardiomyopathies (NICM) have been under-represented with no randomised controlled trials investigating the role of catheter ablation. NICM patients tend to have worse outcomes after catheter ablation of VT compared to patients with ischaemic cardiomyopathy (Dinov et al. 2014). For the treatment of drug-refractory VT storm, catheter ablation is generally considered a safe and effective strategy (Carbucicchio et al. 2008).

In patients with ischaemic cardiomyopathy presenting with recurrent VT, the Euro-VT study suggested that catheter ablation could successfully terminate VT acutely in most patients but around 49% developed VT recurrence during follow-up (Tanner et al. 2010). The observational multi-centre Thermocool VT ablation trial enrolled 231 patients with ischaemic cardiomyopathy and recurrent monomorphic VT to undergo catheter ablation. The primary end-point was freedom from recurrent VT at 6 months, but this was only achieved in 53% of patients. There was a high 1-year mortality rate at 18% whilst procedure-related mortality was 3%.

A number of randomised controlled trials have also been published investigating the safety and efficacy of VT ablation in ischaemic cardiomyopathy. In the SMASH-VT trial, patients with ischaemic cardiomyopathy who were randomised to receive catheter ablation in addition to ICD implantation had a reduced incidence of ICD therapies compared to patients who

received an ICD alone (Reddy et al. 2007). Patients did not receive anti-arrhythmic drugs in this trial and participants were enrolled who had experienced a single episode of VT or ventricular fibrillation, suggesting a low-risk population. In the VTACH study, patients with ischaemic cardiomyopathy and reduced left ventricular ejection fraction were randomised to receive either catheter ablation and an ICD or an ICD alone. Similar to the SMASH-VT study, prophylactic VT ablation prolonged the time to recurrence of VT in this cohort (Kuck et al. 2010). Amiodarone was used in around 35% of patients in each arm. At 2-year follow-up, around 50% of patients in the ablation arm and 70% of patients in the control arm had a recurrence of VT however, suggesting that catheter ablation is insufficient as a stand-alone therapy in this cohort of patients.

The VANISH trial investigated the role of catheter ablation versus an escalation of anti-arrhythmic drug therapy in patients with ischaemic cardiomyopathy and an ICD in-situ who presented with recurrent VT. In this study, catheter ablation was associated with a lower rate of the primary composite end-point of death, VT storm or appropriate ICD shock versus an escalation of anti-arrhythmic drug therapy (Sapp et al. 2016). Around 65% of patients in VANISH were already on amiodarone at baseline, the mean LVEF was 31% in both arms and patients had to have either ≥3 episodes of VT treated with anti-tachycardia pacing, ≥1 appropriate ICD shocks or ≥3 VT episodes within 24hrs at enrolment suggesting a higher-risk cohort compared to SMASH-VT. In these patients, catheter ablation clearly emerged as the favourable option over escalation of anti-arrhythmic medications.

No improvement in all-cause or cardiovascular mortality has been demonstrated by any VT ablation clinical trial. A recent meta-analysis of the main randomised trials in ischaemic cardiomyopathy found that the most consistent benefits of VT ablation was a reduction in

cardiovascular-related hospitalisations driven mainly by reductions in VT storm and ICD shocks (Maskoun et al. 2018). Although these trials were underpowered to detect a mortality benefit, the data highlights the need to improve the efficacy and safety of VT ablation.

Clinical trials in VT ablation have proven to be difficult to perform with long enrolment periods, poor recruitment rates and high cross-over rates across study arms. During the course of long trials, iterative changes in ablation techniques, strategies and technologies have occurred making interpretation of trial results difficult (Mukherjee et al. 2017). There is also significant heterogeneity within trials regarding the mapping and ablation strategy - ablation being guided by either entrainment and activation mapping, pace-mapping or substrate-based strategies. The definition of acute procedural success also varies between trials with some studies targeting the clinical VT alone and defining success with non-inducibility of the clinical VT whilst others have targeted all inducible VTs or used a substrate-based strategy. The reproducibility of programmed stimulation to induce VT itself is variable. Even with substrate-based approaches, some approaches are considered complete and require extensive ablation (e.g. scar homogenisation) where the end-point may be anatomical or incomplete substrate modification strategies (e.g. core isolation) where isolation of segments may be demonstrated by the presence of exit block during pacing from within the isolated segment.

Optimal ICD programming protocols have also changed over time with high-rate therapy and delayed ICD therapy associated with reduced episodes of inappropriate therapy and all-cause mortality compared to conventional programming (Moss et al. 2012). More recently, the Substrate Modification Study (SMS) with contemporary ICD programming, randomised patients with ischaemic cardiomyopathy to catheter ablation plus ICD implantation versus ICD implant alone. There was a failure to meet the primary end-point of time to first VT

recurrence but catheter ablation did reduce the total number of ICD therapies during a follow-up of 2.3 ± 1.1 years (Kuck et al. 2017).

There is some evidence that patients are referred for catheter ablation late in the disease process. The CALYPSO pilot trial found that when screening patients into a trial of ablation versus anti-arrhythmic medications, around 41% of patients had already failed anti-arrhythmic therapy prior to consideration of catheter ablation (Al-Khatib et al. 2015). A recent European Heart Rhythm Association (EHRA) survey found that around 62% of centres would perform ablation after the first episode of monomorphic VT in patients with ischaemic cardiomyopathy (Tilz et al. 2018); in non-ischaemic cardiomyopathy, catheter ablation was used first-line in around 37%. A meta-analysis investigating the impact of early versus late referral for VT ablation suggested reduced VT recurrence and acute complications with early referral in patients with structural heart disease but no differences in total mortality and acute success (Romero et al. 2018).

As a consequence of the limitations to arrhythmia mechanism-directed RF energy delivery in the management of VT, there is increasing interest in substrate-based approaches that target the entire abnormal substrate. An extensive ablation strategy to homogenise scar and target any abnormal potentials in sinus rhythm was found to be superior to reduce VT recurrence compared to an approach where limited ablation of clinical VTs was performed in the multi-centre VISTA trial (Di Biase et al. 2015). A meta-analysis investigating ablation strategy in patients with structural heart disease found that substrate modification was associated with a lower composite end-point of ventricular arrhythmia recurrence and all-cause mortality compared to standard ablation of stable VTs (43% relative risk reduction). Additionally, complete substrate modification (e.g. scar homogenisation) was associated with a lower

recurrence compared to substrate-based approaches with incomplete modification (e.g. core isolation) (Briceno et al. 2018).

Scar dechanneling whereby the channels of 'slow conduction' within the abnormal substrate have been uncovered through physiologic manoeuvres and targeted with catheter ablation to connect regions of electrically unexcitable scar has also been used to achieve acute procedural non-inducibility and reduce VT burden during follow-up (Soejima et al. 2002). Recently, characterisation of scar channels from LGE-MRI based on pixel signal intensity thresholds has been integrated into the navigation system for VT ablation. Interestingly, a lower need for RF delivery, higher non-inducibility rate and improved VT-free survival was demonstrated using MRI-guided scar dechanneling compared to conventional ablation in a non-randomised study (Andreu et al. 2017). Such an approach highlights the potential value in using a structural-based approach to target segments of myocardium responsible for VT rather than a purely electrophysiological approach, with its inherent limitations.

2   Magnetic resonance imaging

This chapter discusses the principles of magnetic resonance imaging, its role in the non-invasive characterisation of the underlying substrate responsible for ventricular arrhythmias and assessment of ablation lesions. The field of interventional magnetic resonance is also introduced and the technical aspects of performing electrophysiology procedures inside a scanner examined.

2.1   Introduction

Magnetic resonance imaging (MRI) is a non-invasive imaging modality that allows comprehensive assessment of cardiac anatomy and function. In addition, tissue characterisation techniques including contrast-enhanced MRI can be used to characterise myocardial scar and differentiate between disease processes (Ambale-Venkatesh and Lima, 2015). MRI can also enable the online monitoring of temperature in different tissues as the magnetic properties of water protons are temperature-dependent (de Senneville et al. 2012), thereby permitting direct visualisation of RF-induced thermal injury.

As noted in the previous chapter, VT in the presence of structural heart disease frequently involves re-entry around or within a region of ventricular scar. The presence of late gadolinium enhancement (LGE) on MRI may identify the fibrotic substrate of VT (Ashikaga et al. 2013) whilst regions of intermediate signal intensity between scar tissue and normal myocardium have been histologically validated as scar borderzone (BZ) (Pop et al. 2013) which may represent the imaging equivalent of slowly conducting tissue. Scar and scar BZ are 3D structures - LGE-MRI is the best available non-invasive technique to define these structures in 3D and is a powerful predictor of ventricular arrhythmia risk (Disertori et al. 2016).

There are a number of potential benefits that the use of MRI in general and interventional MRI, in particular, could offer the electrophysiologist during VT ablation including assessment of structural substrate to complement functional electrophysiological assessment, accurate tracking of catheters to improve intra-procedural guidance and evaluation of ablation lesion formation with soft tissue visualisation (Mukherjee et al. 2019). This chapter explores the basic principles of MRI, image reconstruction and pulse sequences. The application of MRI for scar assessment, temperature mapping and interventional procedures is also discussed.

2.2 MRI physics

2.2.1 Nuclear magnetic resonance phenomenon

The primary source of the MR signal for imaging applications is the hydrogen atom consisting of a single positively-charged proton surrounded by a single negatively-charged electron. Hydrogen nuclei (^{1}H) are abundant in water and fat within biological tissues and is ideally suited for MR imaging. Each nuclei with an odd mass (e.g. ^{1}H) possesses a basic quantum mechanical property termed 'spin' which is a representation of intrinsic angular momentum. The spin of the positively-charged proton (^{1}H) generates a small magnetic field and a magnetic moment. For a ^{1}H nucleus, there are two possible spin states (i.e. direction of the angular momentum), e.g. 'spin-up' or 'spin-down.'

Conventionally, magnetic moments are randomly orientated but following the application of an external magnetic field (B_0), magnetic moments align either with or against B_0. Depending on the orientation of the spin states against B_0, a difference in energy levels may occur (spin-up = lower energy state; spin-down = higher energy state). The energy gap between the two spin states is related to the magnetic field strength and the gyromagnetic ratio (constant

specific to a particular atomic nucleus). At body temperature, the number of spins in each

state are almost equal with a slight excess in the lower energy (spin-up) state. The excess of

these proton magnetic moments can be combined to give the net magnetisation vector which

at equilibrium is parallel to B_0 (z-axis) and is given the value M_0. When particles are placed

within a static external magnetic field, they experience a force perpendicular to the

orientation of angular momentum resulting in a circular motion termed 'precession'. The

precession frequency of a nucleus is proportional to the strength of B_0 and the gyromagnetic

ratio and is described in the Larmor equation:

$$\textit{Equation 1: Larmor equation:} \qquad \omega_0 = \gamma B_0$$

where γ is the gyromagnetic ratio (42.6 MHz/Tesla for ^{1}H) and ω_0 is the Larmor frequency

(which at 1.5T is 64MHz).

2.2.2   Radiofrequency (RF) excitation

In order to perform magnetic resonance imaging, the net magnetisation is displaced out of its

alignment with B_0 through the application of additional oscillating time-varying RF pulses

(B_1) perpendicular to B_0. The B_1 field can be produced by driving an electrical current

through RF transmit coils. In order to flip the net magnetisation of the nuclear spins, B_1 is

applied at the Larmor frequency which enables spin transitions from low energy to high

energy states resulting in excitation. The amplitude and duration of the RF pulse determines

the degree of rotation of net magnetisation and is termed the 'flip angle'. Following

application of the RF pulse, net magnetisation can be split into two components - the

longitudinal component that lies parallel to the z-axis (M_z) and the transverse component that

lies perpendicular to the z-axis and within the plane of the x and y axes (M_{xy}).

Spin-echo based pulse sequences are initially preceded by a 90° RF excitation pulse that transfers M_0 into the transverse plane leaving no component in the z-axis. This is followed by a 180° refocusing pulse which reverses the dephasing of spins due to B_0 field inhomogeneity. If the RF excitation pulse leaves some component of net magnetisation in the z-axis and only transfers a proportion into the transverse plane, a lower flip angle is produced ($<90^0$) - this is typically used to generate the signal in gradient echo pulse sequences. A 180° pulse can also be used to flip M_0 perpendicular to B_0 prior to the application of an excitation pulse and is known as an inversion pulse - these are typically used in inversion recovery pulse sequences. Following cessation of the RF excitation pulse, the transverse magnetisation induces a current (MR signal) which can be detected by a RF receiver coil placed next to the tissue of interest.

2.2.3   Relaxation

The process by which thermal equilibrium is re-established following the termination of a RF excitation pulse is termed relaxation as high energy protons decay back to low energy states. The time taken for decay of the z component of the net magnetisation (longitudinal relaxation) to reach 63% of its equilibrium value is defined as the T1 time. The time taken for decay of the xy component of net magnetisation (transverse relaxation) to 37% of its equilibrium value is defined as the T2 time. Both T1 and T2 relaxation are a function of the size and motion of the molecule upon which the ^{1}H nucleus resides and therefore vary according to the tissue type, e.g. liquids (water/cerebrospinal fluid) have longer T1 and T2 values than dense solids (fat). This information can therefore be used for tissue characterisation during imaging.

As noted earlier, following cessation of the RF excitation pulse, transient fluctuations in coil voltage are created. This signal is called free induction decay (FID) which is produced as the

net transverse magnetisation decays as proton magnetic moments move out of phase to one another. The FID signal is a combined effect of T2 relaxation and additional de-phasing caused by inhomogeneity in the applied magnetic field - a process called T2*-decay. Pulse sequences used in MRI are manipulations of the FID signal involving application of dephasing and rephasing gradients to create calibrated changes in local magnetic fields and alter the Larmor frequency in a given direction. This results in 'echoes' that are used to measure, localise and encode MR signals in space.

2.3   Pulse sequences

The most common types of echoes used in MR pulse sequences are spin echoes and gradient echoes. Balanced steady-state free precession (bSSFP) sequences are created from a combination of spin echo and gradient echo. In general, without the application of pre-pulses, gradient echo and bSSFP sequences are bright-blood whilst spin echo sequences are black-blood. During application of multiple RF pulses, the time interval between the centre of the RF pulse and the resulting echo is called the echo time (TE) whilst the time interval between successive excitation pulses is called the repetition time (TR). The common pulse sequences used in cardiac MRI are described in the section below.

2.3.1   Spin echo

A spin echo sequence is generated through the application of successive pulses - a 90° excitation pulse followed by a 180° refocusing pulse. After the 90° pulse, net magnetisation is tipped into the transverse plane; due to magnetic field inhomogeneities, individual protons precess at different rates causing dephasing. The 180° pulse, rephases these protons causing the FID to increase in amplitude (initial FID decays as a function of T2* but the 180° pulse rephasing results in an echo amplitude that is T2 weighted). The signal that rephases

following the 180° pulse is knows as a spin echo. Adjustment of the TE and TR allows images with different contrast weightings to be obtained.

2.3.2 *Gradient echo*

A gradient echo (GRE) signal is initiated with a single RF pulse which typically uses a flip angle <90° with a smaller degree of transverse magnetisation, but can have any value. Following the RF pulse, a FID signal is generated. An external magnetic field 'gradient' is then applied (causing a calibrated change in local magnetic field) leading to proton spins losing coherence and leading to a dephasing of transverse magnetisation and accelerated decay of the FID signal. A second gradient then reverses the phase shift to recover the FID signal and create the 'gradient echo.' GRE imaging is generally faster than spin echo sequences as only one RF pulse is applied and therefore TE is shorter. A low flip-angle excitation pulse can also allow for a short TR thereby enabling rapid imaging acquisitions.

Whilst each RF pulse in a GRE sequence generates a FID signal, each pair of RF pulses generates a spin echo. If the TR is shorter than the T2 time, the FID signal persists as the 'echo' component starts. The application of gradients can preserve or suppress either the FID or echo signals depending on the time, duration or strength of application. GRE sequences that aim to preserve coherence are called coherent GRE sequences whilst sequences that apply a gradient to dephase residual transverse magnetisation (spoiler gradients) are known as spoiled GRE.

2.3.3 *Balanced steady-state free precession (bSSFP)*

As noted above, a FID signal will occur after each RF pulse and a spin echo after successive pulses. However, if the TR between pulses is less than T2, transverse magnetisation will not

fully dephase and the signal from the FID and echo will merge. A pulse sequence where residual transverse magnetisation remains between RF pulses is known as steady state free precession (SSFP) - i.e. a type of coherent GRE sequence. Dedicated dephasing and rephasing gradients can then be used to refocus the FID and/or echo components of the signal. bSSFP sequences uses balanced gradients along the x, y and z axes that refocuses both the FID and echo components into a single echo. The result is higher signal-to-noise ratio (SNR) as the entire magnetisation vector is utilised to produce the signal and good contrast between blood and myocardium leading to its use as the work-horse of cardiac imaging.

2.3.4   Inversion recovery pulse sequences

A pre-pulse where longitudinal magnetisation (Mz) is inverted by a 180° pulse prior to the spin echo/gradient echo sequence is known as inversion recovery. The time delay between the 180° inversion pulse and the first RF excitation pulse is known as the inversion time (TI). After the application of the inversion pulse, the inverted tissue undergoes T1 relaxation during the TI interval. Different tissues will have varying T1 relaxation times. Therefore, altering the TI interval allows image contrast between tissues to be generated. In order to generate the MR signal (readout), the inversion recovery pre-pulse can be combined with additional pulses and associated gradients (e.g. spin echo, gradient echo or bSSFP) which may further produce a range of image contrasts.

Inversion pulse application allows selective tissue suppression and is widely used in cardiac imaging. Following the inversion of longitudinal magnetisation of tissue, there is gradual recovery of magnetisation. If the TI is set a specific value, tissues with a longitudinal magnetisation of zero will have no signal at that time interval and will be 'nulled.' Inversion recovery pre-pulses are typically used in late gadolinium enhancement (LGE) imaging

whereby the paramagnetic molecule, gadolinium, which shortens T1 time, is used to differentiate between normal and pathological myocardium due to its delayed wash-out from the expanded interstitial space in pathological conditions (e.g. myocardial infarction).

2.4   Slice selection, spatial encoding and image reconstruction

2.4.1   Slice selection

A combination of RF excitation pulses and gradient fields are used to initiate the image formation process and localise the MR signal in three dimensions. In order to selectively excite a slice of tissue, a gradient field (slice selection gradient - G_s) is applied during RF pulse transmission. Resonance of protons will only occur when the frequency of the RF pulse matches the Larmor frequency at a given position along the direction of the gradient. This has the effect of only selectively exciting protons which are perpendicular to the direction of gradient applied and therefore determines the slice of tissue which has been excited. The RF pulse is usually transmitted as a small range of frequencies (bandwidth) which defines the slice thickness.

2.4.2   Phase encoding

A second gradient called the phase encoding gradient (G_p) is then applied which temporarily alters the precession frequency of protons. As the magnetic field strength varies in various parts of the body, the application of G_p leads to a change in the relative phase of protons dependent on their position along the gradient. This allows the spatial position of protons to be mapped according to the phase differences of transverse magnetisation.

2.4.3   Frequency encoding

A third gradient called the frequency encoding gradient (G_f) is then applied in a direction perpendicular to the phase encoding gradient and alters the homogeneity of the main

magnetic field in a calibrated way. Similar to the phase encoding gradient, the frequency encoding gradient alters the precession of protons according to their position along the direction of G_f so that resonant frequency is changed as a function of spatial position.

In combination, G_s, G_p and G_f allow 3D localisation of the MR signal by selecting a given slice and creating a phase shift along a particular axis and a frequency shift along a perpendicular axis in that slice.

2.4.4 *Image reconstruction*

A 2D image can be decomposed into sine waves which vary in frequency, amplitude, phase and direction. Spatial encoding using phase and frequency encoding enables an image to be recorded in this way and the resulting data points representing amplitudes and phases are recorded in a raw data matrix known as k-space. Image space comprised of all pixels that make up an image and k-space are inversely related. Within image space, all MR signals that have been phase and frequency encoded may contribute to a pixel which is part of that image space. Within k-space, each point of the MR signal occupies a particular location - i.e. each point in k-space represents the degree of spatial frequency contained in the image pixel (Ridgeway, 2010). In order to create an image pixel map from the frequency and phase information, a mathematical transformation (Fourier transformation) is required to decode the signals and reconstruct the final image.

2.5   Scar imaging with late gadolinium enhancement

2.5.1 *Contrast-enhanced imaging*

Contrast-enhanced imaging following intravenous administration of contrast agents containing complexes of the small paramagnetic molecule, gadolinium is widely used in cardiac MRI. Gadolinium shortens T1 values in tissue where it accumulates. Following

administration, gadolinium is transferred from the intravascular space to the interstitial/extra-vascular space. Wash-out of gadolinium-based agents are dependent on renal clearance. In normal cardiac tissue, there is a rapid wash-in and wash-out phase. In abnormal tissue such as scarred myocardium (e.g. following myocardial infarction), the interstitial space is expanded and therefore gadolinium accumulates in this space and exhibits a delayed wash-out phase.

In order to identify abnormal tissue with gadolinium accumulation, late gadolinium enhancement (LGE) sequences are used which are T1-weighted pulse sequences preceded by an inversion recovery pulse. Signal from abnormal tissue has a bright signal on T1-weighted images. A TI is chosen where signal from normal myocardium is suppressed (nulled) thereby maximising the contrast between normal and scarred/fibrotic myocardium. A number of factors can affect the optimal nulling of myocardium including the time from contrast injection to acquisition, MR field strength, type of contrast agent, dose and pulse sequence used for image read-out.

Conventionally, LGE imaging is performed 5-15 minutes following administration of contrast with a maximal dose of 0.2mmol/kg. After this period of time, the TI in both blood pool and myocardium increase as gadolinium wash-out occurs and therefore, conventionally, there is a narrow window to perform imaging and discriminate between normal and abnormal tissue. In this thesis, a technique to maintain the blood and myocardial TI in a steady-state through the application of a slow continuous infusion of gadolinium is presented to enable higher resolution scar imaging and compare different contrast-enhanced pulse sequences to identify the optimal method of substrate assessment. The slow infusion of continuous gadolinium to achieve 'contrast steady-state' was first applied to quantify diffuse myocardial fibrosis (Flett et al. 2010).

2.5.2 2D vs 3D imaging

The reference LGE exam most commonly used for myocardial scar imaging is a 2D IR GRE sequence which is acquired using multiple breath-holds. During 2D imaging, tissue within a 2D plane is excited during each breath-hold and a stack of multiple 2D images within a region of interest are acquired to create a 3D volume. In 3D imaging, an entire slab of tissue is excited and imaged. 3D imaging generally provides a better spatial resolution, signal-to-noise ratio (SNR) and can be acquired with an isotropic resolution facilitating multi-planar reconstruction of images to aid interpretation. However, 3D imaging can require prolonged scan times during free-breathing acquisitions whilst both cardiac and respiratory motion, without correction, can corrupt the entire acquisition.

For assessment of myocardial infarcts, 3D LGE can visualise scar with a better SNR and greater image sharpness demonstrating the complexity of heterogenous scars (Peters et al. 2009) compared to 2D LGE. For routine diagnostic purposes, conventional 2D LGE may be sufficient but a higher spatial resolution will allow an improved assessment of scar morphology and peri-infarct tissue, which may be required to define ablation targets for VT ablation. Isotropic 3D LGE imaging will also allow for reconstruction and multi-planar reformatting in any imaging plane, further allowing assessment of scar tissue in different views and therefore aid the identification of channels of tissue that may be important in the maintenance of VT (Basha et al. 2017).

2.5.3 Pulse sequence techniques for LGE imaging

A number of approaches alternative to standard 2D IR GRE have been investigated for LGE scar imaging including phase sensitive inversion recovery (PSIR) reconstruction where the polarity of M_z is taken into account in addition to the magnitude of M_z (Kellman et al. 2002)

and reduces the variation in image quality related to selection of the optimal TI. Additional approaches include 3D LGE to improve spatial resolution and assessment of scar heterogeneity (Basha et al. 2017) and dark-blood LGE using an inversion pulse followed by T_2 magnetisation preparation to simultaneously reduce normal myocardium and blood pool signal intensity and increase scar-blood contrast whilst preserving scar-myocardium contrast (Basha et al. 2018). Different pulse sequence read-outs after the inversion pulse (GRE vs SSFP) can also impact the visualisation of the infarct-blood boundary (Detsky et al. 2007).

Some investigators have performed head-to-head comparisons of LGE sequences to determine the optimal imaging method for different applications. An improved contrast-to-noise ratio (CNR) and qualitative image quality was reported in ischaemic cardiomyopathy patients using a 3D IR GRE technique compared to other breath-hold and free-breathing 2D and 3D techniques (Viallon et al. 2011). Similarly, in patients with structural heart disease referred for VT ablation, an improved matching to EAM-defined scar was reported using scar reconstruction following a 3D IR GRE sequence compared to 2D IR GRE and a 2D IR SSFP sequence (Andreu et al. 2015).

However, given that the wash-in and wash-out kinetics of gadolinium following a single bolus will change the TI during extended scar imaging, it is difficult to be certain that consistent contrast distributions are present during comparison of multiple sequences. To identify the regions of tissue responsible for VT, high-resolution isotropic imaging is required which require prolonged scan times, during which TI may vary significantly. In this thesis, the use of contrast steady-state is applied to compare post-contrast sequences in an experimental model with consistent contrast conditions to determine the optimal imaging technique for 3D scar assessment.

2.5.4   Motion compensation for cardiac and respiratory motion

Motion due to cardiac contraction or breathing can cause significant artifacts and result in blurred images affecting image quality. Broadly speaking, synchronisation with the cardiac cycle through the use of surface ECG electrodes is mandatory to account for cardiac motion. The peak of the R-wave of the ECG can be used as the reference to synchronise the MR sequence with the cardiac cycle. Following this, prospective gating can be applied, where data is acquired during a specific acquisition window within the R-R interval and images reconstructed. Alternatively, retrospective gating, where data is acquired continuously and subsequently re-ordered according to the phase of the cardiac cycle, can be used to reconstruct images and correct for cardiac motion.

A number of techniques may be used to account for respiratory motion. The most straightforward approach is to acquire images during patient breath-holds. A 10-20s breath-hold is typically used at end-expiration to acquire all the data required to reconstruct the image at a time when diaphragmatic motion is minimal. Following a period of rest, the cycle is repeated to acquire consecutive slices.

For patients unable to hold their breath or 3D scans that require prolonged imaging times, free-breathing acquisitions are necessary. A respiratory navigator beam can be used to enable either prospective or retrospective respiratory gating. The navigator is placed on the diaphragm over the lung-liver interface to detect motion of the lungs given that most of the motion is in the foot-head direction. A pre-pulse, called a navigator echo, is used before and/or after the image sequence to locate diaphragm position along the direction of the navigator beam. The signal from the navigator echo are displayed in columns or lines to measure respiratory motion through the duration of the sequence. A pre-defined gating

window is used to accept or reject data depending on whether the diaphragm was in the given window during the respiratory cycle, thereby accepting data only during a still period in the cycle (Lombardi et al. 2018) - *Figure 2-1*. Single-shot acquisition techniques are also possible where all required data are acquired during a single heart beat and phase of the cardiac cycle. The 3D imaging sequences described in this thesis were acquired during free-breathing using prospective respiratory gating.
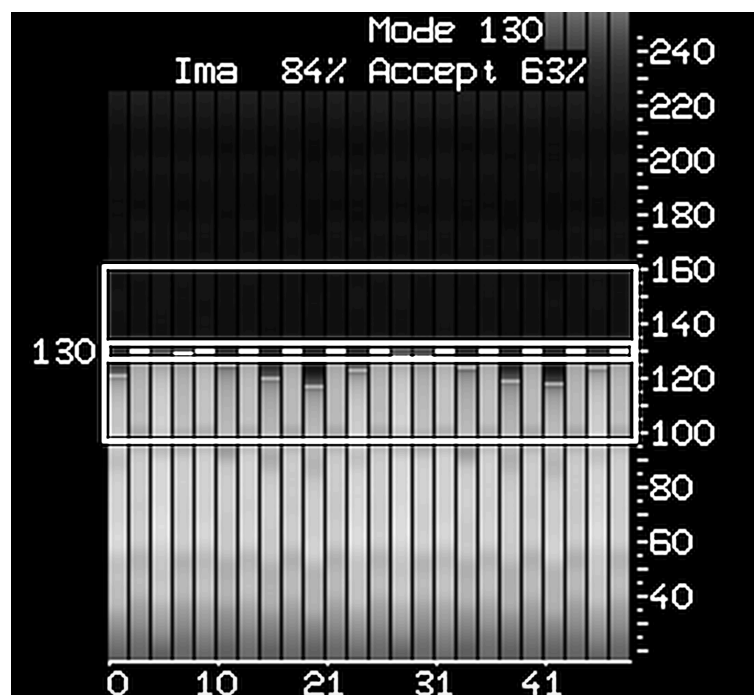
Figure 2-1: Respiratory navigator acceptance window

2.5.5   Analysis and post-processing: core scar and borderzone assessment

There are a number of imaging features that can be extracted from LGE-MRI that could be used to delineate the regions of tissue associated with VT substrate including pixel signal intensity, scar transmurality or tissue thickness and entropy of scar. Spatially complex scar containing a mixture of viable myocardium and electrically-inert scar is thought to represent the substrate for re-entrant VT. Critical isthmus and ablation termination sites have been localised to peri-infarct tissue, defined as regions of dense scar-borderzone transition on MRI

and in regions of scar with >75% transmurality (Piers et al. 2014). Scar heterogeneity with intermediate grades of viable tissue on MRI has been reported to be present at sites containing the critical isthmus for VT (Ashikaga et al. 2007) whilst successful ablation of heterogenous tissue has been associated with non-inducibility of VT in an animal model (Estner et al. 2011).

Tissue characterisation algorithms based on pixel signal intensity have been used to define tissue as either binary (scar or normal myocardium) or ternary (dense scar, borderzone tissue, normal myocardium). These include the full-width at half maximum (FWHM) method whereby manual delineation of a region of interest (ROI) around a region of hyper-intense (scarred) myocardium is selected. The signal intensity at 50% of this value is then used as the threshold to define scar. Other approaches for scar quantification include the n-standard deviation (SD) method whereby a ROI in the remote (normal) myocardium is selected. Thresholds can then be selected based on pixel signal intensity values at 2-SD, 3-SD, 4-SD, 5-SD or 6-SD to define scar. Manual quantification of scar has also been applied based on image segmentations. There is however no agreement on the optimal method or thresholds to categorise scar (Sramko et al. 2019) or any validation of the extent of borderzone tissue and dense scar in large animal models quantified from MRI using whole-mount histology (Pop et al. 2013).

LGE dense scar and borderzone volume can vary significantly depending on the method used for quantification. Borderzone volume can be 2-3 fold higher using FWHM vs n-SD methods whilst dense scar values are higher using the n-SD method of quantification (Mesubi et al. 2015). The FWHM technique appears to be the most reproducible however with the lowest

intra-observer and inter-observer variability (Flett et al. 2011). Differences in MR sequences could also lead to variability in VT substrate identification (Andreu et al. 2015).

Recently, there has been interest in scar entropy, as a measure of tissue inhomogeneity which is independent of signal intensity thresholds to differentiate arrhythmogenic from non-arrhythmogenic scar. High entropy within scar has been associated with an increased risk of ventricular arrhythmias (Androulakis et al. 2019; Gould et al. 2019).

There are limitations in using imaging to define the critical regions of tissue responsible for VT - recently, high-resolution activation mapping data in a porcine infarct model has demonstrated the importance of functional block in defining the borders of a VT isthmus (Anter et al. 2016). Furthermore, a limited specificity of voltage and electrogram characteristics in sinus rhythm have been demonstrated (Anter et al. 2018) suggesting that imaging structural characteristics alone (where there is no equivalent of an electrical 'stress test') are unlikely to identify the optimal sites for ablation. Limitations in the image resolution of current clinical scans (1.4mm^3, as reported in Andreu et al. 2015) can also lead to partial volume effects that may overestimate the volume of heterogenous tissue (Schelbert et al. 2010).

2.5.6   Developments in magnetic resonance techniques to improve substrate assessment
Acquisition of high-resolution imaging is required to detect smaller regions of scar and improve assessment of scar geometry in patients undergoing VT ablation (Basha et al. 2017). 3D LGE imaging can allow acquisitions with a higher spatial resolution compared to 2D LGE but requires prolonged scan durations. Longer scans can lead to changes in contrast agent concentration over time or reduced respirator navigator efficiency due to irregular

breathing patterns (Basha et al. 2017). The use of image acceleration techniques such as compressed sensing has enabled faster acquisition of 3D imaging of higher spatial resolution (1.2mm^3) with acceptable scan duration, image quality and comparable scar characteristics to conventional 3D LGE (Basha et al. 2017). Parallel imaging with a stack-of-spirals acquisition technique has also been used to enable rapid 3D LGE acquisitions in a 12 heart beat-long breath-hold (Shin et al. 2014). 3D free-breathing self-navigating MR sequences have recently been described to overcome the errors associated with respiratory navigator placement and irregular breathing patterns enabling high-resolution visualisation of scar distribution and superior delineation of scar borders (Rutz et al. 2016). A new technique to reconstruct a high resolution image from multiple low resolution views of the same volume (super-resolution reconstruction - SRR) has also shown a good agreement with the bipolar voltage range of scar borderzone (Dzyubachyk et al. 2015). Further developments in these techniques may allow faster imaging with higher spatial resolution and advance the ability of clinical MRI protocols to identify areas of scar critical for re-entrant VT circuits.

The development of dark-blood LGE (DB-LGE) sequences as a technical solution to sub-optimal contrast between scar and blood pool offers promise for improved substrate assessment. DB-LGE sequences have been described that simultaneously reduce normal myocardium and blood pool signal intensity whilst enhancing scar-blood contrast and preserving scar-myocardium contrast (Basha et al. 2018; Kellman et al. 2016). Given that a large proportion of VTs appear to originate in the sub-endocardial region (Tschabrunn et al. 2016), improved contrast between scar and blood pool may improve the detection of substrate in these areas.

2.6   Temperature mapping

Tissue temperature distribution can be estimated using MRI as several MR parameters are temperature-dependent. Intrinsic tissue magnetic properties such as the T1/T2 relaxation time, proton density, diffusion co-efficient, magnetisation transfer and proton resonance frequency (PRF) are sensitive to changes in temperature (Reike V et al. 2008). In cardiac RF ablation, due to the need for real-time application with fast imaging sequences, reduced sensitivity to motion, tissue independence, good temporal and spatial resolution, the PRF method for temperature mapping has been the most widely used for assessment in preference to other techniques.

2.6.1   MR-thermometry with the PRF-shift technique

The resonance frequency of water protons is temperature-dependent (de Senneville et al. 2012) which is thought to be due to the result of rupture, stretching or bending of hydrogen bonds proportional to changes in temperature (Ishihara et al. 1995). PRF-shift based thermometry computation can be derived directly from the MR spectra or phase mapping. For phase mapping, relative temperature changes (ΔT) can be calculated via differences in phase measurements to a reference phase at a given temperature as follows (Winter et al 2016):

Equation 2: PRF shift equation:

$$\Delta T = \frac{\Delta \varphi}{\alpha \cdot \gamma \cdot TE \cdot B_0}$$

where γ is the gyromagnetic ratio, TE is the echo time, α is the temperature dependent chemical shift of water (~0.009-0.01 ppm/$^{\circ}$C, apart from in adipose tissue), B_0 is the static magnetic field strength and $\Delta \varphi$ is the phase variation.

A GRE sequence is most commonly used to compose temperature maps using gradient echoes with a long TE with optimisation to ensure adequate spatial and temporal resolution and good SNR. A series of reference images are initially acquired prior to RF ablation to derive phase of the baseline image. During and following RF ablation, further phase images are acquired. The phase variation is then subtracted to facilitate PRF shift computation and obtain measurements of tissue temperature in each individual pixel of the resulting image (Reike et al. 2008).

There are a number of technical issues that can affect the accuracy of PRF-based thermometry including variations in B_0 during the course of RF ablation, a small degree of tissue dependence of the chemical shift and temperature-dependent changes in the relative permittivity and electric conductivity of tissue which can affect the phase velocity (Winter et al. 2016). In addition, issues with motion (both cardiac and respiratory) is a ubiquitous problem for temperature mapping in the heart. Artifacts can be present due to inter-scan motion (PRF-shift with phase mapping is dependent on acquisition of reference scans prior to ablation and during ablation) and intra-scan motion causing blurring or object ghosting (Reike et al. 2008). Physiological motion can lead to important errors during estimation of tissue temperature and require correction (Mukherjee et. al. 2019). Strategies for motion management include the use of respiratory gating, motion detection and movement registration with navigator echoes, multiple reference acquisitions to sample periodic changes (de Senneville et al. 2007) and referenceless phase correction (Rieke et al. 2004; Reike et al. 2008).

2.6.2 MR-dosimetry

The relationship between temperature elevation and tissue destruction is complex. The volume of tissue necrosis following delivery of RF ablation is not easily calculated and a

number of techniques to estimate lesion size derived from tissue temperature and duration of exposure to ablation have been described. In cardiac RF ablation, the calculation of thermal dose (MR-dosimetry) has been applied to determine when target tissue destruction has been achieved using an integral of temperature elevation and time to derive the thermal dose as follows (Mukherjee et al. 2018; Toupin et al. 2017):

Equation 3: Thermal dose calculation

$$TD = \begin{cases} \int_0^t 2(T(t) - 43)dt & if \quad T(t) > 43°C \\ \int_0^t 4(T(t) - 43)dt & if \quad T(t) < 43°C \end{cases}$$

where *T(t)* represents absolute tissue temperature; the concept of cumulative equivalent minutes (CEM_{43}) is applied whereby for each degree increase above $43°C$, a 2-fold decrease in the time required for the tissue to be thermally destroyed (Chang, 2010) based upon experimental studies of tissue injury. When the thermal dose reaches a critical threshold ($43°C$ for a duration of 240 min), the tissue destruction is believed to have occurred.

Other approaches to quantify lesion volumes include the use of iso-temperature contours from the temperature profiles to delineate ablation lesion boundaries or utilising the Arrhenius equation to determine the relationship between tissue temperature, exposure time and tissue injury (Chang, 2010).

MR-dosimetry can therefore be used to determine the end-point of ablation therapy. In this thesis, the use of MR-thermometry and dosimetry using CEM_{43} to derive the thermal dose, is applied to calculate lesion size when delivering both endocardial and epicardial RF ablation in the left ventricle, inside the MRI scanner.

2.7 Interventional MRI

2.7.1 Introduction

The ability of cardiac MRI to characterise arrhythmia substrate, guide procedures and evaluate ablation lesions has inspired the development of interventional MRI within electrophysiology whereby mapping and ablation can be completed within the MRI environment. Although many investigators have integrated anatomical and scar data from pre-acquired MRIs into the navigation system during catheter ablation (Andreu et al. 2017; Zghaib et al. 2018) these techniques invariably result in registration errors of up to 3.5mm (Roujol et al. 2013). Additionally, conformational changes within cardiac chambers as a result of different loading conditions between the time of imaging and intervention as well as translational changes due to patient movement, cardiac and respiratory motion could all lead to discrepancies between structural data and electrical substrate with potential consequences for the efficacy of catheter ablation (Mukherjee et al. 2018). The mean maximum amplitude of cardiac and respiratory motion for example, during EAM has been estimated to be in the region of 10.2 ± 2.7mm and 8.8 ± 2.3mm respectively (Roujol et al. 2013).

Interventional MRI offers a potential solution to overcome the limitations of image integration as well as utilise the benefits of MR-based catheter tracking and lesion assessment that can only be performed inside a MRI scanner (Chubb et al. 2017). Over the last decade, development of MR-conditional devices and imaging techniques have led to the application of interventional MRI in the setting of cardiac electrophysiology but a number of challenges have been identified. These include the recording of high quality electrograms in an environment with significant electromagnetic interference, the development of clinical-grade MR-compatible devices with similar physical capabilities as their conventional counterparts and establishing robust tools for real-time lesion assessment (Mukherjee et al. 2018). On a

practical level, effective communication is difficult between team members in a noisy environment and novel workflows are evolving to accommodate this hurdle.

From an imaging perspective, there are a number of specific of requirements for interventional MRI compared to diagnostic MRI including the need for faster image acquisition and reconstruction. There are various stages of an interventional MRI procedure including the acquisition of an anatomic procedural roadmap, catheter navigation during the procedure, lesion delivery and evaluation. Each stage requires sequences optimised for their specific purpose. For example, the 'roadmap' sequence will typically need to have a good spatial resolution for definition of anatomy but can have a low temporal resolution. 3D respiratory-navigated, ECG-gated GRE or bSSFP sequences with or without contrast have been used for this stage (Dukkipati et al. 2008). For catheter navigation, sequences with a high temporal resolution are required, typically at least 5-10 frames/second (Bhagirath et al. 2015). Ablation lesion visualisation may use a combination of T1-weighted, T2-weighted, LGE or thermometry sequences to evaluate lesion composition, measure lesion size and evaluate oedema and necrosis.

2.7.2   Technical issues: electrogram fidelity, devices and defibrillation

Accurate recording and characterisation of both surface electrocardiogram (ECG) and intra-cardiac electrograms (EGM) are an essential component of cardiac electrophysiology procedures. During catheter ablation of simple arrhythmias such as atrial flutter, demonstration of bidirectional conduction block created at the cavo-tricuspid isthmus and proven by sequential, timed EGM recordings made along the ablation line during coronary sinus pacing are necessary (Shah et al. 2000). For complex arrhythmias such as ventricular tachycardia, substrate-based mapping techniques rely on the correct identification of low

voltage regions, annotation of abnormal potentials and robust characterisation of electrogram morphologies (Josephson et al 2015).

The MRI environment is considered relatively 'hostile' for the rigorous recording of EGMs as there are many sources of artifact that may distort signals. During MR scanning, RF pulses are deployed that are coupled with fast-switching magnetic gradients which can induce electromagnetic fields around the subject and create voltage artifacts on both the surface ECG and intra-cardiac EGMs (Oster et al. 2010). A second source of signal distortion is the magneto-hydrodynamic effect (MHD). The static magnetic field (B_0) can lead to MHD voltages due to the flow of electrically charged blood particles through the aortic arch in a direction perpendicular to B_0. MHD voltages are superimposed primarily during the S-T phase of the cardiac cycle (period of peak flow) and can have a similar frequency spectrum and magnitude to real electrogram signals - *Figure 2-2* (Tse et al. 2014). The size of MHD voltages may also be affected by the heart rate as a different volume of blood may be ejected from the left ventricle - this may be relevant during EGM recordings in the context of tachycardia or pacing. A third source of artifacts are time-varying magnetic fields that provide position-dependent variation in MR field strength but can lead to induced electric currents in conducting tissues as well as connecting wires (Felblinger et al. 1999).
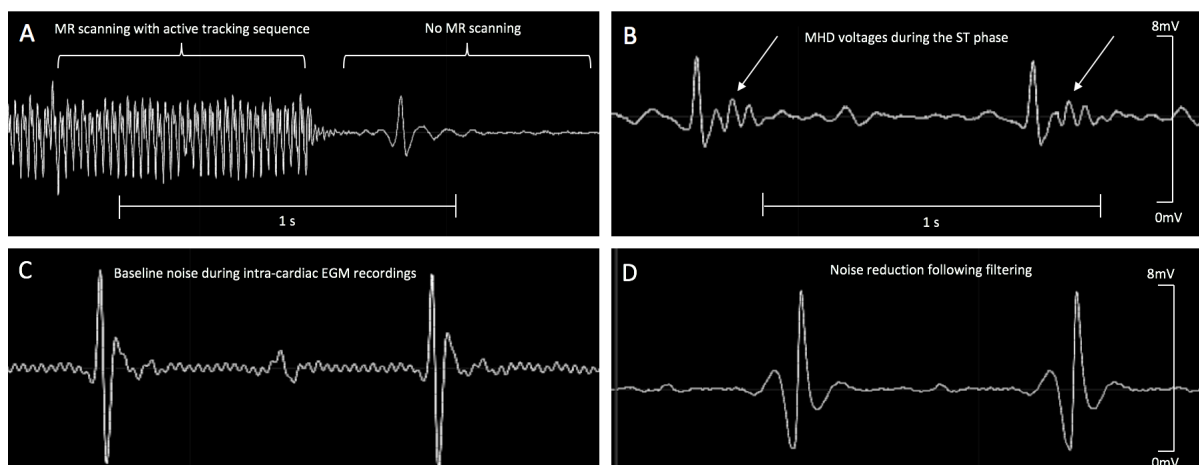
Figure 2-2: Recording surface ECG and intra-cardiac EGMs inside a MRI scanner.

Following the application of a low-pass filter (300Hz), high-pass filter (30Hz), notch filter (60Hz) and RF filters to reduce the 64MHz signal from the MRI scanner, Nazarian et al. (2018) demonstrated the ability to record both atrial and ventricular potentials in normal canines and healthy patients including distinguishing small His potentials with good fidelity. Subsequent studies in patients with atrial flutter have shown that double potentials can be detected along and conduction detour around an ablation line (Hilbert et al. 2016; Chubb et al. 2017). An experimental study in an ovine model estimated that the peak-to-peak amplitude of baseline noise inside the MRI scanner (without scanning) is 10-fold higher than in a conventional X-ray fluoroscopy laboratory (0.10 vs 0.01 mV) whilst the signal-to-noise ratio (SNR) may vary depending on the MRI sequence used during scanning (Elbes et al. 2017). In this study, a low-pass filter with a cut-off frequency of 120Hz gave the best quality EGM signals compared to filter cut-offs at 240 and 500Hz (Elbes et al. 2017). It remains unclear, however, whether low-amplitude abnormal potentials such as fractionated EGMs or late potentials with an amplitude <0.1mV can be detected robustly inside a MRI scanner with limited evidence available from one study (Oduneye et al. 2015). Although a lower value low-pass filter may give the best quality normal EGM signals, it may risk losing the fine high frequency components of abnormal EGMs that are important in substrate evaluation. Further developments in signal processing technologies are needed to improve EGM fidelity and there has been interest in the application of techniques such as adaptive noise cancellation (Wu et al. 2011) artefact modelling and Bayesian filtering for this purpose (Oster et al. 2010). The majority of patients who undergo VT ablation have an implantable-cardioverter defibrillator (ICD) in situ (Tilz et al. 2018). A number of potential adverse effects could

occur during MRI in patients with cardiac devices including device movement, induced current due to rapidly changing gradient magnetic fields, thermal injury with subsequent effects on the sensing and capture thresholds, activation of the reed switch as well as over-sensing and power-on-reset due to electromagnetic interference (Blissett et al. 2018). Although the risks of adverse effects have been reported as low, including imaging with legacy ICD systems (Nazarian et al. 2017), concerns regarding radiofrequency-induced tissue heating and device failure and their potential impact during long procedures lasting several hours, as is often the case during VT ablation, remains. The presence of ICDs also leads to the generation of artefacts; although wideband LGE sequences have been reported to adequately suppress artefacts and preserve diagnostic image quality for LGE imaging (Ranjan et al. 2015; Do et al. 2018) this remains a challenge for real-time MRI-guided procedures.

During VT ablation, haemodynamically unstable arrhythmias are often induced and may require immediate defibrillation. If defibrillation was required inside the scanner bore, the subject would have to be removed from the bore, the MR coil and any connecting wires or catheter instruments would have to be disconnected, the MRI table would need to be undocked, the subject evacuated outside the scanner room and connected to defibrillation pads. This process can be completed in around 60s with practice but nevertheless represents an unacceptable delay and could increase mortality (Schmidt et al. 2016). The inability to perform defibrillation inside a MRI scanner is a major safety hurdle and is a pre-requisite for clinical studies in patients. To date, there are only limited reports of prototype MRI-conditional defibrillation systems to enable electrical defibrillation both inside and outside the scanner bore in swine (Schmidt et al. 2016).

2.7.3 MR-compatible devices and tracking methods

Catheters used in the conventional electrophysiology laboratory typically incorporate ferrous components to grant the mechanical characteristics to enable torque transmission and navigation of tortuous structures. However, these materials can lead to large susceptibility artifacts inside a MRI scanner - although this phenomenon may be used during passive tracking, the susceptibility artifacts from conventional catheters can severely degrade image quality. Instead, materials that create a lower burden of artifacts are preferred including gold, titanium and nitinol with polyester braiding (Ratnayaka et al. 2008). The mechanical performance of MR-compatible catheters is not currently equivalent to their conventional counterparts and this has proven to be an obstacle to more widespread implementation of interventional MRI. The process of RF excitation during MRI can also lead to heating in conductive materials such as wires and transmission lines and make them inherently unsafe requiring re-design of the devices themselves.

There are two principle methods of intra-procedural guidance during interventional MRI - active and passive catheter tracking. Passive catheter tracking enables either positive or negative contrast visualisation by integration of susceptibility artefacts generated from ferromagnetic/paramagnetic materials embedded within a catheter (Grothoff et al. 2014) or using gadolinium or CO_2/N_2O-filled balloon catheters (Ratnayaka et al. 2013). Typically, during passive tracking an in-plane resolution of around 1mm, slice thickness of 6mm and temporal resolution of 4 frames/second has been reported (Nordbeck et al. 2013). Tip tracking accuracy using gadolinium-filled balloon catheters has been estimated to be in the region of ± 0.41mm with imaging reconstructions displayed at a frame rate of around 3 frames/s (Omary et al. 2000). Recently, application of a positive-contrast based passive tracking sequence using partial saturation magnetisation preparation has been shown to

provide improved simultaneous visualisation of both anatomy as well as gadolinium-filled catheters (Velasco-Forte et al. 2017). However, susceptibility artefacts during passive tracking can make devices with ferromagnetic/paramagnetic materials appear larger than their actual size as well as potentially obscure surrounding tissue. Furthermore, with all passive tracking techniques, if the device moves out of the imaging plane, the operator is required to relocate the device which can be time-consuming (Campbell-Washburn et al. 2017). It is also more difficult to track catheters within the expansive 3D space of cardiac chambers compared to in-plane tracking within the lumen of a vessel (e.g. aorta).

Active catheter tracking is an alternative technique whereby micro-coils embedded within the catheter produce a receiver signal to determine location of the device - *Figure 2-3*. An active tracking sequence consisting of intermittent non-selective excitations combined with spatially encoding gradients enable measurement of 1D projections in each space dimension and estimation of the 3D coordinates of the position of the micro-coils (Chubb et al. 2017; Daniels et al. 2016). Real-time estimates of the position of micro-coils can be used to estimate catheter tip orientation. This information can also be used for real-time slice tracking to automatically maintain the catheter tip in the imaging plane during navigation (Chubb et al. 2017). The precision of active tracking during ex-vivo technical validation experiments has been estimated to be in the region of 0.90 ± 0.58mm along the axis of the catheter whilst the angular deviation of catheter orientation from its true direction was $8.5^0 \pm 3.6^0$ (Chubb et al. 2017). Active tracking has been used to perform coronary sinus intubation, activation mapping and trans-septal left atrial access in swine (Grothoff et al. 2017) as well as to guide cavo-tricuspid isthmus ablation in patients with atrial flutter (Hilbert et al. 2016; Chubb et al. 2017).
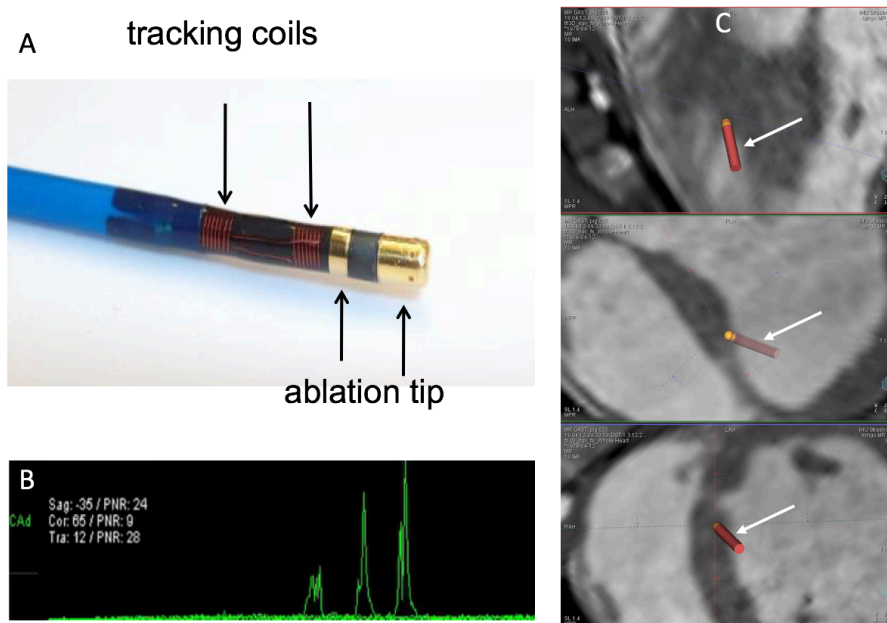
Figure 2-3: Active catheter tracking.

Active catheter tracking using a MR-compatible catheter with gold-tip electrodes and two 2.5mm solenoid receive coils (A). Using a dedicated tracking sequence, the X, Y and Z coordinates of the catheter micro-coils can be determined in 3D space (B) whilst the catheter tip can be displayed as a red icon in three orthogonal MRI projections to guide a MR-EP procedure (C). Reproduced with permission from Mukherjee et al. 2019; Current Cardio Imaging Reports

2.7.4 Communication

The interventional MRI suite is a noisy environment compared to a conventional electrophysiology laboratory. There are also additional personnel required including a MR radiographer and MR physicists who are outside the interventional suite in the control room. Good communication between all team members is a mandatory element to drive interventional MRI procedures. During scanning, MR gradients generate significant acoustic noise to interfere with communication. Headsets with fibre-optic cables, opto-acoustic headsets to subtract gradient noise and wireless headphones have all been used to enable two-way communication between members of the interventional and imaging team (Bhagirath et al. 2015).

2.7.5   Image guidance platforms

EAM systems are in widespread use for catheter ablation of complex arrhythmias. They can facilitate an understanding of arrhythmia mechanism, permit annotation of single or multiple sites of interest, guide catheter navigation to target ablation sites and, when properly used, can dramatically reduce fluoroscopy times and may reduce procedural times (Knackstedt et al. 2008). There has therefore been interest in the development of graphical interfaces to integrate data from real-time imaging into interfaces that closely mimic those of clinical-style EAM systems in order to drive progress in real-time MRI-guided electrophysiology (Wang, 2015). Several major MRI vendors have developed graphical solutions to represent electrical data, enable real-time imaging with active catheter tracking and workflows for catheter ablation - *Figure 2-4*. Philips Healthcare have developed the iSuite system that consists of hardware including a PC and monitor connected to the MR scanner console. A foot pedal also allows an operator to directly control the scanner in real-time from the scanner bore. Additional software capabilities include the ability to perform MRI-guided navigation combining pre-acquired imaging with real-time data, segmentation tools for procedural planning as well as custom modules to perform MR-based device tracking and support MR-thermometry (Chubb et al. 2017).

Similarly, Siemens Healthineers have developed their own interventional MRI platform that allows flexible control of scan plane orientation and image parameters from a dedicated PC connected to the scanner console, load and display volumetric data onto a custom software as well as perform automatic segmentations of pre-acquired data to ensure rapid image processing (Mukherjee et al. 2018). The mapping interface of the software gives the ability to change the colour or rendering styles of loaded segmentations and generate activation and voltage maps based on local activation time or voltage amplitude data using colour

interpolation between mapping points. Active tracking can be superimposed onto real-time imaging datasets allowing the system to deliver the features required of a clinical EAM system as well as having additional capabilities to exploit the benefits of real-time imaging (Mukherjee et al. 2018).

The Vurtigo platform, which is compatible with GE systems is a real-time visualisation application (open-source) that can either import EAMs generated conventionally or compose one using MR-tracked catheters followed by fusion with acquired MR volumes (Campbell-Washburn et al. 2017). A real-time scan control system (RTHawk research platform) which is based on the Heart Vista Cardiac operating system (Heart Vista, Los Altos, CA, USA) acts as a 2D viewer and allows acquisition of real-time sequences. The communication latency between the RTHawk application and Vurtigo has been estimated to be in the region of 6.3 ± 7.7ms (Radau et al. 2011). The system has the ability to visualise, compare and overlay MRI volumes, real-time imaging planes, catheters and surface meshes of EAMs. Further development of features including motion correction of mapping data points and improved signal processing are under evaluation (Radau et al. 2011).
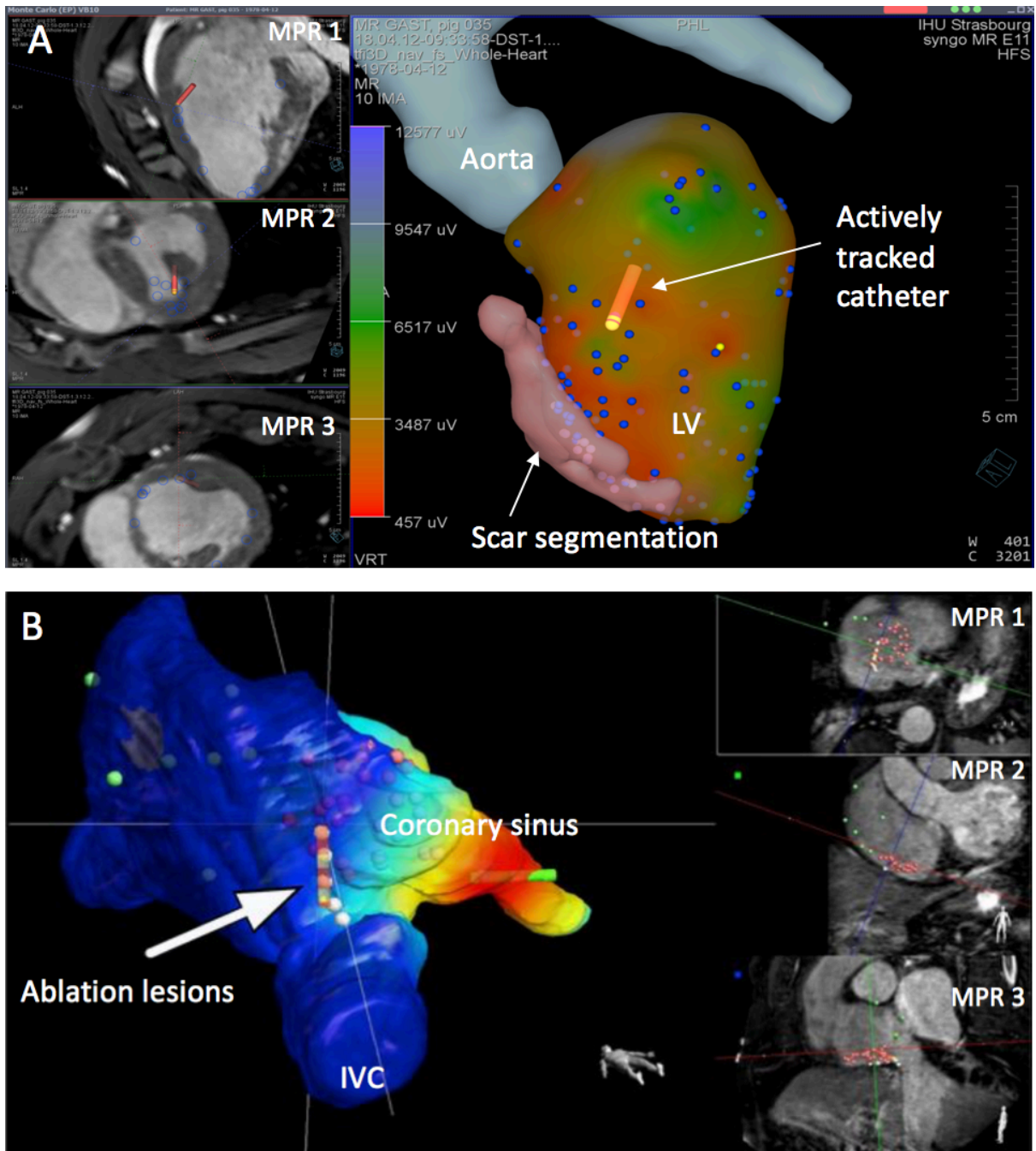
Figure 2-4: Image guidance platforms.

Image guidance software platforms for procedure visualization have been developed by several MRI vendors that are capable of displaying 3D volume roadmaps, real-time imaging planes, cardiac chamber segmentations, electroanatomical maps and actively tracked catheters. Shown here are example screenshots from the Siemens iCMR platform (A) during MRI-guided electroanatomical mapping of the left ventricle in a porcine infarct model and Philips iSuite platform (B) during MRI-guided catheter ablation of the cavotricuspid isthmus in a patient with atrial flutter. Reproduced with permission from Mukherjee et al. 2019; Current Cardio Imaging Reports. LV = left ventricle; IVC - inferior vena cava; MPR = multi-plane reconstruction.

2.7.6 Safety and patient monitoring

There are several safety considerations to performing interventional procedures in the MRI environment including ensuring that ferromagnetic materials are not inadvertently brought near the magnet, adequate preparation of the patient, haemodynamic and ECG-monitoring during the intervention, comprehensive monitoring during anaesthesia and robust evacuation protocols in case of an emergency. Monitoring equipment used need to be MRI-conditional and there are commercially available options for anaesthesia (e.g. Drager Fabius ® MRI) and basic haemodynamic monitoring (Expression, Invivo) (Chubb et al. 2017).

If the patient is sedated or under general anaesthesia during a prolonged interventional procedure, additional monitoring may be required to protect against skin burns due to rapidly switching magnetic gradients and RF pulses. Measurement of the specific absorption rate (SAR) during image acquisition and/or direct measurement of skin temperature can be employed (Lederman, 2005). Conductive material within the patient such as pacemaker/ ICD leads carries a risk of inducing severe burns due to RF-induced heating and all such devices must be carefully screened for safety (Wilson et al. 2019).

In the event of a cardiac arrest or an emergency requiring evacuation of the patient from the MRI environment, specific roles should be assigned to the interventionalist, radiographer and anaesthetist. Staff working within an interventional MRI suite should undergo dedicated training and emergency roles and tasks documented within a standard operating procedure.

SECTION TWO:

METHODOLOGY

3   Methods

In this section, methods which are applicable to one or more chapters are detailed to avoid repetition. Specific study protocols are retained within the individual chapters.

3.1   Animal model

The research protocols were approved by the local institutional review board and complied with French law on animal experiments and the Guiding Principles for the Care and Use of Laboratory Animals published by the National Institutes of Health (8th Edition, National Academies Press, 2011). All animal experiments were performed at the Institut de Chirurgie Guidée par l'image (IHU), Strasbourg, France. Domestic pigs were pre-sedated with a combination of intramuscular tiletamine and zolazepam. Following sedation, endotracheal intubation was performed and general anaesthesia induced and maintained with inhaled isoflurane (1.0 - 2.5%) with mechanical ventilation at 15-20 breaths/min. Percutaneous vascular access was gained from the right femoral artery (7-Fr introducer sheath) under ultrasound guidance. Following arterial access, a bolus of 7000 units of unfractionated heparin was administered intravenously followed by a maintenance infusion of 1000-2000 units/hr. An intravenous lidocaine (1mg/min) and amiodarone infusion (200mcg/kg/min) was also initiated to reduce the risk of ventricular arrhythmias.

3.1.1   Infarct preparation

The protocol was adapted as previously described by Tschabrunn et al. 2016. A 6-Fr Hockey-stick guide catheter (Medtronic, Minneapolis, MN) was advanced to the left main stem and a 0.14in Choice PT extra-support angioplasty guidewire (Boston Scientific, Malborough, MA) was placed in the left anterior descending artery (LAD). A 3.0 x 12mm Emerge Monorail PTCA dilatation catheter (Boston Scientific, Malborough, MA) was placed over the

angioplasty wire in the LAD. A coronary angiogram was performed to assess pre-infarct anatomy, following which the balloon was inflated to 12-14 atm in the mid-LAD distal to the second diagonal branch and maintained for 3 hours. A coronary angiogram was performed at 1 hour and 3 hours after inflation of the balloon to confirm that the artery was still occluded. The creation of infarct was also confirmed by the presence of ST-segment changes in lead V1. A continuous infusion of amiodarone (20mcg/kg/min) and lidocaine (12ml/hr) was administered to reduce the risk of arrhythmias. In the presence of haemodynamically unstable VT or VF at any time during the infarct procedure or at the end of procedure due to reperfusion arrhythmia, DC cardioversion was performed. At the end of the procedure, 0.03mg/kg buprenorphine was administered intramuscularly and a fentanyl patch (125 micrograms/hour) was applied for 72 hours. Animals then underwent a 6-week recovery period prior to imaging and electrophysiology study.

3.2   Magnetic resonance imaging

All MRI scans were performed on a 1.5T scanner (MAGNETOM Aera, Siemens, Erlangen, Germany) with an 18-channel body matrix coil and a 32-channel spine coil.

3.2.1   3D Whole-heart imaging

A 3D, ECG-triggered whole-heart bSSFP acquisition with a 1D diaphragmatic navigator (5 mm gating window) was performed with the following parameters: transverse slice orientation, AP phase encoding, 1.25×1.25 mm^2 in-plane resolution, 256×256 in-plane matrix size, 2.5 mm acquired slice thickness reconstructed to 1.25mm, typically around 100 slices to cover the whole heart, TR/TE = 3.7/1.64 ms, flip angle = 90°, readout bandwidth (per pixel) = 592 Hz, fat suppression, GRAPPA acceleration factor = 2. The trigger delay was set so that the acquisition was performed during mid-diastole and the acquisition window was

set to correspond to the length of the diastolic period (typically ~110ms, corresponding to 30 k-space lines acquired per heartbeat). Following acquisition, the left ventricle, right ventricle, left atrium, right atrium and aorta were manually segmented on each animal using an image processing platform based on a version of Medical Imaging Interaction Toolkit (MITK, Heidelberg, Germany) and saved as Stereolithography (.STL) files. Segmentations were loaded on the iCMR application (Siemens Healthcare) to create a roadmap for mapping and ablation studies.

3.2.2   Active catheter tracking

In order to project the location of the ablation catheter within the context of the cardiac chambers, active catheter tracking using a dedicated MRI tracking sequence, detected by micro-coils within the catheter was used. To perform active catheter tracking during MRI scans, the X, Y, Z coordinates of the catheter microcoils were determined using a custom active tracking sequence/module, which was optionally interleaved with a fast balanced steady state free precession (bSSFP) imaging sequence automatically following the current catheter position. The active tracking sequence comprised three non-selective projection acquisitions along the respective axis. A dynamic imaging coil detuning approach and pre-spoiler were applied to avoid potential background noise, i.e. coil coupling and residual signal effects. Based on the acquired projections, the corresponding signal peaks were detected with a dynamic template-matching algorithm, which used the initial projections to calculate a template per coil and axis. The template was continuously updated with each new projection fulfilling a minimal peak-to-noise ratio to adapt to the changing shape of the projections while manoeuvring the catheter. The detected positions were fed back to both the iCMR platform (Siemens Healthcare) and the MRI scanner to update the rendered catheter position/orientation and imaging plane location respectively. The tracking module was further optimized to run with an ambient acoustic noise and had been found to perform

robustly with an open MR cabin door, in the presence of other electrical equipment (e.g. ventilator, ECG monitoring, etc.) and during RF ablation (Chubb et al. 2017).

3.2.3   Late gadolinium enhancement imaging

To perform 2D standard LGE imaging, a bolus of 0.1mmol/kg gadobutrol (Gadovist) was first administered. After a period of 10 minutes, an inversion time (TI) scout sequence was acquired in a single mid ventricular short-axis slice (bSSFP; TE/TR/α = 1.1ms/2.6ms/30°; slice thickness = 8mm; in-plane resolution = 1.8x1.8mm; FOV = 340x280mm^2) to select the inversion time at which normal myocardium is nulled. A standard clinical 2D LGE was then acquired using a phase-sensitive IR (PSIR) sequence (SSFP; TE/TR/α = 1.21ms/3ms/45°; slice thickness: 8mm; in plane resolution: 1.4 x 1.4mm^2; FOV: 360 x 280 mm^2).

To enable achievement of contrast steady-state, gadolinium was administered via infusion at a rate of 0.0011mmol/kg/min. The TI scout was repeated initially at 5-minute intervals until inversion time reached equilibrium as previously described (Flett et al. 2010). High-resolution 3D late gadolinium enhancement (LGE) imaging was then performed using a free-breathing, respiratory navigator and ECG-gated (in diastole) inversion recovery sequences as described in the individual result chapters.

3.2.4   MR-thermometry and dosimetry

MR-thermometry using the proton resonance frequency shift (PRFS) technique, which is sensitive to temperature changes in real-time was employed to enable real-time monitoring of tissue temperature during MR-guided ablation. To perform MR-thermometry, an ECG-triggered multi-slice single-shot echo planar imaging (EPI) sequence was used with spoiled gradient echo (TR/TE/α=50ms/17ms/60°, FOV=180×180mm^2, voxel size=1.6×1.6mm^2, slice

thickness=5mm, slice number=4, bandwidth=1565Hz/Px, GRAPPA factor=2, partial Fourier=0.75, orientation – short axis). Saturation slabs were used for reduced field of view imaging and inflow saturation to reduce blood signal (de Senneville et al. 2012). Reconstruction of temperature maps was performed offline using a customized multi-baseline approach extending the method previously proposed (Roujol et al. 2010) as follows: A look up table of co-registered MR-phase images was initially created and the MR-thermometry sequence was run for 20 heartbeats before each ablation. Images from the first heart beat served as the reference image. Non-rigid motion was then estimated between the reference and each subsequent magnitude image using an optical flow technique. Phase images were then registered to the reference position using the estimated motion fields. The registration was performed on the complex data instead of the phase images to prevent artifacts due to phase wrap. During ablation, each new phase image was registered to the reference, position as described above. The phase image from the lookup table that best matched the current registered phase image (i.e. minimal mean square error between pair-wise unwrapped phase images) was then selected and used for temperature estimation.

MR-dosimetry derived from MR-thermometry is a technique that can be used to provide a real-time accumulated thermal dose during radiofrequency energy delivery at the intended ablation point. Thermal dose (TD) mapping was calculated on a pixel-wise basis as follows as previously described (Toupin et al. 2017):

$$
TD = \begin{cases} \int_0^t 2(T(t)-43)dt & if \quad T(t) > 43°C \\ \int_0^t 4(T(t)-43)dt & if \quad T(t) < 43°C \end{cases}
$$

Where $T(t)$ represents absolute tissue temperature. Baseline temperature was approximated to 39°C. The thermal dose was considered as lethal when exceeding the equivalent thermal dose

at constant heating of 43°C for 240 seconds. To correct for thermal dose error induced by noise on temperature estimates, thermal dose maps were corrected on a pixel-wise basis as follows:

$$TD_{corr} = TD \cdot e^{-0.5(\ln(2) \cdot \sigma_T)}$$

Where TD_{corr} is the corrected thermal dose and σ_T is the temporal standard deviation of temperature estimates at baseline (measured from the first 20 measurements following the training thermometry step and before the heating process). Width and depth of lesion estimated from thermal dose mapping were measured from the middle slice containing the largest lethal dose area.

3.3 MR-EP Workflow

3.3.1 MR-compatible ablation catheter

A MR-compatible ablation catheter (Vision, Imricor, USA) was used in all animal studies. The catheter is designed to facilitate mapping, delivery of pacing stimuli and ablation lesions within a MRI environment. It contains a MR-conditional lumen with a deflectable tip to facilitate mapping and transmit RF current to the tip electrode for ablation. The shaft is 9Fr and the distal end contains a bipolar pair of tip and ring electrodes that can be used both for recording and stimulation. The electrodes are made out of gold to reduce artefact during MRI scanning (in comparison to conventional platinum). During catheter ablation, a conventional RF generator and a dispersive pad (indifferent electrode) is used in combination with the catheter. The tip electrode has irrigation holes for open loop irrigation of the ablation lesion site when connected to a conventional irrigation pump. The catheter incorporates a fibre optic temperature sensor that is embedded in the tip electrode. For catheter tip location in the MR environment, the

distal tip section of the catheter has two independent solenoid coils for receiving MR signal from the surrounding tissue. These coils are connected to the MR scanner via coax cable inside the catheter body. Additionally, the coax cable has in-line transformers to prevent unintended RF heating (Hilbert et al. 2016).

The catheter has a high-torque shaft with a deflectable tip section. Tip deflection is controlled at the proximal end by a hand-piece in which a piston slides; a thumb knob on the piston controls the piston travel. When the thumb knob is pulled back, the tip is deflected (curved). When the thumb knob is pushed forward, the tip straightens. The high torque shaft also allows the plane of the curved tip to be rotated to facilitate accurate positioning of the catheter tip at the desired site.

At the proximal end of the catheter, an irrigation input port with a standard luer fitting terminates from the open lumen. This irrigation port serves to permit the injection of normal saline to irrigate the tip electrode. During ablation, heparinized normal saline was passed through the irrigation lumen of the catheter and through the tip electrode, to irrigate and cool the tip electrode (Chubb et al. 2017).

3.3.2 *ADVANTAGE-MR electrophysiology recording system*

The Advantage-MR EP recording system allows the operator to perform a range of electrophysiology operations including pacing, ablation, recording of EGMs, data review and monitoring. It is split into three components - a patient interface module (PIM), a digital amplifier/stimulator (DAS) and a host computer workstation. The DAS resides inside the magnet room and connects the catheters to the workstation. It receives, filters and digitizes

the EGM signals, which are optically converted and transmitted to the workstation via a fibre optic cable. Uninterrupted high resistivity wires are used to transmit the EGM signals. The cables are filtered to reduce RF-induced heating and minimise artifacts due to RF-induced noise. The DAS also receives commands from the workstation (e.g. to act as a programmable stimulator) and provides a pathway to transfer ablation energy to the MR-compatible catheter via a standard ablation generator. The computer workstation is located in the scanner control room. It is able to display and record EGMs as well as demonstrate tip temperature data. In addition, it passes cardiac waveform data (e.g. EGM amplitude, local activation time) to the Monte-Carlo image guidance system for cardiac mapping (Mukherjee et al. 2018).

3.3.3   MR-EP Image guidance platform

A custom interventional cardiovascular magnetic resonance (iCMR) image guidance platform (Monte-Carlo, Siemens Healthcare, Erlangen, Germany) was used in this study. The application has the ability to load volumetric data from MRI scans, display multi-plane reconstructions (MPR) in 3 orthogonal planes and transfer segmentations of cardiac chambers derived from previous imaging or imaging acquired at the time of the EAM procedure. An automatic segmentation tool is incorporated within the software to ensure rapid image processing. During the MR-EP procedure, the MPR slices on the iCMR application can follow the tip of the actively tracked catheter to display 3D location of the catheter within the segmentations of the cardiac chambers as well as on the MPR images. The position of the actively tracked catheter is displayed following the implementation of a temporal smoothing algorithm that limits its excursion due to cardiac motion.

The software allows the imaging operator to start/stop sequences remote from the scanner console and configure parameters of each sequence on the MRI scanner. A MR-compatible

foot-switch is also available as part of the application to start or pause an interactive imaging sequence that the electrophysiologist can operate (e.g. to use MPRs to navigate the catheter to a region of interest). The mapping interface of the application allows for changes to the rendering style or colour of a loaded segmentation, as well as place markers in regions of interest (e.g. to highlight EGMs or mark sites of ablation). The iCMR application communicates directly with the Advantage EP Recording system to display recorded activation times and voltage amplitudes. Colour interpolation is used to display this data which is computed by a relaxation algorithm that takes the values on the mapping points as the fixed boundary condition and then performs a linear interpolation on the segmentation surface between these mapping points. These features enable the system to closely mimic that of a clinical EAM system whilst having additional capabilities to utilise imaging data for procedure guidance.

3.3.4   Real-time MR-EP procedure

All EAM studies were performed inside the MRI scanner without the use of fluoroscopy at any point. The left ventricle (LV), right ventricle (RV), left atrium (LA), right atrium (RA) and aorta were manually segmented from the 3D ECG-triggered whole heart bSSFP MRI dataset using the MITK-based platform. Image processing was performed during a 45-minute window following the completion of imaging studies and prior to the start of EAM. During this time, each animal remained inside the scanner in order to minimise translational changes due to subject movement between imaging and mapping. The 3D shells of each chamber were imported into the iCMR guidance platform and displayed using the 3D-whole heart dataset to act as a 'road-map' for mapping studies. The 3D segmentation of scar from the

LGE-MRI was also imported into the iCMR guidance platform and overlaid onto the 3D shell for the LV chamber.

A custom 9Fr, MR-compatible steerable catheter with a single gold 3.5mm tip and ring bipolar electrode (3.5mm inter-electrode spacing) and six circumferential open irrigation ports (Vision-MR, Imricor, Burnsville, MN, USA) was advanced into the LV cavity via retrograde aortic access. A number of modifications were implemented to the MR-compatible catheter from previous versions used in the atria (Hilbert et al. 2016; Chubb et al. 2017) to enable manipulation in the left ventricle - *Figure 3-1*.

Requirements for Ventricular Ablation	Catheter Improvements
Torque transfer within the ventricle	• Designed to navigate increasingly complex vascular pathways • Improved torque response to allow unencumbered rotation and deflection within the ventricle
Maneuverability within the ventricle	• Rigid tip length reduced from 25.4 mm to 16.4 mm
Handle Ergonomics	• Reduced handle diameter • Ergonomic deflection mechanism to deflect/straighten tip • Improved deflection forces
Return to neutral following deflection	• Implemented active return to neutral

Figure 3-1: 2nd generation MR-compatible ablation catheter

Changes made in the 2nd generation MR-compatible Vision, Imricor ablation catheter to enable retrograde aortic access and improved manoeuvrability within the left ventricle. Previous clinical studies published with the Imricor catheter were in patients with atrial flutter using a 1st generation catheter. Images courtesy of Mr Tom Lloyd (Imricor Medical Systems).

These changes enabled improved torque transfer within the ventricle, manoeuvrability and consistency of shape following deflection. The MR-compatible catheter has 2 solenoid micro-coils located 2mm and 11mm proximal to the ring electrode that enabled the location and orientation of the catheter to be detected in 3D space using a dedicated MRI active

tracking sequence. A custom-built MR-EP recording system (Advantage-MR, Imricor, Burnsville, MN, USA) consisting of a digital amplifier, stimulator and host workstation was used to record, display and analyse intra-cardiac electrograms as previously described (Mukherjee et al. 2018). A patient monitoring system suitable for use in the MRI environment (Invivo, Gainesville, Florida) was used to monitor a single lead ECG and invasive arterial blood pressure throughout the pre-clinical studies.

SECTION THREE:

EXPERIMENTAL

DATA

Statement of originality and candidate contributions:

The contrast steady-state technique described in this chapter was first described by Dr Andrew Flett as a non-invasive technique to quantify diffuse myocardial fibrosis (Flett et al. 2010). This technique was subsequently adapted by Dr John Whitaker (King's College London) to enable high resolution 3D LGE imaging with an extended scar acquisition window (manuscript under review).

In this chapter, I have applied the technique described by Dr John Whitaker in an independent cohort of animals to compare the performance of 3D LGE with contrast steady-state to standard clinical 2D LGE. I have performed my own analyses, presented and interpreted the data in my own words. For qualitative comparisons, Dr Adriana Villa (SCMR Level 3, Consultant Radiologist) (King's College London) performed an independent, blinded assessment of image quality as Reader 2 whilst I performed my own assessment of all images acquired as Reader 1.

In addition, I acquired the raw data to facilitate comparisons between multiple 3D LGE sequences in the experimental model, completed all data analyses and wrote the results in my own words. I obtained ethical approval to perform additional MRIs in patients with a history of arrhythmias (including VT) and recruited the patients, acquired images and performed all data analyses described in this chapter. Dr Radhouene Neji assisted with optimisation of the image protocols and acquisition of imaging in the animal datasets. For data analysis, Dr Sebastien Roujol provided the custom software (Mediacare) developed in Matlab (The Mathworks, Natick, MA, USA) and wrote the script to integrate calculation of scar entropy into the Matlab code.

4 High-resolution imaging of ventricular scar: head-to-head comparison of three late gadolinium enhancement (LGE) sequences in a porcine infarct model and application in a cohort of patients with ischaemic cardiomyopathy

4.1 Introduction

The use of cardiac MRI as an adjunctive tool to guide VT ablation is increasing (Mahida et al. 2017). Accurate determination of cardiac anatomy and scar distribution can aid in planning the access route for VT ablation, particularly when scar is intramural or epicardial (Bogun et al. 2009). Image integration of pre-procedural or intra-procedural imaging into the navigation system at the time of ablation, can also be used to define the extent and distribution of arrhythmogenic substrate, focus mapping efforts in regions of interest and potentially improve localisation of the target sites for ablation (Andreu et al. 2017).

The underlying rationale of scar characterisation by cardiac MRI to define target sites for VT ablation is based on the understanding that heterogeneous scar tissue, containing a mixture of normal myocardium and scar, results in slow conduction and represents the substrate for re-entrant VT. These target regions are often located within scar tissue or around scar border-zones. LGE-MRI can be used to index the spatial heterogeneity of necrotic myocardium through the application of signal-intensity based thresholds and classify tissue into infarct core (dense scar) and borderzone (heterogeneous or grey-zone tissue). The extent of heterogeneous tissue, quantified from LGE-MRI, has been related to all-cause mortality in patients with ischaemic cardiomyopathy (Yan et al. 2006) and inducibility of monomorphic VT (Schmidt et al. 2007).

Heterogeneous tissue may have intermediate signal intensities (between that observed in normal myocardium and dense scar) which could be related to the partial volume effect whereby in a given voxel, a mixture of infarct tissue and normal tissue will result in a signal intensity that is an average of the two tissue types. Alternatively, at an interface between infarct and viable myocardium, a region of intermediate signal intensity may be present. During clinical imaging, the spatial resolution of LGE-MRI is frequently >1.5mm in-plane with a slice thickness between 6-10mm. In these scenarios, the partial volume effect can significantly overestimate the peri-infarct borderzone and reduce the accuracy of identification of ablation target sites compared to imaging with a sub-millimetre spatial resolution (Schelbert et al. 2010).

An additional factor that could impact on the signal intensity of heterogeneous tissue is variability in the wash-in and wash-out kinetics of gadolinium within the infarct region and borderzone tissue. Depending on the degree of microvascular damage and remaining capillary perfusion near an infarct borderzone, the wash-out kinetics of gadolinium may vary leading to a higher signal intensity compared to normal myocardium but lower than that of dense scar (Kim et al. 1996; Schmidt et al. 2007).

In order to accurately identify the scar areas critical for re-entry VT circuits, high-resolution 3D imaging is required. Furthermore, isotropic 3D imaging (resolution which is identical in all dimensions) can detect smaller regions of scar and enable multi-planar reconstruction to facilitate visualisation of 'channels' of slow conduction and ablation target sites (Basha et al. 2017). The major limitation of 3D high-resolution isotropic LGE imaging is prolonged scan times during which temporal changes in contrast kinetics can lead to artifacts due to difficulties in nulling healthy myocardium (Basha et al. 2017). Although image acceleration

techniques such as compressed sensing can be used to reduce scan times, recovery of images with under-sampled data can lead to additional artifacts and amplify noise leading to low signal-to-noise ratios (Otazo et al. 2010).

Following delivery of a bolus of gadolinium contrast, there is a reduction in the TI of the blood pool and myocardium which gradually recovers over time. After a period of around 20-30 minutes, an upward drift in the TI results in sub-optimal nulling of healthy myocardium which therefore limits the window during which LGE imaging can be optimally performed. In a seminal study, (Flett et al. 2010) described a method to quantify diffuse myocardial fibrosis using a bolus of gadolinium followed by a slow continuous infusion to achieve blood-myocardium contrast equilibrium. This was then followed by a blood test to measure the volume of distribution of contrast. Recently, (Whitaker et al. unpublished data) adapted this technique using a continuous infusion of contrast to achieve steady-state during LGE-MRI and establish a stable myocardial T1 time, enabling extended acquisition of high-resolution 3D imaging without significant changes in the TI of the blood pool and myocardium.

High-resolution LGE with contrast steady-state could allow detailed characterisation of scar architecture and heterogeneity which is necessary to permit identification of VT ablation target sites. In this chapter, the use of contrast steady-state LGE imaging is applied in an experimental animal model of myocardial infarction to compare 3D post-contrast sequences with consistent contrast distributions and in a cohort of patients with ischaemic cardiomyopathy to demonstrate feasibility of the technique in clinical practice. High-resolution ex-vivo MRI is used in the animal model to validate in-vivo imaging findings.

Qualitative and quantitative comparisons of the technique with conventional 2D LGE imaging is also performed in both the animal model and patients.

4.2   Methods

A porcine model of ischaemic cardiomyopathy was used to enable high-resolution imaging of ventricular scar using the contrast-steady state LGE protocol and systematically compare three 3D LGE techniques for assessment of scar and heterogeneous tissue. Two bright-blood 3D LGE sequences and one black-blood 3D LGE sequence were compared against each other to define the optimal technique for assessment of scar architecture and borderzone. Twelve male domestic pigs (weight 56.6 ± 5kg at the time of imaging) underwent a 180-minute occlusion of the mid left anterior descending artery as described in Section 3.1 followed by a 6-week recovery. All animals then underwent MR imaging in-vivo, followed by euthanasia, extraction of the heart and high-resolution ex-vivo imaging, as described below.

Ten patients with a known scar in the left ventricle underwent a cardiac MRI scan with an adapted contrast-steady state LGE protocol. Patients were recruited from an 'Ablation' MRI list at our institution whereby patients have a pre-procedural MRI prior to a catheter ablation procedure (AF/ PVC or VT ablation). Following demonstration of LV scar, patients were invited back for a research MRI study to undergo the adapted contrast-steady state protocol. In this cohort, 2 patients had a history of sustained VT whilst the remaining patients had either frequent PVCs or AF. The presence of LGE in patients with a history of AF was felt to be likely due to a previous thromboembolic infarct rather than an acute plaque rupture event. As a result, the patient cohort did have a history of arrhythmias but is not reflective of a typical ischaemic cardiomyopathy cohort.

Ethical approval was granted by the local institutional review board (17/LO/0150). Both standard clinical 2D LGE as well as high-resolution 3D LGE imaging were performed after establishment of contrast steady-state.

4.2.1 *Magnetic resonance imaging protocol in porcine model*

All MR imaging was performed on a 1.5T scanner (MAGNETOM, Aera, Siemens Healthcare, Erlangen, Germany). In the animal model, an assessment of LV function was made using cine imaging performed at end-expiration using a standard multi-slice balanced steady state free precession (bSSFP) technique. An ECG-triggered, 3D whole-heart bSSFP acquisition with a 1D diaphragmatic navigator was performed for cardiac chamber segmentation as described in Section 3.2.1. The following parameters were applied: transverse slice orientation, AP phase encoding, 1.25×1.25 mm^2 in-plane resolution, 256×256 in-plane matrix size, 2.5 mm acquired slice thickness reconstructed to 1.25mm, typically around 100 slices to cover the whole heart, TR/TE = 3.7/1.64 ms, flip angle = 90°, readout bandwidth (per pixel) = 592 Hz, fat suppression, GRAPPA acceleration factor = 2.

A bolus of gadolinium contrast (Gadovist, Bayer, Berlin, Germany) at 0.1mmol/kg was then administered. After a period of 10 minutes, a standard 2D LGE scan was performed during end-expiration using a phase-sensitive inversion recovery (PSIR) sequence with the following parameters: bSSFP read-out, 8 short-axis slices, 1.40×1.40 mm^2 in-plane resolution, 8.0 mm slice thickness, TR/TE = 3/1.21 ms, flip angle = 45°, FOV = 360x281mm^2, Pixel bandwidth = 780 Hz/Px. The inversion time (TI) to optimally null normal myocardium was determined using a standard TI scout sequence acquired in a mid-ventricular, short-axis slice during free-breathing, prior to the 2D LGE scan, with the following parameters: bSSFP read-out, 1.80×1.80 mm^2 in-plane resolution, 6.0 mm slice

thickness, TR/TE = 2.6/1.1 ms, flip angle = 55°, FOV = 340 x 276mm^2, Pixel Bandwidth = 1095 Hz/Px.

Following completion of the standard 2D LGE scan, a slow infusion of gadolinium contrast was initiated at a rate of 0.0011mmol/kg/min as previously described (Flett et al. 2010; Whitaker et al. unpublished data). The TI scout sequence was repeated at 3-5 minute intervals to measure the blood and myocardial TI until a steady-state was achieved. Steady-state was maintained for up to 3 hours in each animal to permit the acquisition of multiple 3D isotropic LGE sequences under consistent contrast conditions. Three LGE sequences (bSSFP and GRE read-outs and a black-blood LGE sequence) were then acquired sequentially as follows in 6/11 animals:

1. 3D bSSFP IR LGE - ECG triggered, respiratory navigator-gated, bSSFP read-out, coronal orientation, spatial resolution = 1.2 x 1.2 x 1.2 mm^3, TR/TE = 3.6/1.58 ms, flip angle = 90°, FOV = 400 x 257 x 96 mm^3; Pixel Bandwidth = 930 Hz/Px, 2 R-R interval; GRAPPA acceleration factor = 2; trigger delay = subject-specific determined from a breath-held 2D cine coinciding with the mid-diastolic rest period - acquisition window ranging from 100 to 125ms.

2. 3D GRE IR LGE - ECG triggered, respiratory navigator-gated, GRE read-out, coronal orientation, spatial resolution = 1.2 x 1.2 x 1.2 mm^3, TR/TE = 5.3/1.87 ms, flip angle = 20°, FOV = 380 x 380 x 92 mm^3; Pixel Bandwidth = 365 Hz/Px, 2 R-R interval; GRAPPA factor = 2; trigger delay = subject-specific determined from a breath-held 2D cine coinciding with the mid-diastolic rest period - acquisition window ranging from 100 to 125ms.

3. 3D BOOST LGE (Bright-blood and black-blOOd phase sensiTive inversion recovery sequence) - this sequence exploits alternating T_2-prep-IR and T_2-prep modules to acquire two interleaved bSSFP bright-blood datasets. The T_2-prep acquisition is used as the reference dataset for phase computation and a complimentary, co-registered black-blood LGE PSIR is reconstructed as previously described (Ginami et al. 2017). Prior to data acquisition, a low-resolution 2D image-based navigator (iNAV) is acquired at each heart beat to enable beat-to-beat 2D translational respiratory motion estimation and compensation to achieve 100% scan efficiency leading to predictable scan times compared to diaphragmatic navigator gated sequences with the same acquisition parameters. Image parameters for the 3D BOOST LGE sequence were as follows: ECG triggered, image-navigated, coronal orientation, spatial resolution = 1.2 x 1.2 x 1.2 mm^3, TR/TE = 4.7/1.47 ms, flip angle = 90°, T_2-prep duration = 40ms, FOV = 320 x 320 x 100 mm^3, Pixel Bandwidth = 990 Hz/Px, right-left phase encoding, trigger delay = subject-specific determined from a breath-held 2D cine coinciding with the mid-diastolic rest period - acquisition window ranging from 100 to 125ms. A dedicated 2D BOOST TI scout was acquired prior to acquisition of the 3D LGE sequence. This consisted of a magnetisation-prepared cine sequence where an alternate T_2-prep IR module (odd heartbeats) and T_2-prep module alone (even heart beats) is performed during alternate heartbeats as previously described (Ginami et al. 2017). The optimal TI to null the blood pool was determined from the cine frames acquired during odd heartbeats (T_2-prep IR portion of the sequence).

Following completion of in-vivo imaging, animals were recovered. One week later, ex-vivo studies were performed to validate in-vivo imaging findings. An additional dose of gadolinium contrast (Gadovist, Bayer, Berlin, Germany) at 0.2mmol/kg was administered 10

minutes prior to death of the animal. Rapid intravenous injection of potassium chloride (20mL 10% KCl) was administered to arrest the heart in diastole. The chest cavity was opened and blunt dissection used to extract the heart. Each heart was rinsed in 0.9% normal saline. In order to prevent collapse of the LV, each heart was filled with kinetic sand to maintain the shape of the LV cavity - *Figure 4-1*.
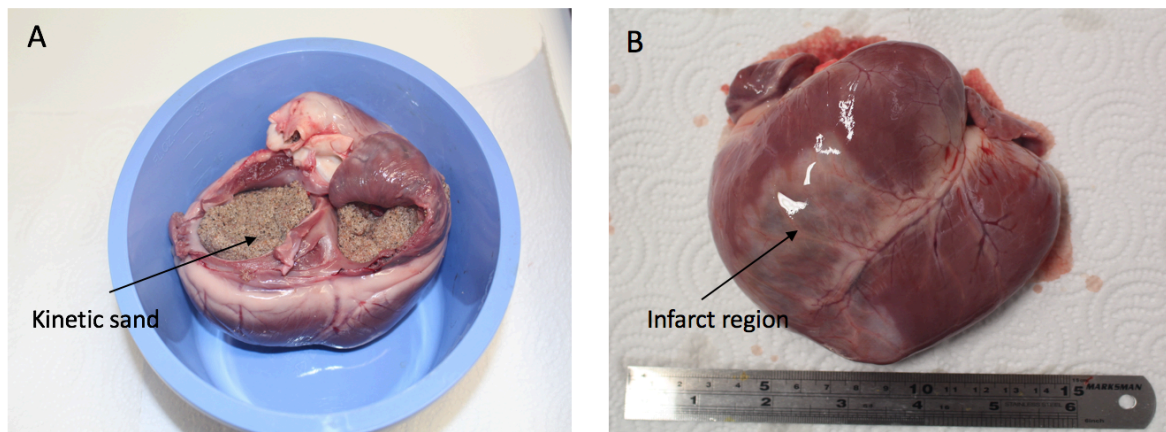
Figure 4-1: Preparation of hearts for ex-vivo imaging.

The LV and RV cavities have a tendency to collapse when removed from the thoracic cavity. In order to maintain the shape of the ventricles during ex-vivo imaging, kinetic sand was used to fill both cavities, preventing collapse (A) and maintaining their shape (B).

Each heart was then submerged in a bath of 0.9% normal saline and ex-vivo imaging performed within 1 hour of euthanasia. A high-resolution 3D T1-weighted spoiled gradient echo sequence was used for ex-vivo imaging with the following parameters: spatial resolution - 0.4 x 0.4 x 0.4 mm^3, TR/TE = 5.4/ 11.2 ms, flip angle = 20°, Pixel Bandwidth = 130 Hz/Px, FOV = 150 x 150 x 100 mm^3.

4.2.2   Magnetic resonance imaging protocol in patients

An adapted CMR protocol was used to enable application of contrast steady-state in patients with ischaemic cardiomyopathy - *Figure 4-2*. Imaging was performed on a 1.5T scanner (MAGNETOM, Aera, Siemens Healthcare, Erlangen, Germany). Each patient was

cannulated and had a single bolus of contrast (0.1mmol/kg) administered prior to entering the scanner. Standard planning scans (localiser, 2-chamber, 4-chamber, short-axis) were acquired followed by commencement of a slow infusion of gadolinium at a rate of 0.0011 mmol/kg/min within 15 minutes after the initial bolus of contrast. Standard 2-chamber, 3-chamber, 4-chamber views and a short-axis stack were then acquired. A TI scout was then repeated until the blood and myocardial TI demonstrated <5% variability and steady-state was achieved. A 2D multi-slice, breath-hold, clinical LGE (bSSFP, PSIR) sequence was performed with the following parameters: TR/TE = 6.0/1.2 ms, flip angle = 45°, in-plane resolution = 1.4 x 1.4 mm, slice thickness = 8 mm, pixel bandwidth = 780Hz/Px, FOV = 292 x 150 mm^2. A 3D isotropic bSSFP IR LGE sequence was then performed whilst contrast steady-state was maintained with the following parameters: ECG triggered, respiratory navigator-gated, coronal orientation, spatial resolution = 1.2 x 1.2 x 1.2 mm^3, TR/TE = 3.6/1.44 ms, flip angle = 90°, FOV = 400 x 260 x100 mm^3; Pixel Bandwidth = 1395 Hz/Px, GRAPPA acceleration factor = 2.
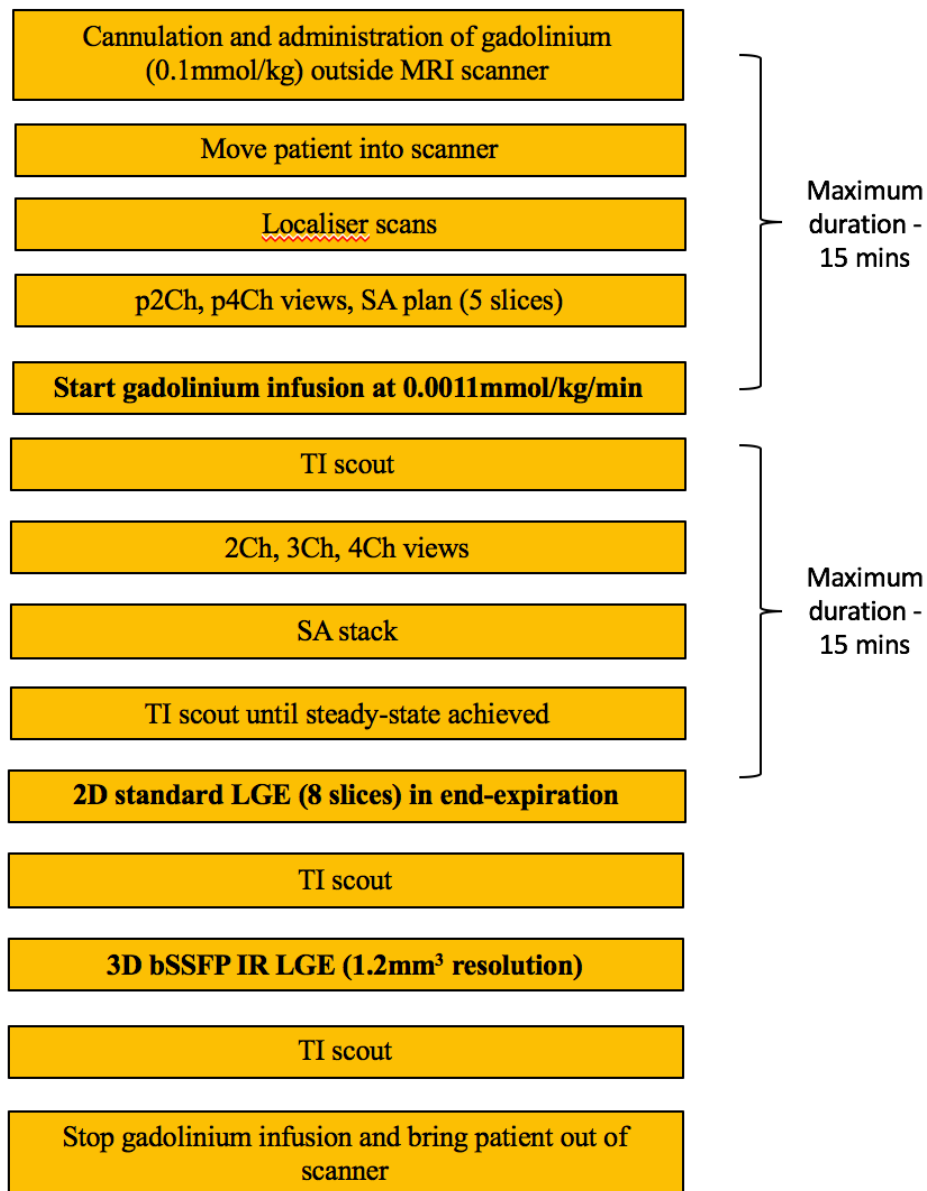
Figure 4-2: Imaging protocol for application of contrast steady-state to enable high-resolution imaging in patients with ischaemic cardiomyopathy.

A single bolus of gadolinium (0.1mmol/kg) is administered outside the scanner. Following localiser and planning scans, the slow infusion of gadolinium diluted in normal saline (0.0011mmol/kg/min) is commenced. Following achievement of steady-state, determined when the myocardial and blood pool TI has <5% variability during multiple TI scouts, the high-resolution 3D LGE sequence is commenced. Total contrast dose does not exceed 0.2mmol/kg at the end of the study.

4.2.3   Qualitative assessment of scar

All imaging datasets were anonymised and stored in a randomised order prior to qualitative assessment. Two independent readers (RKM and AV) graded images using a 5-point Likert scale on the following criteria: scar conspicuity relative to the LV cavity, scar conspicuity relative to adjacent myocardium, presence of artifacts and overall image quality. On this

scale, 0 represents non-diagnostic image quality, 1 = poor image quality, 2 = moderate, 3 = good, 4 = excellent image quality. For lesion conspicuity, 0 = not able to differentiate, 1 = poor differentiation, 2 = moderate differentiation, 3 = good differentiation, 4 = excellent differentiation. For the presence of artifacts, 0 = no artifacts, 1 = minor artifacts, 2 = moderate artifacts, 3 = high artifact level, 4 = non-diagnostic. For transmural scar extent a 4-point scale was used with 0 = 0-24%, 1 = 25-49%, 2 = 50-74%, 3 = 75-100%.

4.2.4   Quantitative assessment of scar

Signal-to-noise (SNR) and contrast-to-noise (CNR) ratios were calculated for the clinical 2D LGE and 3D bSSFP IR LGE sequences in both the animal model and patients. Images were analysed off-line on a OsiriX workstation (www.osirix-viewer.com). SNR and CNR were quantified using the mean signal intensities (SI) within a circular region of interest (ROI) drawn manually within scar, blood pool, and myocardium. An additional ROI positioned within the lungs was used to calculate the background noise intensity and noise standard deviation. For SI_{scar}, a circular ROI was placed encompassing the infarct region (range of ROI size = $50mm^2$ - $250mm^2$ depending on infarct size). $SI_{myocardium}$ was determined from adjacent non-infarct tissue within the same slice. SI_{blood} was determined using a $200mm^2$ circular ROI in the LV blood pool whilst a $200mm^3$ ROI was used for estimation of background noise standard deviation in the lungs.

The LV endocardium and epicardium was manually segmented within a custom software (Mediacare) developed in Matlab (The Mathworks, Natick, MA, USA). Quantification of core infarct and borderzone tissue volume was made through automatic application of the full width at half maximum (FWHM) and 35-50% of maximal pixel signal intensity thresholds respectively to segmentations.

4.2.5 Entropy evaluation

Tissue entropy was used as a parameter derived from LGE imaging to evaluate tissue

heterogeneity independent of signal intensity thresholds. Entropy is a statistical measure of

randomness that can be used to characterise the texture of an image. The underlying

assumption is that regions with varying signal intensity values within scar may represent

tissues of different compositions. A narrow signal intensity distribution suggests low entropy

whilst a wide distribution suggests high entropy. A histogram distribution of pixel signal

intensities with each LGE sequence was created in Matlab with each histogram divided into

256 equidistant bins. The endocardial and epicardial segmentations were applied to each

sequence to quantify entropy across the LV myocardium. The number of pixels within each

bin was counted and entropy (*H*) calculated using the following formula:

Equation 4: Entropy calculation: $\mathbf{H = -\sum(p.*ln2(p))}$

Where $\sum$ = sum; p = normalised histogram counts

The signal intensity (SI) values across subjects and sequences were normalised to a range

between 0 - 1024 in order to avoid SI variation between sequences and subjects from

influencing the results.

4.2.6 Statistical analysis

Statistical analyses were performed using GraphPad PRISM Version 7.0 (GraphPad Inc, CA,

USA) or SPSS (v24, IBM Corporation, New York, USA). All data was screened using

skewness and kurtosis tests and the normality of distribution assessed using the Shapiro-Wilk

test. Qualitative data are reported as means and quantitative continuous data expressed as

mean ± SD. On qualitative analysis, inter-observer variation was evaluated using weighted kappa statistics with extent of agreement rated as follows: $K \geq 0.81$ = excellent; $K = 0.61 - 0.80$, good; $K = 0.41 - 0.60$, moderate; $K < 0.40$ = poor. Statistical significance of kappa values was assessed using a z-statistic. Different sequences were compared using a paired t-test, Wilcoxon matched-pairs signed rank test or a repeated-measures analysis of variance test. Non-parametric ordinal data between two or more groups were compared using a Kruskal-Wallis test. Tukey post-hoc test was used for multiple comparisons. A level of $p < 0.05$ was considered statistically significant, unless otherwise stated.

4.3   Results

Twelve pigs underwent successful balloon occlusion of the mid left anterior descending artery and were subsequently recovered - *Figure 4-3*. One pig died post-MI during MR scanning and did not complete the imaging protocol. In eleven pigs, 2D LGE, 3D bSSFP IR LGE and ex-vivo imaging was successfully acquired with the in-vivo imaging performed during contrast steady-state - *Figure 4-4*. In six of these pigs, three high-resolution 3D LGE sequences (bSSFP, GRE, BOOST) were acquired during contrast steady-state at the same spatial resolution - *Figure 4-5*.
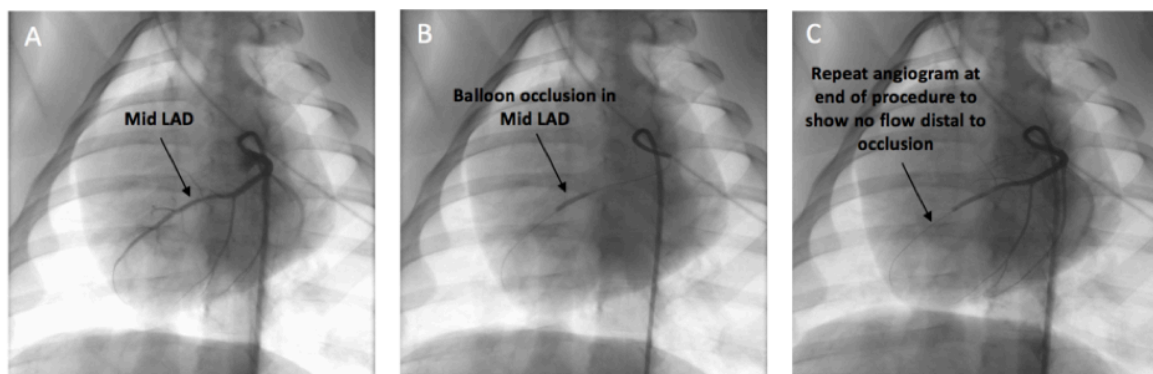
Figure 4-3: Coronary angiograms

Coronary angiograms acquired pre-occlusion (A), during balloon inflation in the mid left anterior descending artery (B) and at the end of the procedure demonstrating no flow distal to occlusion (C).
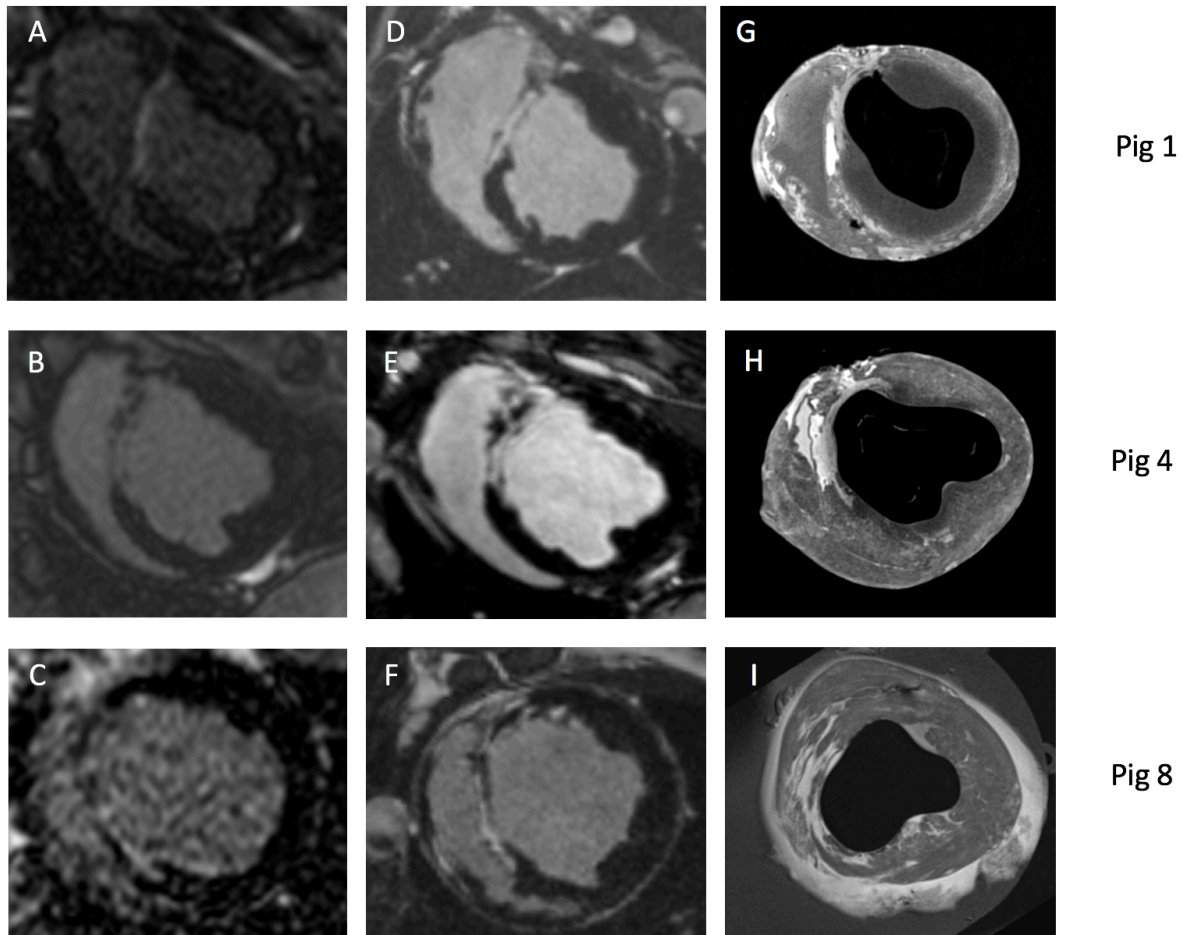
Figure 4-4: Representative LGE and ex-vivo images

Representative slices from three animals demonstrating regions of scar obtained during 2D LGE (A-C), 3D bSSFP LGE (D-F) and ex-vivo imaging (G-I).
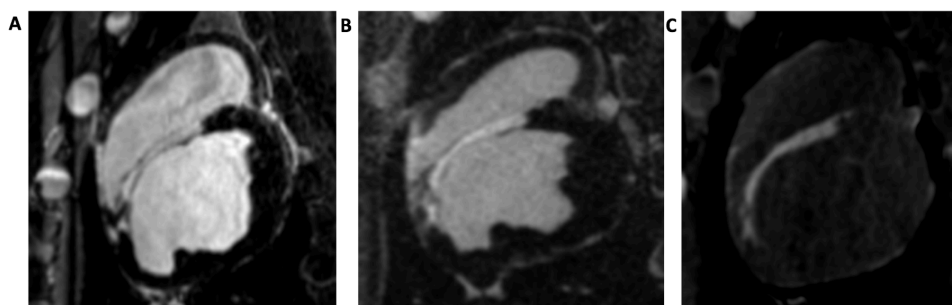
Figure 4-5: Representative images from three LGE sequences

Representative examples of scar seen in the same animal, in the same slice position with the 3D bSSFP LGE (A), 3D GRE LGE (B) and 3D BOOST (C) sequences.

Contrast steady-state was successfully established for LGE imaging in all animals with a total contrast dose not exceeding 0.2mmol/kg - *Figure 4-6*. The mean variation in TI_{blood} and

TI$_{myocardium}$ was 6.5% and 4.8% respectively between the start and end of 2D LGE imaging whilst the mean variation during 3D LGE imaging was <2%. The mean scan duration during 2D LGE imaging was 6.1 ± 1.3 minutes. Mean scan duration during 3D bSSFP LGE, 3D GRE LGE and 3D BOOST were 46.7 ± 3.8, 52.1 ± 5.4 and 26.0 ± 1.2 minutes respectively - *Table 1*.

	2D LGE	3D bSSFP LGE	3D GRE LGE	3D BOOST
Scan duration (mins)	6.1 ± 1.3	46.7 ± 3.8	52.1 ± 5.4	26.0 ± 1.2
Variation in TI$_{blood}$ between start and end of imaging sequence (%)	6.5 ± 5.0	1.2 ± 2.4	0.44 ± 0.76	0.45 ± 0.60
Variation in TI$_{myocardium}$ between start and end of imaging sequence (%)	4.8 ± 4.2	2.0 ± 3.0	0.39 ± 0.67	0.40 ± 0.54

Table 1: Scan durations and variation in TI of the blood pool and myocardium between the start and end of LGE imaging.
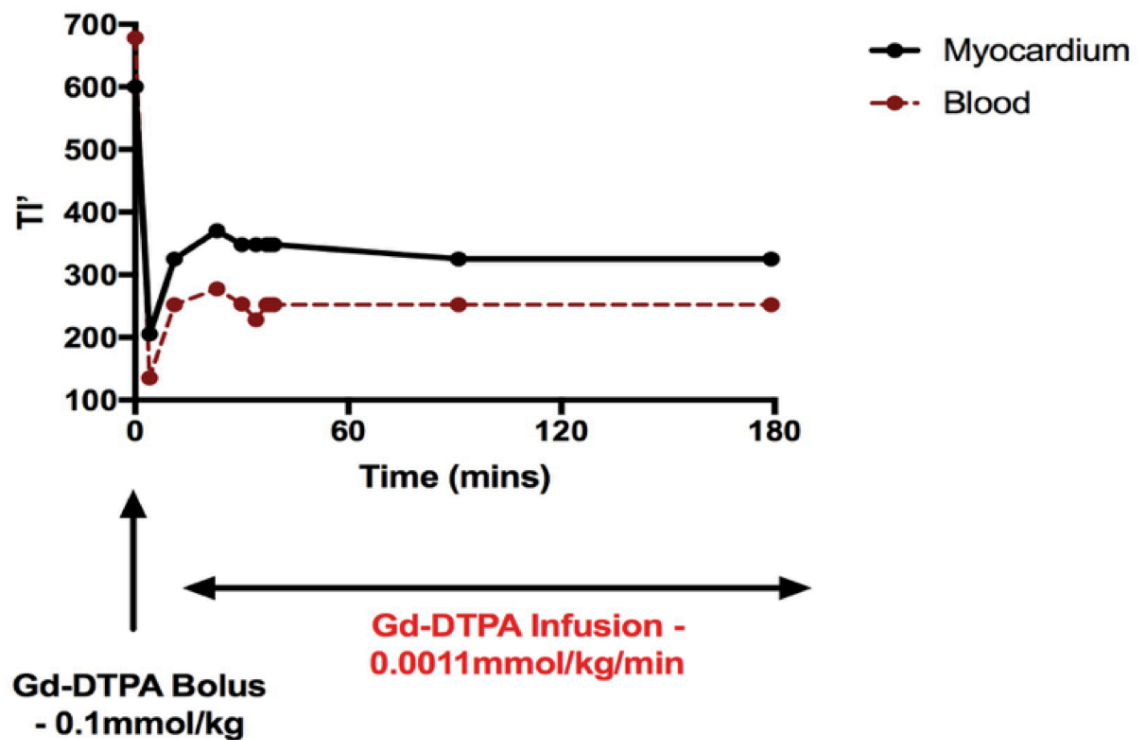
Figure 4-6: Establishment of contrast steady-state

Representative blood and myocardial TI following a bolus of contrast and during a continuous infusion in a pig. Continuous infusion of contrast with steady-state was maintained for up to 180 minutes facilitating extended LGE imaging during consistent contrast conditions.

Ten patients with ischaemic cardiomyopathy were scanned as part of the study protocol. No patients had an implanted device in-situ. One patient was unable to complete the protocol due to a long scan time during 3D imaging and was excluded from the analysis. One patient developed acute kidney injury (AKI) 72 hours after undergoing the contrast steady-state protocol. This patient also underwent a VT ablation during this 72-hour period and had multiple episodes of haemodynamic compromise requiring DC cardioversion during the procedure. He also developed a significant femoral haematoma post-procedure with a >2g/dL drop in haemoglobin. Given these additional factors, it was felt that the contrast steady-state protocol was not responsible for the development of AKI but was reported as a serious adverse event (SAE) to the ethics committee but no change in study protocol was recommended. Patient characteristics are displayed in *Table* 2. The mean acquisition time to

complete the scan protocol was 89.8 ± 4.5 minutes whilst the mean acquisition time for the

3D bSSFP LGE sequence was 49.0 ± 3.5 minutes. Representative images acquired using the

2D LGE and 3D bSSFP LGE sequences are shown in - *Figure 4-7*.

Patient number	Age	Gender	Pathology	LVEF (%)	Rhythm during scan
1	79	Male	ICM	38	Sinus with occasional PVCs
2	66	Female	Thromboembolic	45	Sinus
3	60	Male	Thromboembolic	44	Sinus
4	62	Male	Thromboembolic	42	AF
5	57	Male	Thromboembolic	36	AF
6	55	Male	Thromboembolic	40	AF
7	67	Male	ICM	27	Sinus with runs of slow VT
8	62	Male	Thromboembolic/ Possible DCM	43	AF
9	58	Male	Thromboembolic	39	AF

Table 2: Patient characteristics. The LVEF values reported may be underestimated in the context of scans performed when patients were in AF.

Patient 2
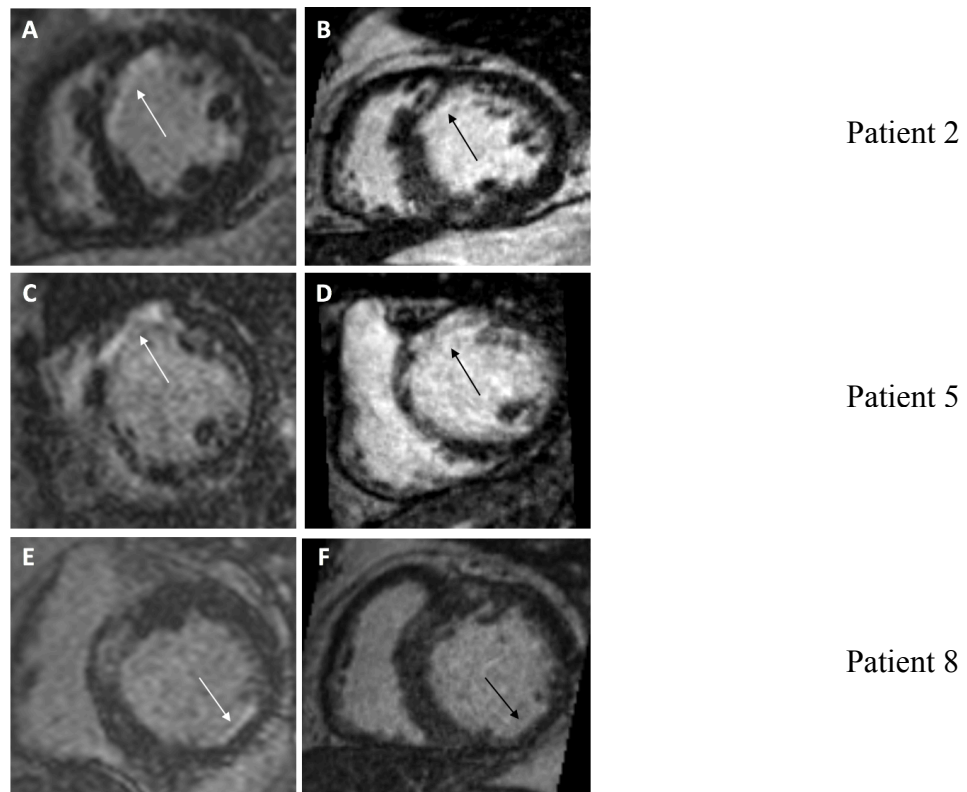
Patient 5

Patient 8

Figure 4-7: Representative LGE images in patients

Representative slices from approximately the same level in three patients demonstrating regions of scar obtained during 2D LGE (A,C,E), 3D bSSFP LGE (B,D,F). Arrows indicate location of scar. An area of possible mid-wall scar in the septum is also noted in Patient 8 raising the suspicion of underlying dilated cardiomyopathy.

4.3.1 Qualitative data analysis - animal study

On qualitative assessment of 2D LGE compared to 3D LGE, there was no difference in scar conspicuity relative to the LV cavity (1.9 vs 2.0; p=0.42) and assessment of transmural scar extent (2.5 vs 2.6; p=0.19). However, scar conspicuity relative to adjacent myocardium (2.0 vs 3.7; p<0.0001) and overall image quality (2.4 vs 3.9; p<0.0001) were significantly improved with 3D LGE imaging. There were significantly more artifacts with 2D imaging (2.3 vs 1.5; p<0.001).

On 3D LGE imaging, inter-rater agreement was moderate on assessment of scar conspicuity adjacent to normal myocardium (K = 0.56; p = 0.039) and presence of artifacts (K = 0.49; p = 0.06), whilst good agreement was present on assessment of transmural scar extent (K = 0.63;

p = 0.014) and overall image quality (K = 0.62; p = 0.026). Inter-rater agreement was poor on assessment of scar conspicuity relative to LV cavity (K = 0.10; p = 0.511). On 2D LGE imaging, inter-rater agreement was good on assessment of overall image quality (K = 0.81; p = 0.006) and transmural scar extent (K = 0.667; p = 0.011) whilst agreement on the presence of artifacts was moderate (K = 0.55; p = 0.009). Inter-rater agreement was poor on assessment of scar conspicuity relative to LV cavity and adjacent to normal myocardium, K = 0.13; p = 0.54 and K = 0.10; p = 0.46, respectively - *Figure 4-8*.
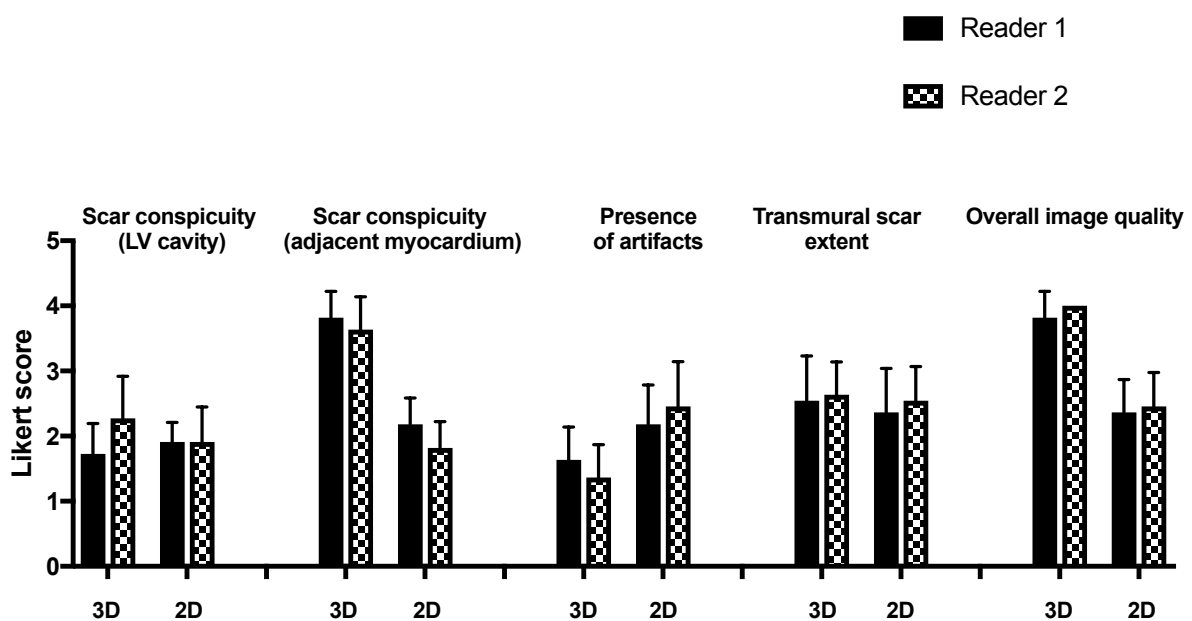
Figure 4-8: Qualitative assessment: 2D vs 3D LGE in animals

Qualitative assessment by 2D and 3D LGE techniques on assessment of scar, presence of artifacts and overall image quality. Mean Likert scores are displayed as assessed by 2 independent readers on a 4-point scale for assessment of scar transmurality and a 5-point scale for all other factors. Error bars represent standard deviation.

During qualitative comparison between the three 3D LGE sequences the BOOST sequence, relative to GRE and bSSFP, had improved scar conspicuity relative to the LV cavity (3.3 vs 2.2 vs 1.8; p<0.001). The bSSFP sequence, however, had improved scar conspicuity relative to adjacent normal myocardium (4.0 vs 3.5 vs 2.6; p<0.0001). The GRE sequence had a higher degree of artifacts whereas the BOOST sequence had the lowest degree (2.1 vs 1.4 vs 0.4; p<0.0001). There was no difference between the sequences on assessment of transmural

scar extent (bSSFP vs GRE vs BOOST = 2.5 vs 2.6 vs 2.6; p = 0.98). Overall image quality

was better with the bSSFP sequence compared to GRE and BOOST (3.6 vs 2.8 vs 2.6; p =

0.0029).

Inter-rater agreement on assessment of transmural scar extent was good to excellent between

bSSFP, GRE and BOOST (K = 0.67 vs 0.67 vs 1.00; p<0.05, respectively). Agreement on

overall image quality was good to excellent between bSSFP and GRE (K = 0.67 vs 1.00; p =

0.083) but poor on BOOST (K = 0.286; p = 0.361). Agreement on the presence of artifacts

was good to excellent between GRE and BOOST (K = 0.71 vs 1.00; p<0.05) but poor on

bSSFP (K = 0.182; p>0.05). Agreement on scar conspicuity relative to the LV cavity was

good on the BOOST sequence (K = 0.67; p=0.04) but poor on bSSFP and GRE (K = 0.28 vs

0.37; p>0.05, respectively). Agreement on scar conspicuity relative to normal adjacent

myocardium was excellent with bSSFP (K = 1.00; p<0.05), moderate with GRE (K = 0.41; p

= 0.014) and poor with BOOST (K = 0.17; p = 0.70) - *Figure 4-9*.
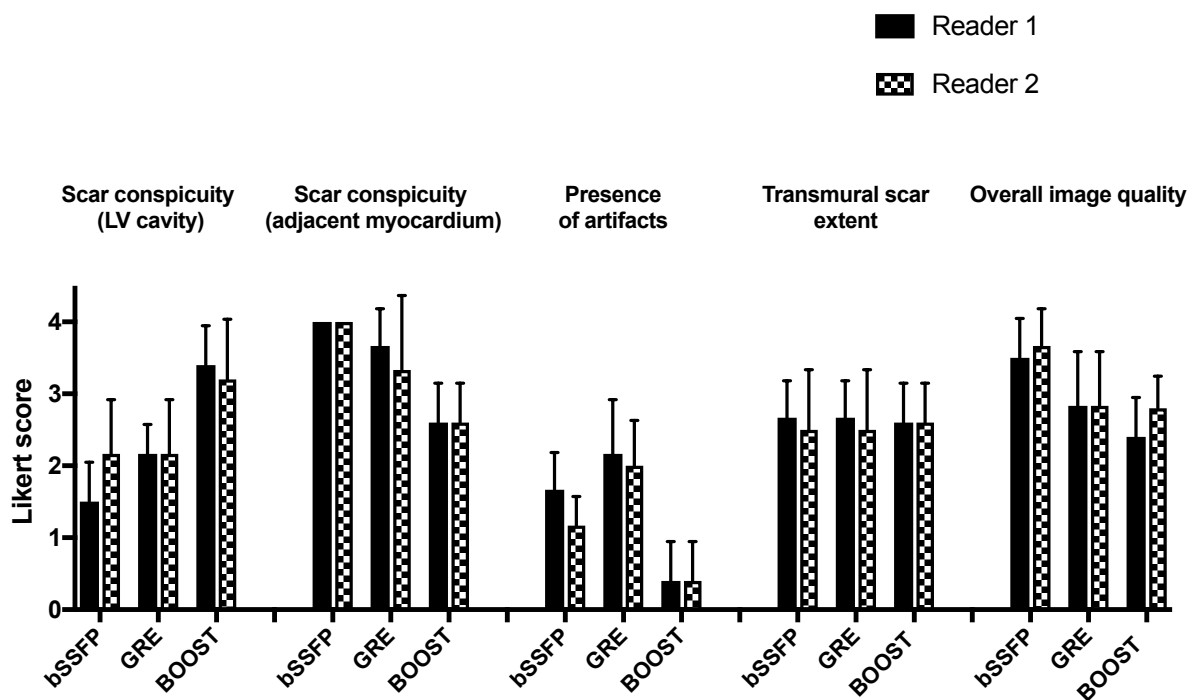
Figure 4-9: Qualitative assessment: three high-resolution 3D LGE sequences

Qualitative assessment of scar, presence of artifacts and overall image quality as assessed between 3 high-resolution 3D LGE sequences. Mean Likert scores are displayed as assessed by 2 independent readers on a 4-point scale for assessment of scar transmurality and a 5-point scale for all other factors. Error bars represent standard deviation.

4.3.2   Quantitative data analysis - animal study

On comparison of 2D vs 3D LGE imaging, the 3D bSSFP dataset provided a statistically significant improvement in the SNR_{scar} and SNR_{blood} (25.2 vs 9.5; $p<0.0001$ and 16.9 vs 10.4; $p = 0.01$, respectively) but not $SNR_{remote\ myocardium}$ (3.3 vs 2.9; $p = 0.28$). An improved CNR between scar and remote myocardium as well as scar and blood pool was also observed with the 3D bSSFP sequence (21.9 vs 6.6; $p<0.0001$ and 8.3 vs -0.9; $p=0.0011$, respectively) - *Figure 4-10.*
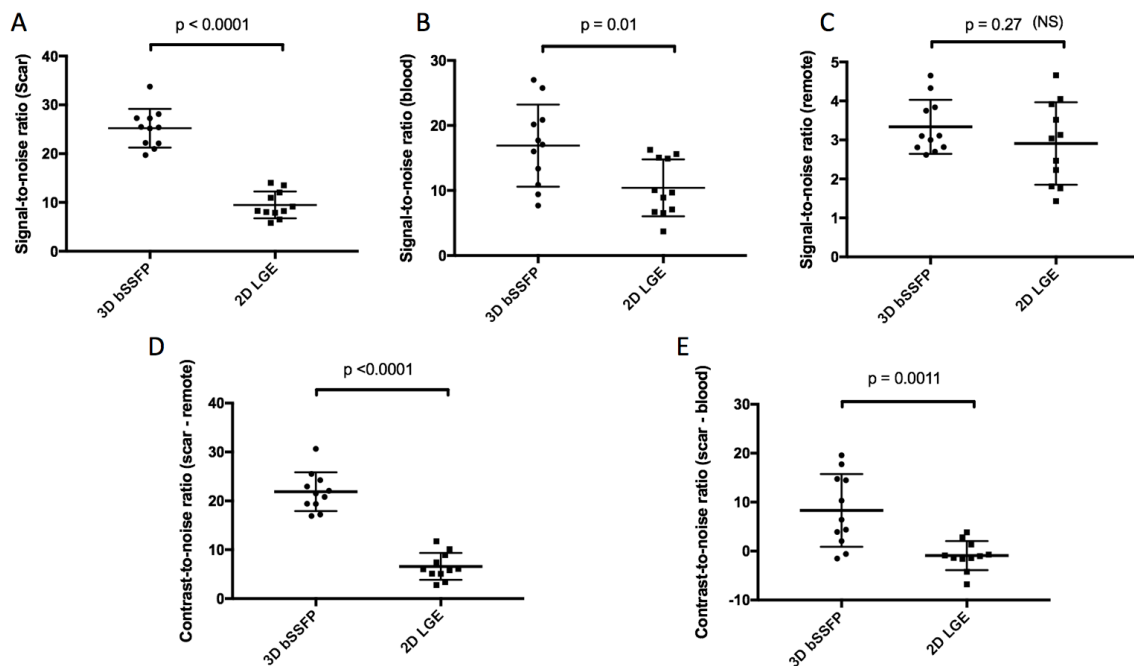
Figure 4-10: Quantitative analysis: SNR and CNR in animal study

Signal to noise ratio (SNR) in scar tissue, blood pool and remote myocardium between 2D and 3D bSSFP LGE and contrast to noise ratio (CNR) between scar and remote myocardium and scar and blood pool. N = 11 animals.

Dense scar volume (FWHM threshold) was not significantly different between 3D bSSFP LGE and high-resolution ex-vivo MRI ($p=0.90$) or between 2D LGE and 3D bSSFP

(p=0.09), however scar volume was significantly higher on 2D LGE vs ex-vivo MRI (p=0.04), likely related to overestimation of scar due to the partial volume effect. Borderzone tissue volume (35-50% maximal signal intensity threshold) was not significantly different between 3D bSSFP LGE and ex-vivo MRI (p=0.28) but was significantly higher with 2D LGE compared to 3D bSSFP (p=0.0033) and ex-vivo MRI (p<0.0001) - *Figure 4-11*.
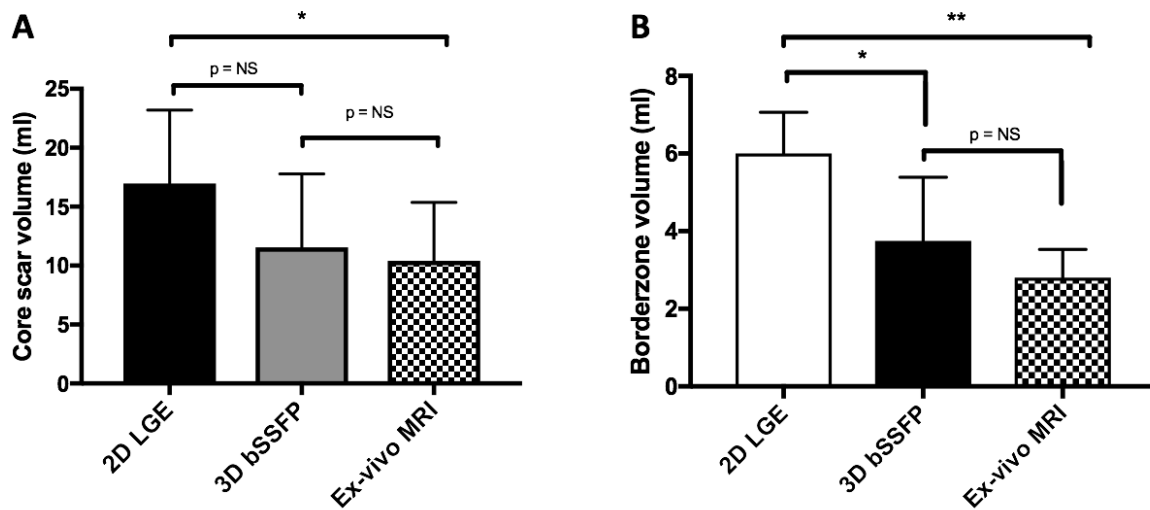
Figure 4-11: Core scar and borderzone volumes in animal study - 2D vs 3D vs ex-vivo MRI

Dense (core) scar (A) and borderzone tissue volume (B) as assessed using a 2D LGE, 3D bSSFP LGE and high-resolution ex-vivo MRI. N=11 animals. *p<0.05, **p<0.0001.

During comparison between the three, 3D LGE datasets and ex-vivo MRI, there was no significant difference in dense (core) scar volume (p=0.71) or borderzone tissue volume (p=0.64) - *Figure 4-12.*
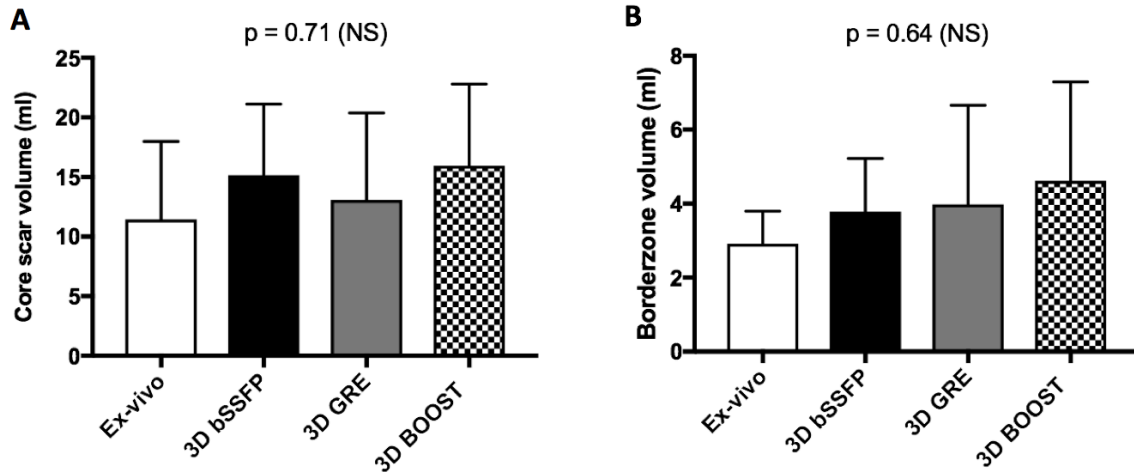
Figure 4-12: Core scar and borderzone volumes: three high-resolution 3D LGE sequences vs ex-vivo MRI

During high-resolution 3D LGE imaging under consistent contrast conditions, there was no difference in dense (core) scar volume (A) or borderzone tissue volume (B) between the bSSFP, GRE or BOOST sequences and ex-vivo MRI.

4.3.3   Mean entropy for assessment of scar heterogeneity - animal study

Mean entropy as a measure of tissue inhomogeneity was used to further evaluate the differences in scar seen with the 2D and 3D LGE sequences. A higher mean entropy was present on 3D bSSFP LGE compared to standard clinical 2D LGE in the same animals with the same scar (7.4 vs 4.8; p<0.0001) suggesting that calculation of scar entropy is sequence and spatial resolution dependent - *Figure 4-13.* A significant difference in mean entropy was also observed during comparison of the 3D bSSFP, GRE and BOOST sequences (p=0.0036). On multiple comparisons, there was no difference between the bSSFP and BOOST sequences (p=0.96) but a significantly higher entropy was observed when these sequences were compared to the 3D GRE (p=0.009 and p=0.007, respectively) - *Figure 4-14.*
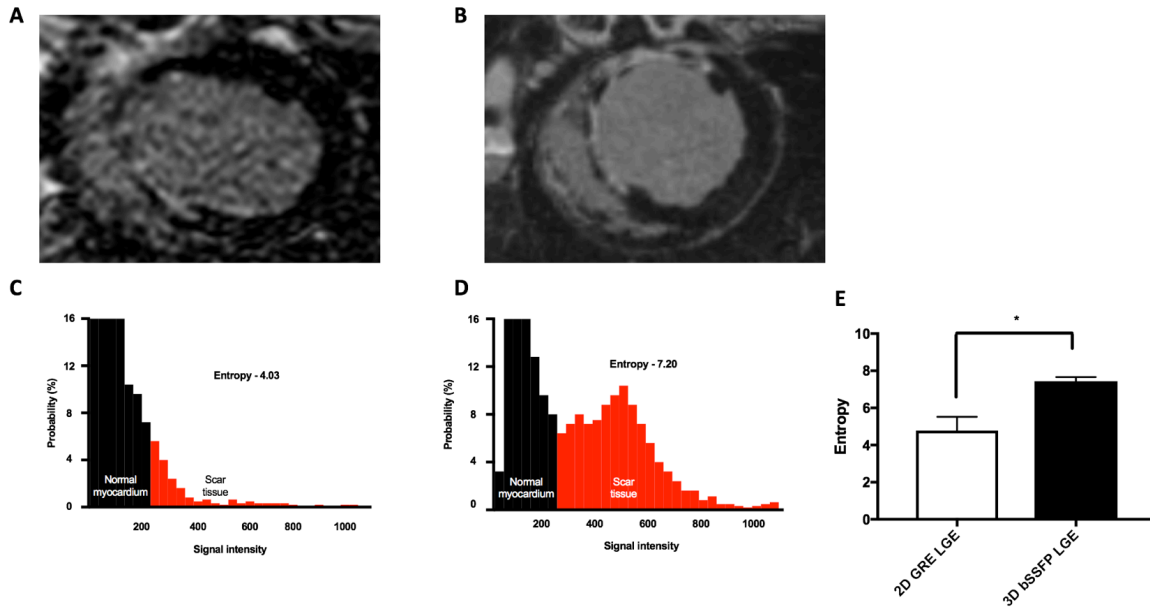
Figure 4-13: Mean entropy of scar - animal study - 2D vs 3D LGE

Mean entropy, as a quantitative marker of scar heterogeneity, was higher with 3D bSSFP LGE imaging compared to 2D LGE. Representative images of the same scar, in approximately the same slice position with 2D LGE (A) and 3D bSSFP LGE (B). Signal intensity histograms in the same animal with 2D LGE (C) and 3D LGE (D) and overall mean entropy in 11 animals (E).*p<0.0001.
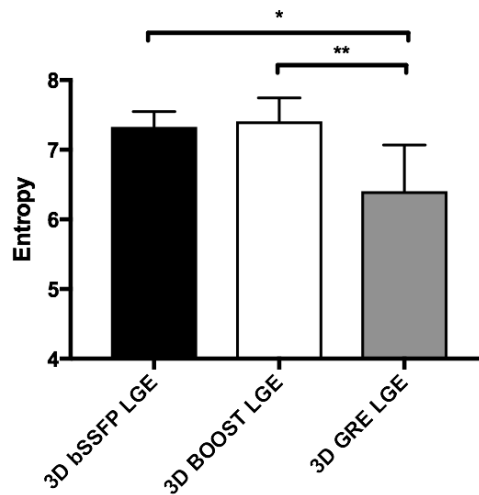
Figure 4-14: Mean entropy of scar - three high-resolution 3D LGE sequences

Mean entropy of scar using the 3D bSSFP, GRE and BOOST sequences. No difference in entropy was observed between the bSSFP and BOOST sequences but the GRE sequence had a statistically significant lower entropy compared to the remaining 3D sequences. *p=0.009; **p=0.007.

4.3.4 Qualitative data analysis - clinical study

Subjectively, in patients with ischaemic cardiomyopathy, scar conspicuity relative to LV cavity and overall image quality were improved with 3D bSSFP with contrast steady-state compared to 2D LGE (2.1 vs 1.6; p = 0.0039 and 2.1 vs 1.7; p=0.02). However, no differences were seen between 3D and 2D LGE on scar conspicuity relative to adjacent myocardium, presence of artifacts or transmural scar extent (2.3 vs 2.2; p=0.45 and 2.1 vs 2.4; p=0.21 and 2.3 vs 2.3; p=0.99, respectively).

Inter-rater agreement on assessment of scar conspicuity relative to LV cavity was moderate across 3D and 2D LGE imaging (K = 0.55 vs 0.41). Agreement on scar conspicuity relative to adjacent normal myocardium was good for 2D LGE (K = 0.79) but poor with 3D LGE (K = 0.23). Agreement on the presence of artifacts was poor across 3D and 2D imaging (K = 0.33 vs 0.27, respectively) whilst agreement on scar transmurality was moderate to excellent for 3D and 2D LGE respectively (K = 0.59 and 1.00). Agreement on overall image quality was poor for 3D imaging (K = 0.25) but moderate for 2D imaging (K = 0.60) - *Figure 4-15*.
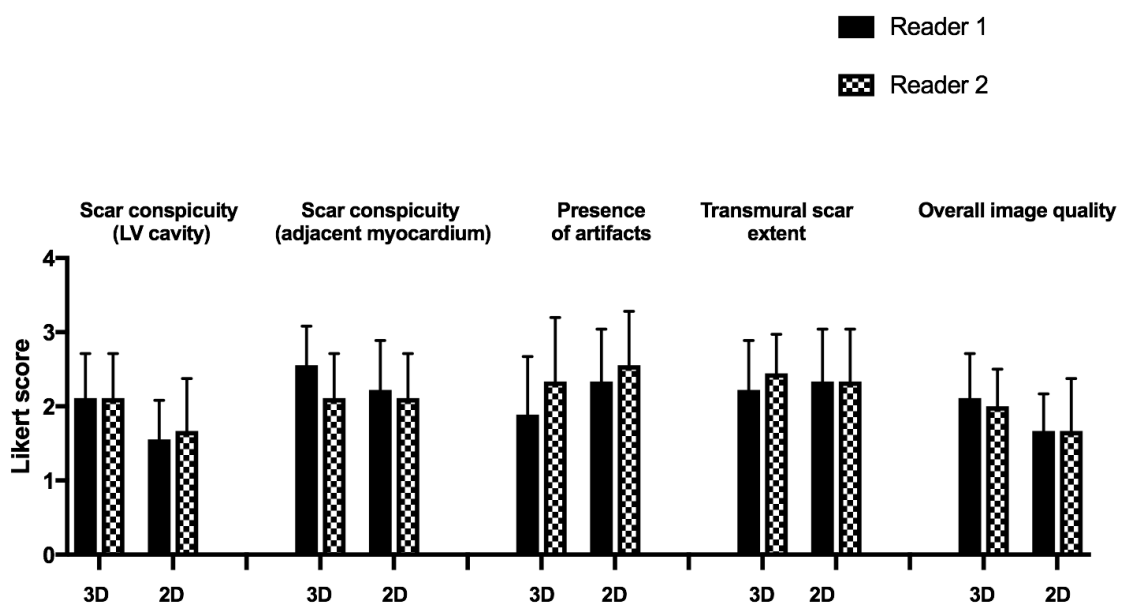
Figure 4-15: Qualitative analysis - clinical study

4.3.5   Quantitative data analysis - clinical study

On comparison of 2D vs 3D LGE imaging, in contrast to the animal studies, there was no difference in SNR_{scar}, SNR_{blood} or SNR_{remote} between sequences (p=0.13, 0.36 and 0.63, respectively). However, $CNR_{scar-remote}$ and $CNR_{scar-blood}$ was improved with 3D bSSFP LGE and reached statistical significance (p=0.032 and 0.046, respectively) - *Figure 4-16.* There was no significant difference in dense (core) scar volume (FWHM threshold) or borderzone tissue volume (35-50% maximal signal intensity threshold) between the sequences (p=0.48 and 0.38, respectively) - *Figure 4-17.*
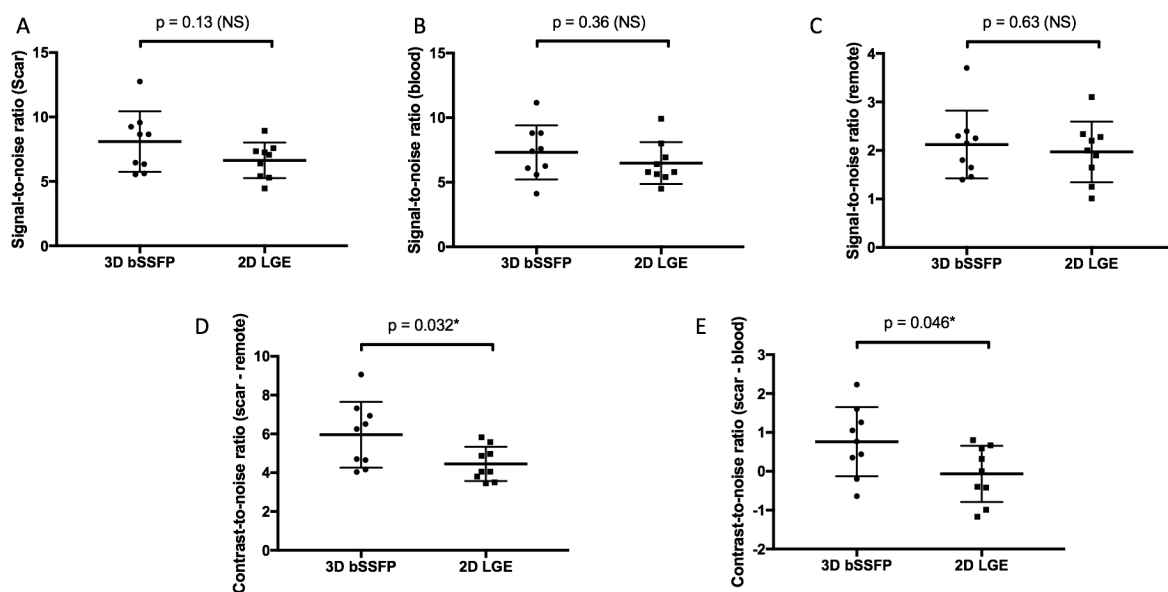
Figure 4-16: Quantitative analysis - clinical study - SNR and CNR

Signal to noise ratio (SNR) in scar tissue, blood pool and remote myocardium between 2D and 3D bSSFP LGE and contrast to noise ratio (CNR) between scar and remote myocardium and scar and blood pool in patients with ischaemic cardiomyopathy. N = 9 patients.
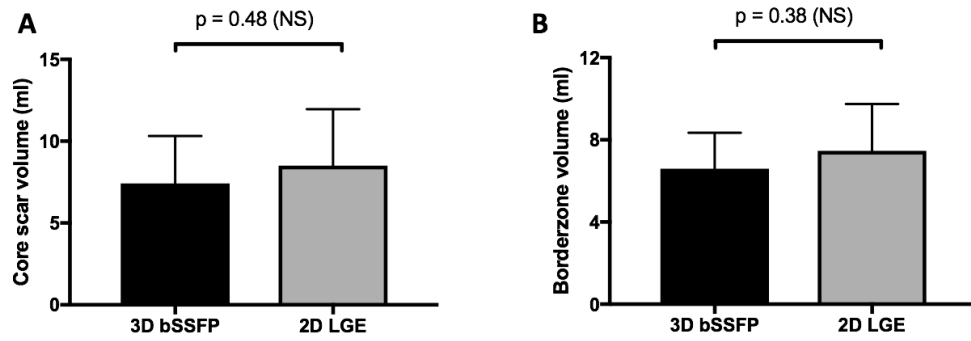
Figure 4-17: Core scar and borderzone volume - clinical study

Dense (core) scar and borderzone tissue volume as assessed using a 2D LGE, 3D bSSFP LGE in patients with ischaemic cardiomyopathy. N=9 patients.

4.3.6 Mean entropy for assessment of scar heterogeneity - clinical study

Mean entropy was significantly higher with 3D bSSFP LGE compared to 2D LGE, consistent with the animal data, however the magnitude of this effect was lower (6.0 vs 5.2; p=0.029) - *Figure 4-18.*
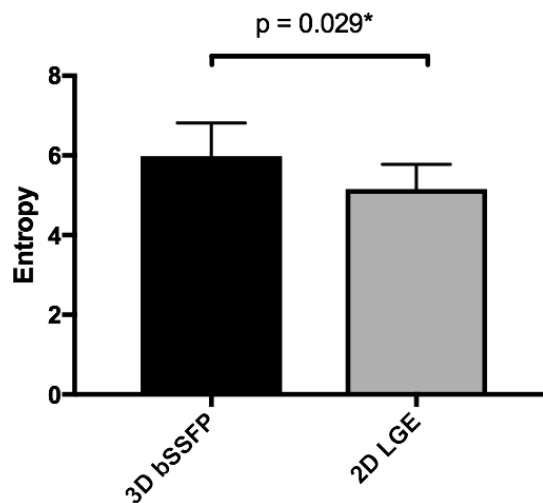
Figure 4-18: Mean entropy - clinical study

Mean entropy of scar using the 3D LGE and 2D LGE sequences in patients with ischaemic cardiomyopathy. A higher entropy value was observed with the 3D sequence, consistent with the results obtained in the animal study.

4.4   Discussion

The principle findings of this study are:

1. A slow infusion of gadolinium to maintain consistent contrast conditions enabled extended scar imaging and a direct head-to-head comparison between multiple 3D sequences.

2. In an animal model, high resolution 3D LGE during contrast steady-state resulted in improved image quality on subjective assessment, improved SNR, CNR and more accurate estimation of dense scar and borderzone tissue volumes compared to standard 2D LGE imaging.

3. The contrast steady-state protocol can be applied in patients but results in prolonged scan times whilst differences between 2D and 3D LGE acquisition modes were attenuated, compared to the animal model.

4. Mean entropy of scar as a measure of scar heterogeneity is dependent on sequence acquisition mode.

Although LGE-MRI has been extensively used for diagnostic purposes to characterise scar location and extent, conventional 2D LGE is of a low spatial resolution with a typical slice thickness of 8-10mm. The 'critical' substrate for re-entrant VT is surviving myocardium within an infarct zone which pathologically consists of surviving myocyte bundles interspersed by fibrous tissue resulting in anisotropic conduction (de Bakker et al. 1993). High resolution ex-vivo imaging has revealed that VT pathways are preferentially located in zones of infarct with a thickness <2mm suggesting that standard LGE techniques are of insufficient resolution to accurately identify surviving tissue (Pashakhanloo et al. 2018).

Furthermore, not all scar is arrhythmogenic and there has been interest in using MRI-derived parameters to discriminate arrhythmogenic from non-arrhythmogenic scar. These include scar borderzone (or gray-zone), transmurality of scar as well as scar complexity (entropy).

Assessment of scar borderzone and transmurality are signal intensity-dependent and increase in proportion to spatial resolution of the MRI sequence used due to partial volume averaging (Schelbert et al. 2010). Scar entropy estimation appears a promising technique for risk stratification of patients at risk for VT (Muthalaly et al. 2018; Gould et al. 2019; Androulakis et al. 2019) but has previously been investigated using standard 2D LGE sequences.

Given the technical challenges in detection of 'critical' regions of VT substrate, higher resolution 3D datasets may lead to improved identification of target areas. Previous studies using MRI to delineate the parts of scar required to sustain VT have mainly employed standard 2D LGE sequences to characterise imaging substrate with in-plane resolution ranging from 1.4 - 2.2 mm but with a slice thickness between 5-8mm (Gupta et al. 2012; Wijnmaalen et al. 2011; Perez-David et al. 2011). More recently, some investigators have used 3D imaging and reported an improved matching of 'conducting channels' to EAM with a 3D GRE LGE sequence compared to 2D GRE LGE and a 2D bSSFP LGE sequence (Andreu et al. 2015). In order to harness the power of MRI during real-time MR-EP, optimisation of LGE protocols to better visualise scar morphology is necessary. The optimal in-vivo LGE spatial resolution reported to date was 1.4mm^3 with a mean scan acquisition time of 16.4 ± 7.2 minutes (Andreu et al. 2015). Using the contrast-steady state protocol, an improved spatial resolution was achieved (1.2mm^3) in this thesis whilst maintaining the optimal TI for myocardial nulling.

4.4.1   2D vs 3D acquisition modes

On qualitative assessment, in both the animal model and patients, an improved overall image quality was reported on 3D vs 2D LGE. In addition, CNR between scar and normal myocardium and scar and blood pool were significantly improved with 3D LGE. A higher scar entropy was present with 3D LGE imaging highlighting the resolution-dependent nature

of entropy estimation. In the animal model, both core scar volume and borderzone tissue volume on 3D LGE more closely approximated the reference standard ex-vivo datasets compared to 2D LGE.

When high resolution 3D LGE with contrast steady-state was applied in patients, the magnitude of difference with 2D LGE was reduced on both qualitative criteria (scar conspicuity, presence of artifacts) and quantitative criteria (SNR in scar and blood pool, core scar/ borderzone tissue volume) resulting in no statistically significant difference in these parameters. These differences could be explained by a number of factors. The animal scans were performed during general anaesthesia with close control of the respiratory cycle and improved scan acquisition efficiency. In contrast, clinical scans were performed in conscious patients with greater variation in their respiratory cycles during prolonged acquisitions. Scan times were longer in patients with reduced acquisition efficiency. In addition, prolonged scan times could have led to patient discomfort and movement affecting overall image quality compared to animals under general anaesthesia. The majority of patients scanned (6 out of 9) experienced episodes of arrhythmia during 3D imaging including slow VT, PVC or atrial fibrillation which resulted in mis-triggering and could have affected image quality. In contrast, only 1 animal experienced an episode of arrhythmia (PVC) during 3D imaging. All animals scanned had received prior treatment with amiodarone and lignocaine (Section 3.1) which could have reduced the incidence of arrhythmias. Given the requirement of high resolution MRI sequences needing repeated cyclical cardiac events to ensure robust imaging, the use of premedication and/or DC cardioversion in patients who are not in sinus rhythm at the time of imaging, prior to ablation, needs further exploration.

4.4.2 Head-to-head comparison between 3D sequences

Direct head-to-head comparisons between multiple LGE sequences can be challenging due to contrast wash-out. In particular, 3D imaging can require prolonged scan durations and few comparisons have previously been made. (Viallon et al. 2011) reported improved image quality and CNR with a 3D GRE LGE technique compared to a 3D bSSFP LGE technique and multiple 2D techniques. However, spatial resolution of all sequences used were lower and did not always include full ventricular coverage compared to this thesis. The order of LGE sequences were randomised to prevent systematic errors due to a change in optimal TI over time. 3D imaging was performed during breath-holds instead of using a free-breathing protocol and isotropic 3D imaging was not performed.

In this thesis, the use of contrast steady-state enabled acquisition of multiple high-resolution isotropic 3D LGE sequences under consistent contrast conditions. In this setting, overall image quality was better with the bSSFP technique qualitatively, but scar conspicuity relative to the LV cavity and absence of artifacts was best with the black-blood LGE technique (BOOST). Black-blood LGE has recently been proposed as an alternative sequence to improve scar-blood contrast and may be useful for detection of sub-endocardial scar and smaller scar regions (Basha et al. 2018; Ginami et al. 2018). Overall there were no significant differences in assessment of core scar volume and borderzone tissue volume between the three, 3D sequences and reference ex-vivo MRI datasets. However, a higher scar entropy was present with the bSSFP and BOOST techniques compared to GRE. Scan acquisition time for the BOOST sequence was also significantly lower and more predictable compared to the bSSFP and GRE sequences due to 2D image-based navigation enabling 100% scan efficiency.

Although conventional LGE imaging uses a GRE readout, it may be desirable to use a SSFP readout due to a higher SNR (Detsky et al. 2007). However, a higher bandwidth may be required with IR-SSFP in order to optimise TR leading to a lower CNR (Viallon et al. 2011). A 22% loss in CNR has been reported during comparison of 2D bSSFP LGE with a 2D segmented GRE LGE acquisition (Huber et al. 2005). The determination of T1 time may be underestimated during IR-GRE acquisitions due to the impact of low flip-angle excitation pulses on longitudinal magnetisation recovery but continuous refocusing of transverse magnetisation with IR-SSFP results in reduced impact on longitudinal magnetisation recovery and subsequently excellent T1 quantification (Scheffler et al. 2001). In this study, the were no differences between the 3D bSSFP and GRE LGE sequences on assessment of core scar and borderzone volumes but qualitatively an improved scar conspicuity relative to adjacent myocardium was noted and subsequently overall image quality. There were also more artifacts with the GRE sequence and longer scan acquisition times. These differences suggest that bSSFP protocol may be the optimal readout acquisition mode for high-resolution 3D LGE imaging in most circumstances. The BOOST sequence may be optimal in the presence of sub-endocardial scar.

4.4.3   Technique for quantification of myocardial scar

In this thesis, the FWHM threshold and 35-50% of maximal signal intensity thresholds were used to quantify dense scar and borderzone tissue, respectively. A variety of methods have been reported in the literature to quantify scar and compared to EAM data. (Andreu et al. 2011) reported that a cut-off of 60% of maximal signal intensity resulted in the best correlation between conducting channels on MRI and EAM. The same group used an automatic algorithm to classify pixels with a signal intensity between 40-60% as borderzone - channels identified using this method identified ~75% of the critical isthmus of clinical VTs (Fernandez-Armenta et al. 2013). Other groups have used a n-SD method whereby core scar

was defined as pixels with a signal intensity ≥3SD above mean signal intensity whilst borderzone tissue was between 2-3SD above mean signal intensity (Estner et al. 2011; Yan et al 2006; Watanabe et al. 2014).

Although LGE volume can vary significantly depending on the thresholding technique used, direct comparisons of quantification methods suggest that the FWHM threshold is the most reproducible and similar to manual quantification (Flett et al. 2011). There is no agreement on the optimal technique for borderzone tissue quantification, however the 35-50% of maximal signal intensity method had a mildly improved ability for the prediction of VT in patients with ischaemic cardiomyopathy compared to the n-SD method, although this did not reach statistical significance (de Haan et al. 2011).

4.4.4   *Entropy as a measure of tissue heterogeneity*

The measurement of scar entropy has emerged as a novel signal-intensity independent parameter to evaluate the complexity of scar. A narrow signal intensity distribution represents low entropy and less inhomogeneity. Tissue harbouring the substrate for VT could theoretically have higher local entropy as a result of inhomogeneity caused by the presence of both surviving myocardium and scar tissue. (Androulakis et al. 2019) reported that patients with ischaemic cardiomyopathy who had a scar entropy ≥ 7.82 had a lower VT-free survival compared to patients with scar entropy <7.82, after adjustment for multi-vessel disease, acute revascularisation, LVEF, scar gray-zone and transmurality. Two subsequent independent cohort of patients with ischaemic and non-ischaemic cardiomyopathy have reported that mean entropy is predictive of subsequent VT (Muthalay et al. 2018; Gould et al. 2019) and could prove useful as a risk stratification tool to determine the need for ICD implantation. All three reports used standard clinical 2D LGE sequences during measurement of entropy.

In this thesis, scar entropy values were sequence and spatial resolution-dependent with higher entropy values with 3D LGE compared to 2D LGE. Furthermore, 3D bSSFP LGE and BOOST also gave significantly higher entropy values compared to 3D GRE LGE imaging. For application during real-time MR-EP, evaluation of higher regional scar entropy values could be a potential approach to identify target sites for ablation and requires further investigation.

4.4.5   Limitations

The LGE sequences evaluated in this study were not compared to histological assessment for validation. Instead, high resolution ex-vivo MRI datasets were used as the reference standard. Despite attempts to maintain the shape of the LV cavity ex-vivo using kinetic sand, there is a tendency for the LV to collapse ex-vivo with subsequent changes to tissue volumes (Whitaker et al. 2019) and this data should therefore be interpreted with caution. Although eleven pigs completed 3D bSSFP LGE imaging combined with 2D LGE, the additional 3D GRE and BOOST sequences could only be completed in six animals due to time constraints within the imaging facility. The 3D GRE sequence was attempted in a further 2 animals but had to be abandoned due to the presence of PVCs in these animals which was increasing the time required for scan acquisition. The 3D bSSFP sequence was chosen as the technique to evaluate high-resolution imaging with contrast steady-state in patients. Due to patient comfort and tolerance considerations, the addition of 3D GRE and BOOST sequences were not evaluated and it is unknown if different results would have been obtained with those techniques. In order to evaluate the performance of high-resolution 3D LGE imaging with contrast steady-state without the confounding effect of device-related artifacts, patients without an ICD in-situ were deliberately studied. Given that VT ablation is primarily an

adjunctive treatment, the majority of patients referred for ablation will have a device in-situ. The performance of high resolution 3D LGE imaging with contrast steady-state in the presence of an implanted device remains unknown and further investigation is required.

The qualitative and quantitative measurements reported in this study are dependent on signal intensity within the acquired MRI scans. Variation in signal intensity between MR images may occur due to type of sequence, haematocrit, renal function, field strength and surface coil proximity and these factors should be taken into account when extrapolating these results to different scenarios.

Although histological evaluation is generally considered the gold-standard to validate imaging data, there are several limitations to using whole-mount 3D histology including the high costs and labour intensive endeavour of creating reconstructed histology slabs from individual slices, challenges in the registration of data between MRI and histology when significant deformations/shrinkage of tissue occurs during histological processing and the lack of a clear histological definition of borderzone tissue (Pop et al. 2013; Glashan et al. 2018). In addition, the definition of borderzone tissue (on histology) can be affected by multiple factors during processing including the magnification technique used, stain used for collaged quantification or using a 2D vs 3D technique for assessment of fibrosis (Schelbert et al. 2010). Given that high-resolution ex-vivo MRI can be used to achieve sub-millimetre spatial resolution, is not affected by perfusion or motion-related artifacts and can be accurately co-registered to in-vivo imaging (Whitaker et al. 2019), this was used to validate the in-vivo MRI data in this study instead of histological assessment.

4.5   Conclusions

This study demonstrates the use of the contrast steady-state protocol to enable high resolution imaging of myocardial scar under consistent contrast conditions and provide an experimental model whereby multiple 3D sequences may be compared against each other. Overall, the 3D bSSFP LGE sequence provided the optimal readout mode in most circumstances whilst the 3D BOOST sequence may be optimal in the presence of sub-endocardial scar. Scar entropy, as a measure of tissue inhomogeneity is sequence and spatial resolution dependent.

Although the contrast steady-state protocol can be applied in patients, both qualitative and quantitative measures of image quality were lower with 3D imaging due to prolonged scan acquisitions, patient tolerance and the presence of arrhythmias.

In the next chapter, the contrast steady-state protocol is applied during real-time MR-EP procedures in the animal model of ischaemic cardiomyopathy to acquire high-resolution 3D bSSFP LGE datasets and assess the association between structural and electrophysiological substrate.

Statement of originality and candidate contributions:

This thesis is submitted as a 'thesis incorporating publication' in accordance with the King's College London guidelines. All publications were published with an open access CC-BY licence and permission has been granted by the publishers to reproduce published manuscripts. The following chapter is adapted from the manuscript below with some sections presented verbatim from the original publication:

Mukherjee RK, Costa CM, Neji R, Harrison JL, Sim I, Williams SE, Whitaker J, Chubb H, O'Neill L, Schneider R, Lloyd T, Pohl T, Roujol S, Niederer SA, Razavi R, O'Neill MD. Evaluation of a real-time magnetic resonance imaging-guided electrophysiology system for structural and electrophysiological ventricular tachycardia substrate assessment. Europace 2019: June 20; Epub ahead of print. PMID: 31219547

I declare that the work presented in this chapter has been primarily carried out by me. I was assisted by Dr John Whitaker in the creation of the porcine infarct model. I was also assisted by Dr James Harrison and Dr Iain Sim in the acquisition of electrophysiology data inside the MRI scanner. Dr Thomas Pohl exported all the data from the iCMR guidance platform and wrote the script to generate 3D shells of voltage, activation and S-QRS maps from the iCMR application. I prepared all imaging protocols with the assistance of Dr Radhouene Neji. I co-ordinated and ran the pre-clinical study, performed data analysis, prepared and wrote the manuscript. Dr Caroline Mendonca Costa assisted with the registration of scar segmentations

derived from MRI and voltage maps. All segmentations and statistical analyses were performed by me.

5 Evaluation of a real-time MRI-guided electrophysiology system for structural and electrophysiological ventricular tachycardia substrate assessment

5.1 Introduction

There is growing interest in the use of real-time magnetic resonance imaging-guided electrophysiology (MR-EP) to treat patients with cardiac arrhythmias (Chubb et al. 2017; Hilbert et al. 2016). Potential advantages of MR-EP procedures include soft tissue visualisation with a high contrast-to-noise ratio, improved assessment of arrhythmia structural substrate using late gadolinium enhancement (LGE) scar imaging, navigation of catheters using dedicated tracking techniques, online monitoring of ablation lesion formation and an evaluation of anatomic and physiologic changes during mapping and lesion delivery (Mukherjee et al. 2018).

Although most preliminary real-time MR-EP studies have been performed in the atria, where significant technical challenges remain for accurate substrate evaluation (Hilbert et al. 2016; Chubb et al. 2017; Paetsch et al. 2019), MRI is the gold standard imaging modality for assessment of ventricular function and scar burden (Dawson et al. 2013). Combined MR-EP techniques could offer synergistic benefits for the evaluation and ablation of ventricular

tachycardia (VT) substrate. Previous studies using conventional mapping systems and image integration where the association between electrical substrate for VT and MRI-derived scar have been investigated, have reported conflicting results. (Wijnmaalen et al. 2011) found that bipolar voltage decreased with increasing scar transmurality in patients undergoing VT ablation. Similarly, (Sasaki et al. 2012) reported an inverse association between bipolar voltage and endocardial and mid-wall scar transmurality. However, other groups have reported a mis-match in scar areas between EAM and MRI in up to 33% of cases (Codreanu et al. 2008). These studies acquired pre-procedural imaging days or weeks prior to an ablation procedure and possible changes in loading conditions and/or rhythm could have occurred since the time of imaging and time of mapping. Furthermore, registration errors on a scale between 3.8 - 4.3mm (Wijnmaalen et al. 2011; Desjardins et al. 2009) have invariably been reported, which could be a significant source of mis-match. The choice of optimal thresholds to define both electrical scar and MRI-derived scar is also an important consideration. Using an optimal bipolar voltage threshold of 1.0mV, a sensitivity of 79% and specificity of 84% was reported in the identification of LGE regions on MRI (Desjardins et al. 2009). Using a signal intensity threshold of 60% of maximum to identify dense scar on MRI, a degree of agreement was reported between bipolar voltage and MR-derived scar, but this agreement remained moderate (Cohen K co-efficient = 0.70) (Andreu et al. 2011). Furthermore, in regions of intermediate bipolar voltage (0.5 - 1.5mV), a disagreement with MR-derived borderzone tissue regions was present in 21.7% of locations (Andreu et al. 2011). The method of analysis has also varied between studies. (Wijnmaalen et al. 2011) divided each short-axis MRI slice into 20 segments to compare the association with bipolar voltage. A similar approach was employed by (Sasaki et al. 2012). A segmental approach for analysis may be less precise compared to a point-by-point registration approach (Audette et al. 2000).

The influence of spatial resolution of MRI on classification of scar areas was also recently described (Lopez-Yunta et al. 2019). In a swine model of myocardial infarction, 25% of voltage-derived scar areas in the LV endocardium were classified as non-enhanced on in-vivo MRI (spatial resolution - 1.5mm^3) whilst 43% of voltage-derived scar areas were non-enhanced on high-resolution ex-vivo MRI (spatial resolution - 0.6mm^3), highlighting the importance of image resolution on the specificity of scar characterisation.

Against this background, this study sought to assess the relationship between structural and electrophysiological substrate using a real-time MR-EP system, a high-resolution 3D LGE sequence (based on work described in the previous chapter) and a point-by-point analysis technique. Real-time MR-EP enables image registration to be performed within a single imaging modality, acquire imaging and electrical data in the same coordinate system and minimise translational changes due to beat-to-beat cardiac motion and respiratory motion.

In this study, we describe the ability of a novel real-time MR-EP system to perform endocardial voltage mapping and limited assessments of delayed conduction in a porcine ischaemia-reperfusion model taking advantage of custom technical developments in a second generation MR-compatible catheter and a dedicated prototype image-guidance platform for interventional procedures. We hypothesised that with the minimisation of registration errors and translational changes expected using a real-time MR-EP platform, an improved association between structural and electrophysiological substrate may be expected.

5.2 Methods

5.2.1 Animal model and infarct preparation

The research protocol was approved by the local institutional review board and complied with French law on animal experiments and the Guiding Principles for the Care and Use of Laboratory Animals published by the National Institutes of Health (8th Edition, National Academies Press, 2011). The research was performed at the Institut de Chirurgie Guidée par l'image (IHU), Strasbourg, France. Seven male domestic pigs (weight - 35.7 ± 5kg; 2 healthy, 5 post infarction) were treated with 800mg amiodarone, twice daily for 4 days prior to and following an infarct procedure and/or imaging and electrophysiology studies. A closed-chest model of myocardial infarction was used as described in Section 3.1.1. The purpose of using two normal heart pigs was to ensure a robust workflow was in place for mapping prior to attempting the procedures in the scar model as well as ensuring that the SNR of EGMs recorded in the normal LV from inside a MRI scanner was sufficient to justify proceeding with experiments in the infarct model where low voltage regions would be present.

5.2.2 Imaging study

All animals underwent a MRI scan for substrate assessment 6 weeks after infarct on a 1.5T scanner (MAGNETOM, Aera, Siemens Healthcare, Erlangen, Germany). Each animal was sedated, intubated and mechanically ventilated as per the infarct procedure for all imaging studies. A 3D ECG-triggered whole heart bSSFP MRI dataset was acquired to enable manual segmentations of cardiac chambers (transverse slice orientation, AP phase encoding, 256 x 256 in-plane matrix size, $TR/TE/\alpha = 3.7ms/1.64ms/90^{o}$, voxel size = $1.25x1.25x2.5mm^{3}$, bandwidth = 895Hx/Px, GRAPPA factor = 2). For scar imaging, contrast was administered (Gadovist, Bayer, Germany) using an initial bolus (0.1mmol/kg) followed by slow infusion of

gadolinium contrast was initiated at a rate of 0.0011mmol/kg/min, as described in Section 4.2.1. High-resolution 3D late gadolinium enhancement (LGE) imaging was performed using a free-breathing, respiratory navigator and ECG-gated (in diastole) inversion recovery, b-SSFP sequence ((TR/TE/α=3.45ms/1.5ms/90°, FOV=339×264×100mm^3, voxel size=1.2×1.2×1.2mm^3, bandwidth=895Hz/Px, GRAPPA factor=2, 2RR acquisition). The choice of 3D LGE sequence was based on the results described in Chapter 4. Based on the LGE-MRI, scar was manually segmented using a version of the Medical Imaging Interaction Toolkit (MITK, Heidelberg, Germany) with the full-width-half-maximum (FWHM) threshold used to define scar and help guide electroanatomic mapping (EAM) during the subsequent procedure.

5.2.3   Real-time MRI-guided electrophysiology procedure

Vascular access was obtained via the femoral artery and vein under ultrasound guidance (9Fr or 10Fr introducer sheath) followed by administration of 100 units/kg of intravenous heparin. Using retrograde aortic access, the custom 9Fr, MR-compatible steerable catheter with a single gold 3.5mm tip and ring bipolar electrode (3.5mm inter-electrode spacing) and six circumferential open irrigation ports (Vision-MR, Imricor, Burnsville, MN, USA) was advanced into the LV cavity without the use of fluoroscopy at any point. Active catheter tracking (Section 3.2.2) was used to place the catheter within the LV and manoeuvre to different locations - *Figure 5-1*. The iCMR image guidance platform (described in Section 3.3.1) displayed the 3D segmentations of each cardiac chamber (LV, RV, LA and RA) imported from the MITK-based platform. The 3D segmentation of scar from the LGE-MRI was overlaid onto the shell of the LV to guide EAM.

A custom MR-EP recording system (Advantage-MR, Imricor, Burnsville, MN, USA) was used to record, amplify, filter, display and analyse intra-cardiac EGMs. The system consisted

of an integrated stimulator which was used to generate pacing stimuli. This system allowed

mapping of activation time and voltage to be combined synergistically with real-time

imaging of anatomy and LGE substrate.
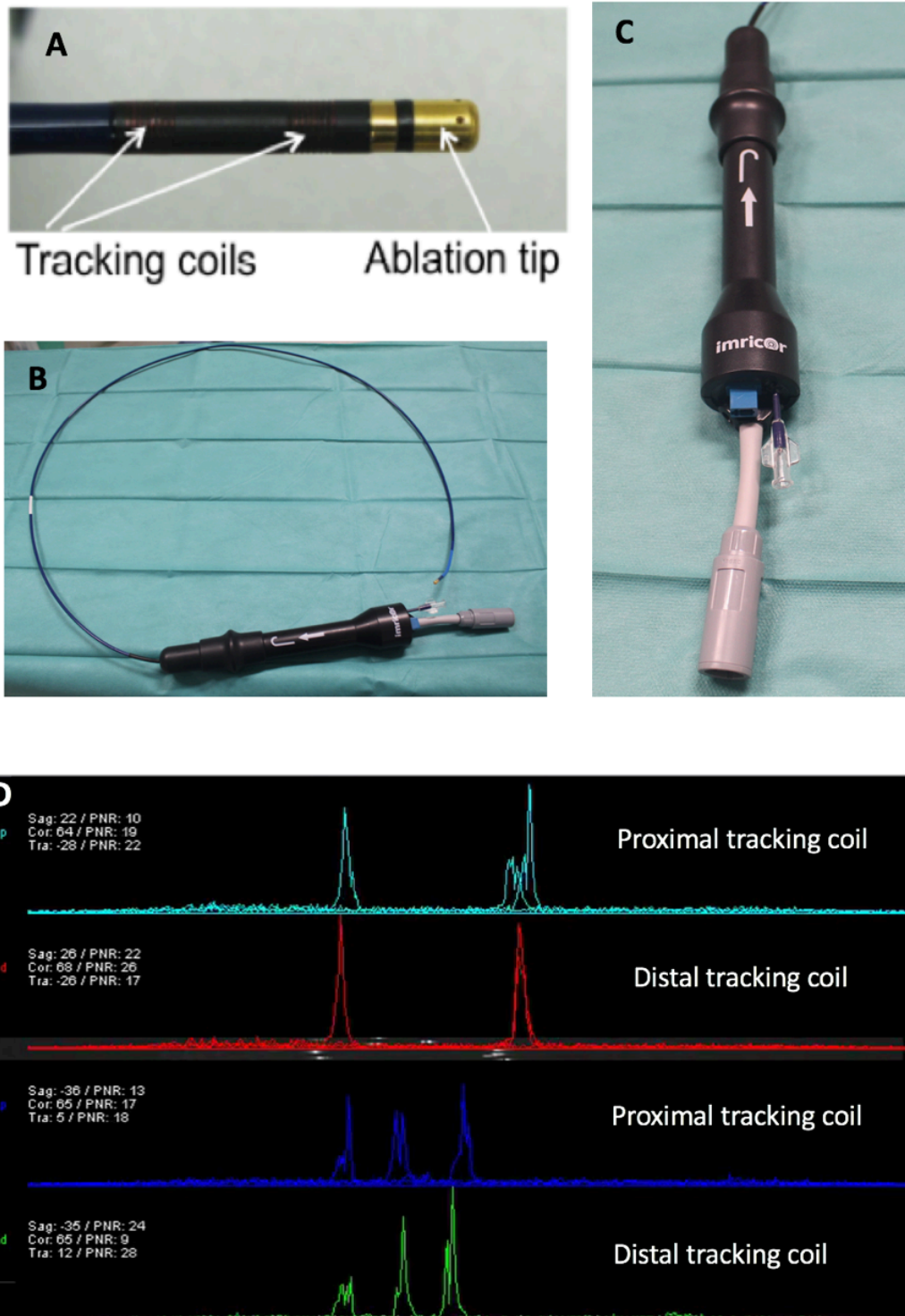
Figure 5-1: MR-compatible catheter, tracking coils and tracking signal

5.2.4   Intra-cardiac electrogram recording and characterisation

Activation and voltage data were acquired during sinus rhythm. For each sampling point, the time delay (LAT) from a fixed intra-cardiac reference point to the initial deflection of the local LV electrogram was measured manually on the EP recording system and data transferred to the iCMR image guidance platform. Similarly, the peak-to-peak voltage amplitude was also measured manually and transmitted to the guidance platform - *Figure 5-2*. Both datasets were used to generate colour-coded activation and voltage maps on the iCMR platform. Areas of focused mapping were based on the location of LGE-derived scar. In order to avoid EGM artifacts due to poor catheter-tissue contact, at least 2 consecutive EGMs had to have the same morphology prior to acceptance of each mapping point. Regions of abnormal myocardium were defined as areas with a bipolar voltage threshold <1.5mV (Tung et al. 2016). EGMs were reviewed off-line at a sweep speed of 100mm/s.

After acquisition of activation and voltage maps, the LV catheter was used to pace during stable sinus rhythm (10mA, 3ms, cycle length 10% shorter than sinus cycle length) from sites of normal myocardium and scar. The time from the stimulus artefact to the surface QRS onset was used to distinguish regions of normal and delayed conduction. Following confirmation of capture, the time duration between the stimulus artefact to QRS onset was recorded. The MR-compatible catheter was sequentially manoeuvred to sites within normal myocardium and scar using active catheter tracking to generate a colour-coded map of stimulus-QRS duration times (S-QRS). Sites with a S-QRS >40ms during pace-mapping in sinus rhythm were considered regions of slow conduction as previously described

(Brunckhorst et al. 2003). Following completion of the MR-EP procedure, pigs were euthanised with potassium chloride and hearts were rapidly dissected for gross pathological examination. Hearts were photographed with areas of ischaemic scar delineated.
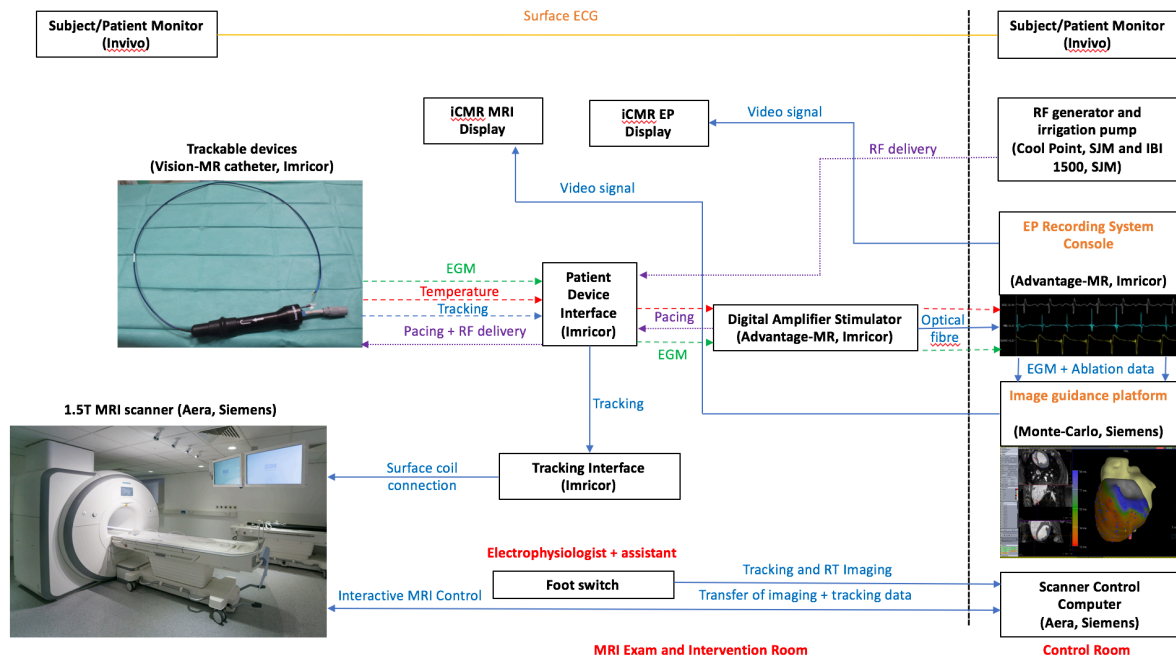
Figure 5-2: MR-EP system set-up

5.2.5 *Image registration, scar segmentation and comparison to voltage maps*

The LGE-MRI imaging was registered to the 3D whole heart MRI datasets using a point-based (landmark) rigid registration to guide EAM. Points were selected within the RV, LV and LA blood pools of each image dataset. Registration was performed on the Medical Imaging Interaction Toolkit (MITK) [https://doi.org/10.1016/j.media.2005.04.005]. Scar was segmented on the LGE-MRI using the FWHM method to normalise signal intensity relative to maximum myocardial signal intensity. First, the LV wall was manually segmented using a custom version of MITK. This was performed using the 'Paint Tool' on the MITK-based platform to derive the endocardial and epicardial border on a slice-by-slice basis with 3D interpolation to minimise discontinuities between slices. Then, the maximum signal intensity

within the LV wall was computed and the voxels with signal intensity above 50% of the maximum intensity (FWHM) were labelled as scar - *Figure 5-3*.
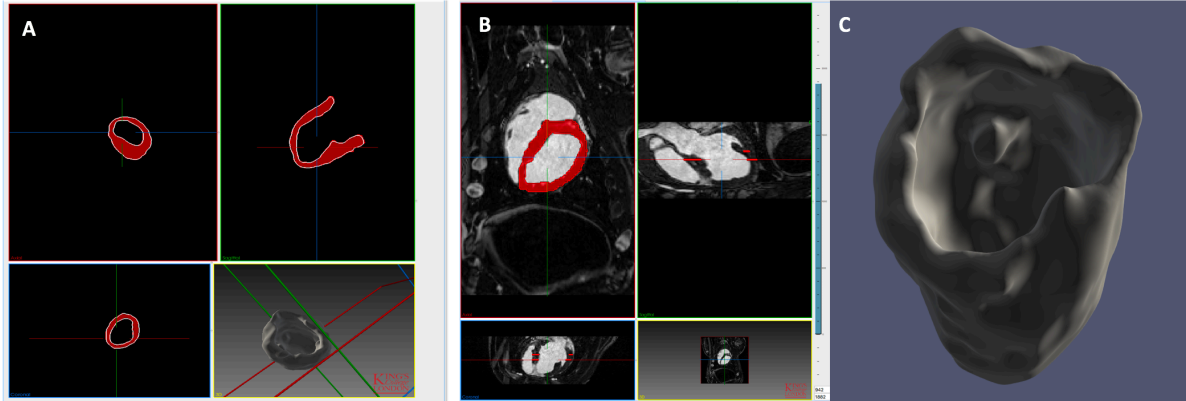
Figure 5-3: Image processing

Representative examples of segmentations of the LV wall (A and B) from 3D LGE-MRI images generated using the custom version of MITK and corresponding 3D shell (C) generated.

To compare the scar segmentation with regions of low voltage, the scar segmentation was mapped onto the voltage map surface mesh. This was achieved in two steps. First, the scar segmentation image was rotated and translated so that it was aligned with the surface mesh. Second, the scar points were mapped onto the surface mesh using the iterative closest point (ICP) method. In addition, the voltage map was converted to a binary map of scar (1) and normal tissue (0). In this ischaemia-reperfusion model, scar has been noted to be transmural in the majority of myocardial segments with LGE (Tschabrunn et al. 2016). The Sorensen-Dice similarity coefficient (DSC) between the two binary maps was then computed on a nodal basis for all regions, scar regions only and regions of normal myocardium. The DSC between LGE scar maps and voltage maps following thresholding at different cut-offs (0.5mV-3.5mV) was also derived. The normal heart pigs (n=2) were not used for assessment of scar concordance and all data reporting ROC curves and DSC refer to infarct hearts only.

5.2.6   Statistical analysis

Data analysis was performed using GraphPad Prism version 7.0 (GraphPad Software, CA, USA) or SPSS v24.0 (IBM Corp. Armonk, NY, USA). Continuous data are represented as mean ± SD and compared using the Student's two-tailed T-test. A 2-sided p value <0.05 was considered statistically significant. For assessment of the accuracy of the MR-EP system to correctly identify scar and delayed conduction, the location of LGE-derived scar was taken as the 'gold standard' of structural substrate. The sensitivity, specificity, positive predictive value and negative predictive value of low voltage points and S-QRS times using the MR-EP system to identify LGE-scar was assessed and used to derive receiver operator characteristic (ROC) curves.

5.3   Results

All pigs that underwent a LAD infarct developed antero-septal scar which was visualised on the LGE images (mean scar volume - 6.80 ± 0.88ml) - *Figure 5-4*. There was no LGE present in healthy pigs that did not undergo the LAD infarct procedure.
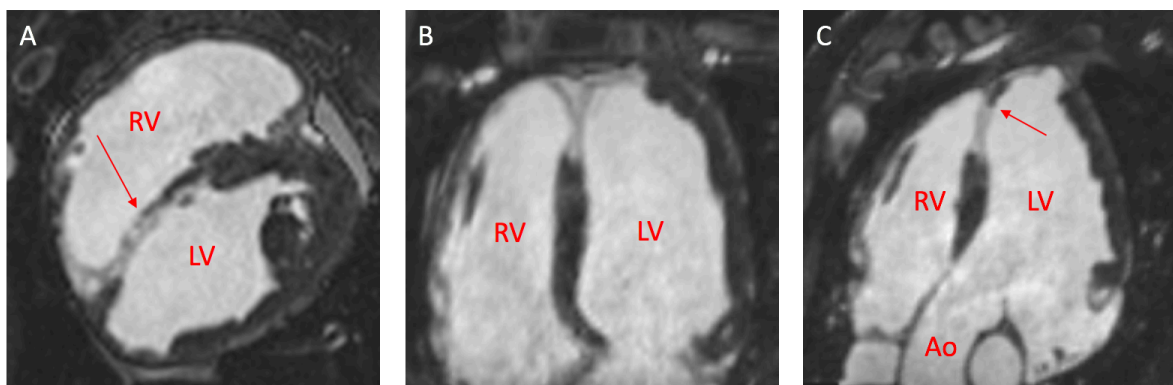
Figure 5-4: LGE-MRI images of infarct

LGE-MRI images acquired 6 weeks post infarct showing region of anteroseptal scar (D-E) - short-axis, 4-chamber and 3-chamber views shown. Red arrows show location and extent of LGE.

5.3.1 Real-time MRI-guided electroanatomical mapping

Segmentations of scar from the LGE-MRI were displayed on the iCMR image-guidance platform as coloured shells to guide EAM - *Figure 5-5*. 445 EGMs (range 30-186) were recorded from all animals in sinus rhythm (including 138 EGMs from regions located within the LGE scar segmentation). Using the MRI-derived LGE segmentation to differentiate between normal myocardium and scar, the mean signal-to-noise ratio (SNR) of EGMs within normal tissue and scar was 44.78 ± 21.91 and 11.67 ± 6.99 respectively (p<0.0001) - *Figure 5-6*. Pacing captured at 103 sites whilst 10 sites which were all in regions of LGE-derived scar did not capture; 56 (54.4%) sites had S-QRS delay $\leq$40ms, 47 (45.6%) sites had a delay of $\geq$40ms whilst 15 (14.5%) had a delay $\geq$80ms. Representative examples of voltage and S-QRS maps obtained using the system are shown in *Figure 5-7*.
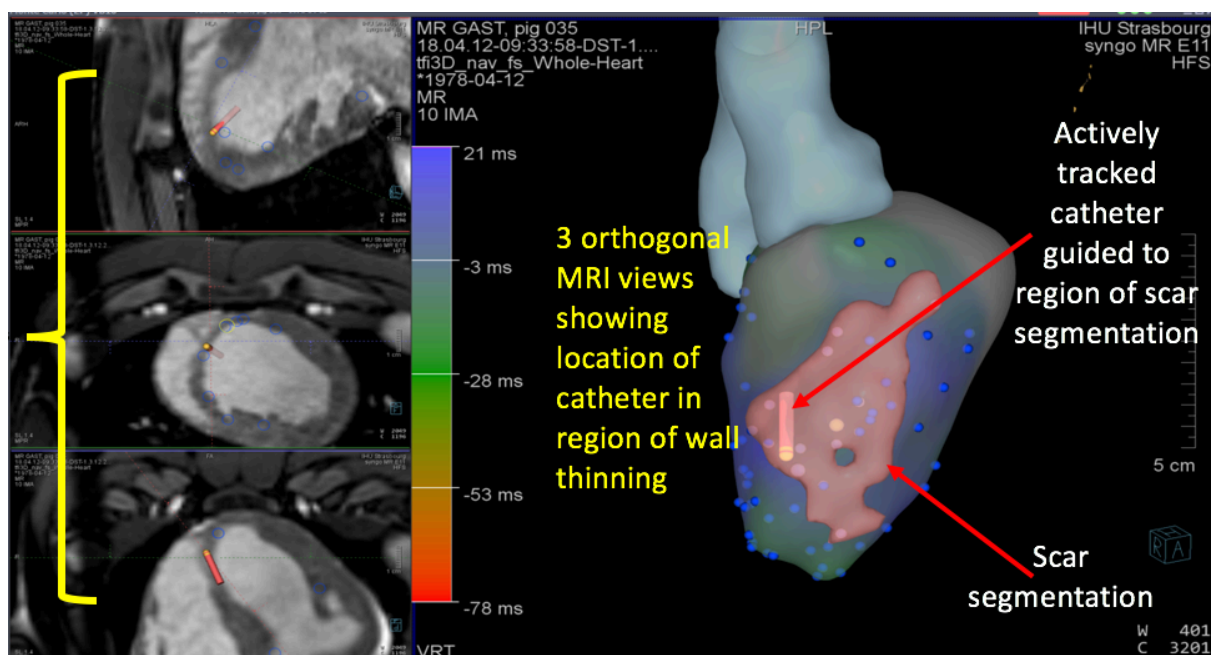
Figure 5-5: Depiction of scar, catheter, segmentations and MRI scans on image guidance platform

Representative depiction of image guidance platform showing 3 orthogonal MRI views demonstrating location of catheter in relation to LV endocardium, 3D segmentation of the left ventricle derived from MRI and scar segmentation from LGE images to guide EAM.
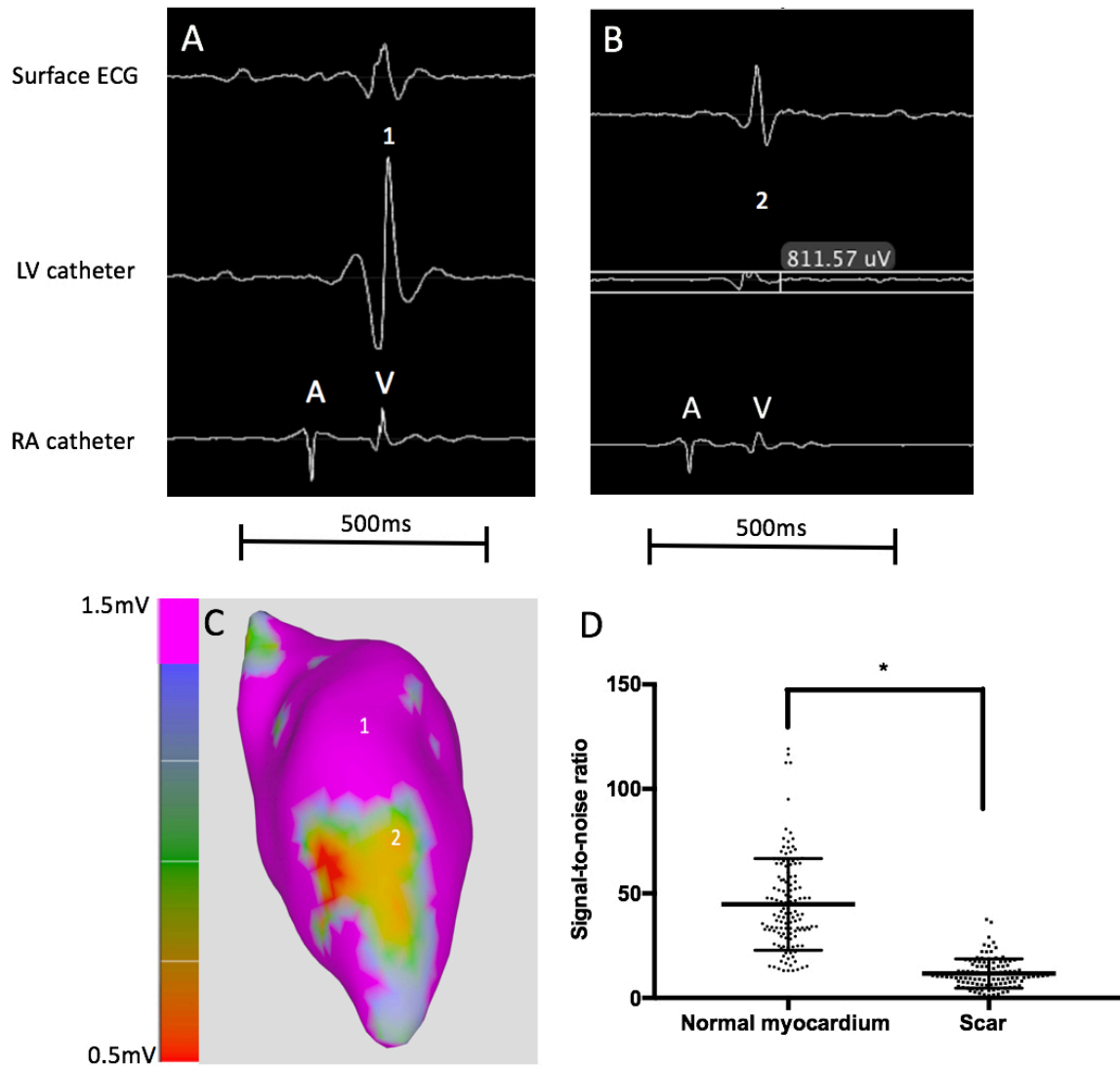
Figure 5-6: Intra-cardiac EGMs obtained inside the MRI scanner and signal-to-noise ratios within normal myocardium and scar tissue

Representative examples of intra-cardiac EGMs obtained using the MR-EP system in a region of normal myocardium (Point 1) and area of scar (Point 2) (A-C). The baseline noise level inside the MRI scanner was in the region of 0.1mV (approximately 10-fold higher than that in the conventional electrophysiology laboratory). Dot-plot showing signal-to-noise ratios obtained for intra-cardiac EGMs in normal myocardium and LGE-derived scar regions from 7 animals; *p<0.0001(D).
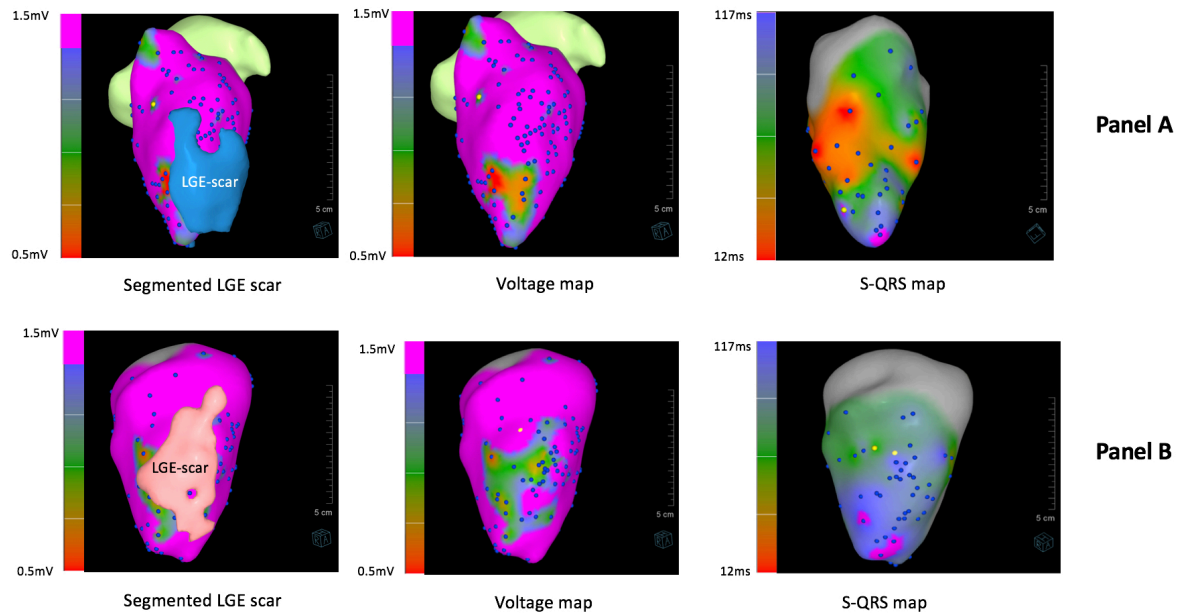
Figure 5-7: Representative examples of segmented LGE scar, voltage and S-QRS maps obtained using real-time MR-EP system in 2 animals (Panel A and B)

5.3.2 Relationship between MRI-derived scar, voltage and delayed conduction

Using conventional (0.5mV-1.5mV) bipolar voltage thresholds, the sensitivity and specificity of voltage mapping using the MR-EP system to identify MR-derived LGE was 57% and 96% respectively (ROC area under curve = 0.907; $p<0.0001$). A S-QRS threshold of >40ms using this system resulted in a sensitivity of 76% and specificity of 73% to identify MR-derived LGE (ROC area under curve = 0.840; $p<0.0001$) - Figure 5. At a threshold of 1.5mV to define abnormal myocardium, the positive predictive value (PPV) and negative predictive value (NPV) of voltage mapping to identify LGE was 86% and 83% respectively. At a threshold of 40ms, the PPV and NPV of S-QRS time using the system to identify LGE was 73% and 79% respectively - *Figure 5-8.*
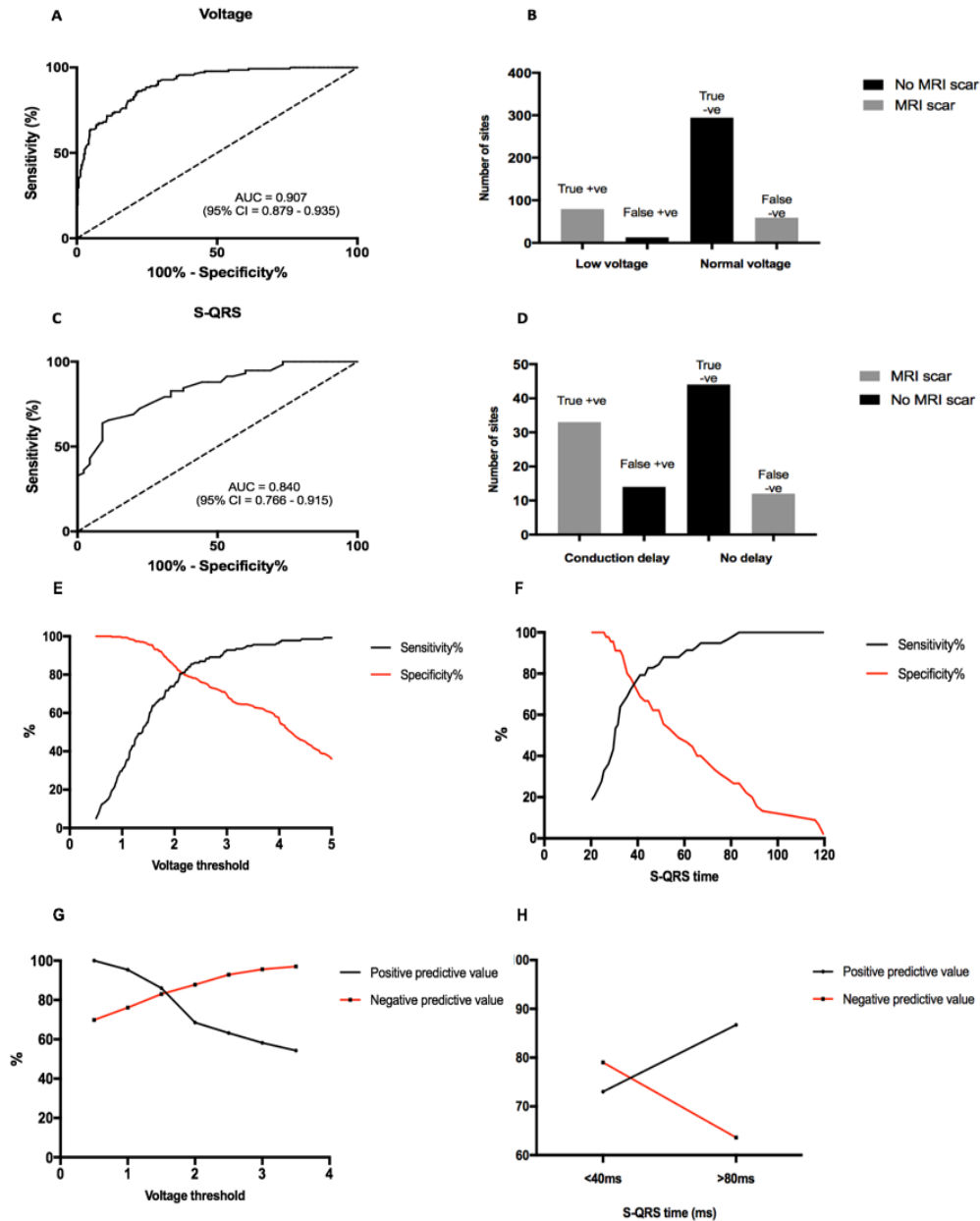
Figure 5-8: ROC curves for prediction of LGE regions using voltage mapping and S-QRS

ROC curves (A and C) for prediction of LGE regions using voltage mapping and S-QRS. Frequency histograms (B and D) displaying the true positive, false positive, true negative and false negative counts of voltage mapping and S-QRS measurements using the real-time MR-EP system to predict MRI-derived scar. Sensitivity, specificity, PPV and NPV of measurements using the system using different normal voltage cut-offs and S-QRS times (E-H).

There was a moderate relationship between low voltage regions in the LV endocardium and LGE-derived scar mapped onto the endocardial surface mesh - *Figure 5-9.* At a voltage threshold of 1.5mV, mean DSC across all nodes was 79.0% ± 6.0%, whilst mean DSC within

scar regions only was 35.0% ± 10.1% and 90.4% ± 8.6% in normal myocardium regions

only. An improvement in DSC within scar regions was observed using a higher voltage cut-

off of 2.0mV and 2.5mV (47.3 ± 9.9% and 60.2 ± 22.4%) at the expense of reduced

agreement across regions of normal myocardium - *Figure 5-10.*
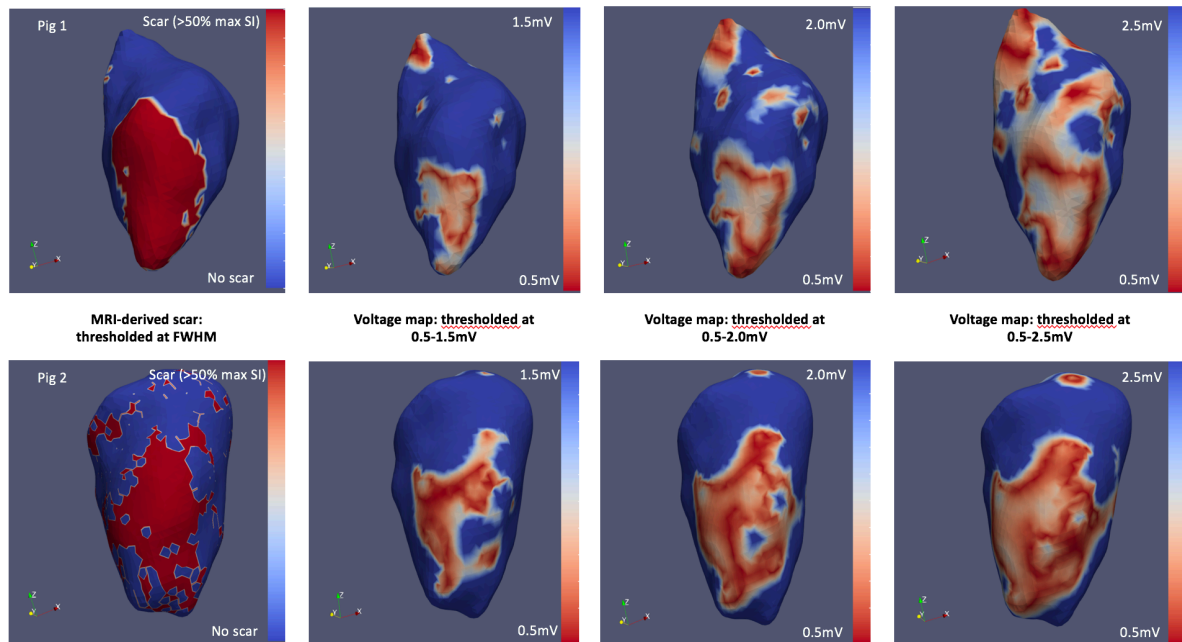
Figure 5-9: Sorenson-Dice similarity co-efficient between MR-derived scar shells and endocardial voltage maps with varying normal voltage thresholds in two representative animals
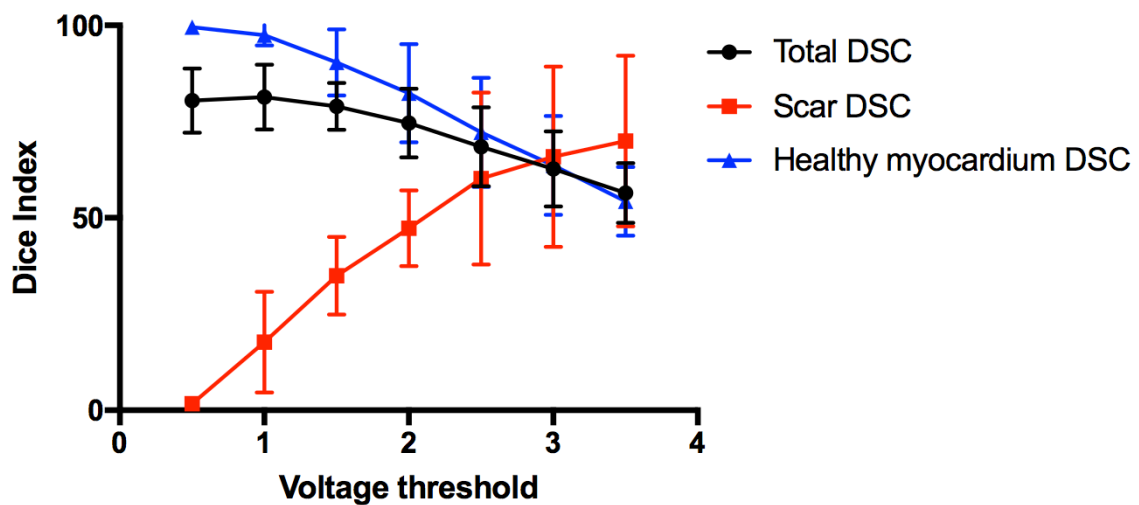
Figure 5-10: Dice similarity co-efficients (DSC) between MR-derived scar shells and endocardial voltage maps acquired using MR-EP system following application of normal cut-off thresholds of 0.5-3.5mV. DSC is shown for overall similarity, similarity across scar nodes and normal myocardium nodes.

5.4   Discussion

This study shows that the prototype real-time MR-EP system can be used to guide catheters to regions of scar using active catheter tracking and to distinguish regions of low voltage and delayed conduction from healthy myocardium. There is a moderate relationship between low voltage and LGE scar using conventional bipolar voltage thresholds. An improved sensitivity for LGE detection may be achieved using higher bipolar voltage cut-offs with this system.

The relationship between local EGM amplitude and scar is complex, in part due to the dependence of voltage on infarct size, heterogeneity and transmurality (Lopez-Yunta et al. 2019). Conventional bipolar voltage thresholds for scar detection may lack sensitivity to fully detect scar as variations in inter-electrode spacing and recording electrode size may affect the representation of EGMs (Tung et al. 2016). Furthermore, although LGE-MRI is the current gold standard for visualisation of ventricular scar post myocardial infarction, the limited spatial resolution of *in vivo* LGE-MRI can result in partial volume effects and limit the specificity of scar characterisation (Lopez-Yunta et al. 2019). Increasing mapping resolution using multi-electrode catheters may also result in detection of a smaller area of low bipolar voltage as each data point represents a smaller tissue area with less far-field contamination (Tschabrunn et al. 2016). The use of multi-electrode catheters could improve the correlation between EAM and imaging as has been shown in a randomised study (Acosta et al. 2018). An additional source of discrepancy when correlating EAM and pre-procedural imaging is registration error due to translational changes (patient movement, cardiac or respiratory motion) or changes in volume, orientation or rhythm of the heart between time of imaging and EAM (Roujol et al. 2016).

The real-time MR-EP system minimises registration error through registration of electrical and structural data within a single imaging modality with the same coordinate system. The 3D whole heart sequence used for chamber segmentation was acquired during the same phase of the cardiac cycle as the 3D LGE to minimise translational changes due to beat-to-beat cardiac motion. Furthermore, both sequences were performed when animals were under general anaesthesia with reduced variability in respiratory motion thereby minimising translational changes due to respiratory motion. Compared to image integration approaches, where positional errors are introduced when registering catheter position to pre-procedural imaging, the MR-EP system tracks catheter position directly using a dedicated tracking sequence that is acquired in the same coordinate system as the 3D whole heart and LGE scans. The main sources of error with the MR-EP system include within scan registration error and catheter tip displacement on the 3D shell with the active tracking sequence. In a cohort of conscious patients scanned with an angiography sequence to create an endocardial mask and a 3D LGE acquisition, the within scan translation error was noted to be 1.9 ± 1.6mm with a rotation error of $0.62 \pm 0.41^\circ$ (Chubb et al. 2018). This is, however, likely to overestimate within scar error with the MR-EP system where translational movements were minimal as animals were under general anaesthesia. Using ex-vivo technical validation, the average tip displacement of the actively tracked catheter using the MR-EP system was measured as 0.90 ± 0.58mm along the axis of the catheter (Chubb et al. 2017) and is likely to be the best estimate of error with this set-up.

In this study, we show that despite the minimisation of registration and translational errors, the relationship between scar delineated using a custom MR-compatible catheter and high resolution isotropic LGE imaging (1.2mm^3) remains moderate when using standard voltage thresholds. An improvement in scar concordance with this system can be achieved using a

higher normal bipolar voltage cut-off. Some investigators have found that abnormal potentials targeted for ablation may be present in tissue classified as 'normal' (>1.5mV) voltage and manual adjustment of bipolar voltage thresholds to higher cut-off values may identify more confluent scar regions incorporating all abnormal signals (Jais et al. 2012). Regions of slow conduction could also be present in tissue of normal bipolar voltage and unmasked during extrastimulus pacing (Acosta et al. 2018).

Although the majority of real-time MR-EP studies published previously have focused on the atria, the full potential of substrate and lesion assessment afforded by such systems is likely to be realised in the context of VT ablation. There are limited data available evaluating real-time MR-EP systems in the ventricle (Nazarian et al. 2008; Oduneye et al. 2013; Oduneye et al. 2015). Our study builds on previous work to characterise the relationship between LGE-derived scar and electrophysiological measurements of low voltage and delayed conduction inside a MRI scanner.

Currently, limited visualisation of soft tissue structures is possible in the electrophysiology laboratory with the use of intra-cardiac ultrasound (ICE), however MRI offers an improved contrast-to-noise ratio and ability to acquire 3D whole heart images or 2D slices in any imaging plane. Furthermore, tissue characterisation techniques such as LGE can be used to identify arrhythmogenic substrate whilst dedicated sequences can be used to monitor tissue temperature during ablation and provide a real-time method of calculating lethal thermal dose (Mukherjee et al. 2018). The novel MR-EP system described is capable of visualising the location and orientation of catheters relative to soft tissue, assess scar with MRI at the time of EAM, enable rapid segmentation and registration of cardiac chambers and potentially monitor formation of ablation lesions (Mukherjee et al. 2018). These features of the MR-EP

system could offer an alternative to conventional fluoroscopy-guided or ICE-guided procedures and improve catheter navigation, delivery of therapy and assess anatomical and physiological changes during VT ablation with the potential to reduce risks and improve outcomes.

A number of technical developments are required prior to the realisation of real-time MRI-guided VT ablation. The development of a MRI-compatible defibrillation system will be a prerequisite prior to any clinical studies and prototypes are currently under evaluation (Schmidt et al. 2016). Current surface ECG monitoring systems inside a MRI scanner are limited to 4-6 surface electrodes; in order to aid the diagnostic electrophysiology requirements of VT ablation, robust 12-lead ECG systems are required. Although high-fidelity 12-lead ECG recordings are possible (Tse et al. 2014), the impact of magneto-hydrodynamic effects and gradient switching-induced voltages within the MRI scanner can still corrupt ECG signals. There is currently a limited availability of MR-compatible devices; the development of MR-compatible multi-electrode catheters with similar capabilities to their conventional counterparts will accelerate progress in the electrophysiological assessment of substrate inside the scanner (Elbes et al. 2017).

5.4.1 *Limitations*

There are several important limitations to this study. We did not define the bipolar voltage threshold that best correlates to histological scar using the MR-compatible catheter - rather two indirect methods of scar assessment were compared to each other. During assessment of S-QRS intervals to assess slow conduction, a single ECG lead was used to derive measurements due to the lack of availability of a MRI-compatible 12-lead ECG; as a result, no assessment of QRS morphology using a 12-lead ECG was performed during pacing.

These measurements should therefore be interpreted with caution as we could not account for local latency although this would be expected to be minimal at the pacing cycle length used. Furthermore, the technique of S-QRS measurements may have limited sensitivity for the detection of regions of myocardium with slow conduction compared to an approach analysing the evoked response to extrastimuli (Acosta et al. 2018). In this model, haemodynamic compromise and death of the animal was inevitable if VT was induced. As there was no means to defibrillate the animal inside the scanner, we deliberately avoided the induction of VT which in turn precluded entrainment mapping. As the location of LGE was used to guide ventricular mapping, there is a degree of sampling bias introduced during collection of mapping points. The purpose of the system being used in this way was to demonstrate the potential advantages and workflow of the MR-EP system. However, in order to perform a stepwise comparison of concordance between imaging scar and electrical scar, it would be necessary to remove this sampling bias by performing EAM independently (without LGE overlaid onto 3D shell) and retrospective evaluation.

There was a large variability in the number of points collected per animal (range: 30-186). This was in part due to the difficulty with catheter manoeuvrability to access different parts of the LV inside the MRI scanner. We used retrograde aortic access to enter the LV rather than trans-septal puncture, due to the difficulties in performing trans-septal puncture inside a MRI scanner. It was difficult to access certain parts of the LV (e.g. LV summit) from retrograde aortic access. As a result, we tried to collect points from the region of LGE as well as a variety of locations where normal myocardium was expected. If it was not possible to sequentially move the catheter to certain locations, we decided not to collect multiple points from the same region as it was likely to add very little to the overall map.

In one particular animal, we were able to successfully acquire 186 points - however this was a relatively prolonged procedure and required > 3 hours of mapping. The animal frequently developed runs of NSVT during the procedure. The decision to stop mapping was influenced by the haemodynamic status of each animal, development of arrhythmias and changes in the manouverability of the catheters during a prolonged procedure.

The MR-EP system used in this study consisted of a single electrode catheter and required manual annotation of activation times and voltages for each point on the EP recording system resulting in substantially lower mapping densities than with contemporary EAM systems. This could have lowered the precision of the sensitivity and specificity measures reported in the study. The development of automated mapping systems and multi-polar catheters for use inside the MRI scanner could better define the relationship between electrophysiological substrate and MR-derived substrate.

5.5   Conclusions

There is a moderate association between low voltage regions and sites of altered conduction determined using a novel real-time MR-EP system with scar derived from LGE-MRI. An improved sensitivity for LGE detection could be achieved using a higher normal voltage cut-off with this system and the respective catheter. Further technical developments in MR-compatible devices will accelerate progress towards real-time MRI-guided VT ablation.

The next chapter builds on the work described to evaluate the accuracy of the MR-EP system in delivering ablation lesions. In addition, a MR technique to assess ablation lesions in real-time (MR-thermometry and dosimetry) is also evaluated.

Statement of originality and candidate contributions:

This thesis is submitted as a 'thesis incorporating publication' in accordance with the King's College London guidelines. All publications were published with an open access CC-BY licence and permission has been granted by the publishers to reproduce published manuscripts. The following chapter is adapted from the manuscript below with some sections presented verbatim from the original publication:

Mukherjee RK, Roujol S, Chubb H, Harrison J, Williams S, Whitaker J, O'Neill L, Silberbauer J, Neji R, Schneider R, Pohl T, Lloyd T, O'Neill M, Razavi R. Epicardial electroanatomical mapping, radiofrequency ablation and lesion imaging in the porcine left ventricle under real time magnetic resonance imaging guidance – an in-vivo feasibility study. Europace 2018: 20(FI2): f254-f262. PMID: 29294008

I declare that the work presented in this chapter has been primarily carried out by me. Dr Sebastien Roujol developed the MR-thermometry imaging protocol and I assisted in the ex-vivo technical validation, including the design of the set-up, catheter handling and analysis of data alongside Dr Henry Chubb. Dr Radhouene Neji and Dr Sebastien Roujol prepared all imaging protocols for in vivo studies. I co-ordinated and ran the pre-clinical study, performed data analysis, prepared and wrote the manuscript. Professor Mark O'Neill, Dr John Silberbauer, Dr James Harrison, Dr Steven Williams and Dr Louisa O'Neill assisted with in vivo catheter ablation studies. Dr Thomas Pohl and Dr Rainer Schneider developed the iCMR guidance platform and exported all the data required for subsequent analysis. Dr Sebastien Roujol wrote the script for analysis of the MR-thermometry and dosimetry data. I performed all histological analysis with the assistance of Dr Mohammed Ikram.

6 Catheter ablation and lesion imaging in the porcine left ventricle under real-time MRI-guidance

6.1 Introduction

The long-term recurrence rate following catheter ablation of VT in patients with structural heart disease has been reported as between 40-60% (Kuck et al. 2010; Stevenson et al. 2008; Al-Khatib et al. 2015). Meanwhile, the risks of VT ablation are considerable with a 5% risk of procedure-related mortality (Santangeli et al. 2017). Significant complications including cardiac tamponade, major bleeding and stroke are also not uncommon. Causes of treatment failure may include an inability to create fully transmural scar, difficulty in reaching regions of myocardium containing arrhythmogenic substrate and inaccurate lesion targeting (Tokuda et al. 2013).

In the conventional electrophysiology laboratory, assessment of the location of ablation lesions is limited and based on either X-ray fluoroscopy with EAM, with no evaluation of soft tissue or through the use of intra-cardiac ultrasound (ICE). Although ICE can be used to assess catheter position and tip-tissue contact, it requires invasive placement, provides a limited field of view and image plane orientation. Furthermore, conventional techniques to determine the size of ablation lesions rely on mathematical modelling of limited surrogate markers including local impedance change, RF power, RF application time, electrode tip temperature and contact force, rather than direct visualisation of lesions (Kolandaivelu et al. 2010).

Real-time MRI guidance during catheter ablation could allow a direct assessment of catheter position and its relation to soft tissue with a high contrast-to-noise ratio (CNR) (Nordbeck et al. 2011). In addition, MRI could be used to monitor lesion development, alongside visualisation of anatomic and physiologic changes during lesion delivery (Guttman et al. 2018). The combination of improved navigation, accurate lesion placement and online visualisation of lesion characteristics could potentially reduce risks and improve the outcome of VT ablation.

Contrast-enhanced MRI with LGE has been used to non-invasively assess RF ablation lesions (Dickfeld et al. 2006) however, acute LGE may grossly overestimate chronic lesion size (Kholmovski et al. 2018). Contrast can also only be given once during a procedure which limits the utility of LGE for real-time interventions. In order to facilitate repeated lesion assessments, the development of non-contrast MR sequences is required. A combination of T1-weighted imaging to visualise lesion necrosis (Guttman et al. 2018) and T2-weighted imaging to assess myocardial oedema can be used concurrently to assess the physiological response post ablation and monitor acute lesion composition (Krahn et al. 2018). However, these sequences are typically performed at the end of a procedure and not in real-time. Recently, there has been significant interest in the development of MR tools to evaluate lesions in real-time and MR-thermometry and dosimetry have emerged as an exciting means to directly monitor tissue temperature and estimate lesion size, respectively (de Senneville et al. 2012).

In this chapter, the accuracy of the MR-EP system previously described, is evaluated to deliver ablation lesions in the porcine left ventricle. In addition, the use of MR-thermometry

and dosimetry to enable real-time visualisation in normal porcine hearts is described including ex-vivo technical development.

6.2   Methods

6.2.1   Ex-vivo technical validation of MR-thermometry

Ex-vivo studies were performed to assess the temperature stability of the MR-thermometry sequence without catheter ablation. In addition, catheter ablation was performed to demonstrate a rise in temperature in the absence of blood flow. Experiments were performed on an ex-vivo porcine thigh preparation which was placed in a custom plastic container and bathed in normal saline. Images were acquired on a 1.5T scanner (MAGNETOM, Aera, Siemens Healthcare, Erlangen, Germany) using an ECG-triggered multi-slice single-shot echo planar imaging (EPI) sequence with spoiled gradient echo with the following parameters: TR/TE/α=50ms/17ms/60°, FOV=180×180mm^2, voxel size=1.6×1.6mm^2, slice thickness=5mm, slice number=4, bandwidth=1565Hz/Px, GRAPPA factor=2, partial Fourier=0.75. The ex-vivo porcine thigh preparation was kept stationary to avoid motion artifacts. Temperature stability was assessed in 10 locations on the thigh preparation through averaging of the temporal standard deviation of temperature within a manually drawn ROI. The MR-thermometry sequence was run for 100s for assessment of stability. For catheter ablation, a MR-compatible ablation catheter (Vision-MR, Imricor, USA) was introduced into the plastic container via a port and placed on the surface of the thigh preparation. A RF ablation generator (Ampere IBI T1500, St Jude Medical, USA) and irrigation pump (Cool Point, St Jude Medical, USA) was positioned outside the scanner room and connected to the catheter. Ten irrigated RF ablation lesions were delivered in different locations at 50W for 60s (irrigation rate -17mL/min) inside the MRI scanner whilst running the MR-thermometry sequence. The sequence was initiated 20s prior to ablation and continued for 20s after the end

of ablation. Reconstruction of the temperature maps was performed offline as described in Section 3.2.4.

6.2.2 Animal model

Animal studies complied with French law on animal experiments and were performed at the Institut de Chirurgie Guidée par l'Image (IHU), Strasbourg, France. Eight female domestic pigs (49.7 ± 8 kg) were pre-sedated with a combination of intramuscular tiletamine and zolazepam. General anaesthesia was induced and maintained with inhaled 1-5% isoflurane and the animals were intubated and mechanically ventilated (20-25 breaths/min). Vascular access (7Fr introducer sheath) for invasive monitoring and administration of medications was obtained through the right and left femoral artery and femoral vein using ultrasound guidance. Epicardial access was successfully gained in four pigs using an anterior percutaneous subxiphoidal puncture under X-ray guidance in a fluoroscopy suite. A custom MR-compatible 10Fr deflectable sheath (Imricor, USA) was placed within the pericardial space for epicardial access. A MR-compatible 9Fr steerable catheter with open irrigation (Vision-MR, Imricor, USA) was manoeuvred into the epicardial space - *Figure 6-1*.
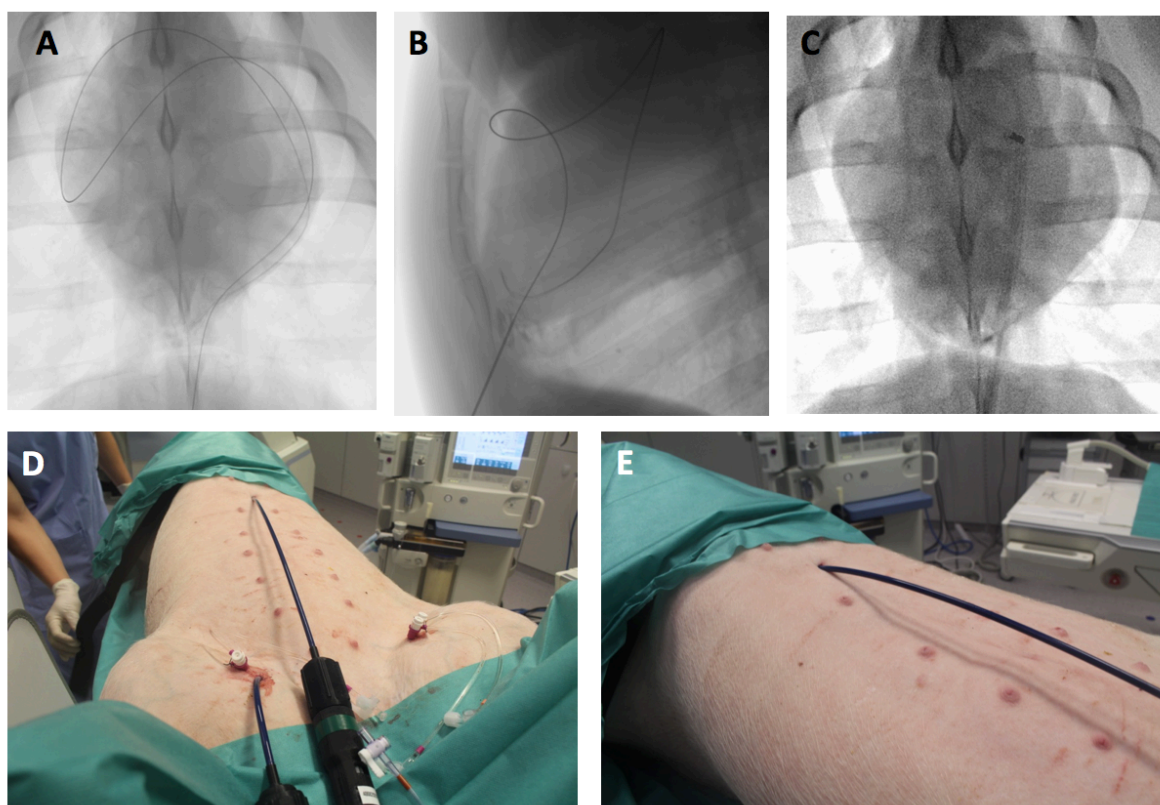
Figure 6-1: Fluoroscopic images demonstrating epicardial access.

Following subxiphoidal puncture, a guidewire is advanced and shown coursing around the heart in the left anterior oblique view (A) and right anterior oblique (B) views. The sheath is in the pericardial space with the MR-compatible catheter coursing in front of the aorta in (C). Photographs showing location of puncture and sheath in a pig (D and E).

The catheters have been described in detail previously (Grothoff et al. 2017). In the remaining four pigs, epicardial access was not possible due to the presence of pericardial adhesions and access to the LV endocardium was gained via retrograde aortic access as described in Section 5.2.3. A custom MR-EP recording system (Advantage-MR) consisting of a digital amplifier and stimulator, patient information module and a host workstation was used to record, display and analyse intracardiac signals, act as a programmable stimulator and deliver ablation energy as previously described (Grothoff et al. 2017). All animals underwent invasive blood pressure and surface ECG monitoring (Invivo Medical, FL, USA) throughout the study. Anticoagulation was maintained with an intravenous bolus of 70units/kg of heparin. A continuous infusion of intravenous lidocaine (12ml/hr) and amiodarone (20mcg/kg/min) was administered prior to ablation. A bolus of intravenous amiodarone

(150mg in 60mls dextrose) was administered as a slow push prior to each ablation lesion delivered. Animals were transferred to a MRI suite following epicardial access for mapping and ablation studies whilst retrograde aortic access was achieved within the MRI scanner using images for guidance.

All MRI scans described below were performed on a 1.5T MR scanner (MAGNETOM, Aera, Siemens Healthcare, Erlangen, Germany). 3D whole-heart MRI for cardiac chamber segmentation, display on the iCMR platform and active catheter tracking was performed as described in sections 3.2.1 and 3.2.2.

6.2.3   Ablation studies

Ablation of the left ventricle was performed by delivering radiofrequency energy (40-60W, irrigation rate 17mL/min, 50-60s duration). Impedance change and catheter tip temperature were continuously assessed. Nineteen discrete ablation lesions were delivered in 8 animals with nine epicardial lesions and ten endocardial lesions. Lesion position was automatically recorded in 3D space and annotated upon the 3D rendering of each heart on the iCMR application. The aim was to create transmural lesions during each discrete ablation. In order to assess the conformational accuracy of lesions on the iCMR application, lesions were placed in discrete locations in the left ventricle and where possible, in a 'X' or 'L' shape to enable the calculation of angles between lesions. Using measurements on gross macroscopic examination as gold standard, conformational accuracy of lesion annotation on the iCMR application was assessed using the angle of intersection between points on two ablation lines measured to the nearest degree. Spatial accuracy was referenced to an anatomical landmark with low spatial variability - the LV apex and was measured to the nearest millimetre.

The total number of ablations delivered in each animal was limited for the following reasons:

1. Large animal models are particularly susceptible to arrhythmias following ablation in the ventricle resulting in ventricular fibrillation (VF) and death of the animal (Toupin et al. 2017), despite the use of anti-arrhythmic medications. In order to maximize the data collected from imaging and reduce the risk of death, we elected to limit the total number of ablations in each animal.

2. In order to characterize RF delivery on CMR without bias from overlapping lesions, discrete lesions were placed in the LV with a distance of at least 1cm from two separate lesions.

6.2.4 MR-thermometry and dosimetry

Real-time lesion imaging could offer an attractive means to titrate energy delivery which could potentially decrease overall procedural time, increase efficacy and reduce procedural risk during MR-guided EP procedures. MR-thermometry and dosimetry using the proton resonance frequency shift (PRFS) technique was employed in this study which is sensitive to temperature changes in real-time and has been most widely studied in non-cardiac ablation (Roujol et al. 2010). The experimental details of the techniques are described in Section 3.2.4.

6.2.5 Non-contrast 3D gradient-echo inversion recovery sequence (GRE IR)

In order to compare MR-dosimetry lesion dimensions with a non-contrast lesion imaging sequence, a subset of animals (4 animals, 8 ablation lesions) underwent additional imaging with a recently described gradient-echo sequence with a long TI (Guttman et al. 2018; Toupin et al. 2017) as follows: T1-weighted, 3D diaphragmatic navigator-gated gradient-echo (GRE) inversion recovery (IR) sequence; image sequence parameters were: TR/TE/Flip angle =

4ms/2.3ms/20°, TI = 700ms; FOV=360x360x100mm^3, matrix = 272 x 272 px, number of slices = 35, voxel size=1.3×1.3×3mm^3, bandwidth=250Hz/Px, GRAPPA factor=2; 2RR acquisition. Regions of signal enhancement on the 3D GRE IR sequence have been recently validated against regions of necrosis on gross pathology in a porcine model of LV ablation (Guttman et al. 2018).

6.2.6   *Gross macroscopy and histological assessment*

Following completion of imaging studies, animals were euthanized with potassium chloride and the heart was rapidly excised and dissected to expose individual ablation lesions. The gross specimens were photographed and fixed in 10% formalin. The ablation lines and surrounding tissue were excised *en bloc* and cut into sections perpendicular to the ablation line. Lesions were photographed and dimensions measured with a ruler. Each cross section was dehydrated, embedded in paraffin, sectioned (6μm sections) and then stained with haematoxylin and eosin.

6.2.7   *Lesion size measurements*

In order to compare 2D thermal dose lesion sizes to gross macroscopy, each heart was dissected to resemble the orientation of the thermal dose images. For measurement of lesion dimensions, the ablation lesion was defined as both the zone of pallor and the surrounding oedematous zone. Depth and width was measured on gross macroscopy and compared to the depth and width dimensions of the lesion on 2D thermal dose maps. For comparison of 2D thermal dose lesion sizes with the GRE IR sequence, four slices were reconstructed from the 3D volume to resemble the equivalent slices and orientation on the thermal dose images. The depth and width was measured for each lesion on both sets of image datasets.

6.2.8 Statistical analysis

Statistical analyses were performed using GraphPad PRISM Version 7.0 (GraphPad Inc, CA, USA). Continuous variables were compared using the Student's two-tailed t-test. Linear regression analysis was performed to assess the relationship between lesion dimensions on image datasets with pathological dimensions and spatial accuracy of the iCMR guidance platform with gross pathology. Bland-Altman analysis and agreement are presented as average difference ± 95% confidence interval (CI). All other data are reported as mean ± SD unless otherwise specified. A level of $p < 0.05$ was considered statistically significant.

6.3 Results

6.3.1 Ex-vivo assessment of MR-thermometry

Within the ex-vivo thigh preparation, the mean temperature variation was $3.2^{o}C \pm 1.2$ in >80% of pixels within each ROI. During RF catheter ablation, a maximum rise in mean temperature variation of $48.2^{o}C \pm 4.7$ was observed in the focal point position at the catheter tip within the ROIs. Within remote ROIs of the thigh preparation, distant from the region of catheter ablation, mean temperature variation was $2.8^{o}C \pm 0.9$ - *Figure 6-2*.
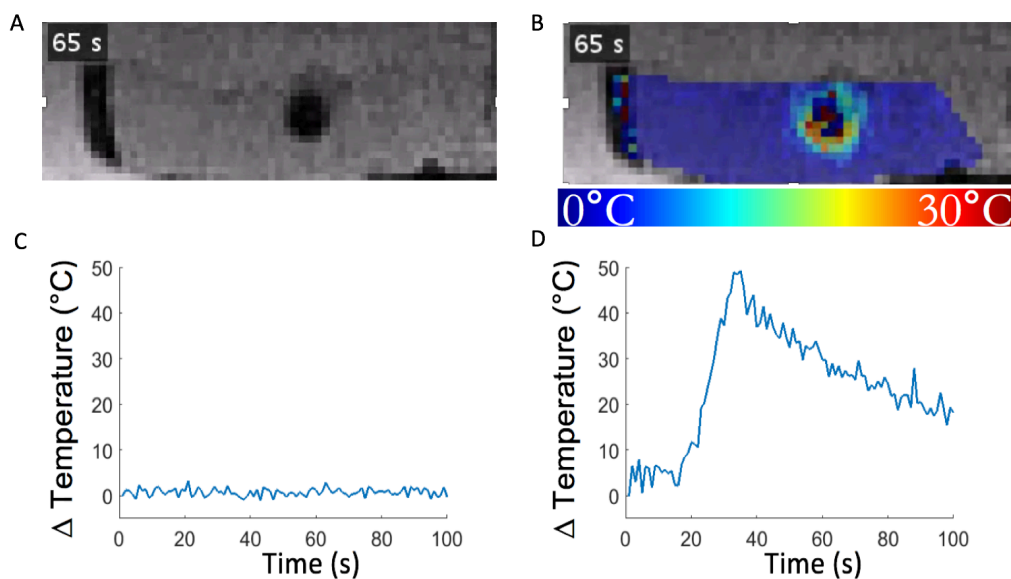
Figure 6-2: Ex-vivo assessment of MR-thermometry.

In a porcine thigh preparation, during catheter ablation, the magnitude image shows the susceptibility artifact created by RF heating at 65s after the start of imaging (A). The temperature map is overlaid onto the corresponding magnitude image (B) and temperature profiles in a remote region (C) and at the focal point position of the catheter tip (D) are shown.

6.3.2 Spatial and conformational accuracy of the MR-EP system during delivery of catheter ablation

All RF ablation lesions in animals were delivered on either the epicardium or endocardial LV surfaces using active catheter tracking (n=19). The locations of ablation lesion delivery were annotated onto the anatomical shells on the iCMR image guidance platform. The spatial accuracy of lesion delivery, compared to the gold standard pathological measurement, was 0.95mm ± 1.03. Linear regression analysis showed a strong association between lesion location on the iCMR platform and gross pathology ($r^2 = 0.93$; $p<0.0001$) whilst Bland-Altman analysis revealed minor bias (-0.947; 95% CI: -8.99 - 7.09). Conformational accuracy of the MR-EP system as assessed by the angle of intersection between ablation lines, was <7 degrees for all measured angles, compared to gross pathology - *Figure 6-3.*
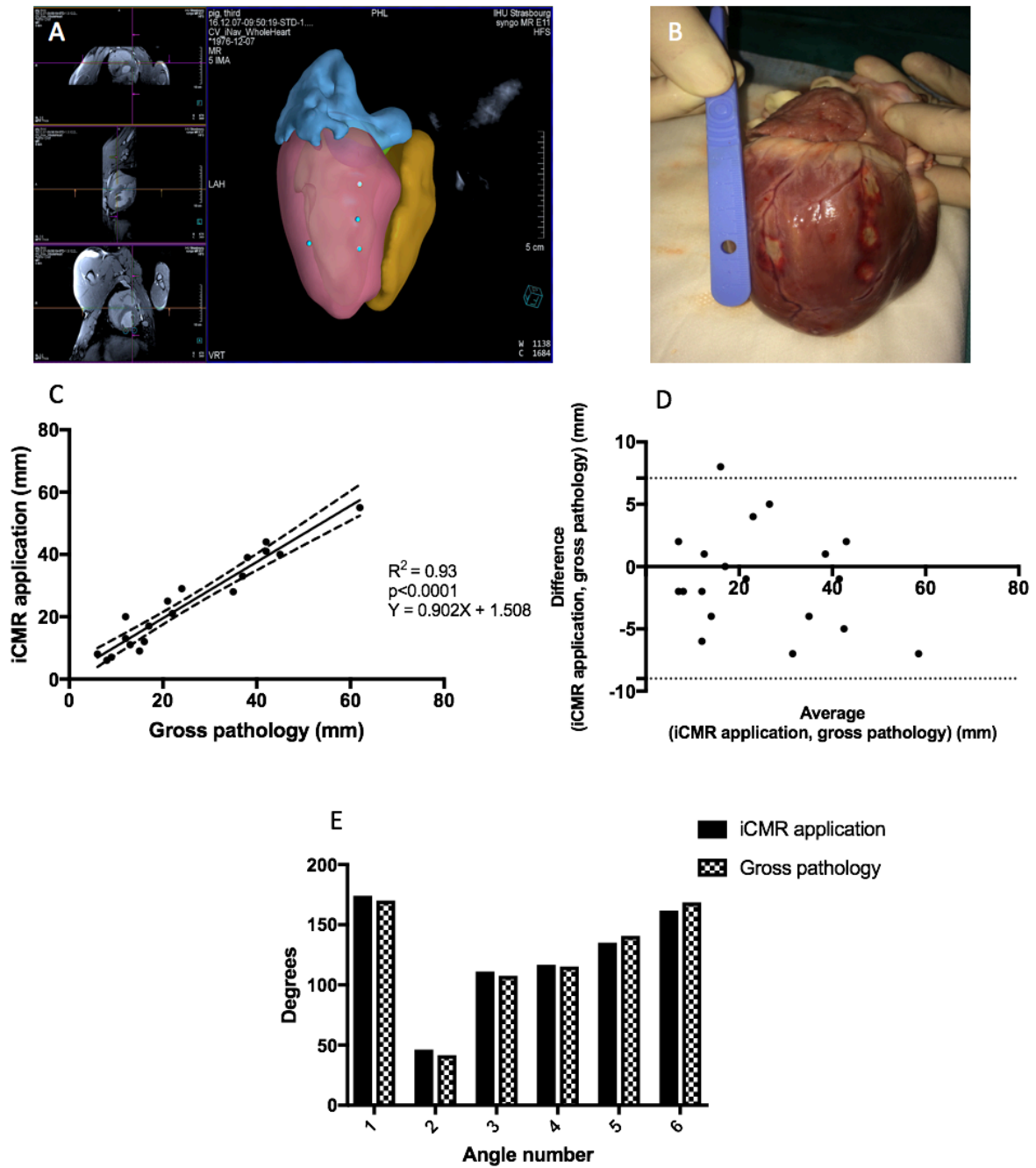
Figure 6-3: Spatial and conformational accuracy of MR-EP system

Ablation lesion location on the iCMR application (A) matched well to absolute site of lesion location on gross pathology (B). A strong association was observed (C) with mean spatial accuracy of <1mm between the iCMR application and gross macroscopy (n=19) with good agreement and minor bias (D). A conformational accuracy <7 degrees was also observed (E) in all angles measured between discrete ablation lesion lines (n=6) on the iCMR application and gross macroscopy.

6.3.3 In-vivo RF ablation with MR-thermometry and lesion size measurements with MR-dosimetry

MR-thermometry was able to demonstrate a localised temperature elevation near the catheter tip during delivery of radiofrequency ablation. Raw magnitude and phase images obtained during RF ablation demonstrated local phase variations associated with ablation-induced susceptibility changes - *Figure 6-4*. Following post-processing, temperature and thermal dose maps were generated and overlaid onto the corresponding magnitude images - *Figure 6-5*.
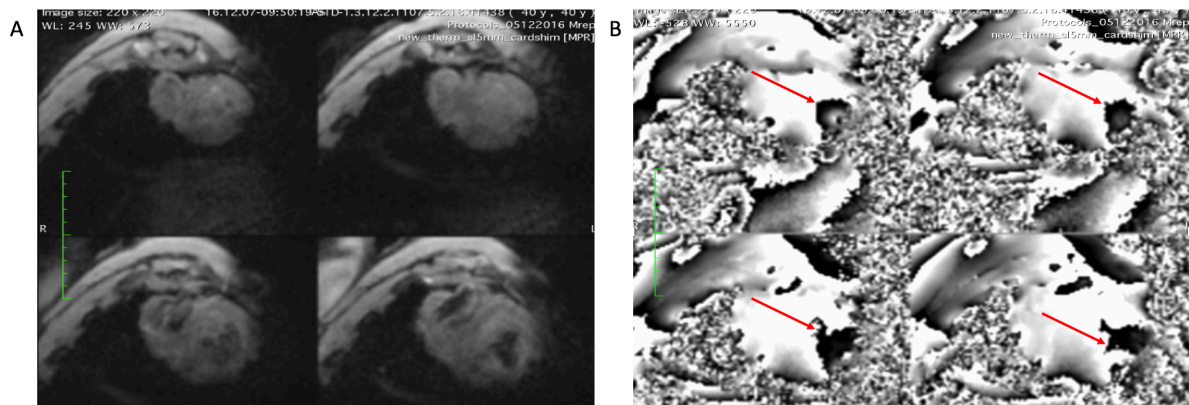
Figure 6-4: Magnitude and phase images of MR-thermometry

Magnitude (A) and phase raw images (B) obtained during RF ablation with the MR-thermometry sequence. Four adjacent slices (5mm slice thickness) are obtained at the level of RF application. Slice selection was determined based on the 3D catheter location determined from the active tracking signal and fed back to the scanner console via the iCMR guidance platform. Red arrows show regions of local phase variations associated with ablation-induced susceptibility changes.
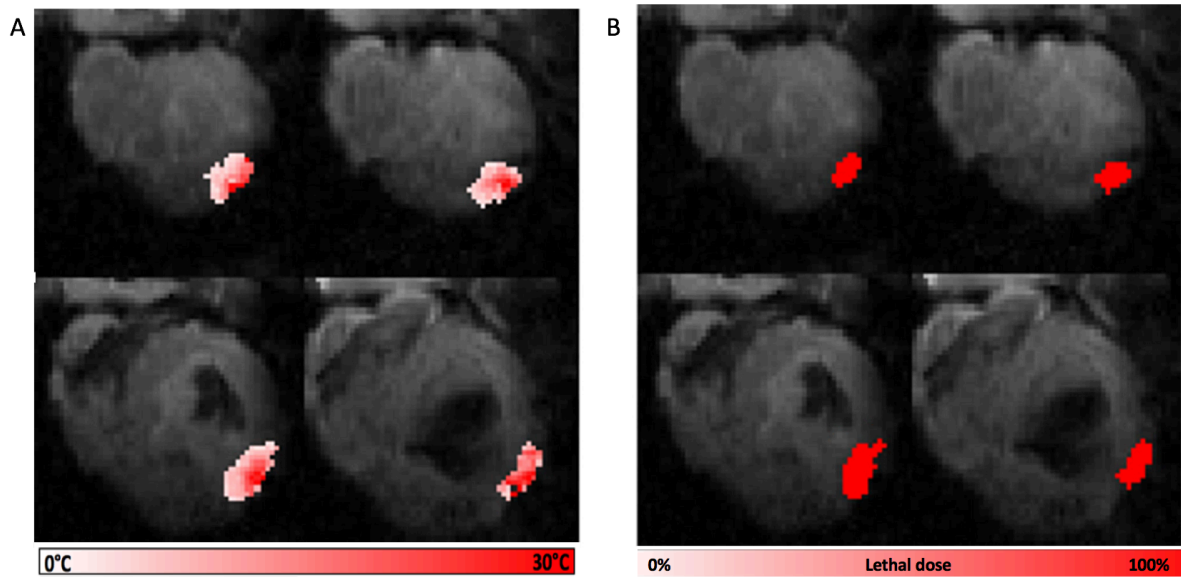
Figure 6-5: ΔTemperature maps

ΔTemperature maps across four slices during RF ablation (A) after 60s are shown overlaid over the corresponding magnitude images. Achieved thermal dose maps (B) are shown across the same slices at the end of treatment.

A maximum temperature difference of 35°C (relative to pixel in area of more remote septum) was observed within 2mm of the irrigated catheter tip (Point 1) whilst a lower temperature difference was observed further away from the catheter tip in the myocardium (Point 2) and no temperature change in a more remote area of myocardium >8mm away from the catheter tip (Point 3) - *Figure 6-6.*
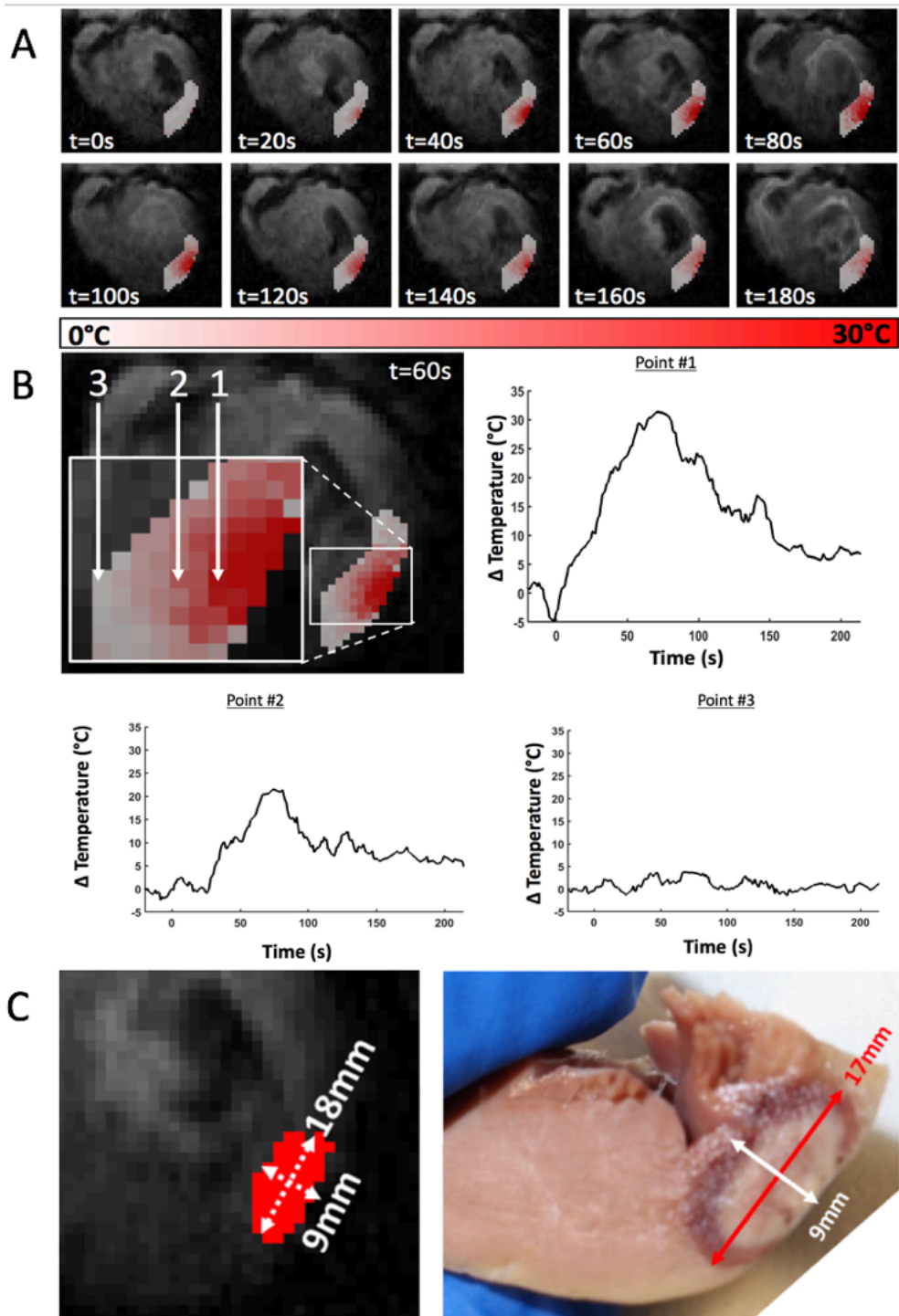
Figure 6-6: MR-thermometry and dosimetry of a representative epicardial ablation lesion with gross pathological lesion dimensions

In-vivo Δtemperature maps (A) shown at different time points relative to the start of the RF heating. Localised temperature elevation can be clearly visualized on the epicardial side of the left ventricle. Temporal profiles (B) obtained using MR-thermometry during epicardial ablation in swine. A maximum temperature elevation of 35°C was observed in a pixel within 2mm of the catheter tip – point 1 (relative to a more remote pixel in myocardium > 8mm away from the catheter tip – point 3). No significant temperature elevation was observed in a pixel located in a remote area. 2D lesion dimensions measured using MR-dosimetry (C) correlate well with measurements on gross macroscopy with mild overestimation of lesion width.

Lesion dimensions measured using MR-dosimetry on thermal dose maps correlated moderately with lesion dimensions on gross pathology (lesion width: $r^2 = 0.77$; lesion depth: $r^2 = 0.76$). On assessment of lesion width, Bland-Altman analysis revealed good agreement and minor bias (0.684; 95% CI: -2.24 - 3.61) whilst on assessment of lesion depth, bias was 1.842; 95% CI: -0.79 - 4.48 - *Figure 6-7.*
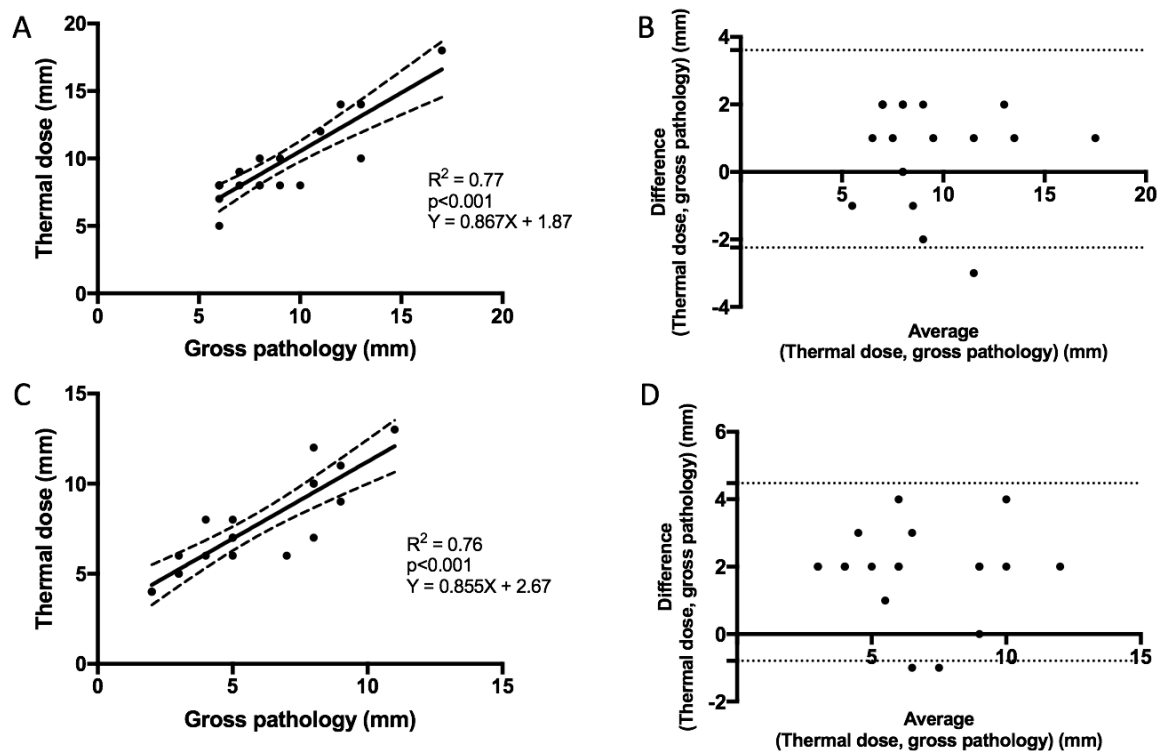
Figure 6-7: Relationship between ablation lesion dimensions on thermal dose maps and gross pathology

Linear regression between ablation lesion width (A) and depth (C) on 2D thermal dose maps and gross pathology (n = 19 lesions). Bland-Altman plots showing the agreement on lesion width (B) and depth (D) size to those dimensions obtained on gross pathological measurements. Dashed/dotted lines indicate 95% confidence bands (A and C) and 95% confidence intervals (B and D). Several points may represent more than one measure given that several lesion dimensions were identical.

6.3.4   Assessment of lesion sizes with non-contrast 3D GRE IR with a long TI and MR-dosimetry

On the 3D GRE IR images, ablation lesions had an increased signal intensity compared to adjacent myocardium, similar to recently described findings (Guttman et al. 2018). The long TI ensured that the blood pool signal was suppressed enhancing the visualisation of lesions -

Figure 6-8. There was a moderate association on lesion width between the 3D GRE images and thermal dose maps ($r^2 = 0.50$) but an improved association on lesion depth between image datasets ($r^2 = 0.81$). Agreement on lesion size measurements between sequences was good (Lesion width bias = 1.201; 95% CI: -2.498 - 4.901; Lesion depth bias = 1.294; 95% CI: -0.466 - 3.054) - *Figure 6-9.*
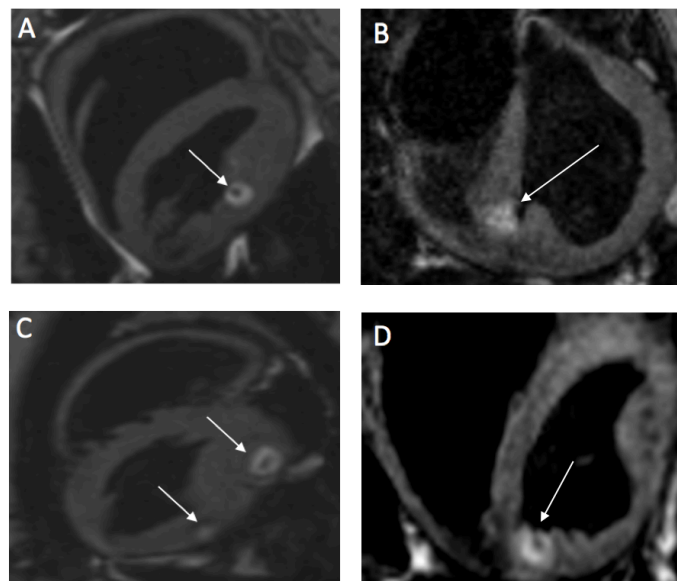
Figure 6-8: Representative images of ablation lesions acquired using a 3D GRE IR sequence with a long inversion time. Lesions are indicated with white arrows.
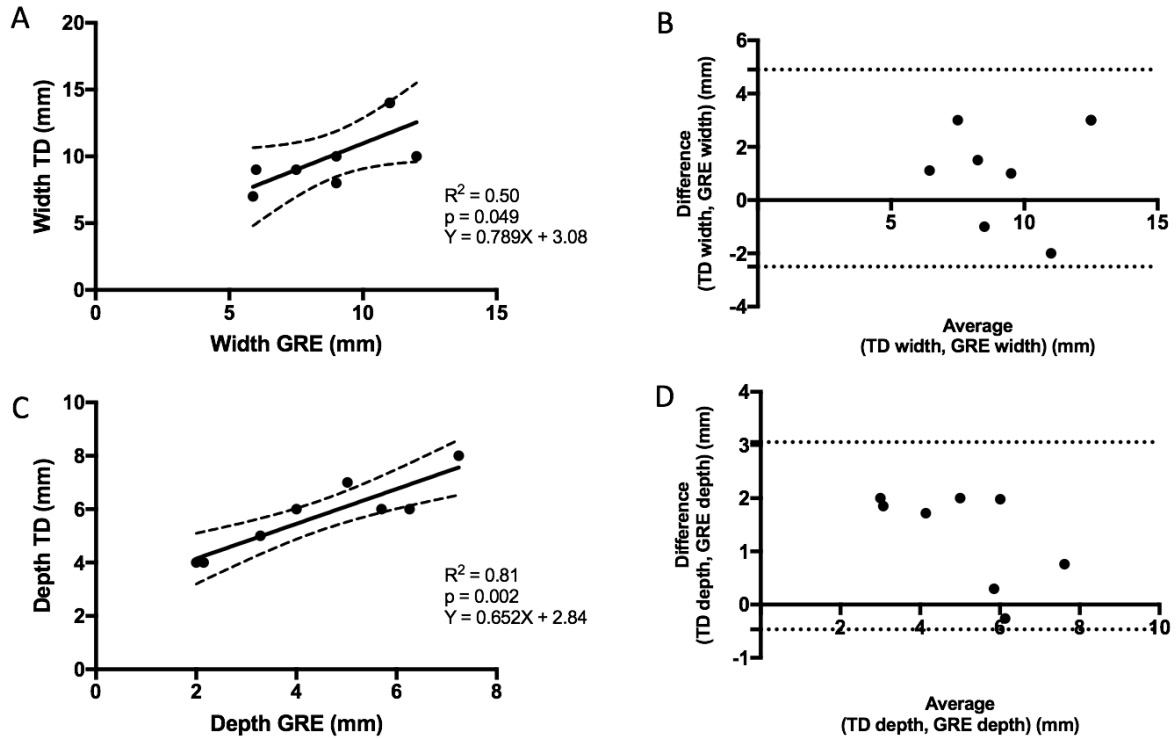
Figure 6-9: Relationship between lesion dimensions on thermal dose maps and 3D GRE IR imaging.

Linear regression between ablation lesion width (A) and depth (C) on 2D thermal dose maps and 3D GRE IR with a long TI (n = 8 lesions). Bland-Altman plots showing the agreement on lesion width (B) and depth (D) size to those dimensions obtained on 3D GRE. Dashed/dotted lines indicate 95% confidence bands (A and C) and 95% confidence intervals (B and D). Several points may represent more than one measure given that several lesion dimensions were identical.

6.3.5   Gross macroscopy and histological assessment

On gross macroscopy, a zone of pallor could be clearly delineated corresponding to the ablation lesion core with a surrounding haemorrhagic zone. Lesion transmurality of >75% was seen in 16/19 ablation lesions. Microscopic histology of acute ablation injury on haematoxylin and eosin staining demonstrated partial loss of membrane borders, nuclear elongation and interstitial oedema - *Figure 6-10.*
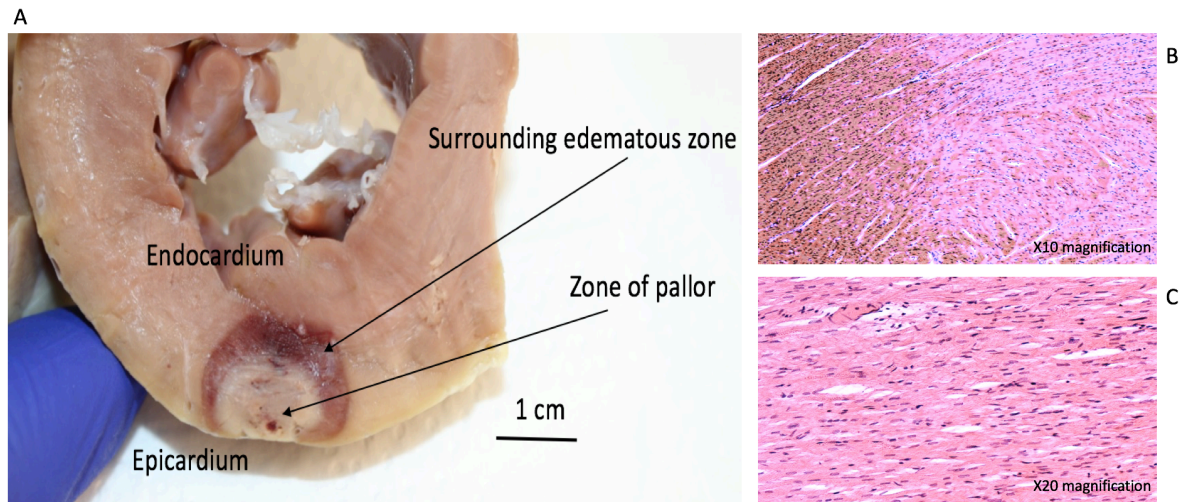
Figure 6-10: Gross pathological and histological appearances of ablation lesion

A zone of pallor with a surrounding oedematous zone is clearly visible on ablation lesions (A). 16/19 lesions showed a >75% transmurality. On microscopic examination (haematoxylin and eosin stain), at 10x and 20x magnification, evidence of loss of membrane borders, interstitial oedema and nuclear elongation was visible within regions of ablated tissue (B and C).

6.4   Discussion

This study demonstrates the feasibility of using real-time MRI guidance to perform both epicardial and endocardial radiofrequency ablation using active catheter tracking in a porcine model. Real-time visualisation of ablation lesions can be achieved using a dedicated MR-thermometry sequence whilst estimated lesion dimensions by MR-dosimetry corresponded to those obtained on gross pathology and a non-contrast 3D GRE IR sequence with a long TI.

Lardo et al. (2000) first described the use of MRI for the spatial and temporal characterisation of RF lesions during MR-guided ablation in mongrel dogs. Regional changes in ablated tissue within the right ventricular (RV) apex were observed using a T2-weighted fast-spin-echo and gadolinium-enhanced T1-weighted gradient-echo sequences. There was a strong correlation between MR-derived lesion area and post-mortem lesion area. Subsequently, in a canine model, four distinct phases of contrast-enhanced signal enhancement were described over a 10-hour time period following epicardial RF delivery (Dickfeld et al. 2006). RF lesions initially had a low signal intensity with increasing enhancement seen in the lesion periphery

at 4-minutes post-ablation which progressively extended to the centre of a given lesion. Full delayed enhancement was observed at approximately 21-minutes post ablation and lesions remained detectable up to 10 hours later. These findings suggested different wash-in and wash-out kinetics of gadolinium in ablation lesions compared to myocardial infarction and may reflect different underlying pathophysiological processes (Dickfeld et al. 2006). More recently, in a canine recovery model, using LGE and T2-weighted oedema imaging, microvascular obstruction volume at 26-minutes post contrast administration appeared to be the best predictor of chronic lesion volume (Ghafoori et al. 2017).

However, administration of exogenous contrast agents can only be given once during a MR-guided ablation procedure. In order to perform repeated assessments at multiple stages of an ablation procedure to characterise lesion formation and potentially titrate therapy based on MR information, the development of sequences without the use of contrast agents are required, ideally which can be performed in real-time.

Celik et al. (2014) described changes in the intrinsic T1 value in lesion cores and intrinsic T2 values in the oedematous regions of RF ablation using MR-relaxometry. Shortening of T1 values were correlated to the presence of ferric iron which could have resulted from a change in iron state inside lesion cores due to conversion of haemoglobin to methaemoglobin during tissue heating. The authors concluded that non-contrast characterisation of T1 changes in ablation lesions may be more reliable than LGE where contrast agent distribution could be affected by changes in membrane permeability and microvascular obstruction (Celik et al. 2014). Dickfeld et al. (2007) characterised the temporal evolution of non-contrast T1 and T2-weighted imaging of RF lesions over a 12-hour time period in mongrel dogs. T2-weighted images demonstrated an elliptical high signal core and a surrounding low intensity rim whilst

T1-weighted images lacked a surrounding rim. These changes were related to central tissue necrosis and transition zone respectively on histopathological examination. More recently, a T1-weighted sequence with a long inversion time (TI = 700ms) has been used to discriminate between chronic scar in a porcine model of myocardial infarction and acute ablation lesions. Enhancement on the non-contrast T1-weighted sequence appeared to be more specific and stationary than LGE (Guttman et al. 2018).

In this study, a real-time technique of lesion assessment (MR-thermometry) was used for lesion imaging, given its potential utility during MR-EP procedures and compared to both non-contrast GRE imaging with a long TI and gross pathological examination.

6.4.1 Demonstration of MR-EP tracking and therapy accuracy

The use of active catheter tracking with a dedicated tracking sequence, detected by microcoils in a MR-compatible catheter has been employed previously (Chubb et al. 2017). The microcoil method is advantageous due to its ability to track multiple coils along the body of the catheter, a faster rate of tracking and choice of guidance using acquired road-maps or real-time imaging (Chubb et al. 2017). Grothoff et al. (2017) reported the use of active catheter tracking to guide intubation of the coronary sinus, trans-septal puncture, activation mapping of the left atrium and ablation of the AV node in pigs. Catheter position was confirmed by passive real-time imaging. Our group have previously demonstrated the feasibility of real-time MRI-guided catheter ablation in patients with typical atrial flutter using active catheter tracking (Chubb et al. 2017). Using a combination of active tracking and catheter visualisation with real-time MR imaging, Hilbert et al. (2016) also performed cavotricuspid isthmus ablation in six patients with a mean procedural time of 109 +/- 58 mins. Complete isthmus block was achieved in 3/6 patients without additional fluoroscopy.

There are little data, however, demonstrating the accuracy of radiofrequency ablation in a real-time MR environment, in the ventricle. Given the challenges of catheter manipulation and lesion delivery inside the MRI environment within the LV, a spatial accuracy of <1mm and conformational accuracy <7 degrees is encouraging. Further work to assess the spatial accuracy of lesion delivery to the scar borderzone tissue with the MR-EP system will be required to ensure that progress is made on a complete MR-based solution for VT substrate modification.

6.4.2   Real-time lesion visualisation

There has been significant interest in the development of MR tools to assess ablation lesions in real-time. Direct monitoring of tissue temperature using MR-thermometry and dosimetry offers an exciting means of exploiting acute physiological changes and could potentially be used to improve the safety and efficacy of catheter ablation. Kolandaivelu et al. (2010) first described the use of MR-thermometry using the Proton Resonance Frequency (PRF) shift technique to quantify tissue temperature changes that lead to ablation lesion formation. In mongrel dogs, the maximum ablation lesion extent during endocardial radiofrequency ablation on MR-thermometry corresponded well to the lesion location, depth on LGE-MRI and pathological examination (Kolandaivelu et al. 2010). Lesion transmurality with MR-thermography was within 20% of that measured by pathology and LGE-MRI. Recently in an ovine model, Toupin et al. (2017) demonstrated that endocardial ablation lesion dimensions on thermal dose images correlated well with 3D T1-weighted images acquired immediately after ablation. The precision of lesion extent in the myocardium was in the region of 1mm – potentially offering a useful MR tool in real-time to guide the safety and efficacy of radiofrequency ablation. The same group have also optimised their thermometry pipeline to improve the spatial resolution achieved (1.6 x 1.6 x 3mm) and display of several slices per

heartbeat to resolve temperature distribution in the myocardium during catheter ablation (Ozenne et al. 2017). Their thermometry method relies on ECG-triggered echo-planar imaging, similar to this thesis, but utilises an optical flow algorithm to perform voxelwise registration of temperature maps in real-time. In addition, a principal component analysis method is employed to compensate for motion-related susceptibility artifacts and a temporal filter applied to increase the precision of temperature measurements (Ozenne et al. 2017). Initial results in healthy volunteers showed excellent temperature stability and in an ovine model of RF ablation, thermal lesion dimensions on dosimetry images were in good agreement with those at gross pathology (Ozenne et al. 2017). The presence of arrhythmia may also impact the precision of temperature measurements. In patients with frequent ectopic beats, the temporal standard deviation of temperature was $2.5^{o}C$, compared to a temporal standard deviation of $1.6^{o}C$ in patients who were in sinus rhythm (Ozenne et al. 2019). A rejection strategy where corrupted phase images during arrhythmia-related beats are removed resulted in an improvement in the precision of temperature measurement whilst maintaining the frame rate (Ozenne et al. 2019). The feasibility of performing MR-thermometry in the presence of persistent arrhythmia, however, remains to be established.

In this thesis, the MR-thermometry pipeline is extended to provide an assessment of epicardial lesion extent during radiofrequency ablation in a separate large animal model. There was a moderate association between lesion width on 3D GRE IR imaging and thermal dose maps but an improved association on lesion depth. This difference could be explained by the accuracy of correspondence between the orientation and position of the 2D magnitude images from MR-thermometry and 3D slices on the GRE imaging. As can be seen in *Figure 6-5,* lesion depth appears consistent across thermometry slices but lesion width can vary considerably depending on the slice chosen for measurements.

Further work is required to assess how real-time lesion imaging relates to chronic transmural lesions – a porcine recovery model of ventricular ablation could be used to confirm long-term efficacy in future studies. In this study, the thermal dose model was used for the prediction of ablation lesion size. Other approaches have also been proposed such as using the maximum temperature peak for each voxel (Toupin et al. 2017; Kolandaivelu et al. 2010). Further work is needed to establish the most accurate model for the prediction of permanent ablation lesions. Of the various approaches available to assess acute ablation injury (LGE, T1-weighted, T2-weighted, MR-thermometry), thermometry remains the only technique with the ability to assess lesions in real-time and would be ideally suited for MR-EP interventions. However, there are several limitations to the technique in its current form that need to be overcome (described below).

6.4.3   Limitations

Following ventricular radiofrequency ablation, large animal models frequently become tachycardic and/or develop ventricular arrhythmias which may affect the quality of the myocardium, blood and phase signal during MR-thermometry. MR-thermometry in the presence of irregular heart rhythm was not evaluated in this study and its feasibility remains to be established, particularly during RF ablation. Further refinements in the thermometry technique may be needed to overcome these limitations (see Section 7.2.3). We did not evaluate chronic ablation injury in this model, therefore further work is needed to evaluate whether thermal dose achieved during acute lesions corresponds to permanent lesion formation in a recovery model. The sensitivity and specificity of MR-thermometry for lesion monitoring during ablation was not assessed whilst the limited number of lesions delivered precluded our ability to assess if the extent of temperature rise could be predictive of lesion

transmurality – these areas could be an important focus of future work. The thermometry data required post-processing offline to generate the data on lesion dimensions. For this data to be useful to the electrophysiologist, a real-time pipeline with visualisation of the thermal dose onto an anatomical shell and demonstration of lesion dimension needs to be developed to guide catheter ablation although this was beyond the scope of this preliminary work.

In order to facilitate VT ablation under MRI guidance in patients, there are still significant hurdles to overcome such as the availability of MRI-conditional defibrillation systems and MR-compatible 12-lead ECG systems. Patients undergoing VT ablation frequently require defibrillation – the time delay associated with removing a patient from the scanner bore before delivery of cardiopulmonary resuscitation and defibrillation could potentially increase the risk of mortality. Although there are prototype MR-compatible defibrillation systems currently undergoing testing, until there are robust systems that are shown to be successfully able to defibrillate patients without increasing the time needed for defibrillation, the uptake of higher-risk MR-guided interventions is likely to be limited.

6.5   Conclusions

This study demonstrates that the real-time MR-EP system can be used to target ablation lesions within the porcine left ventricle with a high degree of spatial and conformational accuracy. Furthermore, MR-thermometry and dosimetry enabled real-time visualisation of ablation injury and estimation of lesion dimensions. There was a good agreement between lesion sizes obtained from thermal dose maps to those obtained from 3D GRE IR imaging and gross pathological examination.

SECTION FOUR:

SUMMARY AND

FUTURE

DIRECTIONS

7 Summary and future directions

7.1 Original contributions

The aim of this thesis was to explore the use of a real-time MR-EP system for the evaluation of structural and electrophysiological ventricular tachycardia substrate and its application for catheter ablation. The potential benefits of MR-guided ablation include accurate 3D substrate assessment at the time of intervention with minimisation of registration error between structural and electrical data, intra-procedural guidance using dedicated MR-tracking techniques and assessment of ablation lesions in real-time. The main drawbacks of the system include limited availability of MR-compatible electrophysiology catheters, 12-lead ECG systems and defibrillators. The procedures are generally more time-consuming, expensive and require a steep learning curve for an electrophysiologist. There is also a lack of evidence currently that the use of MR-EP systems can impact on the safety, efficacy or efficiency of catheter ablation. Although most studies to date utilising MR-EP systems have focused on the atria, where significant technical challenges remain for accurate substrate assessment, the benefits of these systems are likely to be realised in the context of VT ablation. Given these issues, this thesis explored three main areas with respect to MR-guided VT ablation in order to guide the development of this new platform:

1. **Substrate assessment** - There have been numerous studies published using LGE-MRI to assess the substrate for VT. However, the assessment of LV scar heterogeneity which is crucial for identification of target sites for catheter ablation, is dependent on the spatial resolution of the MR sequence used. Differences in the type of LGE sequence used can also influence the image quality, signal-to-noise ratio, contrast-to-noise ratio as well as overall acquisition times. 3D isotropic LGE sequences may provide the optimal method to accurately assess LV borderzone

regions and thereby evaluate regions of scar heterogeneity, however, these require

prolonged acquisition times and/or image acceleration techniques. To date, there have

been few head-to-head comparisons of LGE sequences to determine the optimal

method of LV scar and borderzone tissue assessment. In this thesis, using an

experimental infarct model and a slow infusion of contrast to maintain steady-state, a

direct comparison between three high-resolution LGE sequences was performed

under consistent contrast conditions, alongside ex-vivo validation of results. The use

of contrast steady-state enabled LGE imaging at a resolution of $1.2mm^3$ with

improved performance compared to standard 2D clinical LGE in the animal model.

Furthermore, a 3D LGE sequence with a bSSFP read-out was qualitatively improved

compared to a GRE read-out and a black-blood LGE sequence. These findings have

important implications for clinical MRI protocols in patients pre-VT ablation where

use of standard 2D LGE may be insufficient to aid the electrophysiologist in planning

an ablation procedure. The accurate identification of VT substrate can be challenging

and ablating a region which does not harbour the critical re-entry circuit is an

important factor determining the success of the procedure. 2D LGE is widely used for

diagnostic purposes but may simply not have sufficient resolution to robustly identify

the target sites for VT ablation. Although application of high-resolution 3D LGE with

contrast steady-state in conscious patients proved challenging due to prolonged

acquisition times, incorporation of the protocol immediately pre-ablation in an

anaesthetised patient as part of a MR-EP procedure may prove to be feasible, but

further work will be required to optimise the workflow.

2. **Comparison between structural and electrophysiological substrate** - Multiple

studies have also been published where the association between electrophysiological

substrate (generally bipolar voltage) and MRI-derived scar have been compared. Generally, these studies have relied on pre-procedural imaging acquired days or weeks prior to an ablation procedure where possible changes in loading conditions and/or rhythm between the time of imaging and time of mapping could introduce a registration error and result in mis-match of data. In addition, few studies have utilised high-resolution (<1.5mm^3) LGE imaging for scar assessment. This thesis provides an objective comparison between structural and electrophysiological substrate whereby LGE imaging was optimised using the contrast steady-state protocol, data was acquired within a real-time MR-EP setting where registration error was minimised and a point-by-point analysis technique implemented to achieve improved precision. The main disadvantage of this approach was the limited resolution of EAM data with the MR-EP system due to inherent limitations in the design of the MR-compatible catheter and lack of an automated mapping system for use inside the MR scanner. Nevertheless, a moderate association was found between measurements of bipolar voltage, S-QRS and LGE with this system, despite the minimisation of registration error, highlighting the difficulty in using structural data to predict electrophysiological substrate.

3. **Catheter ablation in the left ventricle with the MR-EP system and real-time lesion imaging** - The ability of the MR-EP system to use active catheter tracking to reach the target region within the LV and ablate both from the endocardium and epicardium was evaluated in this thesis. The MR-EP system provides an opportunity to evaluate anatomical and physiological changes during ablation as well as monitor lesion formation in real-time, in a way which is not possible in the conventional catheter laboratory. This thesis investigated the use of temperature mapping (MR-

thermometry) to directly monitor lesion formation in real-time whilst MR-dosimetry was used to estimate lesion dimensions. There was a good correlation between lesion dimensions using MR-dosimetry to those obtained with a non-contrast T1-weighted sequence and gross pathology. These findings are consistent with those recently reported by the Bordeaux group (Toupin et al. 2017; JCMR) in an ovine model and extend the use of MR-thermometry to assessment of epicardial ablation. Much work is still required to optimise the imaging techniques and demonstrate its ability to predict chronic lesion size, but the study demonstrated the feasibility of the application of MR-thermometry to ventricular ablation.

It is well known that scar pattern can be substantially different in different etiologies of structural heart disease. Typically, in ischaemic cardiomyopathy, compact scar may be present extending from the sub-endocardium to the epicardium with sparing of the endocardial rim. Patients with non-ischaemic cardiomyopathy may have a highly variable scar pattern - previous work has suggested that fibrosis architecture is rarely compact but typically patchy and/or diffuse (Glashan et al. 2018). In dilated cardiomyopathy, scars may be subendocardial, subepicardial, mid-wall or transmural whilst the architecture may be patchy or diffuse. In hypertrophic cardiomyopathy, interstitial fibrosis may be present preferentially involving the septum followed by the lateral and apical LV wall. In ARVC, fibrofatty replacement of myocardium may start in the subepicardium, usually affecting the RV but may also be present in the LV (Sramko et al. 2019).

In order to evaluate the real-time MR-EP system used in this thesis including clinical-grade MR-compatible catheters, a large animal model was required. Although there are small animal models of non-ischaemic cardiomyopathy utilising surgical techniques, genetic

modifications or pharmacological approaches, large animal models of non-ischaemic cardiomyopathy are generally lacking, mainly due to the increasing costs involved. As a result, a porcine model of ischaemic cardiomyopathy was used in this thesis which has recently been well characterised from an electroanatomic, imaging and histopathologic perspective (Tschabrunn et al. 2016).

The imaging techniques used in this thesis were deliberately performed at high spatial resolution in order to evaluate patchy/heterogeneous scar more accurately. It is therefore not expected that the inclusion of patients with non-ischaemic cardiomyopathy with different scar patterns would have necessarily changed the findings reported. It is possible that non-ischaemic scar patterns may have been more difficult to detect, particularly diffuse fibrosis with the imaging techniques described in this thesis. However, the principle that extended scar imaging under conditions of contrast steady-state would enable more detailed scar characterisation would still be expected to apply in non-ischaemic cardiomyopathy patients (where scar would otherwise be detected using standard LGE imaging). The concordance between imaging substrate and electrical substrate may have been affected if non-ischaemic scar was evaluated as patchy and/or diffuse scar remote from the endocardial surface could be difficult to detect on assessment of bipolar voltage due to its limited field of view (compared to unipolar voltage). No group has successfully evaluated unipolar voltage inside a MRI scanner due to the presence of low frequency noise/artifact at a frequency and amplitude that could corrupt near-field signals - this can make signal evaluation challenging. Improvements in noise cancellation and filtering techniques are required to resolve this challenge.

7.2 Future directions

7.2.1 *High resolution imaging of scar and integration into MR-EP systems*

Respiratory-navigated 3D LGE is known to improve the diagnostic yield of MRI in patients with VT, particularly when other diagnostic tests have been negative or even when conventional 2D LGE has revealed no substrate (Hennig et al. 2018). High resolution LGE ($<1.5mm^3$) may be valuable in providing detailed characterisation of 3D scar architecture and aid the delineation of VT ablation target sites. Using a 3D LGE sequence with an in-plane spatial resolution of 1.25 x 1.25mm, slice thickness of 2.5mm and image reconstruction into a stack of 1mm thick slices, (Yamashita et al. 2016) showed that image integration of scar architecture from MRI into the navigation system during VT ablation was successful in identification of 89% of critical isthmuses and 85% of LAVA sites. Furthermore, image integration impacted on procedural management through motivating additional mapping in regions of interest or modifying ablation strategy (Yamashita et al 2016). Given that the ability of MRI to identify heterogeneous tissue of intermediate signal intensity is spatial resolution-dependent (Schelbert et al. 2010), techniques to improve the spatial resolution of clinical protocols are needed. Image acceleration techniques such as compressed sensing can allow acquisition of high-resolution isotropic LGE imaging within scan times of approximately 3-4 minutes (Akcakaya et al. 2012). However, the under-sampled data obtained with compressed sensing protocols invariably results in a lower SNR and consequently CNR. Additionally, non-linear reconstruction of data may reduce the SNR further in the final images (Akcakaya et al. 2012; Basha et al. 2017). The contrast steady-state technique described in this thesis enables extended scar image acquisition, thereby pushing the boundaries of achieved spatial resolution to $1.2mm^3$. However, the animal model used was studied under optimal conditions and all clinical scans were performed in patients who did not have cardiac devices in-situ.

The majority of patients undergoing VT ablation will have an ICD in-situ. Performing MRI scans in the presence of devices has been shown to be safe with minor changes in device parameters occurring occasionally (Nazarian et al. 2017). However, image quality can be degraded significantly in the presence of ICDs. In a cohort of patients undergoing VT ablation, 3D LGE acquisitions were successfully performed but ICD-related artifacts often appeared as a central signal void with a surrounding rim of increased signal intensity (Dickfeld et al. 2011). As a result, LGE could only be fully assessed in 9 ± 4 out of 17 AHA segments and partially assessed in 12 ± 3 segments, limiting the registration of the 3D MRI scar map to the voltage map (Dickfeld et al. 2011). Typically, the inversion pulse used in conventional LGE imaging is spatially non-selective with a spectral bandwidth of 1.1kHz. The resonance offset of the myocardium in the presence of a cardiac device is around 2-6kHz, outside the bandwidth of the inversion pulse and as a result, the myocardium is not adequately nulled which can cause hyper-intense regions mimicking scar tissue (Rashid et al 2014). The incorporation of wideband adiabetic inversion pulses into LGE imaging to facilitate adequate myocardial signal nulling in the presence of devices has enabled a reduction of metal-related artifacts, optimised the clinical yield from MRI and frequently changed clinical management (Bhuva et al. 2019).

Most studies evaluating wideband LGE have used 2D multi-slice LGE with limited spatial resolution and SNR (Do et al. 2018). During 3D LGE imaging in the presence of an ICD, extended signal voids and ripple artifacts can appear compared to 2D imaging due to the spatially varying off-resonance introduced by the ICD and resulting distortion of the slice/slab profile. Recently, a modified wideband 3D LGE technique (spatial resolution: 1.4 x 1.4 x.4mm) has been described in patients with ICDs which replaced the conventional

inversion pulse with a 3.8kHz wideband inversion pulse and increased the bandwidth of the RF excitation pulse to reduce signal voids and ripple artifacts (Rashid et al. 2016). Further work is required to address if the contrast steady-state protocol can be applied to improve the spatial resolution of the 3D wideband sequence and its consequent impact on in-plane artifacts (e.g. readout distortion from the frequency encode process, intra-voxel dephasing) and through-plane artifacts.

In addition to the need for high-resolution 3D LGE imaging to identify VT substrate, real-time MR-EP requires rapid image processing including segmentation and registration. In this thesis, manual segmentation of whole heart anatomy was employed which required around 30 minutes of processing time after imaging and before EAM. Semi-automated segmentation methods (e.g. thresholding), use of shape-constrained deformable models (Chubb et al. 2017) or probabilistic models (Karim et al. 2016) could speed up this process considerably and reduce overall procedure times.

Registration methods to integrate MR-derived scar images to EAM data typically use a combination of landmark and/or surface registration techniques, as employed in this thesis. However, real-time MR-EP provides an opportunity to acquire real-time reference images (e.g. bSSFP cine showing catheter position, regional wall motion, regions of wall thinning) and compare to prior 3D whole-heart road-maps or 3D scar maps. Registration of real-time imaging acquired with different spatial resolutions, plane orientation and acquisition parameters to 3D road-maps can be challenging. Updating the 3D road-map with 2D real-time images with a dynamic registration using extracted image-based features within a multi-scale framework has been described (Xu et al. 2015). This approach requires further validation in the setting of catheter ablation to assess if the accuracy of target delineation can be improved within the framework.

7.2.2   MR-guided EAM

The major limitation of MR-EP is the limited availability of catheters and devices which can be used inside the MRI scanner. Single electrode mapping catheters were used in this thesis requiring manual annotation of individual electrograms to derive activation, voltage and S-QRS data. The development of multi-electrode catheters which can be used inside the MRI environment has recently been reported (Elbes et al. 2017). Further development in catheter technology combined with the production of automated mapping systems that can be used as part of a MR-EP procedure is likely to accelerate progress in the field.

As described in Section 2.7.2, there are multiple sources of signal distortion inside a MRI scanner which can affect the fidelity of EGM signals. It remains unclear at present whether fine myocardial signals (e.g. LAVA) can be robustly detected inside a MRI scanner. Further work to investigate the impact of MR interference on EGM signal characteristics are required and a study is planned to evaluate scar signals in an infarct model with the MR-compatible catheter both inside and outside the MRI scanner. The best approach to track the MR-compatible catheter outside the MR scanner is unclear and may require a combination of fluoroscopy and ICE.

In order to demonstrate the accuracy of MR-guided EAM, a direct comparison with conventional EAM will be required. Given the technical challenges of performing VT ablation under MRI guidance and lack of MR-compatible defibrillation systems currently available, a study is instead planned to use the MR-EP system in patients with adult congenital heart disease undergoing an atrial ablation. This study will afford the opportunity to image atrial substrate with high-resolution 3D LGE and perform EAM using the MR-compatible catheter. As part of the study design, all patients will then be moved to the

catheter laboratory to have a conventional EAM with standard equipment and ablation, as required. In this way, a direct comparison of electrophysiological substrate between MR-guided EAM and conventional EAM can be performed.

Unless the technology available to perform EAM inside the MRI scanner develops sufficiently to compete with conventional EAM, it is possible that the role of MR-EP may simply be to optimise lesion targeting and perform lesion imaging after a conventional EAM has defined targets. Future studies will also have to demonstrate the ability of MR-EP to provide clinical benefit at a reasonable cost.

7.2.3   Development of MR-thermometry and dosimetry protocol

The reliability of MR-thermometry during catheter ablation is highly dependent on the quality of ECG-triggering. There are multiple factors which can lead to inadequate ECG-triggering during catheter ablation including the need for additional RF equipment, poor skin contact with ECG electrodes and strong gradient fields associated with echo-planar imaging sequences. In addition, the large animal models used in this thesis are known to be pro-arrhythmogenic and frequently experienced episodes of catheter-induced ventricular ectopy and occasional runs of VT during catheter ablation. Alternative methods to enable prospective cardiac triggering of the thermometry sequence could resolve these issues.

The MR-compatible catheters used in this thesis contained micro-coils used for tracking of the catheters in 3D space. Using the continuously measured active tracking position as a surrogate for cardiac motion could provide a method to prospectively trigger the thermometry acquisition. Preliminary work in a beating heart phantom - *Figure 7-1,* where the active

tracking modules were interleaved with the thermometry sequence, was performed to evaluate feasibility and temperature stability.
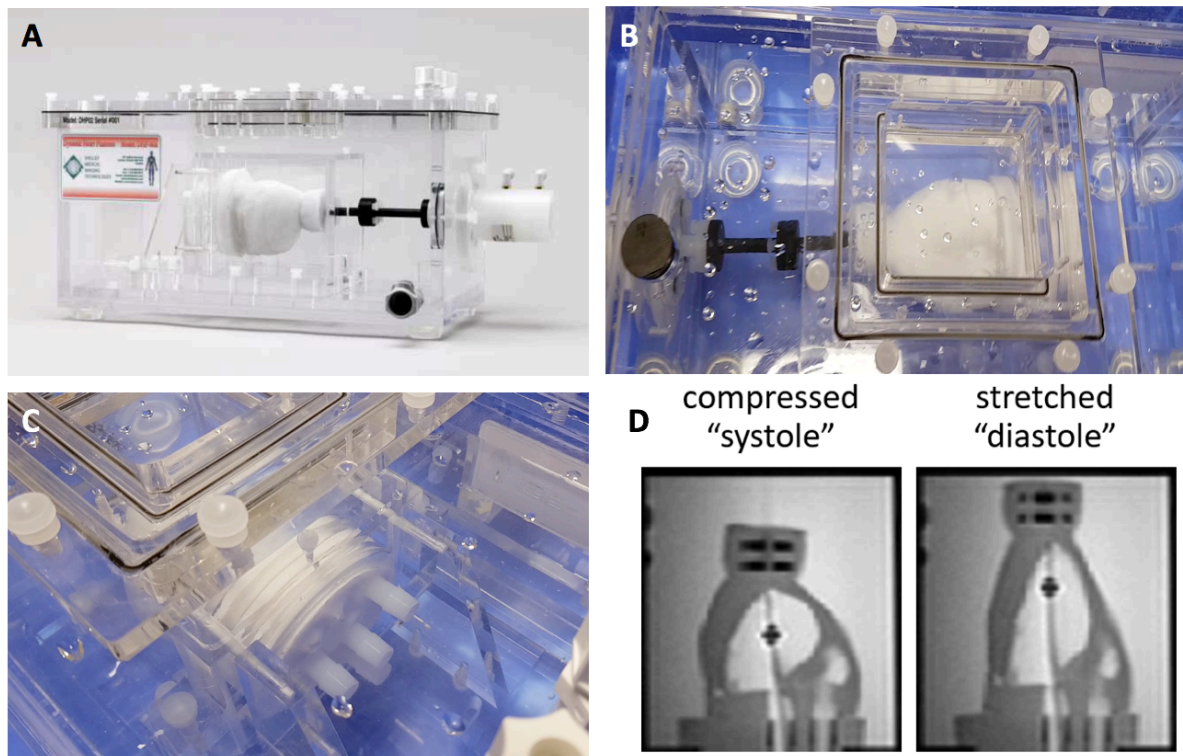
Figure 7-1: Cardiac motion phantom

A MR-compatible cardiac motion phantom (Shelley Medical Imaging Technologies, Canada) (A) comprised of a pneumatic control, acrylic tank, hydrogel heart and cardiac motion control software was used for phantom experiments to evaluate MR-thermometry with active tracking. The phantom containing the hydrogel heart (B) mimics systolic and diastolic motion of the heart and contains ports for catheter devices to be introduced into the heart (C). MR images of the phantom with a catheter in situ acquired during systole and diastole are shown in (D). Images courtesy of Dr Ronald Mooiwer.

In a series of experiments, the MR-thermometry sequence was acquired on an apical slice of the phantom at a heart rate of 60bpm. The sequence was interleaved with active tracking and compared to no triggering and evaluated in a scenario with no cardiac motion. An additional set of measurements were acquired with the phantom beating at 60bpm but triggering using a simulated ECG signal at 80bpm, in order to mimic mis-triggering. The following measurements were then made:

1. Segmentation of visible area of myocardium with all acquisitions - to quantify stability of acquisition

2. Temperature stability - using temperature maps generated from phase data and stability determined through calculation of the standard deviation during all dynamics

During active tracking-based triggering, all heartbeats were successfully detected. There was a strong similarity between myocardial areas detected during active-tracking based triggering and no motion. The temperature stability was $1.12 \pm 0.36^{\circ}$C during active tracking-triggered measurements and $>2.5^{\circ}$C during the mis-triggered scenario - *Figure 7-2*. Future work will focus on translation of this method during in-vivo cardiac RF ablation and will also need to model respiratory motion for accurate estimation of temperature.
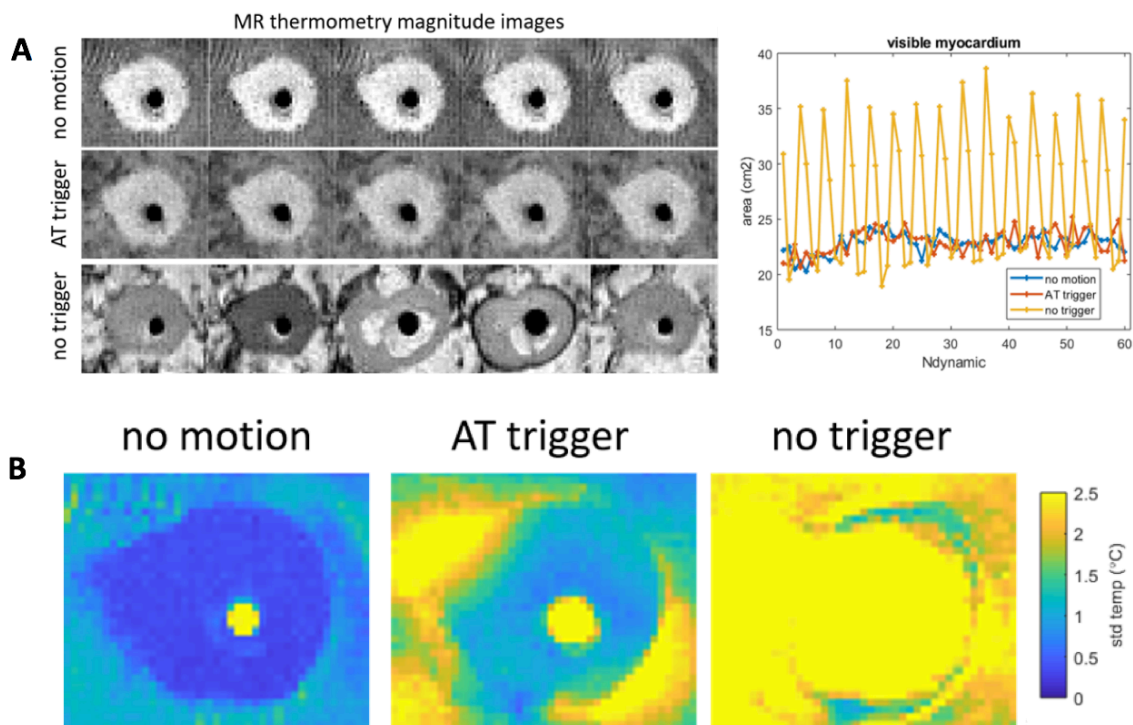
Figure 7-2: MR-thermometry with active-tracking triggering, no triggering and during no cardiac motion

Magnitude images acquired during five time-points using active tracking-triggered thermometry, no triggering and during no cardiac motion (A). The visible myocardial area during each of the three scenarios is also shown (A). A large variation in myocardial area is present in the absence of triggering. Temperature stability measurements are displayed for the three scenarios (B). Images courtesy of Dr Ronald Mooiwer and presented as an abstract at ISMRM 2019 (Mooiwer et al. 2019; Active tracking-based cardiac triggering of MR thermometry for MRI-guided cardiac ablation).

Acknowledgements

I have been fortunate to have had the opportunity to undertake a challenging but highly rewarding project as part of this thesis. Along the way, I have received extensive support and guidance from a number of mentors and colleagues. I would like to thank my supervisors Professor Mark O'Neill and Professor Reza Razavi who have worked tirelessly to support the animal experiments, provide guidance on the direction of this thesis, facilitated collaborations and remained optimistic despite the hurdles.

A large number of clinical colleagues have been involved in the conduct of the studies including Dr James Harrison, Dr Henry Chubb, Dr John Silberbauer, Dr Steven Williams, Dr John Whitaker, Dr Louisa O'Neill and Dr Iain Sim. I have thoroughly enjoyed my discussions and interactions with them and am very grateful for the time they have put in to travel hundreds of miles to support the experiments. I have also received extensive support

from the MR physicists including Dr Sebastien Roujol and Dr Radhouene Neji, in particular. Radhouene has worked tirelessly with me over a number of years to optimise imaging protocols and I am extremely grateful for his patience. Dr Steve Niederer and Dr Caroline Mendonca Costa have helped me with the image processing problems that I have encountered and I am grateful for their expertise. I have spent a significant amount of time working with colleagues in industry, including at Siemens Healthcare and Imricor during this thesis. In particular, I am grateful for the support provided to me by Dr Thomas Pohl, Dr Rainer Schneider and Mr Tom Lloyd. The organisation of the animal experiments in France was a significant logistical challenge and I am grateful for the support provided by Dr Kirstie Opstad, Dr Candice Millard and Dr Sophie Pernot.

Finally, I would like to thank my family, particularly my wife, Selina who has been patient, understanding and provided me with steadfast encouragement throughout this process. Without her support, this thesis would not have been possible and I am forever grateful.

Appendix A: References

Acosta, J., Andreu, D., Penela, D., Cabrera, M., Carlosena, A., Korshunov, V., Vassanelli, F., Borras, R., Martínez, M., Fernández-Armenta, J., Linhart, M., Tolosana, J.M., Mont, L. & Berruezo, A. 2018, "Elucidation of hidden slow conduction by double ventricular extrastimuli: a method for further arrhythmic substrate identification in ventricular tachycardia ablation procedures", *Europace : European pacing, arrhythmias, and cardiac electrophysiology : journal of the working groups on cardiac pacing, arrhythmias, and cardiac cellular electrophysiology of the European Society of Cardiology,* vol. 20, no. 2, pp. 337-346.

Acosta, J., Penela, D., Andreu, D., Cabrera, M., Carlosena, A., Vassanelli, F., Alarcón, F., Soto-Iglesias, D., Korshunov, V., Borras, R., Linhart, M., Martínez, M., Fernández-Armenta, J., Mont, L. & Berruezo, A. 2018, "Multielectrode vs. point-by-point mapping for ventricular tachycardia substrate ablation: a randomized study", *Europace : European pacing, arrhythmias, and cardiac electrophysiology : journal of the working groups on cardiac pacing, arrhythmias, and cardiac cellular electrophysiology of the European Society of Cardiology,* vol. 20, no. 3, pp. 512-519.

Akçakaya, M., Rayatzadeh, H., Basha, T.A., Hong, S.N., Chan, R.H., Kissinger, K.V., Hauser, T.H., Josephson, M.E., Manning, W.J. & Nezafat, R. 2012, "Accelerated Late Gadolinium Enhancement Cardiac MR Imaging with Isotropic Spatial Resolution Using Compressed Sensing: Initial Experience", *Radiology,* vol. 264, no. 3, pp. 691-699.

AL-KHATIB, S., DAUBERT, J.P., ANSTROM, K.J., DAOUD, E.G., GONZALEZ, M., SABA, S., JACKSON, K.P., REECE, T., GU, J., POKORNEY, S.D., GRANGER, C.B., HESS, P.L., MARK, D.B. & STEVENSON, W.G. 2015, "Catheter Ablation for Ventricular Tachycardia in Patients with an Implantable Cardioverter Defibrillator (CALYPSO) Pilot Trial", *Journal of cardiovascular electrophysiology,* vol. 26, no. 2, pp. 151-157.

Ambale-Venkatesh, B. & Lima, J.A. 2015, "Cardiac MRI: a central prognostic tool in myocardial fibrosis", *Nature Reviews Cardiology,* vol. 12, pp. 18-29.

Andreu, D., Berruezo, A., Ortiz-Pérez, J.T., Silva, E., Mont, L., Borras, R., de Caralt, T.M., Perea, R.J., Fernández-Armenta, J., Zeljko, H. & Brugada, J. 2011, "Integration of 3D electroanatomic maps and magnetic resonance scar characterization into the navigation system to guide ventricular tachycardia ablation", *Circulation: Arrhythmia and Electrophysiology,* vol. 4, no. 5, pp. 674-683.

Andreu, D., Ortiz-Pérez, J.T., Fernández-Armenta, J., Guiu, E., Acosta, J., Prat-González, S., De Caralt, T.M., Perea, R.J., Garrido, C., Mont, L., Brugada, J. & Berruezo, A. 2015, "3D delayed-enhanced magnetic resonance sequences improve conducting channel delineation prior to ventricular tachycardia ablation", *Europace : European pacing, arrhythmias, and cardiac electrophysiology : journal of the working groups on cardiac pacing, arrhythmias, and cardiac cellular electrophysiology of the European Society of Cardiology,* vol. 17, no. 6, pp. 938-945.

Andreu, D., Penela, D., Acosta, J., Fernández-Armenta, J., Perea, R.J., Soto-Iglesias, D., de Caralt, T.M., Ortiz-Perez, J.T., Prat-González, S., Borràs, R., Guasch, E., Tolosana, J.M., Mont, L. & Berruezo, A. 2017, *Cardiac magnetic resonance–aided scar dechanneling: Influence on acute and long-term outcomes.* Heart Rhythm: 14; 1121-28.

Androulakis, A.F.A., Zeppenfeld, K., Paiman, E.H.M., Piers, S.R.D., Wijnmaalen, A.P., Siebelink, H.J., Sramko, M., Lamb, H.J., van der Geest, Rob J., de Riva, M. & Tao, Q. 2019, *Entropy as a Novel Measure of Myocardial Tissue Heterogeneity for Prediction of Ventricular Arrhythmias and Mortality in Post-Infarct Patients.* JACC: Clinical Electrophysiology; 5: 480-9.

Anter, E., Tschabrunn, C.M., Buxton, A.E. & Josephson, M.E. 2016, "High-Resolution Mapping of Postinfarction Reentrant Ventricular Tachycardia: Electrophysiological Characterization of the Circuit.", *Circulation,* vol. 134, pp. 314-327.

Anter, E., Kleber, A.G., Rottmann, M., Leshem, E., Barkagan, M., Tschabrunn, C.M., Contreras-Valdes, F.M. & Buxton, A.E. 2018, *Infarct-Related Ventricular Tachycardia: Redefining the Electrophysiological Substrate of the Isthmus During Sinus Rhythm.* JACC: Clinical Electrophysiology; 4; 1033-48.

Arenal, A., Glez-Torrecilla, E., Ortiz, M., Villacastín, J., Fdez-Portales, J., Sousa, E., del Castillo, S., Perez de Isla, L., Jimenez, J. & Almendral, J. 2003, *Ablation of electrograms with an isolated, delayed component as treatment of unmappable monomorphic ventricular tachycardias in patients with structural heart disease.* JACC: 41; 81-92.

Arenal, Á, Hernández, J., Calvo, D., Ceballos, C., Atéa, L., Datino, T., Atienza, F., González-Torrecilla, E., Eídelman, G., Miracle, Á, Avila, P., Bermejo, J. & Fernández-Avilés, F. 2013, *Safety, Long-Term Results, and Predictors of Recurrence After Complete Endocardial Ventricular Tachycardia Substrate Ablation in Patients With Previous Myocardial Infarction.* American Journal of Cardiology; 111: 499-505

Ashikaga, H., Sasano, T., Dong, J., Zviman, M.M., Evers, R., Hopenfeld, B., Castro, V., Helm, R.H., Dickfeld, T., Nazarian, S., Donahue, J.K., Berger, R.D., Calkins, H., Abraham, M.R., Marban, E., Lardo, A.C., McVeigh, E.R. & Halperin, H.R. 2007a,

"Magnetic resonance-based anatomical analysis of scar-related ventricular tachycardia: implications for catheter ablation", *Circulation Research,* vol. 101, pp. 939-947.

Ashikaga, H., Sasano, T., Dong, J., Zviman, M.M., Evers, R., Hopenfeld, B., Castro, V., Helm, R.H., Dickfeld, T., Nazarian, S., Donahue, K., Berger, R.D., Calkins, H., Abraham, R., Marban, E., Lardo, A.C., McVeigh, E.R. & Halperin, H.R. 2007b, "Magnetic resonance-based anatomical analysis of scar-related ventricular tachycardia: implications for catheter ablation", *Circulation Research,* vol. 101, pp. 939-947.

Ashikaga, H., Arevalo, H., Vadakkumpadan, F., Blake, R.C., Bayer, J.D., Nazarian, S., Muz Zviman, M., Tandri, H., Berger, R.D., Calkins, H., Herzka, D.A., Trayanova, N.A. & Halperin, H.R. 2013, *Feasibility of image-based simulation to estimate ablation target in human ventricular arrhythmia*. Heart Rhythm; 10: 1109-16.

Audette, M.A., Ferrie, F.P. & Peters, T.M. 2000, *An algorithmic overview of surface registration techniques for medical imaging*. Medical Image Analysis; 4: 201-17.

Basha, T.A., Akçakaya, M., Liew, C., Tsao, C.W., Delling, F.N., Addae, G., Ngo, L., Manning, W.J. & Nezafat, R. 2017, "Clinical performance of high-resolution late gadolinium enhancement imaging with compressed sensing", *Journal of Magnetic Resonance Imaging,* vol. 46, no. 6, pp. 1829-1838.

Basha, T.A., Tang, M.C., Tsao, C., Tschabrunn, C.M., Anter, E., Manning, W.J. & Nezafat, R. 2018, "Improved dark blood late gadolinium enhancement (DB-LGE) imaging using an optimized joint inversion preparation and T2 magnetization preparation", *Magnetic Resonance in Medicine,* vol. 79, no. 1, pp. 351-360.

Berruezo, A., Fernandez-Armenta, J., Andreu, D., Penela, D., Herczku, C., Evertz, R., Cipoletta, L., Acosta, J., Borras, R., Arbelo, E., Tolosana, J.M., Brugada, J. & Mont, L. 2015, "Scar dechanneling: new method for scar-related left ventricular tachycardia substrate ablation", *Circulation: Arrhythmia and Electrophysiology,* vol. 8, pp. 326-336.

Bhagirath, P., van der Graaf, M., Karim, R., Rhode, K., Piorkowski, C., Razavi, R., Schwitter, J. & Gotte, M. 2015, "Interventional cardiac magnetic resonance imaging in electrophysiology: advances toward clinical translation", *Circulation: Arrhythmia and Electrophysiology,* vol. 8, no. 1, pp. 203-11.

Bhuva, A.N., Kellman, P., Graham, A., Ramlall, M., Boubertakh, R., Feuchter, P., Hawkins, A., Lowe, M., Lambiase, P.D., Sekhri, N., Schilling, R.J., Moon, J.C. & Manisty, C.H. 2019, *Clinical impact of cardiovascular magnetic resonance with optimized myocardial scar detection in patients with cardiac implantable devices*. International Journal of Cardiology: 279; 72-78.

Blissett, S., Chetrit, M., Kovacina, B., Mardigyan, V. & Afilalo, J. 2018, *Performing Cardiac Magnetic Resonance Imaging in Patients With Cardiac Implantable Electronic Devices: A Contemporary Review*. Canadian Journal of Cardiology 2018: 34; 1682-1686.

Bogun, F., Crawford, T., Reich, S., Koelling, T.M., Armstrong, W., Good, E., Jongnarangsin, K., Marine, J.E., Chugh, A., Pelosi, F., Oral, H. & Morady, F. 2007, "Radiofrequency ablation of frequent, idiopathic premature ventricular complexes: comparison with a control group without intervention", *Heart Rhythm,* vol. 4, pp. 863-867.

Bogun, F.M., Desjardins, B., Good, E., Gupta, S., Crawford, T., Oral, H., Ebinger, M., Pelosi, F., Chugh, A., Jongnarangsin, K. & Morady, F. 2009, *Delayed-Enhanced Magnetic*

Resonance Imaging in Nonischemic Cardiomyopathy: Utility for Identifying the Ventricular Arrhythmia Substrate.

Bogun, F., Krishnan, S., Siddiqui, M., Good, E., Marine, J.E., Schuger, C., Oral, H., Chugh, A., Pelosi, F. & Morady, F. 2005, *Electrogram Characteristics in Postinfarction Ventricular Tachycardia: Effect of Infarct Age.*

Briceño, D.F., Romero, J., Villablanca, P.A., Londoño, A., Diaz, J.C., Maraj, I., Batul, S.A., Madan, N., Patel, J., Jagannath, A., Mohanty, S., Mohanty, P., Gianni, C., Della Rocca, D., Sabri, A., Kim, S.G., Natale, A. & Di Biase, L. 2018, "Long-term outcomes of different ablation strategies for ventricular tachycardia in patients with structural heart disease: systematic review and meta-analysis", *Europace : European pacing, arrhythmias, and cardiac electrophysiology : journal of the working groups on cardiac pacing, arrhythmias, and cardiac cellular electrophysiology of the European Society of Cardiology,* vol. 20, no. 1, pp. 104-115.

Brunckhorst, C.B., Stevenson, W.G., Soejima, K., Maisel, W.H., Delacretaz, E., Friedman, P.L. & Ben-Haim, S.A. 2003, *Relationship of slow conduction detected by pace-mapping to ventricular tachycardia re-entry circuit sites after infarction.* Journal of the American College of Cardiology; 41: 802-809.

Callans, D.J., Ren, J.F., Michele, J., Marchlinski, F.E. & Dillon, S.M. 1999, "Electroanatomic left ventricular mapping in the porcine model of healed anterior myocardial infarction. Correlation with intracardiac echocardiography and pathological analysis.", *Circulation,* vol. 100, pp. 1744-1750.

Campbell-Washburn, A., Tavallaei, M.A., Pop, M., Grant, E.K., Chubb, H., Rhode, K. & Wright, G.A. 2017, "Real-time MRI guidance of cardiac interventions", *Journal of Magnetic Resonance Imaging,* vol. 46, no. 4, pp. 935-950.

Carbucicchio, C., Santamaria, M., Trevisi, N., Maccabelli, G., Giraldi, F., Fassini, G., Riva, S., Moltrasio, M., Cireddu, M., Veglia, F. & Della Bella, P. 2008, "Catheter ablation for the treatment of electrical storm in patients with implantable cardioverter-defibrillators: short- and long-term outcomes in a prospective single-center study", *Circulation,* vol. 117, pp. 462-469.

Celik, H., Ramanan, V., Barry, J., Ghate, S., Leber, V., Oduneye, S., Gu, Y., Jamali, M., Ghugre, N., Stainsby, J.A., Shurrab, M., Crystal, E. & Wright, G.A. 2014, "Intrinsic contrast for characterization of acute radiofrequency ablation lesions", *Circulation: Arrhythmia and Electrophysiology,* vol. 7, pp. 718-27.

Chang, I.A. 2010, "Considerations for thermal injury analysis for RF ablation devices", *The Open Biomedical Engineering Journal,* vol. 4, pp. 3-12.

Chubb, H., Karim, R., Roujol, S., Nunez-Garcia, M., Williams, S.E., Whitaker, J., Harrison, J., Butakoff, C., Camara, O., Chiribiri, A., Schaeffter, T., Wright, M., O'Neill, M. & Razavi, R. 2018, "The reproducibility of late gadolinium enhancement cardiovascular magnetic resonance imaging of post-ablation atrial scar: a cross-over study", *Journal of Cardiovascular Magnetic Resonance,* vol. 20, no. 1, pp. 21.

Chubb, H., Williams, S.E., Whitaker, J., Harrison, J.L., Razavi, R. & O'Neill, M. 2017, "Cardiac Electrophysiology Under MRI Guidance: an Emerging Technology", *Arrhythmia and Electrophysiology Review,* vol. 6, pp. 85-93.

Chubb, H., Harrison, J.L., Weiss, S., Krueger, S., Koken, P., Bloch, L.Ø, Kim, W.Y., Stenzel, G.S., Wedan, S.R., Weisz, J.L., Gill, J., Schaeffter, T., O'Neill, M.D. & Razavi, R.S. 2017, *Development, Preclinical Validation, and Clinical Translation of a Cardiac Magnetic Resonance - Electrophysiology System With Active Catheter Tracking for Ablation of Cardiac Arrhythmia*. JACC: Clinical Electrophysiology; 3: 89-103.

Codreanu, A., Odille, F., Aliot, E., Marie, P., Magnin-Poull, I., Andronache, M., Mandry, D., Djaballah, W., Régent, D., Felblinger, J. & de Chillou, C. 2008, *Electroanatomic Characterization of Post-Infarct Scars: Comparison With 3-Dimensional Myocardial Scar Reconstruction Based on Magnetic Resonance Imaging*. Journal of the American College of Cardiology: 52; 839-42.

Creta, A., Chow, A.W., Sporton, S., Finlay, M., Papageorgiou, N., Honarbakhsh, S., Dillon, G., Graham, A., Patel, K., Dhinoja, M., Earley, M.J., Hunter, R.J., Lowe, M., Rowland, E., Segal, O.R., Calabrese, V., Ricciardi, D., Lambiase, P.D., Schilling, R.J. & Providencia, R. 2019, "Catheter ablation for fascicular ventricular tachycardia: a systematic review", *International Journal of Cardiology,* vol. 276, pp. 136-148.

Daniels, B.R., Pratt, R., Giaquinto, R. & Dumoulin, C. 2016, *Optimizing accuracy and precision of micro-coil localization in active-MR tracking*. Magnetic Resonance Imaging; 34: 289-97.

Dawson, D.K., Hawlisch, K., Prescott, G., Roussin, I., Di Pietro, E., Deac, M., Wong, J., Frenneaux, M.P., Pennell, D.J. & Prasad, S.K. 2013, *Prognostic Role of CMR in Patients Presenting With Ventricular Arrhythmias*. JACC: Cardiovascular Imaging: 6; 335-44.

de Bakker, J.M., van Capelle, F.J., Janse, M.J., Tasseron, S., Vermeulen, J.T., de Jonge, N. & Lahpor, J.R. 1993, "Slow conduction in the infarcted human heart. 'Zigzag' course of activation", *Circulation,* vol. 88, no. 3, pp. 915-926.

de Chillou, C., Groben, L., Magnin-Poull, I., Andronache, M., Abbas, M.M., Zhang, N., Abdelaal, A., Ammar, S., Sellal, J., Schwartz, J., Brembilla-Perrot, B., Aliot, E. & Marchlinski, F.E. 2014, *Localizing the critical isthmus of postinfarct ventricular tachycardia: The value of pace-mapping during sinus rhythm*. Heart Rhythm: 11; 175-81.

de Chillou, C., Sellal, J. & Magnin-Poull, I. 2017, *Pace Mapping to Localize the Critical Isthmus of Ventricular Tachycardia*. Cardiac Electrophysiology Clinics: 9; 71-80.

de Groot, N., Schalij, M.J., Zeppenfeld, K., Blom, N.A., Van der Velde, E T & Van der Wall, E E 2003, "Voltage and activation mapping: how the recording technique affects the outcome of catheter ablation procedures in patients with congenital heart disease", *Circulation,* vol. 108, pp. 2099-2106.

de Haan, S., Meijers, T.A., Knaapen, P., Beek, A.M., van Rossum, A.C. & Allaart, C.P. 2011, "Scar size and characteristics assessed by CMR predict ventricular arrhythmias in ischaemic cardiomyopathy: comparison of previously validated models", *HEART,* vol. 97, pp. 1951-1956.

de Senneville, B.D., Roujol, S., Jais, P., Moonen, C.T., Herigault, G. & Question, B. 2012, "Feasibility of fast MR-thermometry during cardiac radiofrequency ablation", *NMR Biomedicine,* vol. 25, pp. 556-562.

de Senneville, B.D., Mougenot, C. & Moonen, C.T.W. 2007, "Real-time adaptive methods for treatment of mobile organs by MRI-controlled high-intensity focused ultrasound", *Magnetic Resonance in Medicine,* vol. 57, no. 2, pp. 319-330.

Della Bella, P., Baratto, F., Tsiachris, D., Trevisi, N., Vergara, P., Bisceglia, C., Petracca, F., Carbucicchio, C., Benussi, S., Maisano, F., Alfieri, O., Pappalardo, F., Zangrillo, A. & Maccabelli, G. 2013, "Management of ventricular tachycardia in the setting of a dedicated unit for the treatment of complex ventricular arrhythmias: long-term outcome after ablation", *Circulation,* vol. 127, pp. 1359-1368.

DENEKE, T., MÜLLER, K., LEMKE, B., LAWO, T., CALCUM, B., HELWING, M., MÜGGE, A. & GREWE, P.H. 2005, "Human Histopathology of Electroanatomic Mapping After Cooled-Tip Radiofrequency Ablation to Treat Ventricular Tachycardia in Remote Myocardial Infarction", *Journal of cardiovascular electrophysiology,* vol. 16, no. 11, pp. 1246-1251.

Desjardins, B., Crawford, T., Good, E., Oral, H., Chugh, A., Pelosi, F., Morady, F. & Bogun, F. 2009, *Infarct architecture and characteristics on delayed enhanced magnetic resonance imaging and electroanatomic mapping in patients with postinfarction ventricular arrhythmia.* Heart Rhythm: 6; 644-51.

Detsky, J.S., Stainsby, J.A., Vijayaraghavan, R., Graham, J.J., Dick, A.J. & Wright, G.A. 2007, "Inversion-recovery-prepared SSFP for cardiac-phase-resolved delayed-enhancement MRI", *Magnetic Resonance in Medicine,* vol. 58, no. 2, pp. 365-372.

Deyell, M.W., Steinberg, C., Doucette, S., Parkash, R., Nault, I., Gray, C., Essebag, V., Gardner, M., Sterns, L.D., Healey, J.S., Hruczkowski, T., Rivard, L., Leong-Sit, P., Nery, P.B. & Sapp, J.L. 2018, "Mexiletine or catheter ablation after amiodarone failure in the VANISH trial", *Journal of cardiovascular electrophysiology,* vol. 29, no. 4, pp. 603-608.

Di Biase, L., Burkhardt, J.D., Lakkireddy, D., Carbucicchio, C., Mohanty, S., Mohanty, P., Trivedi, C., Santangeli, P., Bai, R., Forleo, G., Horton, R., Bailey, S., Sanchez, J., Al-Ahmad, A., Hranitzky, P., Gallinghouse, G.J., Pelargonio, G., Hongo, R.H., Beheiry, S., Hao, S.C., Reddy, M., Rossillo, A., Themistoclakis, S., Dello Russo, A., Casella, M., Tondo, C. & Natale, A. 2015, *Ablation of Stable VTs Versus Substrate Ablation in Ischemic Cardiomyopathy: The VISTA Randomized Multicenter Trial.* Journal of the American College of Cardiology: 66; 2872-2882.

Di Biase, L., Santangeli, P., Burkhardt, D.J., Bai, R., Mohanty, P., Carbucicchio, C., Dello Russo, A., Casella, M., Mohanty, S., Pump, A., Hongo, R., Beheiry, S., Pelargonio, G., Santarelli, P., Zucchetti, M., Horton, R., Sanchez, J.E., Elayi, C.S., Lakkireddy, D., Tondo, C. & Natale, A. 2012, *Endo-Epicardial Homogenization of the Scar Versus Limited Substrate Ablation for the Treatment of Electrical Storms in Patients With Ischemic Cardiomyopathy.* Journal of the American College of Cardiology: 60; 132-141.

Dickfeld, T., Tian, J., Ahmad, G., Jimenez, A., Turgeman, A., Kuk, R., Peters, M., Saliaris, A., Saba, M., Shorofsky, S. & Jeudy, J. 2011, "MRI-Guided ventricular tachycardia ablation: integration of late gadolinium-enhanced 3D scar in patients with implantable cardioverter-defibrillators", *Circulation: Arrhythmia and Electrophysiology,* vol. 4, pp. 172-184.

Dickfeld, T., Kato, R., Zviman, M., Nazarian, S., Dong, J., Ashikaga, H., Lardo, A.C., Berger, R.D., Calkins, H. & Halperin, H. 2007, *Characterization of acute and subacute radiofrequency ablation lesions with nonenhanced magnetic resonance imaging*. Heart Rhythm: 4; 208-14.

Dickfeld, T., Kato, R., Zviman, M., Lai, S., Meininger, G., Lardo, A.C., Roguin, A., Blumke, D., Berger, R., Calkins, H. & Halperin, H. 2006, *Characterization of Radiofrequency Ablation Lesions With Gadolinium-Enhanced Cardiovascular Magnetic Resonance Imaging*. Journal of the American College of Cardiology 47; 370-378.

Dinov, B., Fiedler, L., Schonbauer, R., Bollman, A., Rolf, S., Piorkowski, C., Hindricks, G. & Arya, A. 2014, "Outcomes in catheter ablation of ventricular tachycardia in dilated nonischemic cardiomyopathy compared with ischemic cardiomyopathy: results from the Prospective Heart Centre of Leipzig VT (HELP-VT) Study", *Circulation,* vol. 129, pp. 728-736.

Disertori, M., Rigoni, M., Pace, N., Casolo, G., Masè, M., Gonzini, L., Lucci, D., Nollo, G. & Ravelli, F. 2016, *Myocardial Fibrosis Assessment by LGE Is a Powerful Predictor of Ventricular Tachyarrhythmias in Ischemic and Nonischemic LV Dysfunction: A Meta-Analysis*. JACC: Cardiovascular Imaging: 9; 1046-1055.

Do, D.H., Eyvazian, V., Bayoneta, A.J., Hu, P., Finn, J.P., Bradfield, J.S., Shivkumar, K. & Boyle, N.G. 2018, *Cardiac magnetic resonance imaging using wideband sequences in patients with nonconditional cardiac implanted electronic devices*. Heart Rhythm: 15; 218-225.

Doppalapudi, H., Yamada, T., McElderry, T., Plumb, V.J., Epstein, A.E. & Kay, N. 2008, "Ventricular tachycardia originating from the posterior papillary muscle in the left ventricle", *Circulation: Arrhythmia and Electrophysiology,* vol. 1, pp. 23-29.

Dukkipati, S.R., d'Avila, A., Soejima, K., Bala, R., Inada, K., Singh, S., Stevenson, W.G., Marchlinski, F.E. & Reddy, V.Y. 2011, "Long-term outcomes of combined epicardial and endocardial ablation of monomorphic ventricular tachycardia related to hypertrophic cardiomyopathy", *Circulation: Arrhythmia and Electrophysiology,* vol. 4, pp. 185-194.

Dukkipati, S.R., Mallozzi, R., Schmidt, E.J., Holmvang, G., d'Avila, A., Guhde, R., Darrow, R.D., Slavin, G., Fung, M., Malchano, Z., Kampa, G., Dando, J.D., McPherson, C., Foo, T.K., Ruskin, J.N., Dumoulin, C.L. & Reddy, V.Y. 2008, "Electroanatomic mapping of the left ventricle in a porcine model of chronic myocardial infarction with magnetic resonance-based catheter tracking", *Circulation,* vol. 118, pp. 853-862.

Dukkipati, S.R., Choudry, S., Koruth, J.S., Miller, M.A., Whang, W. & Reddy, V.Y. 2017, *Catheter Ablation of Ventricular Tachycardia in Structurally Normal Hearts: Indications, Strategies, and Outcomes—Part I*. Journal of the American College of Cardiology: 70; 2909-2923.

Dukkipati, S.R., Koruth, J.S., Choudry, S., Miller, M.A., Whang, W. & Reddy, V.Y. 2017, *Catheter Ablation of Ventricular Tachycardia in Structural Heart Disease: Indications, Strategies, and Outcomes—Part II*. Journal of the American College of Cardiology: 70; 2924-2941.

Dzyubachyk, O., Tao, Q., Poot, D.H.J., Lamb, H.J., Zeppenfeld, K., Lelieveldt, B.P.F. & van, d.G. 2015, "Super-resolution reconstruction of late gadolinium-enhanced MRI for

improved myocardial scar assessment", *Journal of Magnetic Resonance Imaging,* vol. 42, no. 1, pp. 160-167.

Elbes, D., Magat, J., Govari, A., Ephrath, Y., Vieillot, D., Beeckler, C., Weerasooriya, R., Jais, P. & Question, B. 2017, "Magnetic resonance imaging-compatible circular mapping catheter: an in vivo feasibility and safety study", *Europace,* vol. 19, pp. 458-464.

Emami, M., Morton, J.B., Chan, K.H. & Roberts-Thomson, K.C. 2019, "Catheter Ablation of Post-Infarct VT: Mechanisms, Strategies and Outcomes", *Heart, Lung and Circulation,* vol. 28, pp. 76-83.

Estner, H.L., Zviman, M.M., Herzka, D., Miller, F., Castro, V., Nazarian, S., Ashikaga, H., Dori, Y., Berger, R.D., Calkins, H., Lardo, A.C. & Halperin, H.R. 2011, *The critical isthmus sites of ischemic ventricular tachycardia are in zones of tissue heterogeneity, visualized by magnetic resonance imaging.* Heart Rhythm: 8; 1942-9.

Felblinger, J., Slotboom, J., Kreis, R., Jung, B. & Boesch, C. 1999, "Restoration of electrophysiological signals distorted by inductive effects of magnetic field gradients during MR sequences", *Magnetic Resonance in Medicine,* vol. 41, no. 4, pp. 715-721.

Fernandez-Armenta, J., Berruezo, A., Andreu, D., Camara, O., Silva, E., Serra, L., Barbarito, V., Carotenutto, L., Evertz, R., Ortiz-Pérez, J.T., De Caralt, T.M., Perea, R.J., Sitges, M., Mont, L., Frangi, A. & Brugada, J. 2013, "Three-dimensional architecture of scar and conducting channels based on high resolution ce-CMR: insights for ventricular tachycardia ablation", *Circulation: Arrhythmia and Electrophysiology,* vol. 6, no. 3, pp. 528-537.

Fernández-Armenta, J., Penela, D., Acosta, J., Andreu, D., Evertz, R., Cabrera, M., Korshunov, V., Vassanelli, F., Martínez, M., Guasch, E., Arbelo, E., María Tolosana, J., Mont, L. & Berruezo, A. 2016, *Substrate modification or ventricular tachycardia induction, mapping, and ablation as the first step? A randomized study.* Heart Rhythm: 13; 1589-95.

Flett, A.S., Hayward, M.P., Ashworth, M.T., Hansen, M.S., Taylor, A.M., Elliott, P.M., McGregor, C. & Moon, J.C. 2010, "Equilibrium contrast cardiovascular magnetic resonance for the measurement of diffuse myocardial fibrosis: preliminary validation in humans", *Circulation,* vol. 122, pp. 138-144.

Flett, A.S., Hasleton, J., Cook, C., Hausenloy, D., Quarta, G., Ariti, C., Muthurangu, V. & Moon, J.C. 2011, *Evaluation of Techniques for the Quantification of Myocardial Scar of Differing Etiology Using Cardiac Magnetic Resonance.* JACC: Cardiovascular Imaging: 4; 150-156.

Frankel, D.S., Mountantonakis, S.E., Zado, E.S., Anter, E., Bala, R., Cooper, J.M., Deo, R., Dixit, S., Epstein, A.E., Garcia, F.C., Gerstenfeld, E.P., Hutchinson, M.D., Lin, D., Patel, V.V., Riley, M.P., Robinson, M.R., Tzou, W.S., Verdino, R.J., Callans, D.J. & Marchlinski, F.E. 2012, *Noninvasive Programmed Ventricular Stimulation Early After Ventricular Tachycardia Ablation to Predict Risk of Late Recurrence.* Journal of the American College of Cardiology: 59; 1529-35.

Gepstein, L., Hayam, G. & Ben-Haim, S.A. 1997, "A Novel Method for Nonfluoroscopic Catheter-Based Electroanatomical Mapping of the Heart", *Circulation,* vol. 95, pp. 1611-1622.

Ghafoori, E., Kholmovski, E.G., Thomas, S., Silvernagel, J., Angel, N., Hu, N., Dosdall, D.J., MacLeod, R. & Ranjan, R. 2017, "Characterization of Gadolinium Contrast Enhancement of Radiofrequency Ablation Lesions in Predicting Edema and Chronic Lesion Size", *Circulation: Arrhythmia and Electrophysiology,* vol. 10, no. 11, pp. e005599.

Ginami, G., Neji, R., Rashid, I., Chiribiri, A., Ismail, T.F., Botnar, R.M. & Prieto, C. 2017, "3D whole-heart phase sensitive inversion recovery CMR for simultaneous black-blood late gadolinium enhancement and bright-blood coronary CMR angiography", *Journal of Cardiovascular Magnetic Resonance,* vol. 19, no. 1, pp. 94.

Glashan CA, Androulakis AFA, Tao Q, Glashan RN, Wisse LJ, Ebert M, de Ruiter MC et al. Whole human heart histology to validate electroanatomical voltage mapping in patients with non-ischaemic cardiomyopathy and ventricular tachycardia. European Heart Journal (2018): 39; 2867-2875.

Gökoğlan, Y., Mohanty, S., Gianni, C., Santangeli, P., Trivedi, C., Güneş, M.F., Bai, R., Al-Ahmad, A., Gallinghouse, G.J., Horton, R., Hranitzky, P.M., Sanchez, J.E., Beheiry, S., Hongo, R., Lakkireddy, D., Reddy, M., Schweikert, R.A., Dello Russo, A., Casella, M., Tondo, C., Burkhardt, J.D., Themistoclakis, S., Di Biase, L. & Natale, A. 2016, *Scar Homogenization Versus Limited-Substrate Ablation in Patients With Nonischemic Cardiomyopathy and Ventricular Tachycardia.*

Gould, J., Porter, B., Claridge, S., Chen, Z., Sieniewicz, B.J., Sidhu, B.S., Niederer, S., Bishop, M.J., Murgatroyd, F., Ganeshan, B., Carr-White, G., Razavi, R., Chiribiri, A. & Rinaldi, C.A. 2019, *Mean entropy predicts implantable cardioverter-defibrillator therapy using cardiac magnetic resonance texture analysis of scar heterogeneity.* Heart Rhythm 16: 1242-1250.

Grothoff, M., Gutberlet, M., Hindricks, G., Fleiter, C., Schnackenburg, B., Weiss, S., Krueger, S., Piorkowski, C., Gaspar, T., Wedan, S., Lloyd, T., Sommer, P. & Hilbert, S. 2017, "Magnetic resonance imaging guided transatrial electrophysiological studies in swine using active catheter tracking - experience with 14 cases", *European Radiology,* vol. 27, pp. 1954-1962.

Grothoff, M., Piorkowski, C., Eitel, C., Gaspar, T., Lehmkuhl, L., Lücke, C., Hoffmann, J., Hildebrand, L., Wedan, S., Lloyd, T., Sunnarborg, D., Schnackenburg, B., Hindricks, G., Sommer, P. & Gutberlet, M. 2014, "MR Imaging–guided Electrophysiological Ablation Studies in Humans with Passive Catheter Tracking: Initial Results", *Radiology,* vol. 271, no. 3, pp. 695-702.

Gulati, A., Jabbour, A., Ismail, T.F., Guha, K., Khwaja, J., Raza, S., Moraji, K., Brown, T., Ismail, N.A., Dweck, M.R., Di Pietro, E., Roughton, M., Wage, R., Daryani, Y., O'Hanlon, R., Sheppard, M.N., Alpendurada, F., Lyon, A.R., Cook, S.A., Cowie, M.R., Assomull, R.G., Pennell, D.J. & Prasad, S.K. 2013, "Association of fibrosis with mortality and sudden cardiac death in patients with nonischaemic dilated cardiomyopathy", *Journal of the American Medical Association,* vol. 309, pp. 896-908.

Gupta, S., Desjardins, B., Baman, T., Ilg, K., Good, E., Crawford, T., Oral, H., Pelosi, F., Chugh, A., Morady, F. & Bogun, F. 2012, *Delayed-Enhanced MR Scar Imaging and Intraprocedural Registration Into an Electroanatomical Mapping System in Post-Infarction Patients.* JACC: Cardiovascular Imaging: 5; 207-10.

Guttman, M.A., Tao, S., Fink, S., Kolandaivelu, A., Halperin, H.R. & Herzka, D.A. 2018, "Non-contrast-enhanced T1-weighted MRI of myocardial radiofrequency ablation lesions", *Magnetic Resonance in Medicine,* vol. 79, no. 2, pp. 879-889.

Halliday, B.P., Gulati, A., Ali, A., Guha, K., Newsome, S., Arzanauskaite, M., Vassiliou, V.S., Lota, A., Izgi, C., Tayal, U., Khalique, Z., Stirrat, C., Auger, D., Pareek, N., Ismail, T.F., Rosen, S.D., Vazir, A., Alpendurada, F., Gregson, J., Frenneaux, M.P., Cowie, M.R., Cleland, J., Cook, S.A., Pennell, D.J. & Prasad, S.K. 2017, "Association between midwall late gadolinium enhancement and sudden cardiac death in patients with dilated cardiomyopathy and mild and moderate left ventricular systolic dysfunction", *Circulation,* vol. 135, pp. 2106-2115.

Haqqani, H.M., Kalman, J.M., Roberts-Thomson, K.C., Balasubramaniam, R.N., Rosso, R., Snowdon, R.L., Sparks, P.B., Vohra, J.K. & Morton, J.B. 2009, *Fundamental Differences in Electrophysiologic and Electroanatomic Substrate Between Ischemic Cardiomyopathy Patients With and Without Clinical Ventricular Tachycardia*. Journal of the American College of Cardiology: 54; 166-173.

Hayashi, T., Liang, J.J., Muser, D., Shirai, Y., Enriquez, A., Garcia, F.C., Supple, G.E., Schaller, R.D., Frankel, D.S., Lin, D., Nazarian, S., Zado, E.S., Arkles, J.S., Dixit, S., Callans, D.J., Marchlinski, F.E. & Santangeli, P. 2018, "Epicardial ventricular tachycardia in ischemic cardiomyopathy: Prevalence, electrophysiological characteristics, and long-term ablation outcomes", *Journal of cardiovascular electrophysiology,* vol. 29, no. 11, pp. 1530-1539.

Hennig, A., Salel, M., Sacher, F., Camaioni, C., Sridi, S., Denis, A., Montaudon, M., Laurent, F., Jais, P. & Cochet, H. 2018, "High-resolution three-dimensional late gadolinium-enhanced cardiac magnetic resonance imaging to identify the underlying substrate of ventricular arrhythmia", *Europace : European pacing, arrhythmias, and cardiac electrophysiology : journal of the working groups on cardiac pacing, arrhythmias, and cardiac cellular electrophysiology of the European Society of Cardiology,* vol. 20, no. FI2, pp. f179-f191.

Hilbert, S., Sommer, P., Gutberlet, M., Gaspar, T., Foldyna, B., Piorkowski, C., Weiss, S., Lloyd, T., Schnackenburg, B., Krueger, S., Fleiter, C., Paetsch, I., Jahnke, C., Hindricks, G. & Grothoff, M. 2016, "Real-time magnetic resonance-guided ablation of typical right atrial flutter using a combination of active catheter tracking and passive catheter visualization in man: initial results from a consecutive patient series", *Europace : European pacing, arrhythmias, and cardiac electrophysiology : journal of the working groups on cardiac pacing, arrhythmias, and cardiac cellular electrophysiology of the European Society of Cardiology,* vol. 18, no. 4, pp. 572-577.

Hsia, H.H., Callans, D.J. & Marchlinski, F.E. 2003, "Characterization of endocardial electrophysiological substrate in patients with nonischemic cardiomyopathy and monomorphic ventricular tachycardia.", *Circulation,* vol. 108, pp. 704-710.

Hsia, H.H., Lin, D., Sauer, W.H., Callans, D.J. & Marchlinski, F.E. 2009, "Relationship of late potentials to the ventricular tachycardia circuit defined by entrainment", *Journal of Interventional Cardiac Electrophysiology,* vol. 26, pp. 21-29.

Hsia, H.H., Lin, D., Sauer, W.H., Callans, D.J. & Marchlinski, F.E. 2006, *Anatomic characterization of endocardial substrate for hemodynamically stable reentrant*

ventricular tachycardia: Identification of endocardial conducting channels. Heart Rhythm: 3; 503-12.

Huber, A.M., Schoenberg, S.O., Hayes, C., Spannagl, B., Engelmann, M.G., Franz, W.M. & Reiser, M.F. 2005, "Phase-Sensitive Inversion-Recovery MR Imaging in the Detection of Myocardial Infarction", *Radiology,* vol. 237, no. 3, pp. 854-860.

Hutchinson, M.D., Gerstenfeld, E.P., Desjardins, B., Bala, R., Riley, M.P., Garcia, F.C., Dixit, S., Lin, D., Tzou, W.S., Cooper, J.M., Verdino, R.J., Callans, D.J. & Marchlinski, F.E. 2011, "Endocardial Unipolar Voltage Mapping to Detect Epicardial VT Substrate in Patients with Nonischemic Left Ventricular Cardiomyopathy", *Circulation: Arrhythmia and Electrophysiology,* vol. 4, pp. 49-55.

Ishihara, Y., Calderon, A., Watanabe, H., Okamoto, K., Suzuki, Y., Kuroda, K. & Suzuki, Y. 1995, "A precise and fast temperature mapping using water proton chemical shift", *Magnetic Resonance in Medicine,* vol. 34, no. 6, pp. 814-823.

J. Oster, O. Pietquin, M. Kraemer & J. Felblinger 2010, *Nonlinear Bayesian Filtering for Denoising of Electrocardiograms Acquired in a Magnetic Resonance Environment*. IEEE Transactions in Biomedical Engineering: 57; 1628-38.

Jais, P., Maury, P., Khairy, P., Sacher, F., Nault, I., Komatsu, Y., Hocini, M., Forclaz, A., Jadidi, A.S., Weerasooriya, R., Shah, A., Derval, N., Cochet, H., Knecht, S., Miyazaki, S., Linton, N., Rivard, L., Wright, M., Wilton, S.B., Scherr, D., Pascale, P., Roten, L., Pederson, M., Bordachar, P., Laurent, F., Kim, S.J., Ritter, P., Clementy, J. & Haissaguerre, M. 2012, "Elimination of Local Abnormal Ventricular Activities: A New End Point for Substrate Modification in Patients With Scar-Related Ventricular Tachycardia", *Circulation,* vol. 125, pp. 2184-2196.

Josephson, M.E., Horowitz, L.N. & Farshidi, A. 1978, "Continuous local electrical activity: a mechanism of recurrent ventricular tachycardia", *Circulation,* vol. 57, pp. 659-665.

Josephson, M.E. & Anter, E. 2015, *Substrate Mapping for Ventricular Tachycardia: Assumptions and Misconceptions*. JACC: Clinical Electrophysiology: 1; 341-352.

Karim, R., Bhagirath, P., Claus, P., James Housden, R., Chen, Z., Karimaghaloo, Z., Sohn, H., Lara Rodríguez, L., Vera, S., Albà, X., Hennemuth, A., Peitgen, H., Arbel, T., Gonzàlez Ballester, M.A., Frangi, A.F., Götte, M., Razavi, R., Schaeffter, T. & Rhode, K. 2016, *Evaluation of state-of-the-art segmentation algorithms for left ventricle infarct from late Gadolinium enhancement MR images*. Medical Image Analysis: 30; 95-107.

KAUTZNER, J., ČIHÁK, R., PEICHL, P., VANČURA, V. & BYTEŠNÍK, J. 2003, "Catheter Ablation of Ventricular Tachycardia Following Myocardial Infarction Using Three-Dimensional Electroanatomical Mapping", *Pacing and Clinical Electrophysiology,* vol. 26, no. 1, pp. 342-347.

Kellman, P., Xue, H., Olivieri, L.J., Cross, R.R., Grant, E.K., Fontana, M., Ugander, M., Moon, J.C. & Hansen, M.S. 2016, "Dark blood late enhancement imaging", *Journal of Cardiovascular Magnetic Resonance,* vol. 18, pp. 77.

Kellman, P., Arai, A.E., McVeigh, E.R. & Aletras, A.H. 2002, "Phase-sensitive inversion recovery for detecting myocardial infarction using gadolinium-delayed hyperenhancement†", *Magnetic Resonance in Medicine,* vol. 47, no. 2, pp. 372-383.

Kholmovski, E.G., Silvernagel, J., Angel, N., Vijayakumar, S., Thomas, S., Dosdall, D., MacLeod, R., Marrouche, N.F. & Ranjan, R. 2018, "Acute noncontrast T1-weighted magnetic resonance imaging predicts chronic radiofrequency ablation lesions", *Journal of cardiovascular electrophysiology,* vol. 29, no. 11, pp. 1556-1562.

Kim, R.J., Chen, E.L., Lima, J.A. & Judd, R.M. 1996, "Myocardial Gd-DTPA kinetics determine MRI contrast enhancement and reflect the extent and severity of myocardial injury after acute reperfused infarction", *Circulation,* vol. 94, no. 12, pp. 3318-3326.

Knackstedt, C., Schauerte, P. & Kirchhof, P. 2008, "Electro-anatomic mapping systems in arrhythmias", *Europace,* vol. 10, pp. 28-34.

Kolandaivelu, A., Zviman, M.M., Castro, V., Lardo, A.C., Berger, R.D. & Halperin, H.R. 2010, "Noninvasive assessment of tissue heating during cardiac radiofrequency ablation using MRI thermography", *Circulation: Arrhythmia and Electrophysiology,* vol. 3, no. 5, pp. 521-529.

Krahn, P., Singh, S.M., Ramanan, V., Biswas, L., Yak, N., Anderson, K., Barry, J., Pop, M. & Wright, G.A. 2018, "Cardiovascular magnetic resonance guided ablation and intra-procedural visualization of evolving radiofrequency lesions in the left ventricle", *Journal of Cardiovascular Magnetic Resonance,* vol. 20, no. 1, pp. 20.

Kuck, K.H., Schaumann, A., Eckardt, L., Willems, S., Ventura, R., Delacrétaz, E., Pitschner, H.F., Kautzner, J., Schumacher, B. & Hansen, P.S. 2010, "Catheter ablation of stable ventricular tachycardia before defibrillator implantation in patients with coronary heart disease (VTACH): a multicentre randomised controlled trial", *Lancet,* vol. 375, pp. 61755-4.

Kuck, K.H., Tilz, R.R., Deneke, T., Hoffmann, B.A., Ventura, R., Hansen, P.S., Zarse, M., Hohnloser, S.H., Kautzner, J. & Willems, S. 2017, "Impact of Substrate Modification by Catheter Ablation on Implantable Cardioverter-Defibrillator Interventions in Patients With Unstable Ventricular Arrhythmias and Coronary Artery Disease: Results From the Multicenter Randomized Controlled SMS (Substrate Modification Study)", *Circulation: Arrhythmia and Electrophysiology,* vol. 10, pp. e004422.

Kumar, S., Tedrow, U.B. & Stevenson, W.G. 2017, *Entrainment Mapping.* Cardiac Electrophysiology Clinics: 9; 55-69.

Lardo, A.C., McVeigh, E.R., Jumrussirikul, P., Berger, R.D., Calkins, H., Lima, J. & Halperin, H.R. 2000, "Visualization and temporal/spatial characterization of cardiac radiofrequency ablation lesions using magnetic resonance imaging", *Circulation,* vol. 102, no. 6, pp. 698-705.

Lederman, R.J. 2005, "Cardiovascular interventional magnetic resonance imaging", *Circulation,* vol. 112, no. 19, pp. 3009-3017.

Ling, Z., Liu, Z., Su, L., Zipunnikov, V., Wu, J., Du, H., Woo, K., Chen, S., Zhong, B., Lan, X., Fan, J., Xu, Y., Chen, W., Yin, Y., Nazarian, S. & Zrenner, B. 2014, "Radiofrequency ablation versus antiarrhythmic medication for treatment of ventricular premature beats from the right ventricular outflow tract", *Circulation: Arrhythmia and Electrophysiology,* vol. 7, pp. 237-243.

Lombardi, M., Plein, S., Petersen, S., Bucciarelli-Ducci, C., Buechel, E.V., Basso, C. & Ferrari, V. 2018, *The EACVI Textbook of Cardiovascular Magnetic Resonance,* Oxford University Press.

López-Yunta, M., León, D.G., Alfonso-Almazán, J.M., Marina-Breysse, M., Quintanilla, J.G., Sánchez-González, J., Galán-Arriola, C., Cañadas-Godoy, V., Enríquez-Vázquez, D., Torres, C., Ibáñez, B., Pérez-Villacastín, J., Pérez-Castellano, N., Jalife, J., Vázquez, M., Aguado-Sierra, J. & Filgueiras-Rama, D. 2019, "Implications of bipolar voltage mapping and magnetic resonance imaging resolution in biventricular scar characterization after myocardial infarction", *EP Europace,* vol. 21, no. 1, pp. 163-174.

Luni, F.K., Zungsontiporn, N., Farid, T., Malik, S.A., Khan, S., Daniels, J., Wu, R., Link, M.S. & Joglar, J.A. 2019, "Percutaneous left ventricular assist device support during ablation of ventricular tachycardia: A meta-analysis of current evidence", *Journal of cardiovascular electrophysiology,* vol. 30, no. 6, pp. 886-895.

Mahida, S., Sacher, F., Dubois, R., Sermesant, M., Bogun, F., Haïssaguerre, M., Jais, P. & Cochet, H. 2017, "Cardiac Imaging in Patients With Ventricular Tachycardia", *Circulation,* vol. 136, no. 25, pp. 2491-2507.

Marchlinski, F.E., Callans, D.J., Gottlieb, C.D. & Zado, E. 2000, "Linear ablation lesions for control of unmappable ventricular tachycardia in patients with ischemic and nonischemic cardiomyopathy", *Circulation,* vol. 101, pp. 1288-1296.

Martin, C.A., Martin, R., Maury, P., Meyer, C., Wong, T., Dallet, C., Shi, R., Gajendragadkar, P., Takigawa, M., Frontera, A., Cheniti, G., Thompson, N., Kitamura, T., Vlachos, K., Wolf, M., Bourier, F., Lam, A., Duchateau, J., Massoullie, G., Pambrun, T., Denis, A., Derval, N., Dubois, R., Hocini, M., Haissaguerre, M., Jais, P. & Sacher, F. 2019, "Effect of Activation Wavefront on Electrogram Characteristics During Ventricular Tachycardia Ablation", *Circulation: Arrhythmia and Electrophysiology,* vol. 12, pp. e007293.

Maskoun, W., Saad, M., Abualsuod, A., Nairooz, R. & Miller, J.M. 2018, *Outcome of catheter ablation for ventricular tachycardia in patients with ischemic cardiomyopathy: A systematic review and meta-analysis of randomized clinical trials*. International Journal of Cardiology: 267; 107-113.

Maury, P., Monteil, B., Marty, L., Duparc, A., Mondoly, P. & Rollin, A. 2018, *Three-dimensional mapping in the electrophysiological laboratory*. Archives in Cardiovascular Diseases: 111; 456-464.

Mesubi, O., Ego-Osuala, K., Jeudy, J., Purtilo, J., Synowski, S., Abutaleb, A., Niekoop, M., Abdulghani, M., Asoglu, R., See, V., Saliaris, A., Shorofsky, S. & Dickfeld, T. 2015, "Differences in quantitative assessment of myocardial scar and gray zone by LGE-CMR imaging using established gray zone protocols", *International Journal of Cardiovascular Imaging,* vol. 31, pp. 359-368.

Mooiweer, R., Schneider, R., Neji, R., Pohl, T., Lloyd, T., Mukherjee, R.K., O'Neill, M., Razavi, R. & Roujol, S. 2019, "Active Tracking-based cardiac triggering of MR thermometry for MRI-guided cardiac ablation", *ISMRM Abstract Book*, Montreal, Canada

Moss, A.J., Schuger, C., Beck, C.A., Brown, M.W., Cannom, D.S., Daubert, J.P., Estes, N.A.M., Greenberg, H., Hall, W.J., Huang, D.T., Kautzner, J., Klein, H., McNitt, S.,

Olshansky, B., Shoda, M., Wilber, D. & Zareba, W. 2012, "Reduction in Inappropriate Therapy and Mortality through ICD Programming", *N Engl J Med,* vol. 367, no. 24, pp. 2275-2283.

Mukherjee, R.K., Chubb, H., Roujol, S., Razavi, R. & O'Neill, M.D. 2019, "Advances in Real-Time MRI-Guided Electrophysiology", *Current Cardiovascular Imaging Reports,* vol. 12, no. 2, pp. 6.

Mukherjee, R.K., O'Neill, L. & O'Neill, M.D. 2017, "Prophylactic Catheter Ablation for Ventricular Tachycardia: Are We There Yet?", *Arrhythmia and Electrophysiology Review,* vol. 6, pp. 125-128.

Mukherjee, R.K., Roujol, S., Chubb, H., Harrison, J., Williams, S., Whitaker, J., O'Neill, L., Silberbauer, J., Neji, R., Schneider, R., Pohl, T., Lloyd, T., O'Neill, M. & Razavi, R. 2018, "Epicardial electroanatomical mapping, radiofrequency ablation, and lesion imaging in the porcine left ventricle under real-time magnetic resonance imaging guidance—an in vivo feasibility study", *Europace : European pacing, arrhythmias, and cardiac electrophysiology : journal of the working groups on cardiac pacing, arrhythmias, and cardiac cellular electrophysiology of the European Society of Cardiology,* vol. 20, no. FI2, pp. f254-f262.

Mukherjee, R.K., Whitaker, J., Williams, S.E., Razavi, R. & O'Neill, M.D. 2018, "Magnetic resonance imaging guidance for the optimization of ventricular tachycardia ablation", *Europace: European pacing, arrhythmias, and cardiac electrophysiology: journal of the working groups on cardiac pacing, arrhythmias, and cardiac cellular electrophysiology of the European Society of Cardiology,* vol. 20, no. 11, pp. 1721-1732.

Mukherjee R.K., Costa C.M., Neji R., Harrison J.L., Sim I., Williams S.E., Whitaker J., Chubb H., O'Neill L., Schneider R., Lloyd T., Pohl T., Roujol S., Niederer S.A., Razavi R., O'Neill M.D. 2019, "Evaluation of a real-time magnetic resonance imaging-guided electrophysiology system for structural and electrophysiological ventricular tachycardia substrate assessment", *Europace: European pacing, arrhythmias, and cardiac electrophysiology : journal of the working groups on cardiac pacing, arrhythmias, and cardiac cellular electrophysiology of the European Society of Cardiology,* vol. 21, no. 9, pp. 1432-1441.

Muthalaly, R.G., Kwong, R.Y., John, R.M., van der Geest, Rob J., Tao, Q., Schaeffer, B., Tanigawa, S., Nakamura, T., Kaneko, K., Tedrow, U.B., Stevenson, W.G., Epstein, L.M., Kapur, S., Zei, P.C. & Koplan, B.A. 2019, *Left Ventricular Entropy Is a Novel Predictor of Arrhythmic Events in Patients With Dilated Cardiomyopathy Receiving Defibrillators for Primary Prevention.* JACC: Cardiovascular Imaging: 12; 1177-1184.

Nakahara, S., Tung, R., Ramirez, R.J., Michowitz, Y., Vaseghi, M., Buch, E., Gima, J., Wiener, I., Mahajan, A., Boyle, N.G. & Shivkumar, K. 2010, *Characterization of the Arrhythmogenic Substrate in Ischemic and Nonischemic Cardiomyopathy: Implications for Catheter Ablation of Hemodynamically Unstable Ventricular Tachycardia.* Journal of the American College of Cardiology: 55; 2355-65.

Nayyar, S., Wilson, L., Ganesan, A.N., Sullivan, T., Kuklik, P., Chapman, D., Brooks, A.G., Mahajan, R., Baumert, M., Young, G.D., Sanders, P. & Roberts-Thomson, K.C. 2014, "High-Density mapping of ventricular scar: a comparison of ventricular tachycardia (VT) supporting channels with channels that do not support VT", *Circulation: Arrhythmia and Electrophysiology,* vol. 7, pp. 90-98.

Nayyar, S., Wilson, L., Ganesan, A., Sullivan, T., Kuklik, P., Young, G., Sanders, P. & Roberts-Thomson, K.C. 2018, "Electrophysiologic features of protected channels in late postinfarction patients with and without spontaneous ventricular tachycardia", *Journal of Interventional Cardiac Electrophysiology,* vol. 51, pp. 13-24.

Nazarian, S., Kolandaivelu, A., Zviman, M.M., Meininger, G.R., Kato, R., Susil, R.C., Roguin, A., Dickfeld, T.L., Ashikaga, H., Calkins, H., Berger, R.D., Bluemke, D.A., Lardo, A.C. & Halperin, H.R. 2008, "Feasibility of real-time magnetic resonance imaging for catheter guidance in electrophysiology studies", *Circulation,* vol. 118, pp. 223-229.

Nazarian, S., Hansford, R., Rahsepar, A.A., Weltin, V., McVeigh, D., Gucuk Ipek, E., Kwan, A., Berger, R.D., Calkins, H., Lardo, A.C., Kraut, M.A., Kamel, I.R., Zimmerman, S.L. & Halperin, H.R. 2017, "Safety of Magnetic Resonance Imaging in Patients with Cardiac Devices", *N Engl J Med,* vol. 377, no. 26, pp. 2555-2564.

NOGAMI, A., SUGIYASU, A., TADA, H., KUROSAKI, K., SAKAMAKI, M., KOWASE, S., OGINOSAWA, Y., KUBOTA, S., USUI, T. & NAITO, S. 2008, "Changes in the Isolated Delayed Component as an Endpoint of Catheter Ablation in Arrhythmogenic Right Ventricular Cardiomyopathy: Predictor for Long-Term Success", *Journal of cardiovascular electrophysiology,* vol. 19, no. 7, pp. 681-688.

Nordbeck, P., Hiller, K.H., Fidler, F., Warmuth, M., Burkard, N., Nahrendorf, M., Jakob, P.M., Quick, H.H., Ertl, G., Bauer, W.R. & Ritter, O. 2011, "Feasibility of contrast-enhanced and nonenhanced MRI for intraprocedural and postprocedural lesion visualization in interventional electrophysiology: animal studies and early delineation of isthmus ablation lesions in patients with typical atrial flutter", *Circulation: Cardiovascular Imaging,* vol. 4, no. 3, pp. 282-294.

Nordbeck, P., Quick, H.H., Ladd, M.E. & Ritter, O. 2013, *Real-time magnetic resonance guidance of interventional electrophysiology procedures with passive catheter visualization and tracking.* Heart Rhythm: 10; 938-9.

Oduneye, S., Pop, M., Shurrab, M., Biswas, L., Ramanan, V., Barry, J., Crystal, E. & Wright, G.A. 2015, "Distribution of abnormal potentials in chronic myocardial infarction using a real time magnetic resonance guided electrophysiology system", *Journal of Cardiovascular Magnetic Resonance,* vol. 17, pp. 27.

Omary, R.A., Unal, O., Koscielski, D.S., Frayne, R., Korosec, F.R., Mistretta, C.A., Strother, C.M. & Grist, T.M. 2000, "Real-time MR imaging-guided passive catheter tracking with use of gadolinium-filled catheters", *Journal of Vascular and Interventional Radiology,* vol. 11, pp. 1079-1085.

Otazo, R., Kim, D., Axel, L. & Sodickson, D.K. 2010, "Combination of compressed sensing and parallel imaging for highly accelerated first-pass cardiac perfusion MRI", *Magnetic Resonance in Medicine,* vol. 64, no. 3, pp. 767-776.

Ozenne, V., Bour, P., de Senneville, B.D., Toupin, S., Vaussy, A., Lepetit-Coiffé, M., Jaïs, P., Cochet, H. & Quesson, B. 2019, "Assessment of left ventricle magnetic resonance temperature stability in patients in the presence of arrhythmias", *NMR in biomedicine,* vol. 32, no. 11, pp. e4160.

Ozenne, V., Toupin, S., Bour, P., de Senneville, B.D., Lepetit-Coiffé, M., Boissenin, M., Benois-Pineau, J., Hansen, M.S., Inati, S.J., Govari, A., Jaïs, P. & Quesson, B. 2017,

"Improved cardiac magnetic resonance thermometry and dosimetry for monitoring lesion formation during catheter ablation", *Magnetic Resonance in Medicine,* vol. 77, no. 2, pp. 673-683.

Paetsch, I., Sommer, P., Jahnke, C., Hilbert, S., Loebe, S., Schoene, K., Oebel, S., Krueger, S., Weiss, S., Smink, J., Lloyd, T. & Hindricks, G. 2019, "Clinical workflow and applicability of electrophysiological cardiovascular magnetic resonance-guided radiofrequency ablation of isthmus-dependent atrial flutter", *European Heart Journal: Cardiovascular Imaging,* vol. 20, pp. 147-156.

Papageorgiou, N., Providência, R., Bronis, K., Dechering, D.G., Srinivasan, N., Eckardt, L. & Lambiase, P.D. 2018, "Catheter ablation for ventricular tachycardia in patients with cardiac sarcoidosis: a systematic review", *Europace : European pacing, arrhythmias, and cardiac electrophysiology : journal of the working groups on cardiac pacing, arrhythmias, and cardiac cellular electrophysiology of the European Society of Cardiology,* vol. 20, no. 4, pp. 682-691.

Pashakhanloo, F., Herzka, D.A., Halperin, H., McVeigh, E.R. & Trayanova, N.A. 2018, "Role of 3-Dimensional Architecture of Scar and Surviving Tissue in Ventricular Tachycardia: Insights From High-Resolution Ex Vivo Porcine Models", *Circulation: Arrhythmia and Electrophysiology,* vol. 11, pp. e006131.

Pathak, R.K., Ariyarathnan, N., Garcia, F.C., Sanders, P. & Marchlinski, F.E. 2019, "Catheter ablation of idiopathic ventricular arrhythmias", *Heart, Lung and Circulation,* vol. 28, pp. 102-109.

Perez-David, E., Arenal, Á, Rubio-Guivernau, J.L., del Castillo, R., Atea, L., Arbelo, E., Caballero, E., Celorrio, V., Datino, T., Gonzalez-Torrecilla, E., Atienza, F., Ledesma-Carbayo, M.J., Bermejo, J., Medina, A. & Fernández-Avilés, F. 2011, *Noninvasive Identification of Ventricular Tachycardia-Related Conducting Channels Using Contrast-Enhanced Magnetic Resonance Imaging in Patients With Chronic Myocardial Infarction: Comparison of Signal Intensity Scar Mapping and Endocardial Voltage Mapping*. Journal of the American College of Cardiology: 57; 184-94.

Peters, D.C., Appelbaum, E.A., Nezafat, R., Dokhan, B., Han, Y., Kissinger, K.V., Goddu, B. & Manning, W.J. 2009, "Left ventricular infarct size, peri-infarct zone, and papillary scar measurements: A comparison of high-resolution 3D and conventional 2D late gadolinium enhancement cardiac MR", *Journal of Magnetic Resonance Imaging,* vol. 30, no. 4, pp. 794-800.

Piers, S.R.D., Tao, Q., de Riva Silva, M., Siebelink, H., Schalij, M.J., van der Geest, Rob J. & Zeppenfeld, K. 2014, *CMR–Based Identification of Critical Isthmus Sites of Ischemic and Nonischemic Ventricular Tachycardia*. JACC: Cardiovascular Imaging: 7; 774-84.

Piers, S., Tao, Q., van Huls van Taxis, CFB, Schalij, M.J., van der Geest, R J & Zeppenfeld, K. 2013, "Contrast-enhanced MRI-derived scar patterns and associated ventricular tachycardias in nonischemic cardiomyopathy: implications for ablation strategy", *Circulation: Arrhythmia and Electrophysiology,* vol. 6, pp. 875-883.

Polin, G.M., Haqqani, H., Tzou, W., Hutchinson, M.D., Garcia, F.C., Callans, D.J., Zado, E.S. & Marchlinski, F.E. 2011, *Endocardial unipolar voltage mapping to identify epicardial substrate in arrhythmogenic right ventricular cardiomyopathy/dysplasia*. Heart Rhythm: 8; 76-83.

Poole, J.E., Johnson, G.W., Hellkamp, A.S., Anderson, J., Callans, D.J., Raitt, M.H., Reddy, R.K., Marchlinski, F.E., Yee, R., Guarnieri, T., Talajic, M., Wilber, D.J., Fishbein, D.P., Packer, D.L., Mark, D.B., Lee, K.L. & Bardy, G.H. 2008, "Prognostic Importance of Defibrillator Shocks in Patients with Heart Failure", *N Engl J Med,* vol. 359, no. 10, pp. 1009-1017.

Pop, M., Ghugre, N.R., Ramanan, V., Morikawa, L., Stanisz, G., Dick, A.J. & Wright, G.A. 2013, "Quantification of fibrosis in infarcted swine hearts by ex vivo late gadolinium-enhancement and diffusion-weighted MRI methods", *Physics in Medicine and Biology,* vol. 58, pp. 5009-28.

Radau, P.E., Pintilie, S., Flor, R., Biswas, L., Oduneye, S.O. & Ramanan, V. 2011, *VURTIGO: Visualization platform for real-time MRI-guided cardiac electroanatomic mapping,* STACOM, Toronto, Canada.

Rajat, Deo. & Albert, C.M. 2012, "Epidemiology and Genetics of Sudden Cardiac Death", *Circulation,* vol. 125, no. 4, pp. 620-637.

Ranjan, R., McGann, C.J., Jeong, E., Hong, K., Kholmovski, E.G., Blauer, J., Wilson, B.D., Marrouche, N.F. & Kim, D. 2015, "Wideband late gadolinium enhanced magnetic resonance imaging for imaging myocardial scar without image artefacts induced by implantable cardioverter-defibrillator: a feasibility study at 3 T", *Europace : European pacing, arrhythmias, and cardiac electrophysiology : journal of the working groups on cardiac pacing, arrhythmias, and cardiac cellular electrophysiology of the European Society of Cardiology,* vol. 17, no. 3, pp. 483-488.

Rashid, S., Rapacchi, S., Shivkumar, K., Plotnik, A., Finn, J.P. & Hu, P. 2016, "Modified wideband three-dimensional late gadolinium enhancement MRI for patients with implantable cardiac devices", *Magnetic Resonance in Medicine,* vol. 75, no. 2, pp. 572-584.

Rashid, S., Rapacchi, S., Vaseghi, M., Tung, R., Shivkumar, K., Finn, J.P. & Hu, P. 2014, "Improved Late Gadolinium Enhancement MR Imaging for Patients with Implanted Cardiac Devices", *Radiology,* vol. 270, no. 1, pp. 269-274.

Ratnayaka, K., Faranesh, A.Z., Guttman, M.A., Kocaturk, O., Saikus, C.E. & Lederman, R.J. 2008, "Interventional cardiovascular magnetic resonance: still tantalizing", *Journal of Cardiovascular Magnetic Resonance,* vol. 10, pp. 62.

Ratnayaka, K., Faranesh, A.Z., Hansen, M.S., Stine, A.M., Halabi, M., Barbash, I.M., Schenke, W.H., Wright, V.J., Grant, L.P., Kellman, P., Kocaturk, O. & Lederman, R.J. 2013, "Real-time MRI-guided right heart catheterization in adults using passive catheters", *European heart journal,* vol. 34, no. 5, pp. 380-389.

Reddy, V.Y., Wrobleski, D., Houghtaling, C., Josephson, M.E. & Ruskin, J.N. 2003, "Combined Epicardial and Endocardial Electroanatomic Mapping in a Porcine Model of Healed Myocardial Infarction", *Circulation,* vol. 107, pp. 3236-3242.

Reddy, V.Y., Reynolds, M.R., Neuzil, P., Richardson, A.W., Taborsky, M., Jongnarangsin, K., Kralovec, S., Sediva, L., Ruskin, J.N. & Josephson, M.E. 2007, "Prophylactic Catheter Ablation for the Prevention of Defibrillator Therapy", *N Engl J Med,* vol. 357, no. 26, pp. 2657-2665.

Ren, J.F., Callans, D.J., Michele, J.J., Dillon, S.M. & Marchlinski, F.E. 2001, "Intracardiac echocardiographic evaluation of ventricular mural swelling from radiofrequency ablation in chronic myocardial infarction: irrigated-tip versus standard catheter", *Journal of Interventional Cardiac Electrophysiology,* vol. 5, pp. 27-32.

Ridgeway, J.P. 2010, "Cardiovascular magnetic resonance physics for clinicians: part I", *Journal of Cardiovascular Magnetic Resonance,* vol. 12, pp. 71.

Rieke, V. & Butts Pauly, K. 2008a, "MR thermometry", *Journal of Magnetic Resonance Imaging,* vol. 27, no. 2, pp. 376-390.

Rieke, V. & Butts Pauly, K. 2008b, "MR thermometry", *Journal of Magnetic Resonance Imaging,* vol. 27, no. 2, pp. 376-390.

Romero, J., Di Biase, L., Diaz, J.C., Quispe, R., Du, X., Briceno, D., Avendano, R., Tedrow, U., John, R.M., Michaud, G.F., Natale, A., Stevenson, W.G. & Kumar, S. 2018, *Early Versus Late Referral for Catheter Ablation of Ventricular Tachycardia in Patients With Structural Heart Disease: A Systematic Review and Meta-Analysis of Clinical Outcomes.* JACC: Clinical Electrophysiology; 4: 374-382.

Rostock, T., Rotter, M., Sanders, P., Takahashi, Y., Jaïs, P., Hocini, M., Hsu, L., Sacher, F., Clémenty, J. & Haïssaguerre, M. 2006, *High-density activation mapping of fractionated electrograms in the atria of patients with paroxysmal atrial fibrillation.* Heart Rhythm: 3; 27-34.

Roujol, S., Anter, E., Josephson, M.E. & Nezafat, R. 2013, "Characterization of respiratory and cardiac motion from electro-anatomical mapping data for improved fusion of MRI to left ventricular electrograms", *PLoS One,* vol. 8, pp. e78852.

Roujol, S., Ries, M., Quesson, B., Moonen, C. & Denis, d.S. 2010, "Real-time MR-thermometry and dosimetry for interventional guidance on abdominal organs", *Magnetic Resonance in Medicine,* vol. 63, no. 4, pp. 1080-1087.

Rutz, T., Piccini, D., Coppo, S., Chaptinel, J., Ginami, G., Vincenti, G., Stuber, M. & Schwitter, J. 2016, "Improved border sharpness of post-infarct scar by a novel self-navigated free-breathing high-resolution 3D whole-heart inversion recovery magnetic resonance approach", *International Journal of Cardiovascular Imaging,* vol. 32, pp. 1735-1744.

S. O. Oduneye, L. Biswas, S. Ghate, V. Ramanan, J. Barry, A. Laish-FarKash, E. Kadmon, T. Zeidan Shwiri, E. Crystal & G. A. Wright 2012, *The Feasibility of Endocardial Propagation Mapping Using Magnetic Resonance Guidance in a Swine Model, and Comparison With Standard Electroanatomic Mapping.* IEEE Transactions in Medical Imaging: 31; 977-83.

S. O. Oduneye, M. Pop, L. Biswas, S. Ghate, R. Flor, V. Ramanan, J. Barry, H. Celik, E. Crystal & G. A. Wright 2013, *Postinfarction Ventricular Tachycardia Substrate Characterization: A Comparison Between Late Enhancement Magnetic Resonance Imaging and Voltage Mapping Using an MR-Guided Electrophysiology System.* IEEE Transactions in Biomedical Engineering: 60; 2442-9.

S. Roujol, T. A. Basha, A. Tan, V. Khanna, R. H. Chan, M. H. Moghari, H. Rayatzadeh, J. L. Shaw, M. E. Josephson & R. Nezafat 2013, *Improved Multimodality Data Fusion of*

Late Gadolinium Enhancement MRI to Left Ventricular Voltage Maps in Ventricular Tachycardia Ablation. IEEE Transactions in Biomedical Engineering: 60; 1308-17.

Santangeli, P., Frankel, D.S. & Marchlinski, F.E. 2014, "End points for ablation of scar-related ventricular tachycardia", *Circulation: Arrhythmia and Electrophysiology,* vol. 7, pp. 949-960.

Santangeli, P. & Marchlinski, F. 2016, "Substrate mapping for unstable ventricular tachycardia", *Heart Rhythm,* vol. 13, pp. 569-583.

Santangeli, P., Frankel, D.S., Tung, R., Vaseghi, M., Sauer, W.H., Tzou, W.S., Mathuria, N., Nakahara, S., Dickfeldt, T.M., Lakkireddy, D., Bunch, T.J., Di Biase, L., Natale, A., Tholakanahalli, V., Tedrow, U.B., Kumar, S., Stevenson, W.G., Della Bella, P., Shivkumar, K., Marchlinski, F.E. & Callans, D.J. 2017, *Early Mortality After Catheter Ablation of Ventricular Tachycardia in Patients With Structural Heart Disease*. Journal of the American College of Cardiology 69: 2105-2115.

Sapp, J.L., Wells, G.A., Parkash, R., Stevenson, W.G., Blier, L., Sarrazin, J., Thibault, B., Rivard, L., Gula, L., Leong-Sit, P., Essebag, V., Nery, P.B., Tung, S.K., Raymond, J., Sterns, L.D., Veenhuyzen, G.D., Healey, J.S., Redfearn, D., Roux, J. & Tang, A.S.L. 2016, "Ventricular Tachycardia Ablation versus Escalation of Antiarrhythmic Drugs", *N Engl J Med,* vol. 375, no. 2, pp. 111-121.

Sasaki, T., Miller, C.F., Hansford, R., Yang, J., Caffo, B.S., Zviman, M.M., Henrikson, C.A., Marine, J.E., Spragg, D., Cheng, A., Tandri, H., Sinha, S., Kolandaivelu, A., Zimmerman, S.L., Bluemke, D.A., Tomaselli, G.F., Berger, R.D., Calkins, H., Halperin, H.R. & Nazarian, S. 2012, "Myocardial structural associations with local electrograms: a study of postinfarct ventricular tachycardia pathophysiology and magnetic resonance-based noninvasive mapping", *Circulation: Arrhythmia and Electrophysiology,* vol. 5, no. 6, pp. 1081-1090.

Scheffler, K. & Hennig, J. 2001, "T1 quantification with inversion recovery TrueFISP", *Magnetic Resonance in Medicine,* vol. 45, no. 4, pp. 720-723.

Schelbert, E.B., Hsu, L.Y., Anderson, S.A., Mohanty, B.D., Karim, S.M., Kellman, P., Aletras, A.H. & Arai, A.E. 2010, "Late gadolinium-enhancement cardiac magnetic resonance identifies postinfarction myocardial fibrosis and the border zone at the near cellular level in ex vivo rat heart", *Circulation: Cardiovascular Imaging,* vol. 3, pp. 743-752.

Schmidt, A., Azevedo, C.F., Cheng, A., Gupta, S.N., Bluemke, D.A., Foo, T.K., Gerstenblith, G., Weiss, R.G., Marban, E., Tomaselli, G.F., Lima, J. & Wu, K.C. 2007, "Infarct tissue heterogeneity by magnetic resonance imaging identifies enhanced cardiac arrhythmia susceptibility in patients with left ventricular dysfunction", *Circulation,* vol. 115, pp. 2006-2014.

Schmidt, E.J., Watkins, R.D., Zviman, M.M., Guttman, M.A., Wang, W. & Halperin, H.A. 2016, "A Magnetic Resonance Imaging-Conditional External Cardiac Defibrillator for Resuscitation Within the Magnetic Resonance Imaging Scanner Bore", *Journal of Cardiovascular Magnetic Resonance,* vol. 10, pp. e005091.

Sen-Chowdhry, S., Prasad, S.K., Syrris, P., Wage, R., Ward, D., Merrifield, R., Smith, G.C., Firmin, D.N., Pennell, D.J. & McKenna, W.J. 2006, *Cardiovascular Magnetic Resonance in Arrhythmogenic Right Ventricular Cardiomyopathy Revisited:*

Comparison With Task Force Criteria and Genotype. Journal of the American College of Cardiology: 48; 2132-40.

Shah, D., Haïssaguerre, M., Takahashi, A., Jais, P., Hocini, M. & Clementy, J. 2000, "Differential pacing for distinguishing block from persistent conduction through an ablation line", *Circulation,* vol. 102, no. 13, pp. 1517-1522.

Shin, T., Lustig, M., Nishimura, D.G. & Hu, B.S. 2014, "Rapid single-breath-hold 3D late gadolinium enhancement cardiac MRI using a stack-of-spirals acquisition", *Journal of Magnetic Resonance Imaging,* vol. 40, no. 6, pp. 1496-1502.

Silberbauer, J., Oloriz, T., Maccabelli, G., Tsiachris, D., Baratto, F., Vergara, P., Mizuno, H., Bisceglia, C., Marzi, A., Sora, N., Guaraccini, F., Radinovic, A., Cireddu, M., Sala, S., Guletta, S., Paglino, G., Mazzone, P., Trevisi, N. & Della Bella, P. 2014, "Noninducibility and late potential abolition: a novel combined prognostic procedural end point for catheter ablation of postinfarction ventricular tachycardia", *Circulation: Arrhythmia and Electrophysiology,* vol. 7, pp. 424-435.

Soejima, K., Stevenson, W.G., Maisel, W.H., Sapp, J.L. & Epstein, L.M. 2002, "Electrically unexcitable scar mapping based on pacing threshold for identification of the reentry circuit isthmus: feasibility for guiding ventricular tachycardia ablation", *Circulation,* vol. 106, pp. 1678-83.

Sramko, M., Hoogendoorn, J.C., Glashan, C.A. & Zeppenfeld, K. 2019, "Advancement in cardiac imaging for treatment of ventricular arrhythmias in structural heart disease", *EP Europace,* vol. 21, no. 3, pp. 383-403.

Stevenson, W.G., Khan, H., Sager, P., Saxon, L.A., Middlekauff, H.R., Natterson, P.D. & Wiener, I. 1993, "Identification of reentry circuit sites during catheter mapping and radiofrequency ablation of ventricular tachycardia late after myocardial infarction", *Circulation,* vol. 88, pp. 1647-1670.

Stevenson, W.G., Wilber, D.J., Natale, A., Jackman, W.M., Marchlinski, F.E., Talbert, T., Gonzalez, M.D., Worley, S.J., Daoud, E.G., Hwang, C., Schuger, C., Bump, T.E., Jazayeri, M., Tomassoni, G.F., Kopelman, H.A., Soejima, K. & Nakagawa, H. 2008, "Irrigated radiofrequency catheter ablation guided by electroanatomic mapping for recurrent ventricular tachycardia after myocardial infarction: the multicenter thermocool ventricular tachycardia ablation trial", *Circulation,* vol. 118, no. 25, pp. 2773-82.

Stevenson, W.G., Friedman, P.L., Sager, P.T., Saxon, L.A., Kocovic, D., Harada, T., Wiener, I. & Khan, H. 1997, *Exploring Postinfarction Reentrant Ventricular Tachycardia With Entrainment Mapping.* Journal of the American College of Cardiology: 29; 1180-1189.

Tanawuttiwat, T., Nazarian, S. & Calkins, H. 2016, "The role of catheter ablation in the management of ventricular tachycardia", *European Heart Journal,* vol. 37, pp. 594-609.

TANNER, H., HINDRICKS, G., VOLKMER, M., FURNISS, S., KÜHLKAMP, V., LACROIX, D., DE CHILLOU, C., ALMENDRAL, J., CAPONI, D., KUCK, K. & KOTTKAMP, H. 2010, "Catheter Ablation of Recurrent Scar-Related Ventricular Tachycardia Using Electroanatomical Mapping and Irrigated Ablation Technology: Results of the Prospective Multicenter Euro-VT-Study", *Journal of cardiovascular electrophysiology,* vol. 21, no. 1, pp. 47-53.

Tilz, R.R., Lenarczyk, R., Scherr, D., Haugaa, K.H., Iliodromitis, K., Pürerfellner, H., Kiliszek, M. & Dagres, N. 2018a, "Management of ventricular tachycardia in the ablation era: results of the European Heart Rhythm Association Survey", *EP Europace,* vol. 20, no. 1, pp. 209-213.

Tilz, R.R., Lenarczyk, R., Scherr, D., Haugaa, K.H., Iliodromitis, K., Pürerfellner, H., Kiliszek, M. & Dagres, N. 2018b, "Management of ventricular tachycardia in the ablation era: results of the European Heart Rhythm Association Survey", *EP Europace,* vol. 20, no. 1, pp. 209-213.

Tokuda, M., Kojodjojo, P., Tung, S., Tedrow, U.B., Not, E., Inada, K., Koplan, B.A., Michaud, G.F., John, R.M., Epstein, L.M. & Stevenson, W.G. 2013, "Acute failure of catheter ablation for ventricular tachycardia due to structural heart disease: causes and significance", *Journal of the American Heart Association,* vol. 2, pp. e000072.

Toupin, S., Bour, P., Lepetit-Coiffé, M., Ozenne, V., Denis de Senneville, B., Schneider, R., Vaussy, A., Chaumeil, A., Cochet, H., Sacher, F., Jais, P. & Quesson, B. 2017, "Feasibility of real-time MR thermal dose mapping for predicting radiofrequency ablation outcome in the myocardium in vivo", *Journal of Cardiovascular Magnetic Resonance,* vol. 19, pp. 14.

Tschabrunn, C.M., Roujol, S., Dorman, N.C., Nezafat, R., Josephson, M.E. & Anter, E. 2016, "High-resolution mapping of ventricular scar: comparison between single and multi-electrode catheters", *Circulation: Arrhythmia and Electrophysiology,* vol. 9, no. 6, pp. e003841.

Tschabrunn, C.M., Roujol, S., Nezafat, R., Faulkner-Jones, B., Buxton, A.E., Josephson, M.E. & Anter, E. 2016, *A swine model of infarct-related reentrant ventricular tachycardia: Electroanatomic, magnetic resonance, and histopathological characterization.* Heart Rhythm: 13; 262-73.

Tse, Z.T.H., Dumoulin, C.L., Clifford, G.D., Schweitzer, J., Qin, L., Oster, J., Jerosch-Herold, M., Kwong, R.Y., Michaud, G., Stevenson, W.G. & Schmidt, E.J. 2014, "A 1.5T MRI-conditional 12-lead electrocardiogram for MRI and intra-MR intervention", *Magnetic Resonance in Medicine,* vol. 71, no. 3, pp. 1336-1347.

Tung, R., Kim, S., Yagishita, D., Vaseghi, M., Ennis, D.B., Ouadah, S., Ajijola, O.A., Bradfield, J.S., Mahapatra, S., Finn, P. & Shivkumar, K. 2016, *Scar voltage threshold determination using ex vivo magnetic resonance imaging integration in a porcine infarct model: Influence of interelectrode distances and three-dimensional spatial effects of scar.* Heart Rhythm: 13; 1993-2002.

Tzou, W.S., Frankel, D.S., Hegeman, T., Supple, G.E., Garcia, F.C., Santangeli, P., Katz, D.F., Sauer, W.H. & Marchlinski, F.E. 2015, "Core isolation of critical arrhythmia elements for treatment of multiple scar-based ventricular tachycardias", *Circulation: Arrhythmia and Electrophysiology,* vol. 8, pp. 353-361.

Velasco-Forte, M.N., Pushparajah, K., Schaeffter, T., Valverde Perez, I., Rhode, K., Ruijsink, B., Alhrishy, M., Byrne, N., Chiribiri, A., Ismail, T., Hussain, T., Razavi, R. & Roujol, S. 2017, "Improved passive catheter tracking with positive contrast for CMR-guided cardiac catheterization using partial saturation (pSAT)", *Journal of Cardiovascular Magnetic Resonance,* vol. 19, pp. 60.

VERGARA, P., TREVISI, N., RICCO, A., PETRACCA, F., BARATTO, F., CIREDDU, M., BISCEGLIA, C., MACCABELLI, G. & DELLA BELLA, P. 2012, "Late Potentials Abolition as an Additional Technique for Reduction of Arrhythmia Recurrence in Scar Related Ventricular Tachycardia Ablation", *Journal of cardiovascular electrophysiology,* vol. 23, no. 6, pp. 621-627.

Viallon, M., Jacquier, A., Rotaru, C., Delattre, B., Mewton, N., Vincent, F. & Croisille, P. 2011, "Head-to-head comparison of eight late gadolinium-enhanced cardiac MR (LGE CMR) sequences at 1.5 tesla: From bench to bedside", *Journal of Magnetic Resonance Imaging,* vol. 34, no. 6, pp. 1374-1387.

Wang, W. 2015, *Magnetic Resonance–guided Active Catheter Tracking.* Magnetic Resonance Imaging Clinics of North America: 23; 579-89.

Watanabe, E., Abbasi, S.A., Heydari, B., Coelho-Filho, O.R., Shah, R., Neilan, T.G., Murthy, V.L., Mongeon, F.P., Barbhaiya, C., Jerosch-Herold, M., Blankstein, R., Hatabu, H., van der Geest, R J, Stevenson, W.G. & Kwong, R.Y. 2014, "Infarct tissue heterogeneity by contrast-enhanced magnetic resonance imaging is a novel predictor of mortality in patients with chronic coronary artery disease and left ventricular dysfunction", *Circulation: Cardiovascular Imaging,* vol. 7, no. 6, pp. 887-894.

Whitaker, J., Neji, R., Byrne, N., Puyol-Antón, E., Mukherjee, R.K., Williams, S.E., Chubb, H., O'Neill, L., Razeghi, O., Connolly, A., Rhode, K., Niederer, S., King, A., Tschabrunn, C., Anter, E., Nezafat, R., Bishop, M.J., O'Neill, M., Razavi, R. & Roujol, S. 2019, "Improved co-registration of ex-vivo and in-vivo cardiovascular magnetic resonance images using heart-specific flexible 3D printed acrylic scaffold combined with non-rigid registration", *Journal of Cardiovascular Magnetic Resonance,* vol. 21, no. 1, pp. 62.

Wijnmaalen, A.P., van der Geest, Rob J, van Huls van Taxis, Carine F B, Siebelink, H.J., Kroft, L.J.M., Bax, J.J., Reiber, J.H.C., Schalij, M.J. & Zeppenfeld, K. 2011, "Head-to-head comparison of contrast-enhanced magnetic resonance imaging and electroanatomical voltage mapping to assess post-infarct scar characteristics in patients with ventricular tachycardias: real-time image integration and reversed registration", *European heart journal,* vol. 32, no. 1, pp. 104-114.

Wilson, S.R., Shinde, S., Appleby, I., Boscoe, M., Conway, D., Dryden, C., Ferguson, K., Gedroyc, W., Kinsella, S.M., Nathanson, M.H., Thorne, J., White, M. & Wright, E. 2019, "Guidelines for the safe provision of anaesthesia in magnetic resonance units 2019", *Anaesthesia,* vol. 74, no. 5, pp. 638-650.

Winter, L., Oberacker, E., Paul, K., Ji, Y., Oezerdem, C., Ghadjar, P., Thieme, A., Budach, V., Wust, P. & Niendorf, T. 2016, "Magnetic resonance thermometry: Methodology, pitfalls and practical solutions", *International Journal of Hyperthermia,* vol. 32, pp. 63-75.

Wissner, E., Stevenson, W.G. & Kuck, K.H. 2012, "Catheter ablation of ventricular tachycardia in ischaemic and non-ischaemic cardiomyopathy: where are we today? A clinical review.", *European Heart Journal,* vol. 33, pp. 1440-1450.

Wu, V., Barbash, I.M., Ratnayaka, K., Saikus, C.E., Sonmez, M., Kocaturk, O., Lederman, R.J. & Faranesh, A.Z. 2011, "Adaptive noise cancellation to suppress

electrocardiography artifacts during real-time interventional MRI", *Journal of Magnetic Resonance Imaging,* vol. 33, no. 5, pp. 1184-1193.

Xu, R., Athavale, P., Krahn, P., Anderson, K., Barry, J., Biswas, L., Ramanan, V., Yak, N., Pop, M. & Wright, G.A. 2015, "Feasibility Study of Respiratory Motion Modeling Based Correction for MRI-Guided Intracardiac Interventional Procedures", *IEEE Transactions on Biomedical Engineering,* , pp. 2899-2910.

YAMASHITA, S., SACHER, F., MAHIDA, S., BERTE, B., LIM, H.S., KOMATSU, Y., AMRAOUI, S., DENIS, A., DERVAL, N., LAURENT, F., SERMESANT, M., MONTAUDON, M., HOCINI, M., HAÏSSAGUERRE, M., JAÏS, P. & COCHET, H. 2016a, "Image Integration to Guide Catheter Ablation in Scar-Related Ventricular Tachycardia", *Journal of cardiovascular electrophysiology,* vol. 27, no. 6, pp. 699-708.

YAMASHITA, S., SACHER, F., MAHIDA, S., BERTE, B., LIM, H.S., KOMATSU, Y., AMRAOUI, S., DENIS, A., DERVAL, N., LAURENT, F., SERMESANT, M., MONTAUDON, M., HOCINI, M., HAÏSSAGUERRE, M., JAÏS, P. & COCHET, H. 2016b, "Image Integration to Guide Catheter Ablation in Scar-Related Ventricular Tachycardia", *Journal of cardiovascular electrophysiology,* vol. 27, no. 6, pp. 699-708.

Yan, A.T., Shayne, A.J., Brown, K.A., Gupta, S.N., Chan, C.W., Luu, T.M., Di Carli, M.F., Reynolds, H.G., Stevenson, W.G. & Kwong, R.Y. 2006, "Characterization of the peri-infarct zone by contrast-enhanced cardiac magnetic resonance imaging is a powerful predictor of post-myocardial infarction mortality", *Circulation,* vol. 114, pp. 32-39.

Zghaib, T., Ipek, E.G., Hansford, R., Ashikaga, H., Berger, R.D., Marine, J.E., Spragg, D.D., Tandri, H., Zimmerman, S.L., Halperin, H., Brancato, S., Calkins, H., Henrikson, C. & Nazarian, S. 2018, "Standard Ablation Versus Magnetic Resonance Imaging-Guided Ablation in the Treatment of Ventricular Tachycardia", *Circulation: Arrhythmia and Electrophysiology,* vol. 11, no. 1, pp. e005973.

Appendix B: Awards, Publications and Presentations

Awards

2018: Finalist, Early Career Award (Translational), Society of Cardiovascular Magnetic Resonance, Barcelona, Spain

2018: Travel Award, Society of Cardiovascular Magnetic Resonance, Barcelona, Spain

2017:   Research Group of the Year (Mark O'Neill, Steven Williams, John Whitaker, <u>Rahul</u>

<u>Mukherjee</u>, Louisa O'Neill, James Harrison, Henry Chubb) – School of Biomedical

Engineering and Imaging Sciences, King's College London

Peer-reviewed publications (First author only)

1) **<u>Mukherjee RK</u>**, Costa CM, Neji R, Harrison JL, Sim I, Williams SE, Whitaker J,
     Chubb H, O'Neill L, Schneider R, Lloyd T, Pohl T, Roujol S, Niederer SA, Razavi R,
     O'Neill MD. Evaluation of a real-time magnetic resonance imaging-guided
     electrophysiology system for structural and electrophysiological ventricular
     tachycardia substrate assessment. <u>Europace</u> 2019; 21(9): 1432-1441. PMID:
     31219547

2) **<u>Mukherjee RK</u>**, Chubb H, Roujol S, Razavi R, O'Neill MD. Advances in real-time
     MRI-guided electrophysiology. <u>Current Cardiovascular Imaging Reports</u> 2019; 12: 6.
     PMID: 31501689

3) **<u>Mukherjee RK</u>**, Williams SE, Niederer SA, O'Neill MD. Atrial fibrillation ablation
     in patients with heart failure: one size does not fit all. <u>Arrhythmia and</u>
     <u>Electrophysiology Review</u> 2018; 7(2): 84-90. PMID: 29967679

4) **<u>Mukherjee RK</u>**, Whitaker J, Williams SE, Razavi R, O'Neill MD. Magnetic
     resonance imaging guidance for the optimization of ventricular tachycardia ablation.
     <u>Europace</u> 2018; 20 (11); 1721-32. PMID: 29584897

5) **Mukherjee RK**, Roujol S, Chubb H, Harrison J, Williams S, Whitaker J, O'Neill L, Silberbauer J, Neji R, Schneider R, Pohl T, Lloyd T, O'Neill M, Razavi R. Epicardial electroanatomical mapping, radiofrequency ablation and lesion imaging in the porcine left ventricle under real time magnetic resonance imaging guidance – an in-vivo feasibility study. Europace 2018: 20(FI2): f254-f262. PMID: 29294008

6) **Mukherjee RK**, O'Neill L, O'Neill MD. Prophylactic catheter ablation for ventricular tachycardia: Are we there yet? Arrhythmia and Electrophysiology Review 2017; 6(3):125-8. PMID: 29018520

International presentations (First author only)

1) **Mukherjee R**, Costa CM, Neji R, Harrison J, Sim I, Williams SE, Whitaker J, Chubb H, O'Neill L, Schneider R, Lloyd T, Pohl T, Roujol S, Niederer SA, Razavi R, O'Neill M. Evaluation of a real-time MRI-guided electrophysiology system for structural and electrophysiological ventricular tachycardia substrate assessment in a porcine model. Heart Rhythm Society Scientific Sessions, San Francisco, California, USA, May 2019.

2) **Mukherjee RK**, Costa CM, Neji R, Harrison J, Sim I, Williams SE, Whitaker J, Chubb H, O'Neill L, Lloyd T, Pohl T, Roujol S, Niederer SA, Razavi R, O'Neill M. Pre-clinical evaluation of a real-time MRI-guided electrophysiology system for ventricular tachycardia. EHRA, 16-19th March 2019, Lisbon, Portugal.

3) **Mukherjee R**, Ginami G, Neji R, Roujol S, Williams SE, Chubb H, Whitaker J, O'Neill L, Pohl T, Schneider R, Lloyd T, Razavi R, Botnar R, O'Neill MD, Prieto C.

Ablation lesion visualisation using non-contrast simultaneous bright and dark blood whole-heart MRI during real-time MR-guided electrophysiology. Heart Rhythm Society Scientific Sessions, Boston, Massachusetts, USA, May 2018. *Heart Rhythm (15):5; May Supplement 2018: S178-S283*

4) **Mukherjee R**, Williams SE, Neji R, Roujol S, Harrison J, Whitaker J, Chubb H, O'Neill L, Sim I, Pohl T, Schneider R, Lloyd T, Razavi R, O'Neill MD. High-power, short-duration atrial ablation can achieve transmural lesions and can be visualised on MRI in a porcine model. Heart Rhythm Society Scientific Sessions, Boston, Massachusetts, USA, May 2018. *Heart Rhythm (15):5; May Supplement 2018: S178-S283.*

5) **Mukherjee RK**, Whitaker J, Roujol S, Neji R, Ginami G, Villa A, Chubb H, O'Neill L, Williams SE, Silberbauer J, Wright M, O'Neill M, Botnar R, Prieto C, Razavi R. 3D High resolution imaging of ventricular scar: head-to-head comparison of three late gadolinium enhancement (LGE) sequences in a porcine infarct model at 1.5T. Society of Cardiovascular Magnetic Resonance, Barcelona, Spain. 31st January - 3rd February 2018.

6) **Mukherjee RK**, Harrison JL, Roujol S, Neji R, Chubb H, Williams S, Whitaker J, O'Neill L, Silberbauer J, Pohl T, Lloyd T, O'Neill M, Razavi R. Assessment of acute ablation injury in the swine left ventricle delivered using real-time MRI guidance. EHRA Europace - Cardiostim, Vienna, Austria. 18th - 21st June 2017. *Europace (2017) 19; Supplement 3; iii402.*

7) **<u>Mukherjee RK</u>**, Chubb H, Harrison J, Williams S, Whitaker J, O'Neill L, Ginami G, Botnar R, Prieto C, Silberbauer J, Lloyd T, Pohl T, Schneider R, Roujol S, Neji R, Razavi R, O'Neill M. Epicardial electro-anatomical mapping and radio-frequency ablation in the swine left ventricle under real time MRI guidance. Heart Rhythm Society Scientific Sessions, Chicago, Illinois, USA. 10-13th May 2017. *Heart Rhythm (14): 5: May Supplement 2017; S191.*

Appendix C: Additional data

2D LGE   3D LGE   Ex-vivo MRI
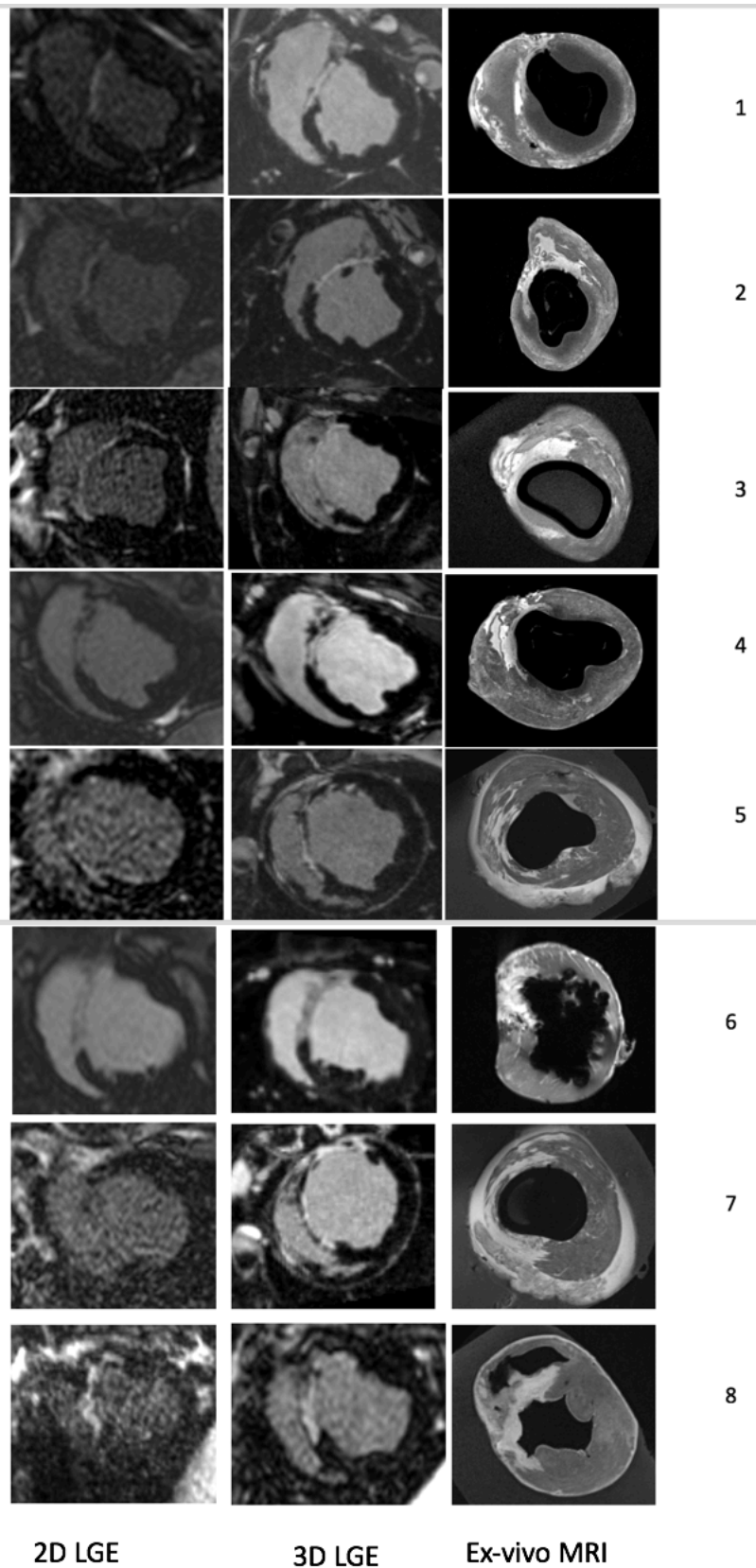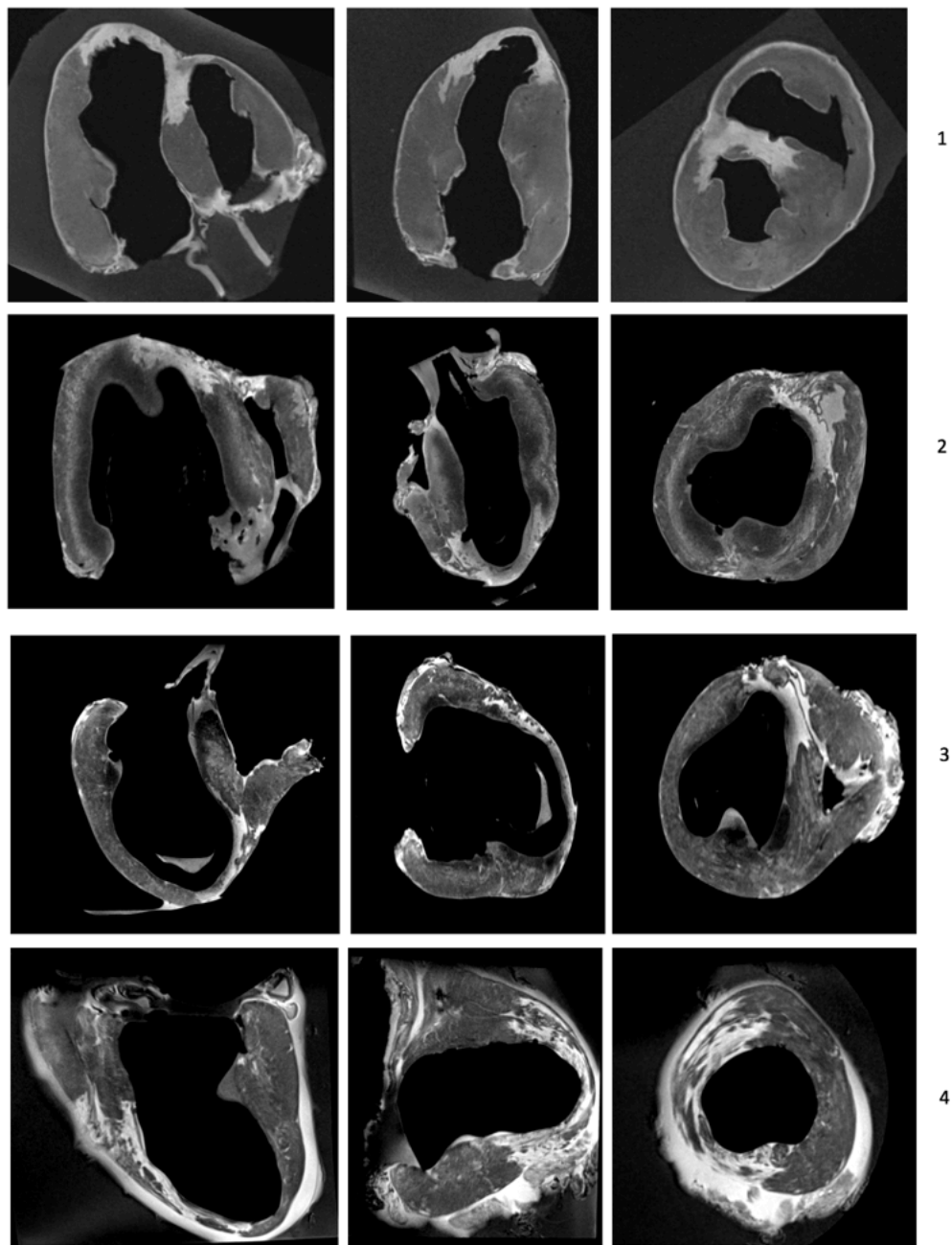
Appendix Figure 1: Additional raw MRI images showing 2D LGE, 3D LGE and ex-vivo MRI datasets acquired in different animals at approximately the same slice location.
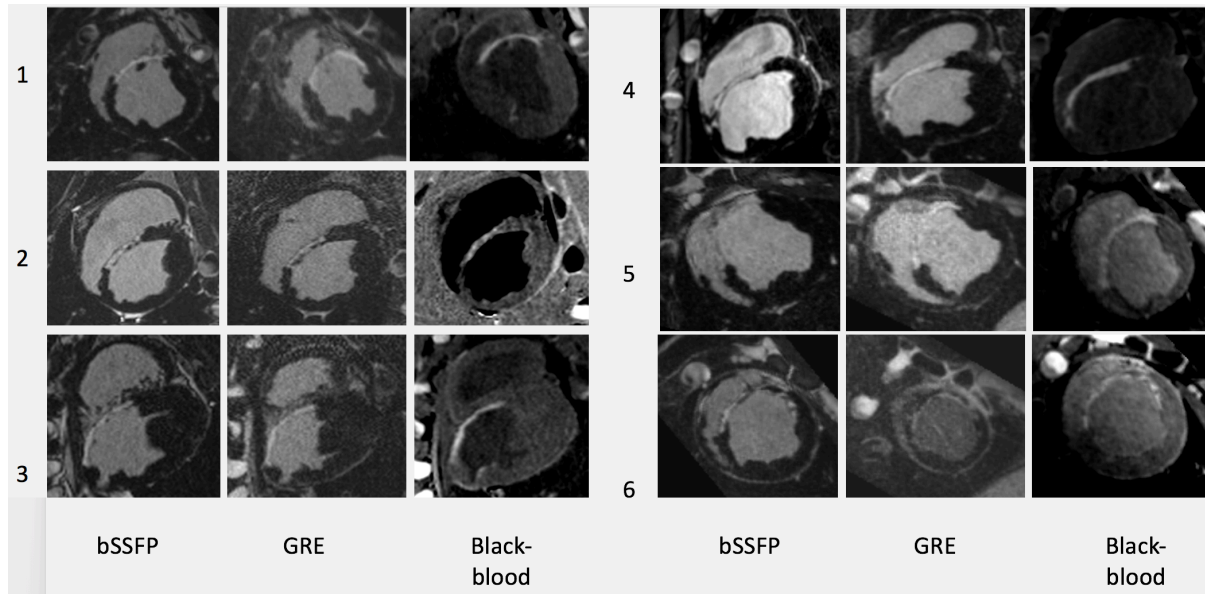
Appendix Figure 2: Additional raw MRI images showing 3D bSSFP, 3D GRE and 3D black-blood LGE sequences from 6 animals at approximately the same slice location.

Appendix Figure 3: Additional raw ex-vivo MRI datasets showing multi-plane reconstructions in 3 views in different animals.
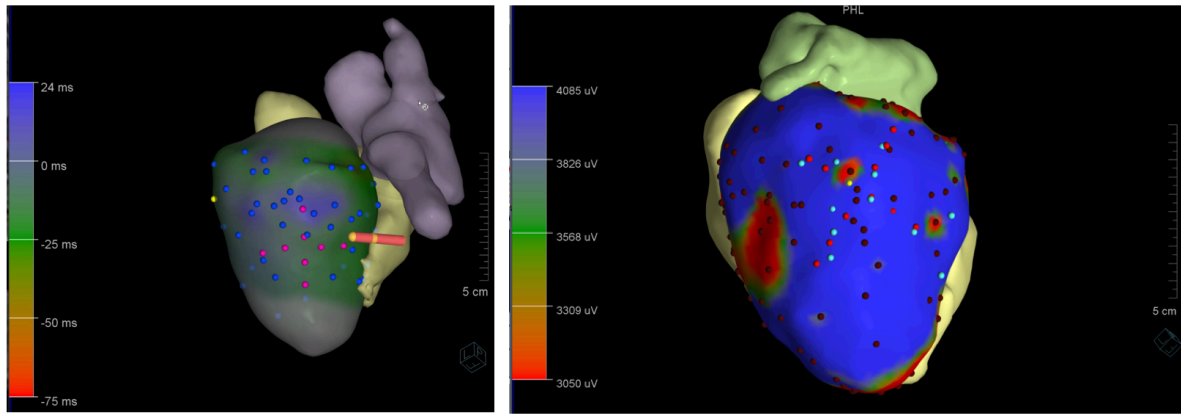
Appendix Figure 4: Activation and voltage map acquired in normal porcine hearts under real-time MRI guidance.

Appendix D: Ethical approvals

MINISTERE DE L'EDUCATION NATIONALE,
DE L'ENSEIGNEMENTSUPERIEUR ET DE LA RECHERCHE

Paris, le jeudi 3 mars 2016

Direction générale
de la recherche
et de l'innovation

Service de la performance,
du financement et de la
contractualisation avec les
organismes de recherche

Département de la culture
scientifique et des relations
avec la société

Expérimentation animale -
Autorisation de projet

Affaire suivie par
Didier HOFFSCHIR
Conseiller scientifique
auprès du DGRI

Florence HERVATIN
Chargée de mission

Téléphone
01 55 55 84 05
Fax
01 55 55 99 59
Mél.
florence.hervatin-queney
@recherche.gouv.fr

1 rue Descartes
75231 Paris Cedex 05

Objet : Notification d'autorisation de projet utilisant des animaux à des fins scientifiques

Monsieur,

En application des dispositions du code rural et de la pêche maritime, notamment ses articles R. 214-87 à R.214-126, le projet :
- référencé sous le numéro *APAFIS#3593-2016011510263648 v2*
- ayant pour titre : « *MR-GAST-VT Phase 1 Study* »,
- déposé par l'Établissement Utilisateur : IRCAD, numéro d'agrément D6748216, dont le responsable est *Monsieur Jacques MARESCAUX*
- et dont le responsable de la mise en œuvre générale du projet et de sa conformité à l'autorisation est *Monsieur Jacques MARESCAUX,*

est autorisé.

L'autorisation de projet est accordée, sous réserve de la validité de l'agrément de l'Établissement Utilisateur, pour une durée de *7 mois* à partir du 03/03/2016

Le projet précité a été évalué sur le plan éthique par le Comité d'éthique en expérimentation animale n°38 et a reçu un avis *favorable*.

Ce projet ne fera pas l'objet, à l'issue de sa réalisation, d'une appréciation rétrospective.

Pour la ministre et par délégation
l'adjointe du chef du service de la performance,
du financement et de la contractualisation avec
les organismes de recherche

Christine COSTE

Monsieur Jacques MARESCAUX
IRCAD

225

NHS
Health Research Authority

London - Westminster Research Ethics Committee

4 Minshull Street
Manchester
M1 3DZ

Telephone: 0207 104 8012

Please note: This is the favourable opinion of the REC only and does not allow you to start your study at NHS sites in England until you receive HRA Approval

---

21 March 2017

Professor Mark O'Neill
Professor of Cardiac Electrophysiology and Consultant Cardiologist
King's College London
4th Floor, North Wing
St Thomas' Hospital
SE1 7EH

Dear Professor O'Neill

Study title:	**Magnetic resonance imaging (MRI) to guide treatment of abnormal heart rhythms**
REC reference:	17/LO/0150
Protocol number:	1.0
IRAS project ID:	217417

Thank you for your submission responding to the Committee's request for further information on the above research and submitting revised documentation.

The further information has been considered on behalf of the Committee by the Alternate Vice-Chair and Dr Yash Patel.

We plan to publish your research summary wording for the above study on the HRA website, together with your contact details. Publication will be no earlier than three months from the date of this opinion letter. Should you wish to provide a substitute contact point, require further information, or wish to make a request to postpone publication, please contact hra.studyregistration@nhs.net outlining the reasons for your request.

Confirmation of ethical opinion

226

On behalf of the Committee, I am pleased to confirm a favourable ethical opinion for the above research on the basis described in the application form, protocol and supporting documentation as revised, subject to the conditions specified below.

Conditions of the favourable opinion

The REC favourable opinion is subject to the following conditions being met prior to the start of the study.

Management permission must be obtained from each host organisation prior to the start of the study at the site concerned.

Management permission should be sought from all NHS organisations involved in the study in accordance with NHS research governance arrangements. Each NHS organisation must confirm through the signing of agreements and/or other documents that it has given permission for the research to proceed (except where explicitly specified otherwise).
Guidance on applying for NHS permission for research is available in the Integrated Research Application System, www.hra.nhs.uk or at http://www.rdforum.nhs.uk.

Where a NHS organisation's role in the study is limited to identifying and referring potential participants to research sites ("participant identification centre"), guidance should be sought from the R&D office on the information it requires to give permission for this activity.

For non-NHS sites, site management permission should be obtained in accordance with the procedures of the relevant host organisation.

Sponsors are not required to notify the Committee of management permissions from host organisations

Registration of Clinical Trials

All clinical trials (defined as the first four categories on the IRAS filter page) must be registered on a publically accessible database within 6 weeks of recruitment of the first participant (for medical device studies, within the timeline determined by the current registration and publication trees).

There is no requirement to separately notify the REC but you should do so at the earliest opportunity e.g. when submitting an amendment. We will audit the registration details as part of the annual progress reporting process.

To ensure transparency in research, we strongly recommend that all research is registered but for non-clinical trials this is not currently mandatory.

If a sponsor wishes to request a deferral for study registration within the required timeframe, they should contact hra.studyregistration@nhs.net. The expectation is that all clinical trials will be registered, however, in exceptional circumstances non registration may be permissible with prior agreement from the HRA. Guidance on where to register is provided on the HRA website.

It is the responsibility of the sponsor to ensure that all the conditions are complied with before the start of the study or its initiation at a particular site (as applicable).

Ethical review of research sites

NHS sites

The favourable opinion applies to all NHS sites taking part in the study, subject to management permission being obtained from the NHS/HSC R&D office prior to the start of the study (see "Conditions of the favourable opinion" below).

Approved documents

The final list of documents reviewed and approved by the Committee is as follows:

Document	Version	Date
Covering letter on headed paper [Cover Letter]	1	19 October 2016
Covering letter on headed paper [Cover Letter]	2	16 February 2017
Covering letter on headed paper [Cover Letter]	3	16 February 2017
Evidence of Sponsor insurance or indemnity (non NHS Sponsors only) [Sponsor Insurance]	1	29 June 2016
GP/consultant information sheets or letters [GP Letter]	1	10 January 2017
IRAS Application Form [IRAS_Form_09012017]		09 January 2017
Letter from funder [Letter from funder]	1	15 June 2015
Letters of invitation to participant [Patient Invitation Letter]	1	19 October 2016
Participant consent form	2	20 February 2017
Participant information sheet (PIS)	4	20 February 2017
Research protocol or project proposal [Research protocol]	3	10 February 2017
Summary CV for Chief Investigator (CI) [Mark O'Neill CV]	1	19 November 2016

Statement of compliance

The Committee is constituted in accordance with the Governance Arrangements for Research Ethics Committees and complies fully with the Standard Operating Procedures for Research Ethics Committees in the UK.

After ethical review

Reporting requirements

The attached document "After ethical review – guidance for researchers" gives detailed guidance on reporting requirements for studies with a favourable opinion, including:

- Notifying substantial amendments
- Adding new sites and investigators
- Notification of serious breaches of the protocol
- Progress and safety reports
- Notifying the end of the study

The HRA website also provides guidance on these topics, which is updated in the light of changes in reporting requirements or procedures.

User Feedback

The Health Research Authority is continually striving to provide a high quality service to all applicants and sponsors. You are invited to give your view of the service you have received and the application procedure. If you wish to make your views known please use the feedback form available on the HRA website:
http://www.hra.nhs.uk/about-the-hra/governance/quality-assurance/

HRA Training

We are pleased to welcome researchers and R&D staff at our training days – see details at
http://www.hra.nhs.uk/hra-training/

17/LO/0150	Please quote this number on all correspondence

With the Committee's best wishes for the success of this project.

Yours sincerely

Mr Robert Goldstein
Chair

Email: nrescommittee.london-westminster@nhs.net

Enclosures: "After ethical review – guidance for researchers"

Copy to: Mr Keith Brennan, Kings College London
                     Ms Jennifer Boston, Guy's and St Thomas' NHS Foundation Trust